

Oxidation/Pyrolysis Chemistry as Related to
Fuel Sooting Tendencies

Kenneth Brezinsky and Irvin Glassman

Princeton University
Mechanical and Aerospace Engineering Department
Princeton, NJ 08544

Introduction

The obvious practical importance of understanding soot formation processes has motivated a series of studies examining both the macroscopic, phenomenological parameters that affect soot formation such as flame type and temperature and the microscopic, chemical processes that may be responsible for the rate controlling soot initiation steps.

At Princeton University, premixed and diffusion flame experiments have been conducted and have revealed the relationship between the sooting tendency of hydrocarbon fuels and temperature (1,2,3). The tendencies exhibited by fuels are different when measured in the two types of flames. Under premixed conditions, an increased flame temperature has been found to decrease the formation of soot. The details of the initial fuel structure, such as the isomeric distribution of side chains, degree of conjugation and aromaticity are unimportant to the sooting tendency except insofar as they contribute to the total number of C-C bonds. The general conclusions that have been deduced are that soot forms in the post flame region from an essential precursor, probably acetylene, and the sooting tendency of a particular fuel depends primarily on the balance between the amount of soot precursor it forms (a function only of the number of C-C bonds) and the amount of precursor consuming OH radicals the fuel produces. The OH attack increases faster with temperature than does the soot precursor formation (1). The OH concentration is also proportional to the H/C ratio, which, too, is a function of the number of C-C bonds (1).

Diffusion flame experiments have led to the observation of almost completely opposite patterns. An increase in the diffusion flame temperature has been shown to increase the sooting tendency of a hydrocarbon fuel. The particular structure of the fuel affects the degree of soot formation through the mechanism by which the fuel pyrolytically decays. Since different fuels have different pyrolysis mechanisms, the nature of the initial fuel structure becomes a significant determinant in the degree of soot formation. Furthermore, soot is formed in the pre-flame, fuel region. Consequently, oxidation at the flame front consumes fuel, fuel fragments and soot particles. Particles break through the flame front and become observed as soot only when there are lowered temperatures in a localized area and insufficient oxygen to consume both the molecular hydrocarbons and the soot particles.

The details of the chemical mechanisms of the pyrolysis and oxidation processes that so strongly impact the sooting tendencies of various hydrocarbon fuels could not be revealed by the types of premixed and diffusion flame experiments that were performed. Insight into chemical mechanisms, however, has been obtained from chemical kinetic, flow reactor studies conducted at Princeton. Studies of the oxidation of benzene (4), toluene (5), ethyl benzene (6), propyl benzene (7,8), butyl benzene, alpha methyl naphthalene (10), butadiene (11), ethylene (12), propane (13), butane (14) and

other hydrocarbons have revealed many of the mechanistic steps by which these fuels decompose. A limited number of pyrolysis studies have also yielded mechanistic information for oxygen free conditions. Despite the information obtained from the flow reactor studies, the absence of a chemical, soot formation mechanism has prevented the linking of the flow reactor derived mechanisms with the pyrolysis and oxidation chemistry that must be responsible for the phenomenological observations of the flame studies.

A recently developed soot formation mechanism by Frenklach et al. (15), that evolved from a sequence of shock tube experiments on acetylene pyrolysis can serve as a partial framework for connecting known chemical mechanisms with macroscopically determined sooting tendencies. The mechanism proposes a sequence of events starting from acetylene, proceeding through butadienyl and vinyl acetylenyl radicals to the formation of a phenyl radical (Table 1). From the phenyl radical, the growth of large polycyclic aromatics leading to soot would proceed relatively easily. This soot formation sequence should be appropriate for the post-flame region of a sooting premixed flame and the pre-flame fuel region of a diffusion flame.

In this paper, a first attempt is made at using the postulated soot formation mechanism of Frenklach et al., as a framework for relating flow reactor derived oxidation and pyrolysis mechanisms to soot related, fuel and intermediates decomposition processes. In order to logically develop the relationship, the set of Princeton experiments will first be described, the results obtained from them succinctly stated and then the proposed chemical relationships discussed.

Experimental

In both the premixed and diffusion flames the effects of temperature and fuel structure on the propensity to soot have been examined by changing the amount of diluent, usually nitrogen. Fuel structure effects were examined by the careful selection of a wide variety of hydrocarbon compounds. However, the two types of flames are very different in the manner in which the fuel and oxidizer come together at the flame front. As a consequence, there are profound effects on the above mentioned relationships between temperature, fuel structure and sooting tendency.

In a premixed flame, fuel, oxidizer and diluent are mixed upstream of the flame front and arrive at the flame front as components of a homogeneous gas. In the Princeton experiments (1), preset quantities of nitrogen and oxygen were mixed with a variable amount of fuel and fed to a Bunsen type tubular burner. The sooting limit was determined by increasing the fuel flow rate while the oxygen and nitrogen flow rate were kept constant. When luminous continuum radiation was detected at the sides of the conical flame, the fuel flow rate was decreased just enough to cause the radiation to disappear. The average fuel flow rate associated with both the appearance and disappearance of luminosity was used to calculate the critical equivalence ratio for the onset of soot. To establish the critical equivalence ratio at another temperature, the same procedure was repeated with a different preset quantity of nitrogen.

A diffusion flame is unlike a premixed flame in that the fuel and oxidizer meet in a reaction zone as a result of molecular and turbulent diffusion. The Princeton diffusion flame studies(2,3) were conducted with a burner in which a central tube delivered fuel into an outer tube containing flowing air. An excess of oxidizer led to the elongated shape characteristic of an overventilated flame. The sooting tendency of a particular fuel was established using this burner by varying the volumetric fuel + diluent flow rate for a given amount of air. When visibly obvious soot particles exited

from an annulus around the top of the flame, the soot height, i.e. the length of the luminous zone measured from the burner lip to the flame apex, was measured. Sooting heights for different fuels with different amounts of added nitrogen or argon diluent were evaluated in order to establish the sooting propensity at different temperatures.

For the chemical mechanism studies, the Princeton flow reactor was used (16). The flow reactor is a tubular, high temperature, turbulent reactor that is designed to permit the examination of oxidation and pyrolysis processes without complications due to the diffusion of heat and mass. Species concentrations with respect to time for a dilute reacting flow are obtained by withdrawing samples with a water cooled probe at discrete, well characterized locations within the tube. Analysis of the chemical content of each sample is performed with either gas chromatography or gas chromatography/mass spectrometry as is needed. Concentrations at the various locations in the reactor are related to the extent of reaction by taking into account the flow velocities within the reactor. Experiments examining the oxidation and pyrolysis of various hydrocarbon fuels have all been conducted at one atmosphere pressure and in a 900 to 1200K temperature range. The temperature range of the flow reactor, though lower than the range of hydrocarbon adiabatic flame temperatures, is nevertheless quite relevant to the chemistry of soot formation processes. The 900-1200K range corresponds both to the temperature in a flame where the initial fuel decomposition occurs and also the temperature of the zone of a flame where soot particles are first observed (17).

Results

For premixed flames, the sooting tendency (as a function of the adiabatic premixed flame temperature) for a wide variety of hydrocarbons is shown in Figure 1 (1). The critical effective equivalence ratio, i.e. the ratio of the stoichiometric oxygen necessary to convert all the fuel to CO and H₂O to the experimental amount, is used as a measure of the sooting tendency in the premixed flame. The larger is the critical equivalence ratio, the smaller is the tendency of fuel to soot. Therefore, from Figure 1 it can be seen that ethane at all temperatures has a much smaller tendency to soot than does methylnaphthalene. The single, most obvious trend in Figure 1 is that for all fuels, the sooting tendency decreases as the flame temperature is increased. Furthermore, the change in sooting tendency with temperature is roughly the same for all fuels regardless of fuel type. Consequently, a vertical slice through Figure 1 at any one temperature should permit an ordering of sooting tendencies that is representative of those at all temperatures.

Such an ordering is presented in Figure 2 for a flame temperature of 2200K (1). The abscissa, "number of C-C bonds", represents the total number of carbon to carbon bonds in the parent fuel molecule when each single carbon-carbon bond is considered to contribute one, each double bond contributes two and each triple bond contributes three to the total number of bonds. The predictive correlation of Figure 2, which is independent of a detailed knowledge of isomeric structures, conjugation and even aromaticity, implies that fuel structure is an inconsequential factor in soot formation in premixed flames. The results of these premixed flame experiments along with those that have examined the post-flame region as a function of initial fuel type (18), suggests that soot formation occurs in the post flame region from a universal soot precursor whose concentration but not nature is affected by the structure of the initial fuel.

The results of a diffusion flame study of the sooting tendency of hydrocarbons as a function of temperature is shown in Figure 3 (19). The

sooting tendency is measured by the inverse of the volumetric flow rate at the smoke height. The smaller the inverse flow rate the smaller the tendency to soot. The sooting tendency of different classes of species varies widely from class to class but is relatively constant within a class. For example, aromatic compounds such as benzene, ethylbenzene and methylnaphthalene soot much easier than do the small alkenes such as propene, butene and even cyclohexene. The classes of compounds also have very different sooting temperature dependencies as revealed by the slopes of each line in Figure 3. However, in contrast to the behavior of hydrocarbon fuels in premixed flames, fuels show an increasing sooting tendency with increasing flame temperature.

A structure independent correlation of the type available for premixed flames cannot be developed from the diffusion flame results. It appears that initial fuel morphology does play an important part in the tendency of a fuel to soot as is evidenced in Figure 3 by the groupings of sooting tendency according to class of hydrocarbon. Since hydrocarbon fuels will pyrolytically decompose at the temperatures present in the oxygen-free fuel stream a distance far from the flame front, the conclusion can be drawn that the effect of initial fuel structure on sooting tendency is manifested through pyrolysis processes.

Flow reactor studies of hydrocarbon fuels, unfortunately, cannot be so concisely summarized in three plots as were the flame results. Generally, each oxidation study is conducted at rich, stoichiometric and lean equivalence ratios at one or more temperatures. From the many species concentration profiles with respect to time that are obtained, mechanistic information is deduced. The mechanism of the high temperature oxidation of benzene/phenyl radical that was developed from a series of such flow reactor oxidation studies is displayed in Figure 4 (16). This mechanism, as well as the one for butadiene that follows, were chosen for display from among the many that have been obtained from flow reactor studies because of their particular relevance to important elements of the soot formation process.

The mechanism of Figure 4 indicates that benzene is oxidized in a step by step process involving C_6 , C_5 and C_4 stable radicals. At the temperature of the oxidation studies, 1000-1200K, oxidative attack was the predominant mode of decomposition, since purely pyrolytic processes are too slow. The benzene oxidation sequence as outlined ends with the ring opening formation of either butadiene or the butadienyl radical. The oxidation characteristics of butadiene have been the object of another, different set of flow reactor studies (11). These studies have resulted in the development of a mechanism that extends the benzene mechanism just presented. This butadiene/butadienyl oxidation mechanism is given in Figure 5.

Discussion

Before discussing the relationship between flame and flow reactor experimental results, the assumption must be made that the diffusion of species in flames affects the rates of reactions but not the basic pathways of a chemical mechanism that would occur in a reduced diffusion, flow reactor environment. Some preliminary, direct comparisons of flame species obtained from the probe sampling of a diffusion flame and flow reactor pyrolysis experiments appear to support this conclusion (20). Presumably, diffusion of species would also leave the basic mechanisms of oxidation and pyrolysis in premixed flame essentially unaffected.

Therefore, premixed sooting flames can be conceptually viewed as flames in which the fuel rapidly breaks down in an oxidizing environment to acetylene; the acetylene passes through the flame front, and then reacts to form soot. If the initial fuel is benzene, it is oxidized in the homogeneous

pre-flame region to mostly CO, H₂O and a small amount of acetylene. The acetylene that survives the flame front then grows through the Frenklach mechanism (15) back up to phenyl radicals and/or benzene. In some sense, the process is symmetric with respect to the flame front. The benzene oxidation mechanism derived from the flow reactor is applicable both to the rapid pre-flame benzene decomposition processes and the post-flame benzene and/or phenyl radical consumption reactions.

The pre-flame benzene decomposition oxidation reactions, if very rapid, will lead by the step by step mechanism of Figure 4 to a large buildup of acetylene. Since a large concentration of acetylene on the pre-flame side near the flame front would presumably lead to a large acetylene concentration in the post-flame region, these oxidation reactions are soot enhancing.

In contrast, any oxidation reactions in the post-flame region that consume species involved in the Frenklach soot growth mechanism will be soot retarding and perhaps even inhibiting. For example, vinyl acetylene, a key species in the soot formation mechanism, may be attacked by an O atom leading to the formation of allene and CO as indicated in Figure 5. Though the allene, through subsequent reactions may contribute species, such as acetylene, that can enter back into soot formation mechanism they do so at a lower molecular weight level with a consequent delay in the formation of soot. Therefore, the oxidation processes serve to drain species out of the soot formation route.

In a similar way, the formation of phenoxy or phenol from phenyl and/or benzene can occur in the post-flame region because of some O₂ and significant quantities of OH and O that are found there. The phenoxy quickly decomposes to cyclopentadienyl which itself will be oxidized. Thus the post-flame benzene consuming reactions interfere with the further growth of large molecules by removing or delaying the concentration growth of an essential soot building block, the phenyl radical. These reactions are therefore soot inhibiting.

Paradoxically, it appears that oxidative attack on some soot formation intermediates could actually contribute to soot formation. For example, butadienyl radical is postulated to be a key species in the route leading to the first aromatic ring. The butadienyl radical can decompose to vinyl acetylene as indicated in Figure 5 through reaction with O₂ or collision with a third body designated as M. The decomposition reaction with O₂, when the concentration of O₂ is high enough, may even be faster than the unimolecular decomposition. Since it is known from sampling in flames (21) that a considerable fraction of the initial O₂ persists into the post-flame region, the accelerative effect of O₂ on the rate of soot formation may be significant.

The benzene oxidation mechanism of Figure 4, when developed into a detailed mechanism of the type now available for smaller hydrocarbons and coupled with an advanced flame model, can potentially yield an analytic prediction of the amount of acetylene that is formed in the pre-flame region and which then survives into the post-flame zone.

In diffusion flames, soot formation can be viewed conceptually to be the result of fuel pyrolysis reactions occurring in the relatively oxygen free pre-flame, fuel stream. Consequently, the soot formation mechanism of Frenklach et al., which is, in fact, a pyrolysis mechanism, would be most appropriate for the fuel stream reactions of diffusion flames. However, in contrast to the situation for premixed flames, there is no experimental indication that hydrocarbon fuels must break down to acetylene before building back up to larger molecules. Pyrolysis reactions in the fuel stream that produce directly any of the larger members of the soot formation route would contribute to an increased sooting tendency. An indication of the routes

through which fuel decomposition might feed large species into the soot formation route could come from flow reactor pyrolysis experiments augmented by higher temperature mechanistic information available in the literature.

An obvious example of such a case is the pyrolysis chemistry of benzene. Flow reactor pyrolysis experiments have indicated that though it is difficult to decompose benzene thermally, when the molecules do break apart they form vinyl acetylene, butadiene and acetylene (22). Higher temperature experiments performed in a very low pressure pyrolysis apparatus (23) revealed the formation of these same intermediates as well as others. High temperature shock tube pyrolysis experiments corroborate both of these experimental findings and emphasize the importance of phenyl radical formation (24). Clearly, benzene fuel in a diffusion flame not only will decompose pyrolytically to the starting material in the soot formation mechanism, acetylene, but also provides some of the essential vinyl acetylene and phenyl radical building blocks necessary for the formation of the polycyclic aromatics. In view of the intermediates known to be formed during benzene pyrolysis, it is not surprising that the data of Figure 3 indicate that benzene soots very easily.

However, it is not necessary that the hydrocarbon pyrolysis processes form the exact C_2 , C_4 and C_6 species that appear in the soot formation mechanism. Sometimes, it is sufficient for the pyrolytic decomposition simply to produce stable intermediates which themselves appear to easily form the appropriate species. An interesting demonstration of this point results from a flow reactor examination of the major pyrolysis intermediates of iso-octane and n-octane (25). Though both fuels pyrolytic decomposed rather quickly, each one produced a different major intermediate. The pyrolysis of iso-octane was found to yield primarily iso-butene and some propene. The corresponding pyrolysis of n-octane yielded mostly ethylene and also some propene. The diffusion flame data of Figure 3 indicates that iso-octane has a significantly greater tendency to soot than does n-octane. In fact, the sooting tendency of iso-octane is close in magnitude to that of its primary pyrolysis intermediate, iso-butene. In contrast, the sooting tendency of n-octane approaches the reduced value of ethylene, its major pyrolysis intermediate. The comparison between the sooting tendency of the two isomeric octanes, and their pyrolysis intermediates is another example of the importance of initial fuel structure to sooting in a diffusion flame.

Experimental results on the addition of small amounts of oxygen to the fuel side of various sooting diffusion flames have yielded some interesting insights into the relationships between sooting tendency and chemical mechanism. The oxygen effect was found to be exceptionally strong in ethene, less so in propene, and negligible for the alkane fuels (26,27,28,29,30,31). It would appear that the normal radical pool formed during thermal pyrolysis of most fuels in diffusion flames is so large that the additional radical reactions due to the presence of small amounts of oxygen lead to no overall gain in the extent of the radical pool which governs the overall pyrolysis rate. This pyrolysis condition is true for all aliphatic hydrocarbons except ethene, and to some extent propene. For ethene, oxygen increases the radical pool extensively. Consideration of the bond strengths in ethene and propene would lead one to perhaps expect the trend postulated. Verification was shown (31) by computations in which a comprehensive chemical kinetic mechanism for the oxidation of butane (14), developed in part with flow reactor data, was adapted to apply to the pyrolysis of ethene, propene and acetylene. Although there are no experimental data for oxygen effects on accelerating the sooting of acetylene, from bond strength considerations one would expect a strong

effect and the flow reactor based computations do show substantial increase in the radical pool with oxygen addition. Similarly one would expect the same for benzene. Although no computations for benzene were performed, experimental results (29) show that oxygen accelerates the sooting of benzene.

There is, of course, a temperature effect when considering the role of oxygen in accelerating pyrolysis of fuels. The higher the temperature, the less is the accelerative effect (32,33). Most fuels show increased pyrolysis rates with oxygen addition at lower temperature (32,33). The comparisons made in the previous paragraph were for high temperatures (~100-1300 K). In laminar diffusion flames the temperature time history of a pyrolyzing fuel element is short compared to low temperature flow and static reactors. Since it has been established that the onset of soot formation in a diffusion flame coincides with the points on the temperature profiles corresponding to about 1300 K (17,34), it is very apparent that the high temperature comparisons are the ones of importance. This temperature sensitivity can lead one to conclude that the initiation step is accelerated in addition to increasing the radical pool. The computations (31) appear to confirm this statement. The general pyrolysis mechanism does not seem to change otherwise. Flow reactor experimental results confirm that there is no appreciable, if any, accelerative effect of oxygen on the pyrolysis of propane, propene or butane (33) at high temperatures and an appreciable effect on ethene (35).

Summary

The relationships between flame studies of the sooting tendencies of various hydrocarbon fuels and chemical mechanisms derived from flow reactor experiments have been developed. The mechanisms for the oxidation of benzene and butadiene, in particular, have been related to both sooting premixed and diffusion flames despite the large difference in basic flame structure. A recently developed soot formation mechanism has provided the linking framework between chemical mechanism and observable sooting tendencies. The same framework has permitted the application of flow reactor based chemical models to the prediction and explanation of the effect of oxygen addition on sooting diffusion flames.

Acknowledgements

The authors wish to thank Mr. George Sidebotham and Mr. Harjit Hura of Princeton University for helpful discussions and for providing preliminary experimental data. The support of the Air Force Office of Scientific Research under Contract F49620-82-K-0011 is also greatly appreciated.

References

1. Takahashi, F. and Glassman, I., *Combust. Sci. & Technol.*, 1984, Vol. 37, pp. 1-19.
2. Glassman, I. and Yaccarino, P., *The Combust. Inst.*, 18th Symp. (Int'l.) on Combustion, 1981, pp. 1175-1183.
3. Gomez, A., Sidebotham, G. and Glassman, I., *Comb. and Flame* 58, 45-57 (1984).
4. Venkat, C., Brezinsky, K., and Glassman, I., *Int. Symp. Combust.* 19, 143 (1982).
5. Brezinsky, K., Litzinger, T.A. and Glassman, I., *Int. J. Chem. Kinet.* 16, 1053 (1984).
6. Litzinger, T.A., Brezinsky, K. and Glassman, I., *Comb. and Flame* 63, 251 (1986).
7. Litzinger, T.A., Brezinsky, K. and Glassman, I., *J. of Phys. Chem.*, 1986, 90, 508.
8. Litzinger, T.A., Brezinsky, K. and Glassman, I., *Combust. Sci. & Technol.*, 1986, Vol. 50, pp. 117-133.

9. Brezinsky, K., Litzinger, T.A. and Glassman, I., 21st Symp. (Int'l.) on Combustion, 1986.
10. Litzinger, T.A., Brezinsky, K. and Glassman, I., Eastern States Section/Combust. Inst. Paper #68, 1985.
11. Brezinsky, K., Burke, E.J. and Glassman, I., Int. Symp. Combust. 20, 613 (1985).
12. Westbrook, C.K., Dryer, F.L. and Schug, K.P., 19th Symp. (Int'l.) on Combustion, 1982, pp. 153-166.
13. Hautman, D.J., Schug, K.P., Dryer, F.L. and Glassman, I., Combust. Sci. & Technol. 25, 219 (1981).
14. Pitz, W.J., Westbrook, C.K., Proscia, W.M. and Dryer, F.L., Int. Symp. Combust. 20, 831 (1985).
15. Frenklach, M., Clary, D.W., Gardiner, W.C., Jr. and Stein, S.E., 20th Symp. (Int'l.) on Combustion, 1984, pp. 887-901.
16. Brezinsky, K., Prog. Energy Combust. Sci., 1986, Vol. 12, pp. 1-24.
17. Kent, J. and Wagner, H. Gg., Int. Symp. Combust., 20th, p. 1007.
18. Harris, S.J. and Weiner, A.M., Combust. Sci. & Technol., 1984, Vol. 38, pp. 75-87.
19. Glassman, I., COMBUSTION, Academic Press, 1987.
20. Sidebotham, G. and Hura, H., Princeton University, unpublished data.
21. Bittner, J.D. and Howard, J.B., Int. Symp. Combust. 18, 1105 (1981).
22. Weckman, E., Princeton University, unpublished data.
23. Smith, R.D. and Johnson, A.L., Comb. and Flame 51: 1-22 (1983).
24. Kiefer, J.H., Mizerka, L.J., Patel, M.R. and Wei, H.-C., J. Phys. Chem. 1985, 89, 2013-2019.
25. Brezinsky, K. and Dryer, F.L., Central States/Western Section/Combustion Institute, WSSCI Paper # 3-5A, 1985.
26. Chakeraborty, B.B. and Long, R., Comb. and Flame 12, 469 (1968).
27. Deardon, P. and Long, R., J. Appl. Chem. 18, 243 (1968).
28. Jones, J.M. and Rosenfeld, J.L.J. Comb. and Flame 19, 427 (1972).
29. Wright, F.J., Fuel 53, 232 (1974).
30. Schug, P., Manheimer-Timmat, Y., Yaccarino, P. and Glassman, I., Comb. Sci. and Tech. 22, 235 (1980).
31. Hura, H. and Glassman, I., Comb. Sci. and Tech. 53, 1(1987).
32. Walker, P.W., Reaction Kinetics (Spec. Periodical Rep., Chem. Soc. London) 1, 172 (1975).
33. Murphy, S.L., Brezinsky, K. and Glassman, I., Eastern States Section/The Combustion Institute Meeting, Paper No. 10 (1982). See also Murphy, S.L., Princeton University M.S.E. Thesis, 1982.
34. Gomez, A. and Glassman, I., 21st Symp. (Int'l.) on Combustion (1986).
35. Hura, H., Princeton University, private communication (1987).

Acetylene Soot Formation Mechanism

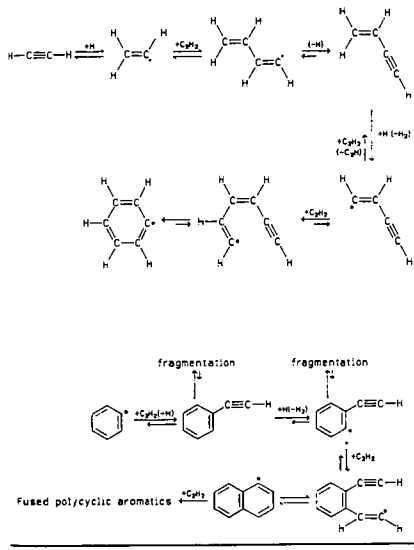


Table 1

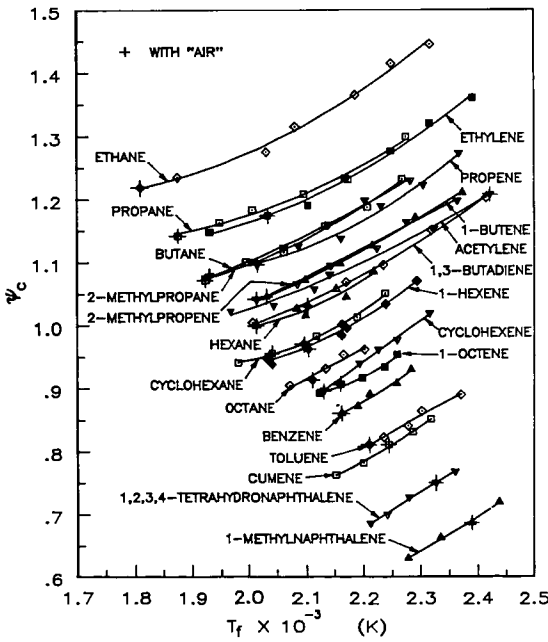


Figure 1. The critical effective equivalence ratio at sooting as a function of adiabatic flame temperature (from ref. 1)

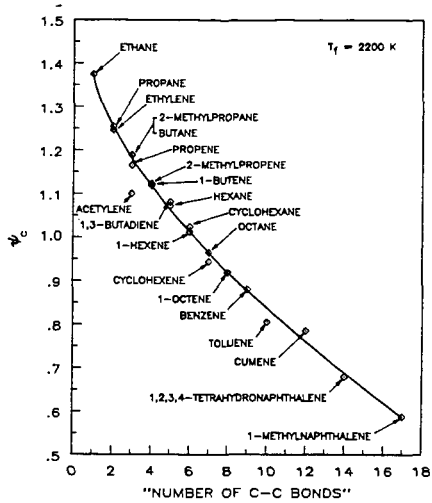


Figure 2. The correlation between the critical equivalence ratio at sooting and the number of C-C bonds (from ref. 1).

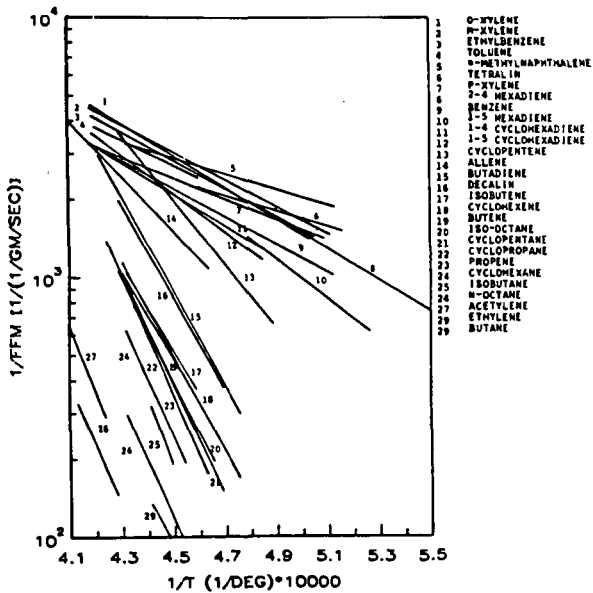


Figure 3. The sooting tendency of some hydrocarbon fuels as a function of the reciprocal of the calculated adiabatic flame temperature (from ref. 19).

**The Formation of Soot and Polynuclear Aromatic Compounds in the
Low-Temperature Pyrolysis of Alkynes**

by

Julian Heicklen

Department of Chemistry and Environmental Resources Research Institute,
The Pennsylvania State University, University Park, PA 16802

Abstract

The pyrolysis of vinylacetylene ($\text{CH}_2=\text{CH}-\text{C}\equiv\text{CH}$), 2-methylbut-1-ene-3-yne ($\text{CH}_2=\text{C}(\text{CH}_3)-\text{C}\equiv\text{CH}$), acetylene-vinylacetylene mixtures and acetylene-styrene mixtures at 300-550°C produced polymer and adducts (or dimers) in parallel independent homogeneous second-order reactions. At the temperatures of the studies, the polymerization reaction dominates, but because the Arrhenius parameters are smaller for the polymerization process, it should become relatively less important above $\approx 850\text{K}$. The respective Arrhenius A factors are about $10^{6.5}$ and $10^{8.0} \text{ M}^{-1} \text{ sec}^{-1}$ for polymerization and adduct formation (or dimerization) and the respective activation energies are about 90 and 125 kJ/mole.

The adducts (or dimers) are cyclic compounds some of which are aromatic. With continued heating they can lose hydrogen and condense to higher polynuclear aromatic compounds. The polymer chars on heating, presumably because of hydrogen evolution. The second-order removal processes dominate over unimolecular decomposition at the temperatures studied and can remain significant for temperatures in excess of 1200K. Both second-order processes should be important in soot formation.

Early Work

Soot and the aromatic compounds are well-known products of the low-temperature pyrolysis of hydrocarbons. They include polynuclear aromatic compounds, some of which are carcinogenic.

The pyrolysis of C_2H_2 has been studied for over 50 years, an early work being done by Pease (1929) who reported only polymerization at 400-600°C. Munson and Anderson (1963) studied the reaction in a flow reactor between 500 and 850°C. Apparently they were the first to show that the exclusive initial product is vinylacetylene. In a companion study, Hou and Anderson (1963) found that no free radicals were formed at temperatures up to 700°C in the pyrolysis of acetylene, vinylacetylene or diacetylene.

Cullis and Franklin (1964) studied the pyrolysis of C_2H_2 from 500-1000°C and confirmed that the sole initial product was vinylacetylene. The diacetylene seen comes from the heterogeneous decay of the vinylacetylene. They found the reaction to be second order in C_2H_2 , and to be unaffected by the presence of other hydrocarbons. By comparing their results with earlier work, they concluded that a single mechanism prevails for the pyrolysis of C_2H_2 from 350-2500°C. The reaction is second order with $\log(k, M^{-1} s^{-1}) = 10.8 - 41,600/\theta$ where $\theta = 4.575 T$ (Cullis and Read, 1970). Palmer and Cullis (1965) have pointed out that vinylacetylene is the sole initial product at temperatures at least up to 1300°C. Subsequent work by Ogura (1977) of the shock decomposition of C_2H_2 gave $\log(k, M^{-1} sec^{-1}) = 11.39 + 0.26 - (46,000 + 1400/\theta)$ from 1000-1670K.

Extended pyrolysis of C_2H_2 does produce many other products. Stehling et al (1962) studied the reaction at 600-900°C and found benzene as the main product at 600°C with some vinylacetylene and styrene present. At 700°C, indene, naphthalene, and other unidentified products were seen. Above 800°C, H_2 and C_2H_4 became important, though they were seen along with CH_4 for very extended conversions at 600°C. The aromatic compounds are produced at temperatures up to 800°C, at which temperature they start dehydrogenating. The vinylacetylene reached a maximum concentration at 600-650°C. The aromatic compounds formed must come from reactions of vinylacetylene, either by itself or with C_2H_2 .

The first study on vinylacetylene pyrolysis was done by Ikegami (1963). He studied the reaction at 300-400°C and found two processes, a rapid polymerization and a slow decomposition to produce mainly H_2 , C_2H_4 , C_2H_6 , CH_4 , and small amounts of C_2H_2 . The rate was second order in C_4H_4 with a rate coefficient of $1.85 \times 10^8 \exp(-25,300/1.987T) M^{-1} s^{-1}$.

The pyrolysis of vinylacetylene was also studied by Cullis et al (1967) and Cullis and Read (1970). They studied the reaction between 300 and 620°C and found it to be quite different below and above 500°C. Below 500°C only polymerization occurred in a second order reaction with an activation energy of 28 kcal/mole. These results agree with those of Ikegami (1963). Above 500°C it was found that polymerization was accompanied by large amounts of low molecular weight products, mainly H_2 and C_2H_2 , though CH_4 , C_2H_4 , and soot were also formed. Diacetylene and methylacetylene were not produced under any conditions.

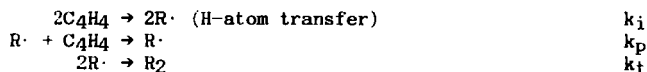
Cullis and Read (1970) found that the addition of C_2H_2 to vinylacetylene had no effect on the vinylacetylene pyrolysis at $478^\circ C$, even for an acetylene concentration twice that of vinylacetylene. On the other hand, Yampol'skii et al (1968) found that at $800-950^\circ C$, vinylacetylene removal was slower in a mixture of 0.5% vinylacetylene and 99.5% C_2H_2 than in a mixture of 0.5% vinylacetylene and 99.5% Xe, and they reported the respective rates in terms of first order removal coefficients. Furthermore in the presence of C_2H_2 , though the vinylacetylene removal rate was reduced, benzene was produced.

Polymer Formation

The pyrolyses of several alkyne systems have been studied in our laboratory from $300-550^\circ C$. The dominant product in all cases is a yellow polymer which settles on the wall of the reaction vessel. This polymer is stable at $\approx 300^\circ C$, but slowly becomes black over a period of weeks at higher temperatures. Presumably hydrogen is being evolved from the polymer and it becomes soot.

The systems studied include pure vinylacetylene ($CH_2=CH-C\equiv CH$), pure 2-methylbut-1-ene-3-yne ($CH_2=C(CH_3)-C\equiv CH$), vinylacetylene-acetylene (C_2H_2) mixtures and acetylene-styrene ($C_6H_5CH=CH_2$) mixtures. In all cases the rate of disappearance of reactants was homogeneous, second order, and unaffected by the addition of excess N_2 or He. For the pure C_4H_4 and C_5H_6 systems the reaction was second order in the reactant, whereas for the mixed systems, the removal rate for C_2H_2 or C_8H_8 was first order in each reactant. The rate coefficients and temperature ranges used are summarized in Table 1.

Presumably the polymerization occurs through a free-radical addition mechanism. For the pure C_4H_4 system the basic mechanism would be:

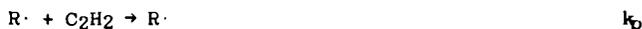


which leads to the rate law

$$-d[C_4H_4]/dt = (2k_i + k_p(k_i/k_t)^{1/2})[C_4H_4]^2$$

The mechanism and rate law for the C_5H_6 system is analogous. Since $2k_i$ is small compared to $k_p(k_i/k_t)^{1/2}$, the overall Arrhenius A factor for the reaction is given by $A_p(A_i/A_t)^{1/2}$. The expected values for A_i and A_p are $\approx 10^8 M^{-1} \text{sec}^{-1}$ since these are typical second-order reactions. Radical-radical termination reactions occur near collision frequency, and since $R\cdot$ is a large radical, we expect $A_t \approx 10^{11} M^{-1} \text{sec}^{-1}$. Thus the overall A factor should be $10^8 \times (10^8/10^{11})^{1/2} = 106.5 M^{-1} \text{sec}^{-1}$ in agreement with the observation of Lundgard and Heicklen (1984) for C_4H_4 and Chanmugathas and Heicklen (1985) for C_5H_6 . The overall activation energy is $E_p + E_i/2$ since $E_t \approx 0$ and is about 90 kJ/mole.

For the $C_2H_2-C_4H_4$ system the initiation and termination steps are the same as for pure C_4H_4 , since C_2H_2 self polymerization was negligibly slow under the conditions of the study. However an additional propagation step is needed:



so that

$$-d[C_2H_2]/dt = k_p(k_i/k_t)^{1/2}[C_2H_2][C_4H_4]$$

in agreement with the observations. The values for the overall Arrhenius A factor and activation energy should be similar to those for the one-compound polymerizations, as indeed they are.

The C₂H₂-C₈H₈ polymerization is considerably more complex and not completely understood. The polymerization of either compound alone was negligibly slow under the conditions studied, yet copious amounts of polymer were produced in the mixed system. A tentative mechanism has been suggested (Chanmugathas and Heicklen, 1987) in which initiation occurs by the interaction of 2C₈H₈ molecules:



The R₁· radical presumably does not add readily to styrene, but does add readily to C₂H₂



where the distinction between R₁· and R₂· radicals is that the former has a styrene end group, whereas the latter has an acetylene end group. The R₁· radicals can also terminate:



The R₂· radicals add preferentially to C₂H₂ to regenerate R₂· type radicals, but occasionally they generate a different radical, R₃·, which adds preferentially to styrene to give an R₁· type radical:



This mechanism leads to the rate laws

$$-d[C_8H_8]/dt = 2k_1[C_8H_8]^2 + k_2(k_1/k_3)^{1/2} [C_2H_2][C_8H_8]$$

$$-d[C_2H_2]/dt = k_2(k_1/k_3)^{1/2} [(k_4 + k_{4b})/k_{4b}] [C_2H_2][C_8H_8]$$

If $2k_1 \ll k_2(k_1/k_3)^{1/2}$, then C₈H₈ removal is first-order in both reactants and the rate coefficient parameters should be similar to those for the other systems in agreement with the observations. The C₂H₂ removal rate is first-order in both reactants but is much larger than that for C₈H₈ by the factor $(k_4 + k_{4b})/k_{4b}$.

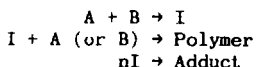
Many addition polymers have a ceiling temperature at which their rate of depolymerization equals their rate of polymerization, and the polymer is not produced at higher temperatures. Usually this occurs because the polymerization process produces C-C single bonds which are the weakest bonds in the polymer and are ruptured on heating. This does not appear to

be the case with polymers produced from acetylenes. C-C single bonds are formed but they are sandwiched between C=C double bonds giving rise to a conjugation effect. Thus the C-C single bond energies are strengthened to >400 kJ/mole while the tertiary vinylic C-H bonds are weakened to ≈335 kJ/mole. Therefore instead of depolymerization at high temperature, C-H bond scission occurs and hydrogen is released leaving behind a char (or soot). Thus the polymerization followed by charring could be an important soot-producing process in the low-temperature pyrolysis of hydrocarbons.

It is interesting to see at what temperatures the polymerization process is important. This can be computed precisely for C₄H₄ since its first-order decomposition rate has been measured recently by Hidaka et al (1986) to be $6.1 \times 10^{13} \exp(-335 \text{ kJ/mole-RT}) \text{ sec}^{-1}$. With this expression and the Arrhenius parameters obtained by Lundgard and Hecklen (1984) for total C₄H₄ removal at low temperatures where polymerization predominates, we can obtain $[\text{C}_4\text{H}_4]^{1/2}$, the concentration of C₄H₄ where equal amounts of it disappear by unimolecular decomposition and polymerization. The curve marked polymerization in Fig. 1 shows a plot of $\log([\text{C}_4\text{H}_4]^{1/2})$ vs. temperature. From this curve it can be seen that the polymerization dominates over decomposition at 1000K for C₄H₄ pressures in excess of 0.1 Torr or at 1200K for C₄H₄ pressures in excess of 20 Torr. Soot formation through polymerization is important at temperatures up to at least 1200K and may be significant at temperatures up to 1400K.

Adduct Formation

Adduct formation occurs along with polymerization. Thus in the single reactant systems dimers are produced along with polymer, but no trimers or tetramers were seen. In the mixed systems adducts of the two reactants were observed. Both polymerization and adduct formation (dimerization) are initial processes as determined by examining time histories of the curves of growth. Furthermore they are completely independent of each other and do not proceed through a common intermediate. This conclusion comes from the rate laws by the following argument. Let us assume that the two processes have some common intermediate I. Then the general mechanism would be



where A and B are the two reactants. This general mechanism requires that the rate law for polymer formation be of higher order than for adduct formation, contrary to observation. Therefore the two processes cannot have a common intermediate. The adduct formation occurs by a concerted or diradical process. Presumably the polymerization occurs via a mono radical chain mechanism.

In our laboratory, acetylene and vinylacetylene mixtures were pyrolyzed at 400-500°C in the absence and presence of O₂ or NO (Chanmugathas and Hecklen, 1986). The major product of the interaction between C₂H₂ and C₄H₄ was polymer, but benzene was also produced. Both the C₂H₂ removal and C₆H₆ formation rates were first-order in C₂H₂ and C₄H₄. The rate coefficient parameters are listed in Tables 1 and 2, respectively. Benzene formation occurred by two processes: a concerted molecular mechanism (≈60%) and a singlet diradical mechanism (≈40%).

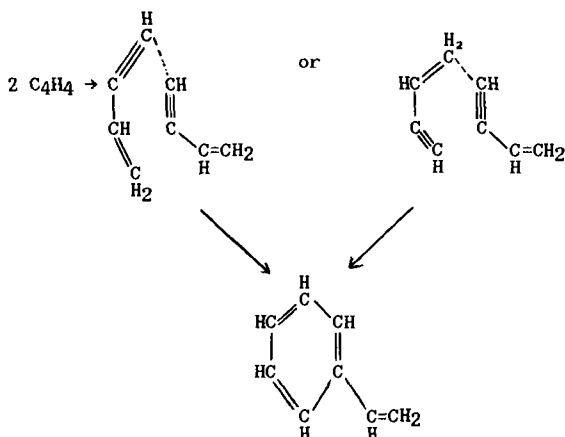
In order to investigate the low temperature (below 500°C) pyrolysis of vinylacetylene as an avenue for polynuclear aromatic hydrocarbon formation, it is essential to look at the formation of higher molecular weight products. Due to experimental limitations, however, the two early studies (Ikegami, 1963; and Cullis and Read, 1970) in this temperature range were only able to monitor lower molecular weight products such as H₂, CH₄, C₂H₂, C₂H₄, C₂H₆, C₃H₆ and in one case benzene. Also, kinetic data were limited to vinylacetylene removal rates as a function of temperature.

Therefore, a study was undertaken in our laboratory in order to obtain more detailed kinetic information about the low-temperature pyrolysis of vinylacetylene, paying particular attention to higher molecular weight products formed during the early stages of reaction. Thus we have examined the pyrolysis of vinylacetylene at 300-450°C (Lundgard and Heicklen, 1984). Vinylacetylene removal was found to be second-order with rate coefficients similar to those reported by Ikegami (1963) and Cullis and Read (1970). In agreement with the earlier work, we found no effect of added gases (N₂, He in our case) and that the main product was polymer which coated the reaction vessel walls. However, in addition we found that 20% of the vinylacetylene was converted to styrene, a dimer of vinylacetylene. This provided the first direct evidence of how aromatics are produced from the pyrolysis of smaller hydrocarbons.

The reaction for vinylacetylene removal and C₈H₈ formation is homogeneous, second-order in reactant, and independent of the presence of a large excess of N₂ or He. However C₈H₈ formation is about half-suppressed by the addition of the free radical scavengers NO or O₂. The major reaction for C₄H₄ removal is polymerization. In addition four C₈H₈ isomers, carbon, and small hydrocarbons are formed. The three major C₈H₈ isomers are styrene, cyclooctatetraene (COT), and 1,5-dihydropentalene (DHP).

The C₈H₈ compounds are formed by both molecular and free radical processes in a second-order process with an overall $k \approx 3 \times 10^8 \exp(-122 \text{ kJ/mole RT}) \text{ M}^{-1}\text{-sec}$ (average of packed and unpacked cell results). The molecular process occurs with an overall $k = 8.5 \times 10^7 \exp(-188 \text{ kJ/mole RT}) \text{ M}^{-1}\text{-sec}$. The COT, DHP, and an unidentified isomer (d), are formed exclusively in molecular processes with respective rate coefficients of $4.4 \times 10^4 \exp(-77 \text{ kJ/mole RT})$, $1.7 \times 10^5 \exp(-89 \text{ kJ/mole RT})$, and $3.1 \times 10^9 \exp(-148 \text{ kJ/mole RT}) \text{ M}^{-1}\text{-sec}$. The styrene is formed both by a direct free-radical process and by isomerization of COT.

Lundgard and Heicklen (1984) pointed out that the mechanism for styrene formation could involve a modified Diels-Alder reaction with either of two intermediates:



With either of the transition states it is necessary to transfer a hydrogen atom before ring closure.

In order to distinguish which intermediate is involved in styrene formation a study was made of the pyrolysis of 2-methylbut-1-ene-3-yne: $\text{CH}_2=\text{C}(\text{CH}_3)-\text{C}\equiv\text{CH}$ (hereafter referred to as C_5H_6). For this molecule the two intermediates will give different products. The head-to-head addition will give a meta-substituted product, while the head-to-tail addition will give a para-substituted product.

The pyrolysis of 2-methylbut-1-ene-3-yne (C_5H_6) has been studied from 375–450°C in a quartz reaction vessel in the absence and presence of O_2 or NO (Chanmugathas and Heicklen, 1985). From 375–425°C, the rates of disappearance of reactant and of formation of dimers are second order in C_5H_6 . The major product is polymer, with the dimers accounting for about 3% of the C_5H_6 consumed. In addition toluene and p-xylene are produced, their production coming, at least in part, from decomposition of the C_5H_6 dimers ($\text{C}_{10}\text{H}_{12}$). Also trace amounts of CH_4 , C_2H_4 , C_2H_6 , and C_3H_6 are formed. The rate coefficient parameters for C_5H_6 removal and $\text{C}_{10}\text{H}_{12}$ formation in the absence of O_2 or NO are listed in Tables 1 and 2, respectively.

The reaction mechanism for dimer formation is analogous to that in vinylacetylene (C_4H_4) pyrolysis (Lundgard and Heicklen, 1984), except that in the C_4H_4 system cyclooctatetraene is seen as an unstable product that isomerizes to styrene, whereas in the C_5H_6 system, the dimethylcyclooctatetraene apparently is too unstable to be detected. The dimers detected were 2,6-dimethylstyrene (P4), p-isopropenyltoluene (P5), and 2 other unidentified dimers (P3) with nearly identical gas chromatographic retention times. From the effect of the radical scavengers and by comparison of the C_4H_4 and C_5H_6 systems, the following mechanistic characteristics were determined:

- 1) The direct formation of styrene in the C_4H_4 system comes from a

head-to-head "modified Diels-Alder" 6-member cycloaddition which proceeds through a diradical intermediate.

2) There is no conclusive evidence for a direct head-to-tail "modified Diels-Alder" 6-member cycloaddition. However, if it does occur, it does not involve diradicals, but must be concerted. Presumably this is how the unquenchable C_6H_6 is formed in the $C_2H_2-C_4H_4$ reaction.

3) Cyclooctatetraene is formed in concerted, non-free radical mechanisms which may proceed both by head-to-head and head-to-tail 8-member cycloadditions. For the C_5H_6 system, the head-to-head adduct isomerizes to P3, whereas the head-to-tail adduct isomerizes to P3, P4, and/or P5. Kinetic data suggest that P3 is not produced from the cyclooctatetraene intermediate, in which case, head-to-head addition would not occur.

It appears that the head-to-head additions are free radical in nature and proceed mainly through a 6-membered ring intermediate, while head-to-tail additions are a concerted molecular process and proceed mainly through an 8-membered ring intermediate.

Chanmugathas and Hecklen (1987) have found that styrene adds to acetylene in a homogeneous second-order reaction with a rate coefficient of $\log(k[C_{10}H_{10}], M^{-1}sec^{-1}) = 8.24 \pm 0.62 - (143 \pm 9)kJ/mole-RT$ from 450-550°C to produce methyl indene and 1,2-dihydronaphthalene as initial products. These products then decay to produce indene and naphthalene, respectively.



1,2 dihydronaphthalene



naphthalene



methylindene



indene

These experiments suggest how larger polynuclear aromatic systems may be produced. Presumably if vinylacetylene were added to styrene, then vinylnaphthalene might be produced, which in turn could add to acetylene to product anthracene and phenanthrene.

In summary we have discovered a new class of reactions: the second-order homogeneous reaction of alkynes to form adducts. There are three pieces of evidence that these reactions are homogeneous. First, all four systems studied give normal homogeneous second-order Arrhenius preexponential factors of $\log(A, M^{-1}sec^{-1}) \approx 8$. Second the addition of a large excess of inert gas (N_2 or He) had no effect on the rate coefficients. Third, for the one system in which packed vessels were used, the rate constants for vinylacetylene dimerization was unaffected by a change in surface-to-volume ratio of 59.

At the temperatures for which these systems were studied, the polymerization process was much more important than adduct formation. However its Arrhenius parameters are smaller than those for adduct formation (see Tables 1 and 2). Thus at higher temperatures the relative importance of adduct formation will become greater. We can use the rate coefficients for adduct formation for C_4H_4 obtained by Lundgard and Hecklen (1984) and for C_4H_4 unimolecular decomposition of $6.1 \times 10^{13} \exp(-335 kJ/mole-RT) sec^{-1}$ obtained by Hidaka et al (1986) to obtain $[C_4H_4]_{1/2}$ when the two processes

for C₄H₄ removal are equal. This C₄H₄ pressure is shown in Fig. 1 as a function of temperature by the curve marked dimerization. The dimerization becomes more important than polymerization at temperatures above 860K. It is equal to unimolecular decomposition at 10 Torr pressure of C₄H₄ at 1250K and can play a significant role at even higher temperatures.

The dimerization or adduct formation forms aromatic compounds which can continue to add acetylenic compounds to form polynuclear aromatic compounds which become more and more graphitic as the number of aromatic rings grow. Thus this may be an important, or even the major, path to soot formation at temperatures of $\geq 1200\text{K}$.

References

- Chanmugathas, C. and J. Hecklen, Intern. J. Chem. Kinetics, **17**, 871 (1985).
- Chanmugathas, C. and J. Hecklen, (1986) Intern. J. Chem. Kinetics, **18**, 701.
- Chanmugathas, C. and J. Hecklen (1987) submitted for publication.
- Cole, J. A., J. D. Bittner, J. P. Longwell, and J. B. Howard (1984) Combustion and Flame, **56**, 51.
- Cullis, C. F. and N. H. Franklin (1964) Proc. Roy. Soc., **A280**, 139.
- Cullis, C. F., I. A. Read, and D. L. Trimm (1967) Intern. Symp. Comb., **11**, 391.
- Cullis, C. F. and I. A. Read (1970) Trans. Faraday Soc., **66**, 920.
- Hidaka, Y., K. Tanaka, and M. Suga (1986) Chem. Phys. Lettr., **130**, 195.
- Hou, K. C. and R. C. Anderson (1963) J. Phys. Chem., **67**, 1579.
- Ikegami, T. (1963) Rev. Phys. Chem. Japan, **33**, 15.
- Lundgard, R. and J. Hecklen (1984) Intern. J. Chem. Kinetics, **16**, 125.
- Munson, M. S. B. and R. C. Anderson (1963) Carbon, **1**, 51.
- Ogura, H. (1977) Bull. Chem. Soc. Japan, **50**, 1044.
- Okabe, H. (1981) J. Chem. Phys., **75**, 2772.
- Okabe, H. (1983) J. Chem. Phys., **78**, 1312.
- Palmer, H. B. and C. F. Cullis (1965) "Chemistry and Physics of Carbon" P. L. Walker, ed., Marcel Dekker, NY, **1**, 265.
- Pease, R. N. (1929) J. Am. Chem. Soc., **51**, 3470.
- Stehling, F. C., J. D. Frazee, and R. C. Anderson (1962) Intern. Symp. Comb., **8**, 774.
- Yampol'skii, Yu. P., V. Maksimov, and K. P. Lavrovskii, J. Phys. Chem. USSR (Engl. trans.) **182**, 940 (1968); Dokl. Akad. Nauk SSSR, **182**, 1344 (1968).

Table 1: Summary of Total Removal Rate Coefficients

Reactant 1	Reactant 2	$\text{Log}(A_1)$ $M^{-1}\text{sec}^{-1}$	$\text{Log}(A_2)$ $M^{-1}\text{sec}^{-1}$	E_1 , kJ/mole	E_2 , kJ/mole	Temp. °C	Reference
C ₄ H ₄	C ₄ H ₄	8.57	-	105	-	300-400	Ikegami (1963)
"	"	9.32	-	117	-	336-475	Cullis and Read (1970)
"	"	6.22	-	79	-	300-450	Lundgard and Heicklen (1984) ^a
"	"	7.10	-	91	-	300-450	Lundgard and Heicklen (1984) ^b
C ₅ H ₆	C ₅ H ₆	6.79	-	80	-	375-450	Chanmugathas and Heicklen (1985)
C ₂ H ₂	C ₄ H ₄	6.26	-	71	-	400-500	Chanmugathas and Heicklen (1986)
C ₂ H ₂	C ₈ H ₈	7.53	6.63	91	99	450-550	Chanmugathas and Heicklen (1987)

a) Unpacked cell.
b) Packed cell.

Table 2: Summary of Adduct Formation Rate Coefficients

Reactant 1	Reactant 2	$\text{Log}(A, M^{-1}\text{sec}^{-1})$	$E, \text{kJ/mole}$	Temp. °C	Reference
C ₄ H ₄	C ₄ H ₄	8.50	122	300-450	Lundgard and Heicklen (1984)
C ₅ H ₆	C ₅ H ₆	7.40	111	375-450	Chanmugathas and Heicklen (1985)
C ₂ H ₂	C ₄ H ₄	8.65	126	400-500	Chanmugathas and Heicklen (1986)
C ₂ H ₂	C ₈ H ₈	8.27	143	450-550	Chanmugathas and Heicklen (1987)

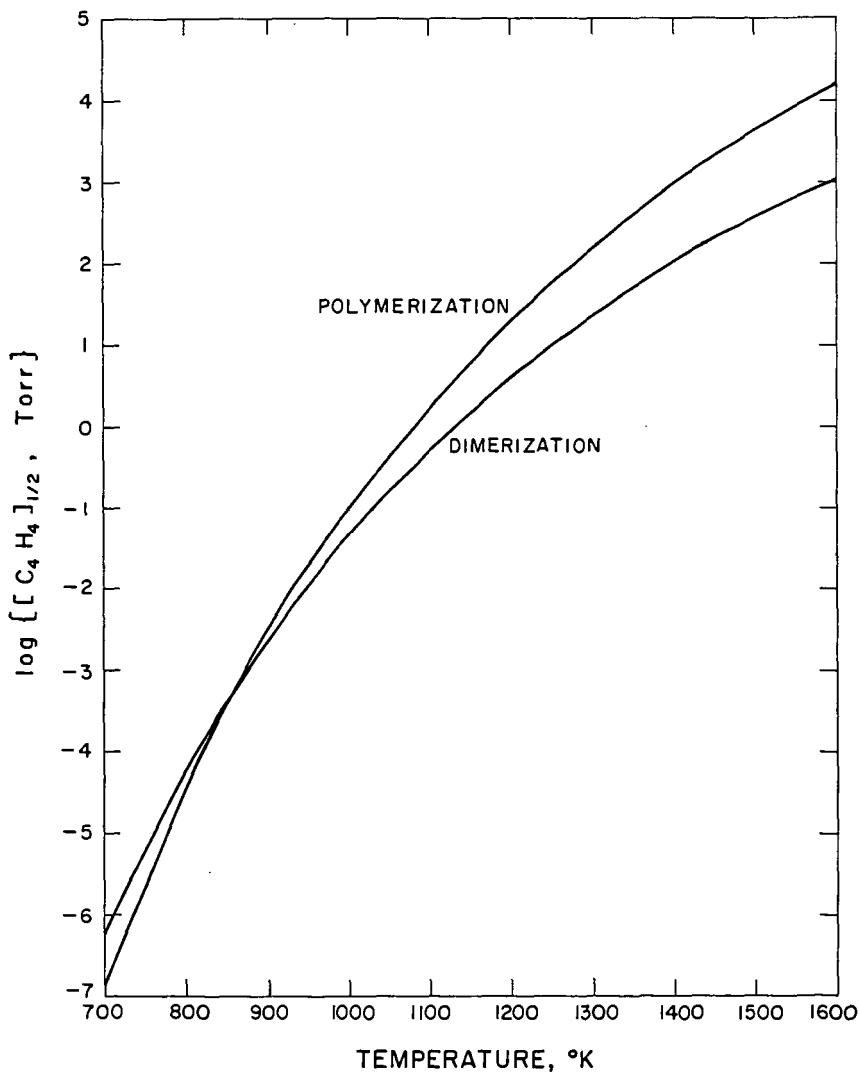


Fig. 1: Plot of the C_4H_4 pressure where unimolecular decay is equal to second-order removal vs. temperature.

Kinetic Mechanism for Pyrolysis
of Acetylene Near 1000K

by M. B. Colket, III

United Technologies Research Center, East Hartford, CT 06108

INTRODUCTION

Recently a mechanism for acetylene pyrolysis was proposed to describe experimental data obtained from a single-pulse shock tube (1) over the temperature range of 1100 to 2000K. The kinetic mechanism is similar to those proposed previously (2,3) and includes mechanisms to describe formation of vinylacetylene, benzene, and phenylacetylene. Subsequently, a subset of this mechanism was modified and used (4) to match decay profiles of acetylene as well as product formation for pyrolysis data obtained in a flow reactor (5) at temperatures of 873 to 1173K.

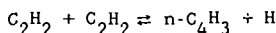
It is the objective of this study: (a) to extend the mechanism (4) to include formation of higher molecular weight species, with a detailed discussion of growth from one to two rings; (b) to discuss the possible role of the 'odd' radical, $i\text{-C}_4\text{H}_3$; (c) to discuss some uncertainties with modeling PAH formation.

Description of Model

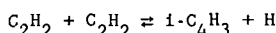
The kinetic model used in this study is listed in Table I and contains 89 reactions and 43 species. CHEMKIN and LSODE were used for integration of the rate equations. For modeling of the flow reactor data, constant temperature and pressure conditions were imposed whereas, for the shock tube data, a shock tube code modified (1) to simulate quenching in a single-pulse shock tube was utilized.

Thermodynamic parameters (except for those of vinyl radicals) are the same as those used and reported previously (1) for the lower molecular weight species. Parameters for species with molecular weights above 100 AMU were obtained from Stein (6) and are believed to be identical to those used in Frenklach, et. al. (3) Reference data for vinyl radicals and heavier species are reported in Table II. Stein's thermodynamic data for vinyl radicals were adopted since his heat of formation (68.4 kcal/mole) is higher than that used by Colket (1) (65.7 kcal/mole) and is closer to some recent determinations. In addition, Stein's reference value for entropy is higher (by 2 eu) than that used by Colket. Fortunately, the differences in values are nearly offset when determining equilibrium constants ($\ln K_{eq} = -(\Delta H - T\Delta S)/RT$) and changes in chemical kinetic modeling results are minimal.

The chemical kinetic model differs from that used previously (4) in that C_2H , C_4H_2 , C_4H , $i\text{-C}_4\text{H}_3$, C_6H_2 , and C_6H and associated reactions were included. In addition, species and reactions related to formation of polycyclic aromatics were also added. Of particular note is a modification in the dominant bimolecular initiation step. Previously the reaction



was used with a rate constant of $\log (k/\text{sec}^{-1}) = 14.54 - 68000/4.58T$. In the present study the reaction

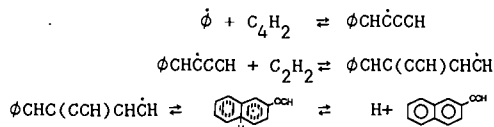


which has a lower endothermicity was employed with a rate of $\log (k/\text{sec}^{-1}) = 14.54 - 60500/4.58T$. This larger rate constant for initiation is required to counterbalance termination steps omitted previously.

Formation of Fused Rings

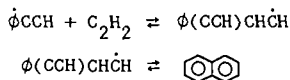
This work was guided substantially by the significant contributions of Bittner, Howard, and Palmer (7) and of Frenklach, et. al (3). An important conclusion of the former work is that ring growth is dominated by addition of aryl radicals to triple bonds, followed by addition of acetylene to the resultant vinylic (aromatic) radical, cyclization, and loss of an H-atom.

i. e.,



Other than reverse processes, the main competitive process which can inhibit ring growth is the thermal decomposition of the vinylic adducts (i. e., loss of H-atoms). Bittner, et. al, reached specific conclusions regarding the importance of the thermal decomposition of the vinylic adduct relative to its addition to acetylene. However, these conclusions may have to be re-examined, since calculations were based on low pressure flame conditions rather than those of a high pressure combustor.

Frenklach, et. al, included at least six separate reaction sequences for growth from a single to a fused ring. One reaction sequence, however, was found to dominate although a second played a minor, but contributing role. The second (minor) reaction sequence is comparable to that proposed by Bittner, et. al (see above) although phenyl radicals add to acetylene, rather than diacetylene. The dominant reaction sequence was found to be initiated by H-atom abstraction from the ortho position on phenylacetylene, followed by acetylene addition and cyclization.



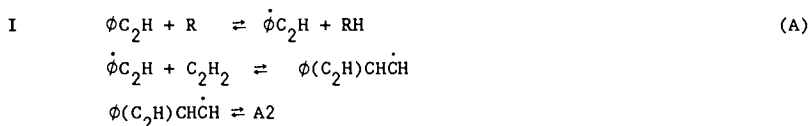
The resultant aryl radical can subsequently add to triple bonds to continue growth to higher order polycyclic aromatics. Due to the lack of experimental

rate data for reactions involving abstraction, addition, cyclization, or ring fracturing of polycyclic aromatics, Frenklach, et. al, selected generic rate constants for classes of reaction.

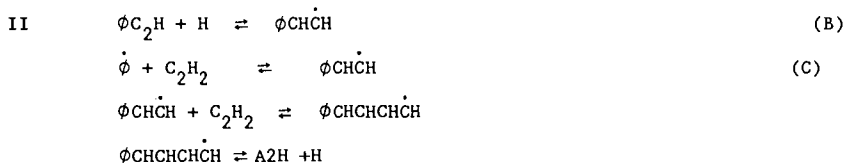
Rate constants for reactions involving aromatic species as listed in Table I were selected using the same technique of Frenklach, et. al, i.e., rate constants for a class of reactions are equated. Previously (3), values for several of these classes were assigned since experimental data was sparse. In this study, we have where possible updated the reaction rate data to be consistent with recently available determinations.

Predictions from the model (at 973K, 20% acetylene, and one atmosphere) are compared to the data from Munson and Anderson (5) in Fig. 1 for acetylene decay and production of benzene. In Fig. 2, predictions of production of styrene, naphthalene, and phenanthrene are shown. Although there is no experimental data from Munson and Anderson for these species, the final concentration of naphthalene is similar to other results (8) near 1000-1100K. The predicted value for styrene is about a factor of ten high.

Initially, only the dominant and minor mechanism (as identified by Frenklach, et. al) were included in the reaction sequence, specifically Mechanisms I and II:



and



where A2 represents the 1-naphthyl radical and A2H, naphthalene.

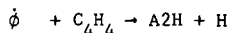
The net contribution of the second sequence to the formation of A2H (or A2) dominates over that of the first by several orders of magnitude. For the specific conditions considered in this study, this fact can be easily explained.

At the low temperature ($\approx 1000\text{K}$) and the high initial concentrations of acetylene, forward reaction rates can be shown to dominate. Ignoring the contribution of Reaction C and taking the radical, R, in Reaction A to be an H-atom, then the relative rate is simply the rate of H-atom abstraction from the ring by H-atoms relative to the rate of H-atom addition to the acetylenic group in phenylacetylene. The value (9) of k ($C_6H_6 + H \rightarrow C_6H_5 + H_2$)

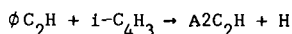
at 1000K is about 10^{10} cc/mole-sec. The rate constant for H-atom addition to acetylene, according to Ellul, et. al (10), extrapolates to 2×10^{12} cc/mole-sec at 1000K. Using these rate constants as estimates for k_A and k_B , respectively, Mechanism II is approximately 200 times faster than the first. The dominance of the Mechanism II becomes more apparent when the contribution of Reaction C is considered, since Reaction C is two to three orders of magnitude faster than Reaction B. Consequently, the second sequence is more than four orders of magnitude faster than the first. This is opposite to the trend observed by Frenklach, et. al. This strong discrepancy can be explained by a combination of (a) the higher temperatures of their study which enhance thermal decomposition of the radical adducts; (b) the lower partial pressures of acetylene in their study (40 torr vs. 150 torr in this study) which reduce the rate of radical addition to acetylene; and (c) the use by Frenklach of a high, temperature independent rate constant for Reaction A (with R as H-atom). Their rate constant was selected to be 10^{14} cc/mole-sec whereas, Kiefer, et. al's expression (9) gives 1.6×10^{12} cc/mole-sec at 1600 K.

Consequently, a reanalysis of dominant reactions occurring in a practical device should be performed for the specific ambient conditions. A preliminary analysis of the kinetic model indicates that the Mechanism II will dominate at temperatures of 1500-1700K for high pressure combustors, in which local acetylene concentrations may be at least an order of magnitude larger than considered in this and previous studies.

Also found to contribute a minor but significant role at 973K are the overall reactions



and



both of which require H-atom shifts prior to cyclization. The second of these could be part of a very attractive sequence (as shown in Fig. 4) depending on the concentration of $i-C_4H_3$ radicals.

Role of $i-C_4H_3$

It is recognized that thermochemistry plays a significant role in the ability to model the above processes. Frenklach, et al. (11) have demonstrated quantitatively that uncertainties in thermochemistry drastically affect computed results. An interesting and possibly important thermochemical aspect of acetylene pyrolysis is due to the rather large difference between the heats of formation of the two isomers of C_4H_3 , i.e., $HCCCH\dot{C}H$ and $HCC\dot{C}CH_2$. The separation in this work was taken to be 10 kcal/mole, although Steiń (6) and Bittner (12) give 8 and 15 kcal/mole, respectively. Due to its relative stability, the isomer with the unpaired electron on the secondary carbon atom ($i-C_4H_3$) becomes a dominant radical in the acetylene system. The situation is exacerbated if an isomerization step ($i-C_4H_3 \rightleftharpoons n-C_4H_3$) is not included. Depending on temperature, the

concentration of $i\text{-C}_4\text{H}_3$ is two to three orders of magnitude higher than that of its isomer and an order higher than that of the vinyl radical. Consequently, it is logical that $i\text{-C}_4\text{H}_3$ plays a significant role in termination, and quite possibly in ring formation and growth.

The importance of this radical to chain termination or to ring formation and growth is dependent critically on (a) the thermodynamics of the C_4H_3 isomers; (b) the isomerization rate (equated in this work to a rate suggested (13) for the $i\text{-propyl} \rightleftharpoons n\text{-propyl}$ isomerization); and (c) rate constants for reactions forming and destroying $i\text{-C}_4\text{H}_3$. Reactions which dominate formation of $i\text{-C}_4\text{H}_3$ include H-atom abstraction from vinylacetylene by phenyl, vinyl and H-atoms. The principal destruction mechanism in the present study is the isomerization to $n\text{-C}_4\text{H}_3$.

Uncertainties

Significant uncertainties in both rate constants and mechanisms still exist. The initiation step in acetylene pyrolysis has been a matter of unresolved discussion for nearly thirty years. There is perhaps just as much uncertainty in the termination step(s). In this work, recombination of $\text{C}_2\text{H}_3 + \text{C}_2\text{H}_3$, $\text{H} + \text{C}_2\text{H}_3$, $i\text{-C}_4\text{H}_3 + i\text{-C}_4\text{H}_3$, and $\text{H} + i\text{-C}_4\text{H}_3$ all contributed to termination, yet there is essentially no data available on the absolute value of their rate constants (although some information on reverse reactions is available). The addition of H-atoms to acetylene is critically important to this mechanism, yet there is no data on this reaction near or above 1000K. Rate constants for reactions of similar types have been equated in this work; however, changes in rate constants depending on molecular size may be quite significant. Molecular and ionic processes have been ignored in the present study; however, there is as yet no proof against their occurrence. It is believed, however, that due to the reasonable agreement between the present model and experiments, contributions due to such reactions are perhaps small.

Conclusions

A chemical kinetic model, revised to include growth of aromatic rings predicts profiles of acetylene decay and formation of benzene, vinylacetylene, ethane, and hydrogen which are in agreement with experimental flow reactor results near 1000K. In addition the model predicts the formation of styrene, phenylacetylene, naphthalene and other fused rings. An analysis of the detailed model indicates that the dominant route for growth from a single to a fused ring is due to addition of phenyl radicals to two acetylenes. Addition of phenyl to vinylacetylene was proposed and may play a significant role depending on pressure and relative concentrations. Uncertainties associated with the role of the $i\text{-C}_4\text{H}_3$ radical were discussed and a mechanism involving sequential addition of $i\text{-C}_4\text{H}_3$ to phenylacetylene and the resultant products was proposed as a conceptually attractive mechanism for ring growth. Uncertainties related to the heat of formation and rate of isomerization to $n\text{-C}_4\text{H}_3$ prevent quantitative predictions as to the importance of such a mechanism.

Acknowledgements

This work has been supported by the Air Force Office of Scientific Research (AFSC) under Contract No. F49620-85-C-0012. The United States government is authorized to reproduce and distribute reprints for governmental purposes, notwithstanding any copyright notation herein.

References

1. Colket, M. B., Twenty-First Symposium (International) on Combustion. The Combustion Institute, 1987, to be published.
2. Tanzawa, T., and Gardiner, W. C., Jr., *Combust. Flame* 39, 241 (1980), also *J. Phys. Chem.* 84, 236 (1980).
3. Frenklach, M., Clary, D. W., Gardiner, W. C., Jr., and Stein, S., Twentieth Symposium (International) on Combustion, p. 887, The Combustion Institute, 1985; also see Frenklach, M., Clary, D. W., and Ramachandra, M. K., NASA Contractor Report 174880, May 1985.
4. Colket, M. B., Palmer, H. B. and Seery, D. J. Submitted for publication, 1987.
5. Munson, M. S. B., and Anderson, R. C., *Carbon* 1, 51 (1963).
6. Stein, S., Personal communication, 1987.
7. Bittner, J. D., Howard, J. B., and Palmer, H. B., Soot in Combustion Systems and Its Toxic Properties, ed. by J. Lahaye and G. Prado, p. 95, Plenum Press, 1983.
8. Stehling, F. C., Frazee, J. D. and Anderson, R. C., Eighth Symposium (International) on Combustion, p. 774, Williams and Wilkins Co., Baltimore 1962.
9. Kiefer, J. H., Mizerka, L. J., Patel, M. R., and Wei, H.-C., *J. Phys. Chem.* 89, 2013 (1985).
10. Ellul, R., Potzinger, P., Reimann, B., and Camilleri, P., *Ber. Bunsenges. Phys. Chem.* 85, 407 (1981).
11. Frenklach, M., Clary, D. W., Gardiner, W. C., Jr. and Stein, S. E., Shock Waves and Shock Tubes, Proceedings of the Fifteenth International Symposium, Ed. by D. Bershader and P. Hanson, p. 295, Stanford University Press, 1986.
12. Bittner, J. D., Ph.D dissertation, Massachusetts Institute of Technology, 1981.
13. Benson, S. W., Thermochemical Kinetics, J. Wiley and Sons, New York, 1976.

TABLE I
 REACTIONS FOR ACETYLENE PYROLYSIS NEAR 1000K
 $\log k = \log A + n \log T - E/R/T/2.303$ *

Reactions	Forward Rate Constant			Reverse Rate Constant		
	logA	n	E	logA	n	E
1 2C2H2=1-C4H3+H	14.54	0.0	60.5	13.49	0.0	0.2
2 H+C2H2=C2H3	12.92	0.0	2.7	12.96	0.0	41.6
3 C2H3+C2H2=n-C4H5	12.88	0.0	8.0	14.86	0.0	44.1
4 n-C4H5=C4H4+H	13.00	0.0	33.0	12.39	0.0	-5.4
5 n-C4H5+C2H2=l-C6H7	12.18	0.0	5.0	14.25	0.0	41.0
6 c-C6H7=l-C6H7	14.48	0.0	50.0	11.36	0.0	0.4
7 C6H6+H=c-C6H7	13.60	0.0	4.3	13.12	0.0	24.6
8 C2H3+C4H4-C6H6+H	11.60	0.0	0.0	0.00	0.0	0.0
9 C4H4+n-C4H5-A1C2H3+H	13.50	0.0	5.0	0.00	0.0	0.0
10 A1C2H3+H=A1C2H2S+H2	14.00	0.0	14.5	13.09	0.0	19.7
11 C2H4+C6H5=A1C2H3+H	11.57	0.0	2.1	12.92	0.0	1.4
12 C6H6+H=C6H5+H2	14.40	0.0	16.0	12.39	0.0	9.5
13 C2H2+C6H5=A1C2H2	12.00	0.0	4.0	13.72	0.0	42.2
14 C2H3+C4H4=C2H4+n-C4H3	13.00	0.0	10.0	13.09	0.0	9.5
15 C4H4+C6H5=C6H6+n-C4H3	12.48	0.0	0.0	13.04	0.0	3.1
16 l-C6H5=n-C4H3+C2H2	13.40	0.0	36.1	11.11	0.0	0.0
17 C6H5=l-C6H5	13.54	0.0	65.0	10.25	0.0	1.7
18 C2H3+C6H6=C2H4+C6H5	13.48	0.0	13.0	13.00	0.0	9.3
19 2C2H3=C4H6	13.40	0.0	0.0	17.15	0.0	104.9
20 C4H4=n-C4H3+H	15.00	0.0	100.0	12.91	0.0	-7.9
21 C6H6=C6H5+H	15.70	0.0	107.9	13.05	0.0	-3.2
22 n-C4H5+H=C4H4+H2	13.00	0.0	0.0	12.99	0.0	66.0
23 n-C4H5+H=C4H6	13.00	0.0	0.0	14.84	0.0	107.9
24 n-C4H5+n-C4H3=2C4H4	12.70	0.0	0.0	14.18	0.0	69.5
25 n-C4H5+C2H3=C4H4+C2H4	12.00	0.0	0.0	13.57	0.0	69.0
26 C2H3+H=C2H4	12.85	0.0	0.0	15.00	0.0	107.2
27 C6H5+C2H3=A1C2H3	12.60	0.0	0.0	16.11	0.0	106.5
28 C2H3+H=H2+C2H2	13.00	0.0	0.0	13.57	0.0	65.5
29 C2H4+H=C2H3+H2	14.84	0.0	14.5	13.30	0.0	11.7
30 C4H4+H=n-C4H3+H2	13.90	0.0	14.5	12.42	0.0	11.0
31 C4H6+H=n-C4H5+H2	14.00	0.0	14.5	12.76	0.0	10.9
32 C4H6+C2H3=n-C4H5+C2H4	13.18	0.0	10.0	13.52	0.0	9.5
33 C6H5+C6H6=C12H10+H	11.80	0.0	11.0	13.38	0.0	9.2
34 C2H4+M=C2H3+H+M	16.16	0.0	81.8	14.01	0.0	-25.4
35 2i-C4H3=C4H4+C4H2	11.00	0.0	0.0	14.35	0.0	47.8
36 i-C4H3+H2=C2H2+C2H3	10.70	0.0	20.0	11.18	0.0	14.8
37 C4H4=i-C4H3+H	15.20	0.0	95.0	12.72	0.0	-2.1
38 C2H+C4H4=C2H2+i-C4H3	13.60	0.0	0.0	12.48	0.0	27.9
39 n-C4H3=C2H2+C2H	14.30	0.0	57.0	13.56	0.0	3.0
40 i-C4H3=C4H2+H	12.00	0.0	49.0	12.86	0.0	-0.2
41 n-C4H3=C4H2+H	12.60	0.0	40.0	13.04	0.0	1.4
42 n-C4H3=i-C4H3	13.00	0.0	35.0	12.58	0.0	45.7
43 i-C4H3+H=C4H2+H2	13.00	0.0	0.0	14.47	0.0	55.2
44 n-C4H3+H=C4H2+H2	12.48	0.0	0.0	13.53	0.0	65.9

* NOTES: Units for A: cc,moles,sec., Units for E: kcal/mole.
 = represents forward and reverse directions included in model.
 - represents forward direction only included in model.

(CONTINUED NEXT PAGE)

TABLE I (continued)
 REACTIONS FOR ACETYLENE PYROLYSIS NEAR 1000K
 $\log k = \log A + n \log T - E/R/T/2.303$ *

Reactions	Forward Rate Constant			Reverse Rate Constant		
	logA	n	E	logA	n	E
45 C4H4+H=1-C4H3+H2	14.49	0.0	14.5	12.62	0.0	21.9
46 C6H5+C4H4=C6H6+1-C4H3	12.18	0.0	0.0	12.31	0.0	13.8
47 C2H3+C4H4=C2H4+1-C4H3	12.70	0.0	10.0	12.36	0.0	20.2
48 C4H4=C2H+C2H3	15.70	0.0	115.0	12.93	0.0	-7.8
49 H2+M=2H+M	12.35	-5	92.5	11.74	-5	-11.9
50 C2H2+M=C2H+H+M	16.62	0.0	107.0	15.25	0.0	-17.9
51 C2H+H2=H+C2H2	12.85	0.0	0.0	13.60	0.0	20.5
52 C2H+C2H2=C4H2+H	13.60	0.0	0.0	14.78	0.0	15.4
53 C2H+C4H2=C6H2+H	13.60	0.0	0.0	14.97	0.0	15.1
54 C4H+C2H2=C6H2+H	13.30	0.0	0.0	14.91	0.0	8.1
55 C4H+H2=H+C4H2	13.30	0.0	0.0	14.30	0.0	13.5
56 C6H+H2=H+C6H2	13.30	0.0	0.0	14.53	0.0	10.3
57 C2H+C6H6=C6H5+C2H2	13.30	0.0	0.0	12.05	0.0	14.1
58 C4H+C6H6=C6H5+C4H2	13.30	0.0	0.0	12.29	0.0	7.0
59 C2H3+C4H2=C4H4+C2H	13.48	0.0	23.0	13.70	0.0	5.4
60 2C6H5=C12H10	12.48	0.0	0.0	16.57	0.0	108.3
61 C2H+C4H4=C2H2+n-C4H3	13.60	0.0	0.0	12.91	0.0	17.2
62 A1C2H3+H=A1C2H2+H2	14.50	0.0	14.5	13.29	0.0	11.7
63 A1C2H2S=A1C2H+H	13.00	0.0	45.0	13.11	0.0	0.8
64 A1C2H2=A1C2H+H	12.30	0.0	37.0	12.71	0.0	0.8
65 A1C2H2+C2H2=A1C4H4	12.88	0.0	8.0	14.81	0.0	44.5
66 A1C4H4=A2H+H	10.00	0.0	0.0	13.32	0.0	18.5
67 C6H5+C4H4=A2H+H	11.60	0.0	0.0	17.14	0.0	56.4
68 A1C2H+C2H3=A1C2HP+C2H4	13.70	0.0	13.0	14.02	0.0	10.5
69 A1C2H+H=A1C2HP+H2	14.40	0.0	16.0	13.18	0.0	10.7
70 A1C2H+C2H=A1C2HP+C2H2	13.30	0.0	0.0	12.85	0.0	15.2
71 A1C2H+1-C4H3-A2C2H+H	11.60	0.0	0.0	0.00	0.0	0.0
72 A1C2H+C2H3-A2H+H	11.60	0.0	0.0	0.00	0.0	0.0
73 A1C2HP+C4H4=A1C2H+1-C4H3	12.18	0.0	0.0	11.51	0.0	12.6
74 A1C2HP+C2H2=A1C2HV	12.30	0.0	4.0	13.70	0.0	41.8
75 A1C2HV=A2	11.00	0.0	0.0	14.14	0.0	53.4
76 A2C2H2=A2C2H+H	12.30	0.0	37.0	12.71	0.0	0.8
77 A2+C2H2-A2R5+H	12.30	0.0	4.0	0.00	0.0	0.0
78 A2C2H2+C2H2=A2C4H4	12.88	0.0	8.0	14.81	0.0	44.5
79 A2C4H4=A3H+H	10.00	0.0	0.0	13.32	0.0	20.7
80 A2H+H=A2+H2	14.40	0.0	16.0	12.88	0.0	10.7
81 A2H+H=A2P+H2	14.40	0.0	16.0	12.88	0.0	10.7
82 C2H3+A2H=C2H4+A2	13.70	0.0	13.0	13.72	0.0	10.5
83 C2H3+A2H=C2H4+A2P	13.70	0.0	13.0	13.72	0.0	10.5
84 A2P+C2H2=A2C2H2	12.30	0.0	4.0	13.70	0.0	41.8
85 A2C2H+H=A2C2HX+H2	14.40	0.0	16.0	13.49	0.0	10.7
86 A2C2H+C2H3=A2C2HX+C2H4	13.70	0.0	13.0	14.33	0.0	10.5
87 A2C2HX+C2H2-A3	12.30	0.0	4.0	0.00	0.0	0.0
88 A3+C2H2-A4H+H	12.30	0.0	4.0	0.00	0.0	0.0
89 A3H+H=A3+H2	14.40	0.0	16.0	13.18	0.0	10.7

* NOTES: Units for A: cc,moles,sec., Units for E: kcal/mole.
 = represents forward and reverse directions included in model.
 - represents forward direction only included in model.

TABLE II
 Selected Thermodynamics at 300K
 (from Stein(6))

Species	Identification	Heat of Formation (kcal/mole)	Entropy (eu)
C2H3	vinyl	68.4	56.5
A1C2H3	styrene	35.3	82.6
A1C2H2	A1CHCH	91.2	85.2
A1C2H2S	A1CCH2	83.2	83.8
A1C2H	phenylacetylene	75.2	76.4
A1C2HP	A1C2H	133.6	79.0
A1C2HV	A1(C2H)CHCH	146.6	95.1
A1C4H4	A1CHCHCHCH	104.7	98.0
A2	1-naphthyl	94.4	83.6
A2P	2-naphthyl	94.4	83.6
A2H	naphthalene	36.1	79.7
A2C2H	2-naphthylacetylene	91.5	90.9
A2C2H2	A2CHCH	107.4	99.7
A2C2HX	A2C2H	149.9	92.1
A2C4H4	A2CHCHCHCH	121.0	112.5
A2R5	acenaphthylene	61.7	87.2
A3	phenanthrenyl	108.5	96.8
A3H	phenanthrene	50.1	94.2
A4H	pyrene	55.2	96.5

FIG. 1 MODEL PREDICTIONS vs. DATA OF REF. 5
C₂H₂ and C₆H₆ Concentrations at 973K

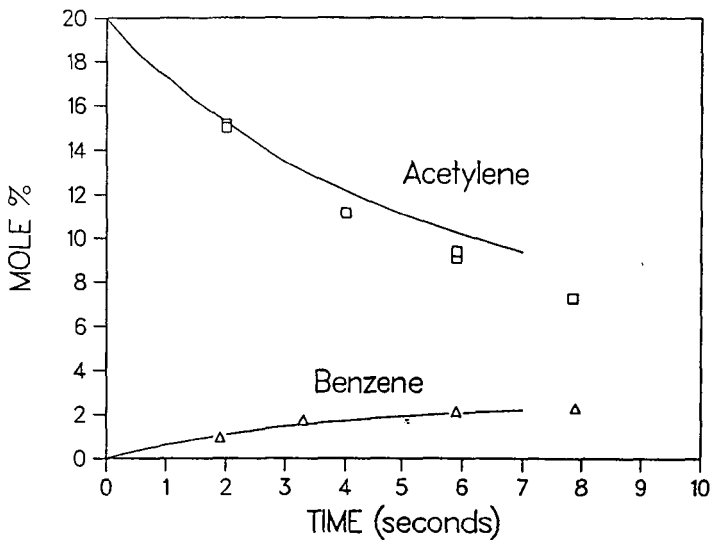
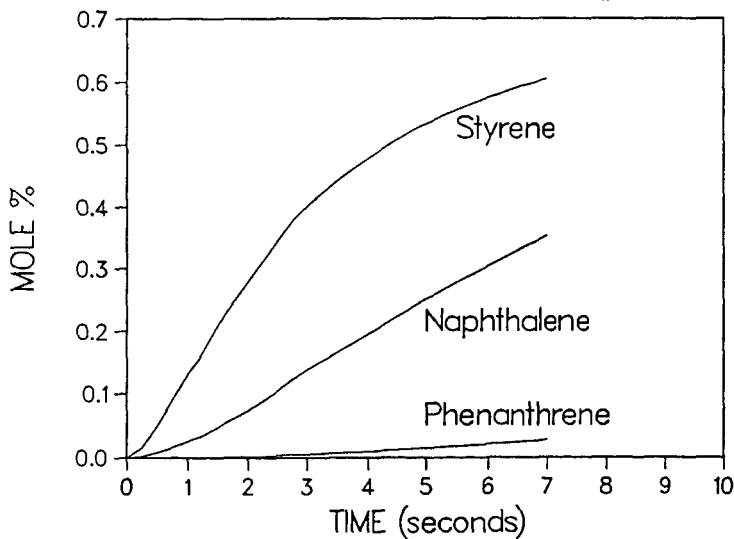


FIG. 2 PYROLYSIS OF 20% ACETYLENE AT 973K
Formation of Aromatic Products (predictions)



A MECHANISTIC INVESTIGATION OF SOOT PRECURSORS

S. H. Bauer^(a) and P. M. Jeffers^(b)

(a) Department of Chemistry, Baker Laboratory,

Cornell University, Ithaca, New York 14853-1301

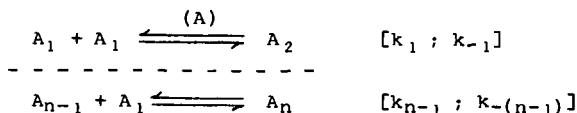
(b) Department of Chemistry, SUNY-Cortland, Cortland, NY 13045

INTRODUCTION

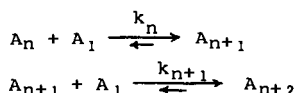
Fuels with low H/C ratios are particularly prone to soot production during combustion; aromatic species generally (but not universally) do so more readily than aliphatics. It is now well recognized that "soot" is not a singular material. Besides characterizing the variety of soots with respect to composition, volatile content, and structure, extensive efforts have been devoted to determining conditions which promote the development of soot in flames and in internal combustion engines. Many studies have been reported on the effects of inhibitors; reviews abound (1). During the past decade chemical kinetics investigations have proliferated with the hope of unraveling the mechanisms for its generation, ultimately to permit control of the types and magnitudes of soot emissions. There is general agreement on species types which initiate condensed aromatic ring growth (2); there is still disagreement as to whether ions play a major role (3); there is overall agreement on the spacial distribution of PAH in flames, as measured mass spectrometrically (4); composition constraints on fuel/oxidizer ratios for the inception of sooting, and the temperature range in flames wherein soot appears are sufficiently well-defined (5).

In this report our objectives are: **A.** To call attention to the differences and the conceptual similarities between the sooting process and a kinetic model for nucleation/condensation. **B.** List the types of precursors required for sooting, and the underlying experimental basis. **C.** Present a minimal set of reactions, with rate constants, which model the observed time evolution of condensed molecular structures (soot precursors). This list must incorporate a repetitive growth cycle for continued condensation. As a minimum, the model must semiquantitatively reproduce observed delay times for the onset of condensation. **D.** Present qualitative spectral data which support **C.**

A. The characteristic kinetic features of a typical nucleation/condensation mechanism (6) are: (a) An initial binary association sequence which reaches steady state at some small number (n) (7):



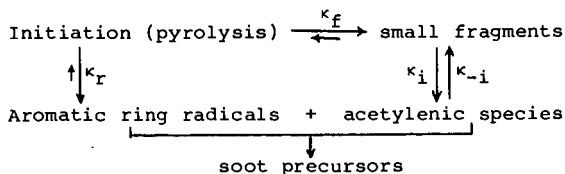
Note that at this stage the rates of association/condensation are nearly balanced for each step: $k_{n-1}(A_1) \approx k_{-(n-1)}$. No activation energies are involved; association is driven by a decrease in enthalpy; dissociation is favored by an almost equal $T\Delta S$ term. This is followed by (b),



wherein steady state is achieved by unidirectional flow, such that $k_{n+1} \approx k_n$, with insignificant reversibility. Here the enthalpy factor completely dominates. The magnitude of n at which this "switch-over" occurs characterizes the critical size nucleus.

The contrast with soot production from C/H fragments is striking. The initial lag is due to: (α_1) the rate of pyrolysis of the fuel, to generate small reactive fragments, generally referred to as "acetylenic species", and (α_2) their partial recombination to [in some cases --- the direct production of] aromatic ring radicals; activation energies control these steps. Hence, minimal temperatures of ≈ 1500 K are required. It is likely that a dynamic local equilibrium similar to the steady state (a), develops between these small highly reactive radicals. When adequate levels of both types of species are attained, stage (β) follows; i.e. an essentially unidirectional growth sequence, wherein the acetylenic species add onto the aromatic radicals, in analogy with (b). Thus, there occurs a "switch-over" which has the appearance of a catastrophic onset of sooting. Since at all times in (β) the driving enthalpy for growth is countered by an opposing $T\Delta S$ term, at some higher temperature the latter quenches sooting (≈ 2100 K). This accounts for the bell-shaped generation profile [soot yield vs temperature] reported by many observers.

B. What are the essential precursors which operate in regions (α_1) and (α_2)? Observations, previously reported for shock tube pyrolysis studies of ten polycyclic aromatics (8), guided our choice of the smallest species which have to be incorporated in a minimal mechanism. For shock durations of < 700 μ s, over the temperature range 1500-2200 K, acetylene, tetramethylpentane, acenaphthene or acenaphthalene, when individually pyrolyzed, yielded insignificant amounts of soot. However, any aliphatic/aromatic combination under the same shock conditions produced copious amounts of soot. Clearly, two types of molecular species are required for the onset of sooting. It follows that one should anticipate longer delays when a single type is initially present because of the time required to generate the other type. Schematically,

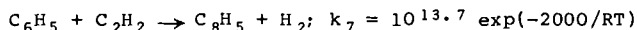


The relative magnitudes of k_f and k_r are determined by the structures of the fuel.

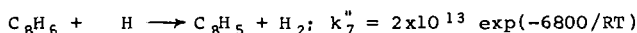
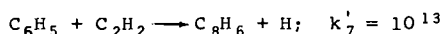
C. Two sets of reactions with appropriate rate constants are listed in Tables I and II, for benzene and toluene, respectively. We attempted to identify the smallest number of essential steps, not to list all reactions which plausibly occur concurrently with soot initiation.

C_6H_6 : For the benzene pyrolysis our final set consists of 18 reactions with 18 H/C species (plus Ar), although at least twice that number of reactions and species [30] were considered during the preliminary calculations. Not included in Table I are intermediate radical stabilization steps.

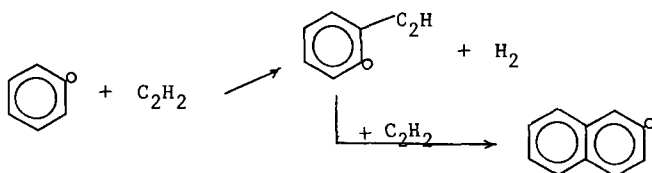
We also treated the addition of acetylene as a single step:



rather than a two reaction sequence:



The typical growth cycle is illustrated by



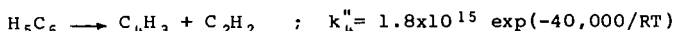
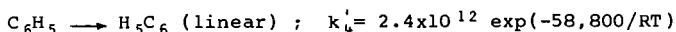
At each cycle one ring is added and a new radical is generated which repeats the cycle. As ring condensation proceeds there are possibilities for alternate routes to yield other observed products, for example R12; it was included because biphenyl is a commonly found product, although no further reactions of biphenyl occur other than the reverse of its formation. The other stable molecular products incorporated in this mechanism are C_2H_2 , C_4H_2 , $H_{10}C_{18}$, and $C_{22}H_{12}$. It is necessary to assign an upper limit to the largest species incorporated in the computer code; we chose $C_{22}H_{12}$ which serves as a "sink". Tests show that the concentration/time patterns for the last three species, for any selected terminus, remains essentially unchanged when the largest assumed unit was varied [$C_{18} + C_{20} + C_{22}$]. Clearly, the two-step growth sequence continues until the system is quenched.

Kinetic calculations, to model rates of production of soot precursors by pyrolysis, were performed with the Mitchell/Kee (9) shock kinetics program. All reactions were considered reversible, with their reverse rate constants calculated within the program by reflection through their equilibrium constants. Most of the unavailable thermodynamic parameters were estimated by Benson's group contribution recipe.

Figure 1 is a plot of the computed concentration-time profiles for 1% C_6H_6 in argon, reflected shock heated to 2120 K (initial). It shows the expected general features. During early times the mole fractions of H, C_2H_2 , C_4H_2 and H_2 rise, that of C_6H_6 slowly declines and nearly steady state concentrations of C_6H_5 and C_8H_5 develop. The higher molecular weight products then slowly begin to grow, in sequence of increasing carbon content. The time dependence of the imposed cut-off at C_{22} provides a measure of the delay time for the onset of avalanche soot growth. Note that after a gradual decline, C_6H_6 drops sharply as do all the heavier species even though all reactions

were treated reversibly. $C_{22}H_{12}$ (the terminal species) increases (designated as the soot initiator). Eventually, after the lower carbon content species had passed through maximum levels, C_2H_2 , C_4 's and H_2 dominate.

A measure of the sensitivity of this mechanism to the rate constant for initiation (R1) was obtained by using a value derived by reflection of Frenklach's (1) estimate for the reverse of R1, 1×10^{13} mole/cc-sec, whereas the curves in Fig. 1 were calculated with k_1 about a factor of ten larger, as suggested by M. C. Lin (10); it is very close to the value reported by Fujii and Asaba (11). A faster initiation rate results, with a much earlier appearance of heavy products and considerably more extensive (eventual) destruction of benzene. When the one step phenyl radical decomposition (R5) was replaced by the sequence:

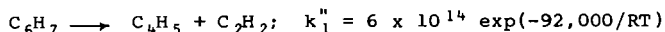
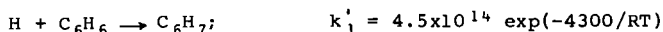


a dramatically slower depletion of all the low molecular species was indicated. This merits further investigation, possibly by direct assay of the time dependence for appearance of C_4H_3 .

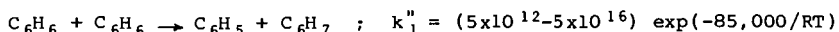
The proposed mechanism is sensitive to one more feature --- the initial concentration of C_2H_2 . If one starts a calculation, as for Fig. 1, but with added C_2H_2 (mole fraction of 0.005), the production of all the heavy products is strongly accelerated. This accounts for our observations that soot formation from acenaphthene or acenaphthalene is significantly accelerated when C_2H_2 [or tetramethylpentane, which readily produces C_2H_2] was included in the initial mixture.

Two variations of the mechanism were found to exert a moderate effects on the rate of heavy product formation. The C_2H_2 addition sequence via one step, rather than two steps, delays somewhat the appearance of the final product. Reducing the value of k_{12} by a factor of 100 makes at most a 15-20% change in heavy species mole fractions at 5 μ sec, with slightly larger differences in $C_{12}H_{10}$ and C_8H_6 concentrations at earlier times.

Finally, several factors were found to have slight or negligible effects. These non-critical factors include deletion of radical stabilization steps, incorporating an initial [artificially] high H atom concentration, the value for k_7 [acetylene addition to phenyl], and the inclusion of an alternate initiation process:



Reduction of E_a from 92 to 80 kcal/mole for the second step had no effect. Substituting the bimolecular reaction:



for R1 failed to provide sufficient radical species for the pyrolysis sequence to proceed.

$C_6H_5CH_3$: The adequacy of our minimalist approach to develop a mechanism for the precursor stage of sooting is illustrated by the analysis of our shock tube data for toluene. The initiation steps (Table II) differ from those for benzene (steps 1-6, Table I) but thereafter the growth sequences are the same. Here also the calculated and observed delay times are in acceptable agreement. Six additional species must be included (C_7H_8 ; C_7H_7 ; C_3H_3 ; CH_3 ; CH_4 and C_2H_2). Reactions T 1, 2, 4, 5 and 6 were taken from Mizerka and Kiefer (12). The combined effect of reactions T2, T3, and T8 is to generate rapidly significant concentrations of C_6H_5 and C_6H_6 . No effort was made to determine which reaction path is most effective. At temperatures around 1800°K and higher T2 is a significant pathway for the initial breakup of toluene. The rate constant for T3 was assumed to be (1/4) that for T4, and both are exothermic. T7 is a reasonable sink for CH_3 radicals, while the recombination of C_3H_3 's [T8] maintains the reaction sequence alive in a simple fashion. All the initially estimated rate constants were used in the calculations without subsequent adjustments. The possibility that there are steps in the sequence T 1-8 which are not essential for the "minimal" mechanism was not fully tested; it appears that T7 could be dropped.

Our conclusion is that a few additional steps added to the simplified mechanism proposed for benzene, can account in a quantitative way for many features of the pyrolysis of aromatics, in general. For soot production, the major pathways are evident and inherently reasonable.

D. What experimental evidence exists, or can be developed, to support the above proposals? Other than direct mass spectrometric detection of PAH, one must look for some *in situ* diagnostic technique. Absorption and fluorescence spectra (5) are indicated, but there are obvious limitations. The samples consist of complex brews, characterized by superposed broad spectral bands. Thus, there is little likelihood that one could identify specific species. But, we are concerned with molecular types; the saving feature is the absence of oxygen or nitrogen chromophoric structures. The recorded spectra in the near uv, visible and down to the near infrared must arise from condensed polycyclic aromatics, either the stable species, as reported in the literature (12) or their radicals. To distinguish between general turbidity and characteristic absorptions, one should measure the temporal wavelength dependence of light loss on passage through the reacting medium, and its dependence on temperature. Also, a condition for the adequacy of a minimal mechanism is that it correctly predict the temperature dependence of the time delays of the growth of condensed polycyclic aromatics.

EXPERIMENTAL

Since a large diameter shock tube was not available to measure the time dependent spectra transverse to the shock flow, we had to resort to recording integrated absorption spectra by passing the probing beam axially along the shock direction. The data were resolved by imposing an additional integration step in the analysis. A 1" I.D. stainless steel shock tube (Fig. 2a) was fitted with a clear plastic end-wall at the driver section; a quartz window and filter terminated the test section. A He/Ne laser beam (6328 Å), directed along the axis of the tube, was aimed at a small aperture inserted between the quartz end plate and the narrow band pass filter. The phototube output was recorded simultaneously with the output of two pressure trans-

ducers located 1 cm and 11 cm from the downstream end. In later experiments the laser was replaced by a Xe lamp and the phototube by a monochromator/linear array of diodes for scanning other regions of the spectrum (Fig. 2b).

The signals from the piezo-gauges allow evaluation of the shock speed and dwell time. Since the gas at different initial positions along the tube is heated for different lengths of time, the extent of light absorption (or scattering) must be integrated along the entire tube length. Let $A_n(x; t')$ be the instantaneous concentration of the n^{th} absorbing species, where $t' = t_w - x/u_r$; t_w is the laboratory time for shock reflection at the quartz window, x is the return distance from the window at the location of the reflected shock, and u_r the reflected shock speed. Then, the recorded light loss is:

$$I^\lambda(t')/I_0^\lambda = \exp \left[- \int_n u_n(\lambda, T_5) \int_0^{u_r t'} A_n(t_w - x/u_r) dx \right]. \quad [1]$$

Here we assumed that no chemical processing and no absorption (at the probing wavelength) occurs during the incident shock.

Reflected shock temperatures ranged from 1400°K to 2200°K, and were controlled by varying both the initial pressure of the test gas and the diaphragm thickness. Residence times were generally about 700 μ sec, followed by a rapid quench due to expansion. Analysis by g.c. of the shock heated samples (both gas phase and condensable species) indicated that during the test time the products had not achieved their equilibrium concentrations at the reflected shock temperatures.

I. The molecular species which strongly absorb red light (He/Ne) appear after an extended induction period which is temperature dependent. [Typical shapes are illustrated by the curves in Fig. 3b.] In turn, these absorbers are removed by continued condensation. Hence the initial flattening and the subsequent slow growth of absorption. We noted that substantial light loss occurred even in some cases where little soot was produced. Curves of $\ln(I/I_0)$ vs t (corrected for emission) were sigmoidal and often saturated at $I > 0$. We presume that the recorded light loss was due primarily to absorption by transient species, which are precursors of soot particles, and to a lesser extent by soot, which forms during the later stages of the experiment. The absorbing species at $\lambda 6328$ must be condensed ring entities, such as the para sequence of the acene series (12), and/or radicals of similar structure (Fig. 4). For the 2% runs, the concentration-time profiles for $C_{20}H_{11}$ [designated as the representative absorber of $\lambda 6328$] were integrated, per eq. [1]. These curves show all the salient features of the recorded (I/I_0) traces, i.e. the sigmoid shape following a delay, a relatively sharp rise and a slow approach to saturation. The computed times selected for minimal detection of absorption (at 3x noise level) check quite well with the measured values (Table III).

II. Absorption curves over a range of wavelengths (400-800 nm) were obtained with the second experimental configuration (Fig. 2b). Typical time/wavelength spectra at two extremes are shown in Fig. 3a and Fig. 3b. No significant differences appear over a spectral range of 20 nm. However, there are clear, significant differences between the spectral scans at 811 and 392 nm. First, the delay times are shorter and the rise times are faster for the same shock speeds, indicating more rapid rates for generating the smaller species which absorbed

near the uv, compared with the much longer delay times for the appearance of the larger species, which absorb in the near infrared. Second, a two step process appears at 800 nm, where the initial relatively fast rise is followed by a slower continued increase in absorption, demonstrating subsequent growth, since the absorption edge continues to move toward the longer wavelength.

Two types of information are presented by these plots (recorded at 100 nm intervals, 400-800 nm); delay times (t_i) which measure induction times for the development of absorbing species, and rise times $[(t_f - t_i)/2]$, which are mean inverse rates of production of these species. For any specified shock temperature (T_5), a plot of t_i vs mean λ has a positive slope, as expected for a sequential growth of absorbers with leading edges progressing toward the red. For any specified λ , t_i is longer the lower the shock speed (T_5).

Because of the restricted range of final densities covered in these experiments, the half-times for attaining the first saturation level do not permit us to determine whether the global process is first or second order. However, graphs of $\ln k_u \approx 10^6 \ln 2 / t_{1/2, \mu s}$ vs $1/T_5$ (Fig. 5) clearly show nesting of points for the sequence of λ 's, as expected, assuming that the leading edges of the absorption curves measure the larger units at longer wavelengths. At any T_5 , the k_u 's are consistently larger when derived from 400 nm traces compared with 800 nm traces.

ACKNOWLEDGMENTS

This program was supported by the U. S. Department of Energy under contract DE-AC01-80 ER 10661.A004. We sincerely thank Dr. R. J. Kee for copies of the Sandia computer codes, Professor C. F. Wilcox, Jr. for extensive discussions of the possibilities and limitations of the Diels-Alder addition sequence, and Professor J. H. Kiefer for discussions of his shock tube pyrolysis experiments of toluene and ethylbenzene.

REFERENCES

1. Sections on SOOT & COMBUSTION GENERATED PARTICULATES can be found in every Symposium (International) on Combustion [Combustion Institute], starting with the 15th (1974) through the 21st (1986). Also: Wagner, H. Gg., 17th Symposium (International) on Combustion, The Combustion Institute, Pittsburgh, 1978, p. 3; Haynes, B. S. and Wagner, H. Gg., Prog. Energy Comb. Sci. 1981, 7, 229.
2. Frenklach, M., Clary, D. C., Gardiner, W. C. and Stein, S. E., 20th Symposium (International) on Combustion, The Combustion Institute, Pittsburgh, 1984, p. 887; Bockhorn, H., Fetting, F. and Wenz, H., Ber. Bunsenges. Phys. Chem. 1983, 87, 1067; Homan, K. H., 20th Symposium (International) on Combustion, The Combustion Institute, Pittsburgh, 1984, p. 857.
3. Keil, D. G., Gill, R. J., Olson, D. B. and Calcotte, H. F., 20th Symposium (International) on Combustion, The Combustion Institute, Pittsburgh, 1984, p. 1129 -- favor ionic mechanisms; Bertrand, C. and Delfan, J-L., Comb. Sci. and Tech. 1985, 44, 25; discount significant contributions from ions.

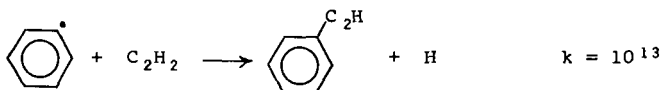
4. Longwell, J. P., 19th Symposium (International) on Combustion, The Combustion Institute, Pittsburgh, 1982, p.1339.
5. Smith, K. C., et al., Comb. and Flame, 1985, 62, 157; Frenklach, M., Hsu, J. P., Miller, D. L. and Matula, R. A., Comb. and Flame, 1986, 64, 141.
6. Bauer, S. H. and Frurip, D. J., J. Phys. Chem. 1977, 81, 1015.
7. Bauer, S.H., Wilcox, C.F., Jr. and Russo, S., J. Phys. Chem. 1978, 82, 59.
8. Bauer, S. H. and Zhang, L-M., 14th International Symposium on Shock Tubes and Waves, Ed. R. D. Archer and B. E. Melton, New S.W. University Press, 1983, p. 654.
9. Mitchell, R. E. and Kee, R. J., Sandia National Laboratories, Livermore, CA, SAND-82-8205 (March, 1982).
10. Hsu, D. S. Y., Lin, C. Y. and Lin, M. C., 20th Symposium (International) on Combustion, August 1984. See also: Kieffer, J. H., et al., J. Phys. Chem. 1985, 89, 2013.
11. Fujii, N. and Asaba, T., 14th Symposium (International) on Combustion, The Combustion Institute, p. 433 (1973).
12. Clar, E., Polycyclic Hydrocarbons, 1964, Academic Press, London; Clar, E., The Aromatic Sextet, 1972, J. Wiley & Sons, London; Stern, E. S. and Timmons, C. J., Electronic Absorption Spectroscopy in Organic Chemistry, 1970, Edward Arnold, London; Karcher, W., et al., Ed., Spectral Atlas of Polycyclic Aromatic Compounds, 1983, D. Reidel, Dorchester.

TABLE I

	MINIMAL MECHANISM (C ₆ H ₆)	log A	E ₀ (cal mole ⁻¹)	Ref.
1.	C ₆ H ₆ = C ₆ H ₅ + H	15.7	108000.	10
2.	C ₂ H + C ₆ H ₅ = C ₆ H ₅ + C ₂ H ₂	13.3	0.00	2
3.	C ₂ H ₂ + C ₂ H ₂ = C ₄ H ₃ + H	12.3	65000.	a
4.	C ₆ H ₅ = C ₄ H ₃ + C ₂ H ₂	14.8	82800.	b
5.	C ₄ H ₃ = C ₂ H ₂ + C ₂ H	10.76	52500.	2
6.	C ₄ H ₃ + Ar = Ar + C ₄ H ₂ + H	16.0	45000.	c
7.	C ₆ H ₅ + C ₂ H ₂ = C ₈ H ₅ + H ₂	13.7	2000.0	2
8.	C ₆ H ₅ + C ₂ H ₂ = C ₁₀ H ₇	13.0	0.00	2
9.	C ₁₀ H ₇ + C ₂ H ₂ = C ₁₂ H ₇ + H ₂	13.0	2000.0	2
10.	C ₁₂ H ₇ + C ₂ H ₂ = C ₁₄ H ₉	13.0	0.00	2
11.	C ₁₄ H ₉ + C ₂ H ₂ = C ₁₆ H ₉ + H ₂	13.0	2000.0	2
12.	C ₆ H ₅ + C ₆ H ₆ = C ₁₂ H ₁₀ + H	11.0	11000.	d
13.	C ₁₆ H ₉ + C ₂ H ₂ = H ₁₀ C ₁₈ + H	12.74	10000.	e
14.	C ₁₆ H ₉ + C ₂ H ₂ = C ₁₈ H ₉ H ₂	13.0	2000.0	2
15.	C ₁₈ H ₉ + C ₂ H ₂ = C ₂₀ H ₁₁	13.0	0.00	2
16.	C ₂₀ H ₁₁ + C ₂ H ₂ = C ₂₂ H ₁₂ + H	12.74	10000.	e
17.	H ₂ + Ar = H + H + Ar	(12.08) ^T ^{1/2}	92600.	
18.	C ₆ H ₆ + H = C ₆ H ₅ + H ₂	13.3	6600.	c

Footnotes for TABLE I

- a. J. Warnatz, *Ber. Bunsengesell. Phys. Chem.* 1983, 87, 1008 but $E_0 = \Delta H_{\text{reaction}} = 67.4 \text{ kcal mole}^{-1}$ (rather than $54 \text{ kcal mole}^{-1}$).
- b. T. Asaba and N. Fujii, 13th Symposium (International) on Combustion, The Combustion Institute, Pittsburgh (1971), p.155.
- c. Values of A are those given in (2), but with selected E_0 's.
- d. A slightly adjusted value based on --- C. T. Brooks, S. J. Peacock and B. G. Renber, *J. Chem. Soc. Farad. Trans. I*, 1979, 75, 652 and ref. (b).
- e. Based on the reaction:



For (13) and (16) we assumed a somewhat lower A value and inserted $E_0 = 10 \text{ kcal mole}^{-1}$, because in these the H atom is lost from the ring rather than from the added moiety (C_2H_2).

TABLE II
Initiation Steps for Toluene

MINIMAL MECHANISM ($\text{C}_6\text{H}_5\text{CH}_3$)	log A	E_0 (cal mole ⁻¹)	Ref.
T1 $\text{C}_7\text{H}_8 = \text{C}_7\text{H}_7 + \text{H}$	12.9	72,600	9
T2 $\text{C}_7\text{H}_8 = \text{C}_6\text{H}_5 + \text{CH}_3$	11.6	90,000	9
T3 $\text{H} + \text{C}_7\text{H}_8 = \text{C}_6\text{H}_5 + \text{CH}_4$	$1 + 4 \log T$	2,100	estimated
T4 $\text{H} + \text{C}_7\text{H}_8 = \text{C}_7\text{H}_7 + \text{H}_2$	$1.6 + 4 \log T$	2,100	9
T5 $\text{C}_7\text{H}_7 = \text{C}_3\text{H}_3 + 2\text{C}_2\text{H}_2$	14.0	84,800	9
T6 $\text{C}_7\text{H}_7 + \text{H} = \text{C}_3\text{H}_3 + \text{C}_4\text{H}_3 + \text{H}_2$	14.65	80,000	9
T7 $\text{C}_2\text{H}_6 + \text{Ar} = 2\text{CH}_3 + \text{Ar}$	14.6	88,400	estimated
T8 $\text{C}_3\text{H}_3 + \text{C}_3\text{H}_3 = \text{C}_6\text{H}_6$	13.0	-	estimated

TABLE III
Experimental Condition for Representative Shocks

Composition	P_1 (Torr)	u_1 (mm/ μsec)	T_5 (°K)	$\rho_5 \times 10^3$ (g/cc)	Exp'tl Δt (μsec)	Calc Δt (μsec)
2.0% toluene	110	.893	1612	1.93	340	320
"	95	.943	1700	1.64	100	
"	85	.962	1725	1.82	70	
"	65	1.02	1812	1.37	40	50
2.0% benzene	85	.926	1767	1.41	240	240
"	95	.926	1767	1.55	380	
"	85	.926	1767	1.41	360	
"	65	.980	1910	1.51	50	60
"	65	1.00	1950	1.56	50	40

p_1 (Torr): total pressure of fuel plus Ar; Δt (μsec) is interval between the onset of the reflected shock and the toe of the absorption trace.

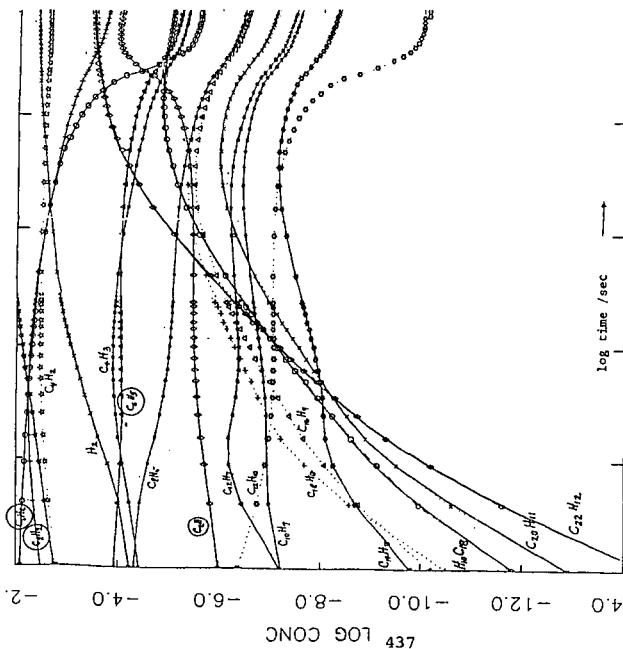


Figure 1. Calculated dependence of mole fraction on time, of various species, for shock heated benzene in argon. $T_1(\text{initial}) = 2120\text{K}$; $T_2(\text{final}) = 1907\text{K}$.

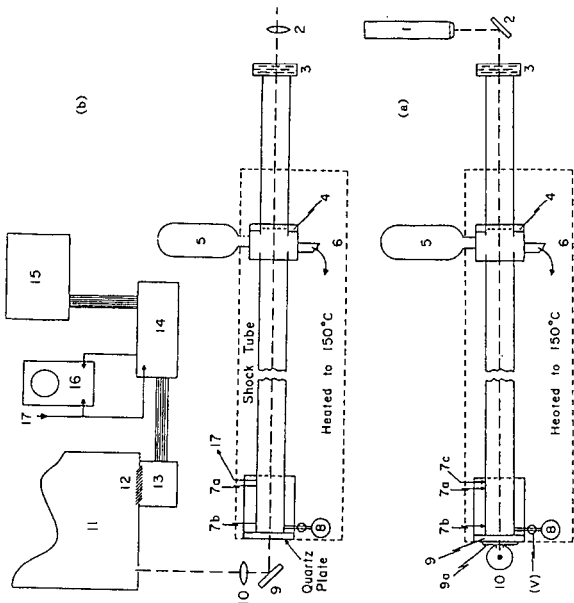
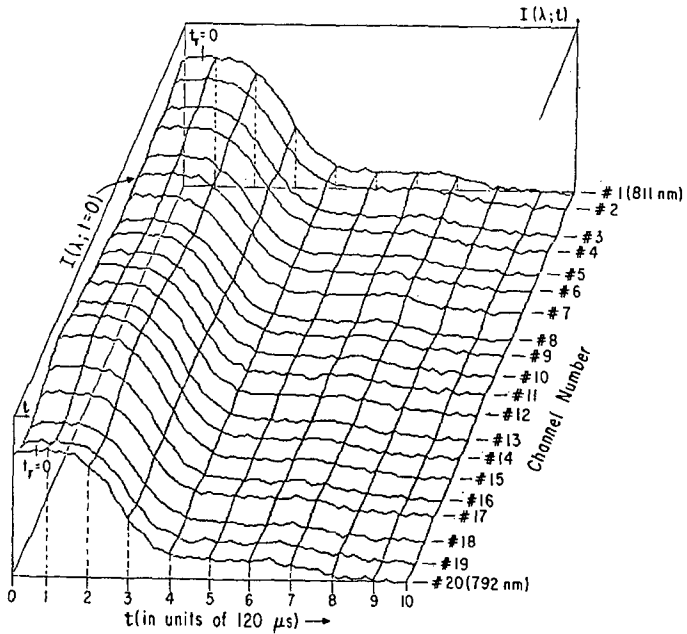
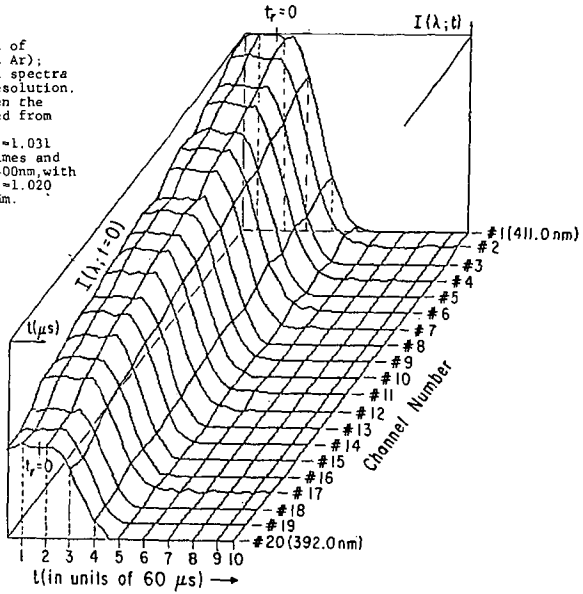


Figure 2. Schematic of shock tube and optical configuration. 1. Microprobe; 2. Plastic back-plate; 3. Diaphragm location; 4. Piezo gauges; 5. Quartz crystal; 6. Sampling port; 7. Piezo gauges; 8. Quartz window; 9. Quartz plate; 10. Microprobe; 11. Monochromator; 12. Linear array detectors; 13. Amplifiers and digitizers; 14. Read and hold; 15. Computer.

Figure 3 Absorption spectra of shock heated toluene (2% in Ar); reflected shock regime. All spectra were recorded with $20 \mu\text{s}$ resolution. $t_r=0$ indicates the time when the incident shock was reflected from the quartz end plate.

(a) Incident shock speed $u_1=1.031 \text{ mm}/\mu\text{s}$. Compare the delay times and absorption rise times for 400 nm , with
 (b) Incident shock speed $u_1=1.020 \text{ mm}/\mu\text{s}$, of spectra at 800 nm .



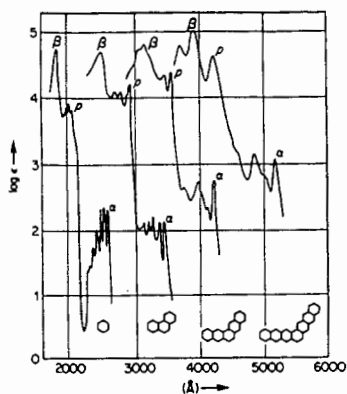
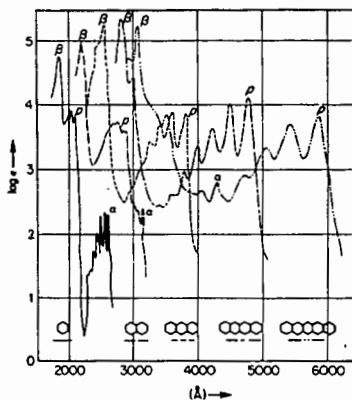


Figure 4. Absorption spectra in the phenylene series



Absorption spectra of the acene series

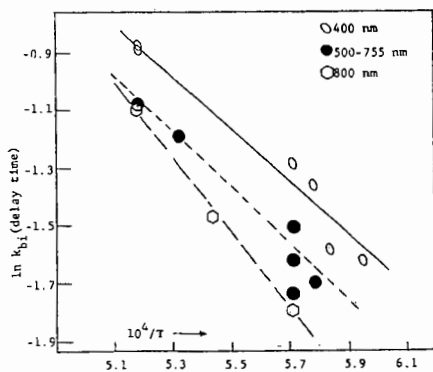


Figure 5a. The delay time for onset of absorption is the reciprocal of a mean bimolecular rate constant (arbitrary units) which decreases with the size of the absorbing units. The largest absorbers (at 800 nm) require a larger activation energy.

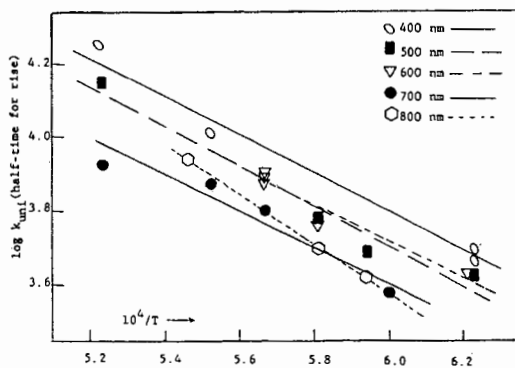


Figure 5b. The mean half-times for generating the larger absorbers increases with increasing size. The 800 nm absorbers require a larger activation energy (≈ 30 kcal/mole) compared to those which absorb at 400 nm (≈ 24 kcal/mole).

COMBUSTION TUBE SOOT FROM A DIESEL FUEL/AIR MIXTURE

L. B. Ebert and J. C. Scanlon

Exxon Research and Engineering; Annandale, NJ 08801

C. A. Clausen

University of Central Florida; Orlando, FL 32816

INTRODUCTION

Used by the Chinese to make inks many years before Christ (1), soot was an environmental nuisance by the time of the industrial revolution (2). Today, soot can be both useful (the carbon black industry) and detrimental (diesel exhaust), so that investigations of soot can impact wide-ranging areas. Curiously, although there is intuitive understanding about the commonality of soots from a variety of sources, including furnace flames, piston engines, combustion chambers, or premixed flames (2), there is no general agreement about the detailed molecular structure of soot. Recently, Zhang, O'Brien, Heath, Liu, Curl, Kroto, and Smalley (ZOHLCKS) proposed to interrelate soot with carbon clusters of icosahedral symmetry (3). They suggested that "the polycyclic aromatic molecules known to be present in high concentrations in sooting flames may therefore adopt pentagonal rings as they grow, so as to generate spheroidal structures which maximize the number of C-C linkages," ultimately yielding a soot nucleus consisting of "concentric, but slightly imperfect spheres" (3). Thus, ZOHLCKS proposed that the spherical morphology of soot particles arose from soot "molecules" of nearly spherical symmetry.

In this paper, we discuss the structural and chemical characterization of soot formed in a combustion tube, in part to address the ZOHLCKS proposal, in part to develop information to compare soot to a variety of other carbonaceous materials.

EXPERIMENTAL DETAILS

Samples of soot were generated at the University of Central Florida by the combination of no. 2 diesel fuel (C-13 NMR aromaticity 19%) with air in a combustion tube of inner diameter 9.8 cm. Sample 1 was generated by injecting the air and fuel (at a mass ratio of 5:1) preheated to 75°C into the combustion tube heated to 1150°C. For sample 2, the combination of air preheated to 600°C with diesel fuel preheated to 350°C in an unheated combustion tube led to spontaneous ignition. The combustion process was allowed to proceed under basically adiabatic conditions; the flame tem-

perature reached a maximum of $\sim 900^\circ \text{C}$. Further information on the diesel fuel is available (4).

X-ray diffraction was performed on a Siemens D-500 using copper radiation. Debye internal interference calculations were done as previously reported (5-7).

Elemental analysis of sample 2 was done by Galbraith. Duplicate runs made on carbon and hydrogen yielded average values of $\% \text{C} = 90.08$ (89.94, 90.21) and $\% \text{H} = 1.76$ (1.82, 1.69) for an average H/C atomic ratio of 0.23. The sample had 0.22%N (N/C= 0.002) and 4.64%O (O/C=0.04). Ash by thermogravimetric analysis was 0.19%.

Sample 2 was reacted with potassium naphthalene (-1) in tetrahydrofuran (THF) at room temperature. A solution of 30 minute old naphthalene radical ion (0.380 g, 2.97 mmol naphthalene in 25.810 g THF; with 2.498 g, 63.9 mmol K°) was added to 0.675 g sample 2. After 2 hours 15 minutes, there was a consumption of 0.404 g, 10.3 mmol K° , determined by weighing the solid K° ; that the total K° uptake of 10.3 mmol exceeded the amount of naphthalene (2.97 mmol) suggested that the deposit was reacting. After 23 hours 15 minutes, there was a consumption of 0.536 g, 13.7 mmol K° and the solution was quenched at 0°C with the addition of solution of 2.836 g CD₂I in 1.845 g THF. The solution was allowed to stand at room temperature under inert gas for 24 hours, and then was filtered through a medium porosity frit. Following drying, the entrained solids weighed 2.589 g; following rotary evaporation, the material which passed the filter weighed approximately 0.29 g. A Bruker MSL was used for D-2 in the solid state (55.283 MHz).

RESULTS AND DISCUSSION. X-RAY DIFFRACTION.

Figure 1 gives the diffraction pattern of sample 2 over the range $15 - 105^\circ 2\theta$ (Cu). There are four readily observed diffraction peaks, which fall into the range normally associated with the (002), (100), (004), and (110) peaks of graphite or other benzenoid arrays. There are no (hkl) peaks having non-zero hk and non-zero l (e.g., (101)), suggesting that the material is turbostratic, meaning that there is no well-defined registry between adjacent planes (as found in the ABAB stacking sequence of graphite). The most intense peak, the (002), arises from interference between approximately parallel aromatic entities, and thus gives information about aromatic stacking. Figure 2 shows that sample 1 and sample 2 have (002) peaks of different widths. Sample 1 has $d(002)$ at 3.63 Å of width 0.122 radians, corresponding to a crystallite size in the direction of aromatic stacking of 12 Å; sample 2 has $d(002)$ at 3.60 Å of width 0.070 radians, corresponding to a crystallite size of 20 Å. (Scherrer constant = 0.9).

The (100) and (110) diffraction peaks give information about the size of the benzenoid array. As given in Figure 3, the linewidths of these peaks suggest sizes of 22 to 28 Å, if one uses a Scherrer constant of 1.84. However, as pointed out by Warren and Bodenstein in a study of carbon blacks (8) and by Ergun (9), the use of the 1.84 constant can give unreliable results for in-plane crystallite sizes < 50 Å. For crystallite sizes near 20 Å (8), the Scherrer constant is about 1.4 for the (100) and about 1.6 for the (110), which then give us crystallite sizes of 21 Å (100) and 19 Å (110).

Knowledge of the lattice constants can allow us to predict microscopic density. For graphite, which has $a_0 = 2.45$ Å (= C - C bond distance of $1.415 \text{ Å} \times \sqrt{3}$) and $c_0 = 6.74$ Å, one obtains a unit cell volume of $(a^2)c \times 0.866 = 35.0 \text{ Å}^3$. This unit cell has four carbon atoms, so we have $8.76 \text{ Å}^3/\text{C}$ atom. This yields a predicted density of 2.28 gram/cm^3 . If we consider the effect of the different c_0 of the soot on density (e.g., (002) at 3.60 Å instead of 3.37 Å), we calculate a unit volume of $9.36 \text{ Å}^3/\text{C}$ atom and a density of 2.13 gram/cm^3 . The changes associated with a_0 are smaller, and in the other direction. Intuitively, and on the basis of the (100) peak, we would expect a limiting sp^2 - sp^2 bond distance of 1.39 Å, and correlative a_0 of 2.41 Å. If we consider the effect of both the increased c_0 and the possible decreased a_0 on density, we find a volume of $9.05 \text{ Å}^3/\text{C}$ and a density of 2.21 gram/cm^3 . The key point from these calculations is that the increase in c_0 found in the soot can change the predicted density only about 7%; this change is not enough to account for the observed densities of 1.8 to 2.0 gram/cm^3 typically found in soots (M. Frenklach, personal communication).

Having appreciable amounts of hydrogen, the soot is better viewed as a "large" polynuclear aromatic rather than as a "small" graphite. Because hydrogen-hydrogen and carbon-hydrogen interactions are key structural determinants for aromatic hydrocarbons, the densities are much lower for the aromatics than for graphite: naphthalene (1.145), anthracene (1.25), phenanthrene (1.182), biphenylene (1.24), pyrene (1.27), picene (1.324), perylene (1.341), and coronene (1.38). Relating observed density to wgt% carbon for the above aromatics, we obtain

$$\text{density} = 0.10814 (\%C) - 8.988 \quad R = .9546$$

If one extrapolated to graphite, using the densities of these hydrocarbons as a guide, one obtains a density of only 1.826.

What do we expect for a soot of spherical carbon clusters? One must consider effects due to intramolecular scattering (analogous to the (100) and (110) peaks in benzenoid

arrays) and due to intermolecular scattering (analogous to the (002) and (004) peaks in graphite).

For intramolecular interference, we have simulated the scattering from one truncated icosahedron of bond length 1.54 Å using the formalism of Debye internal interference, and the results are given in Figure 4. In the figure, the x axis is linear in k , with $k = 2\pi/d = 4\pi\sin\theta/\lambda$ (θ = Bragg angle, λ = wavelength of x-radiation), and one sees two peaks in the range $k = 0.8$ to 2.8 , neither of which are observed in our soot. As one changes the bond length of the icosahedron, one will change the peak maxima in a predictable way, with the coefficient relating bond length to d value given by the Miller index of the peak (5,6). For instance, for the (002) peak in a stack of seven parallel coronene molecules, changing the interplanar spacing from 3.20 Å to 3.95 Å changes the observed d value from 3.16 Å to 3.87 Å (5, 6).

For intermolecular interference between spheroids, let us assume that we can place all carbon atoms on the surface of one spheroid at a distance of ca. 3.6 Å from carbon atoms of some other spheroid. In this way, we can get a "(002)" peak at 3.6 Å, as observed in the soot, but one notes that the linewidth of such a peak will correspond only to a "stack" of two aromatics (crystallite size ca. 7.2 Å). If one goes to the concentric shell model (Figure 4 of ref. 3), one can obtain a larger apparent stack height; to account for the data on sample 2, one would need 5 to 6 shells (20 Å/3.6 Å) to obtain the observed (002) linewidth. Such an entity would have a large fraction of non-protonated (quaternary) aromatic carbon atoms, just as graphite does, and, from a chemical point of view, would be more like graphite than aromatic hydrocarbons. To address this more fully, we performed chemical experiments on sample 2.

BACKGROUND. CHEMICAL REDUCTION.

The use of potassium naphthalene (-1) in THF to reduce fossil fuel materials has been reviewed by Stock (10) and by Ebert (11). If one wants to distinguish graphite-like chemistry from polynuclear aromatic hydrocarbon chemistry, reduction by naphthalene (-1) followed by alkylation by alkyl iodide is useful because different products are obtained. Graphite is reduced by naphthalene (-1) and correlatively intercalated by K^+ and THF; the potassium intercalate is not alkylated by alkyl iodides. Aromatic hydrocarbons of reduction potential less negative than the -2.5 V (vs. SCE) of naphthalene (-1) will be reduced to anions, which can then (usually) be alkylated by alkyl iodides to give products in which the alkyl group is attached to an sp^3 -hybridized carbon of the reduced aromatic.

With respect to the reduction, there has been a belief in the literature that aromatic hydrocarbons can form numer-

ous highly charged poly-anions driven by the presence of excess alkali metal. Examples include the dianion of naphthalene (10) and tetraanions of pyrene and perylene. Noting that the difference in reduction potential between the radical anion and dianion of anthracene is 0.48 V (12), one would expect the dianion of naphthalene to have a reduction potential of at least -2.98 V (vs. SCE), near that of K° itself; we are unaware of any work in which a second reduction peak has been measured for naphthalene and in fact with pyrene third and fourth reduction peaks are not seen (13).

Relevant to the shell proposal for soot of ZOHLCKS (3), Stock proposed that the reductive alkylation of coal suggested a model "in which molecular fragments of coal are peeled away from the solid as layers from an onion" (10). To address this, we performed reductive methylation (with CD_3I) of Burning Star coal to determine if methyl groups added preferentially to the "soluble" phase (14). The coal consumed 10.4 mmol K/g, and, following alkylation, 52% of the product carbon was in the "THF-soluble" phase and 48% in the "THF-insoluble" phase. Solid state 2D NMR showed CD_3 groups in both phases, with the THF-soluble phase having only 87% of the deuterium of the insoluble phase, on a per carbon atom basis! The spectrum of the insolubles showed only a first order quadrupole split spectrum (separation = 51.7 G, indicative of three-fold rotation of bound $-CD_3$ groups) but the solubles showed a strong (averaged) central peak and a quadrupolar split line. Significantly, these results for coal, which are those expected for alkylation of aromatics and heterocyclics, are similar to what we report here for soot.

RESULTS AND DISCUSSION. REDUCTIVE ALKYLATION.

At 23 hours 15 minutes, the soot took up 15.9 mmol K/gram, correcting for consumption of potassium by naphthalene(-1). Figures 5 and 6 give the 2D NMR of the solid solubles and insolubles, and we see that the soot has behaved like a polynuclear aromatic in being alkylated by CD_3I . Figure 7 gives the 2D NMR of the solubles in methylene chloride, showing CD_3 groups bound primarily to sp^3 carbon, as expected for the reductive alkylation of polynuclear aromatics (15); some methylation of oxygen does occur.

One might be concerned with contamination of the THF-soluble sample by vast amounts of 1,4 dimethyl 1,4 dihydro naphthalene. Actually, naphthalene (-1) reduces methyl iodide to methyl radicals, in contrast to anions of larger aromatics which do in fact undergo alkylation (15, 16). Analysis of the THF-solubles by GC/MS, with quantification by flame ionization detection, shows the ratio of naphthalene to the most abundant dimethyl dihydro naphthalene to be 19.7/1; this is consistent with solution phase ^{13}C NMR which

shows three sharp aromatic peaks at 125.7, 127.7, and 133.3 δ , the shift positions of naphthalene itself. The underlying aromatic envelope goes from 120 to 146 δ , and there are aliphatic peaks at 14.2, 22.8, 25.9, 29.4, 29.7, 30.09, 30.34, 31.98, 34.26, and 37.46 δ . Aliphatic carbon bound to oxygen is suggested by a peak at 68 δ .

In conclusion, we see that the soot anion, in being alkylated by CD₁, behaves as anions of larger polynuclear aromatics, such as perylene and decacyclene (16) and not like the anion of graphite with K⁺. Naphthalene, with excess K⁺, behaves as naphthalene (-1).

Acknowledgements--We thank Mike Matturro for giving us the atomic coordinates of the 60 atom truncated icosahedron, Rod Kastrup for for the high resolution NMR spectra, and Manny Garcia for the D-2 NMR of solid samples.

REFERENCES

1. Y. Schwob, Chem. Phys. Carbon, 15, 109 (1979).
2. H. GG. Wagner, 17th Symposium on Combustion, pp. 3-19 (1978).
3. Q. L. Zhang, S. C. O'Brien, J. R. Heath, Y. Liu, R. F. Curl, H. W. Kroto, and R. E. Smalley, J. Phys. Chem., 90, 525 (1986).
4. Oak Ridge National Laboratory report ORNL/TM-9196 (November 1983).
5. L. B. Ebert, J. C. Scanlon, and D. R. Mills, Preprints, Petroleum Division of the Amer. Chem. Soc., 28(5), 1353 (1983).
6. _____, Liq. Fuels Technology, 2, 257 (1984).
7. _____, Preprints, Petroleum Division of the Amer. Chem. Soc., 30(4), 636 (1985).
8. B. E. Warren and P. Bodenstein, Acta Cryst., 18, 282 (1965).
9. S. Ergun, Chem. Phys. Carbon, 3, 211 (1968).
10. L. M. Stock, in Coal Science, Academic, 1982, pp. 161-282.
11. L. B. Ebert, in Chemistry of Engine Combustion Deposits, Plenum, 1985, pp. 303-376,
12. A. J. Bard and L. R. Faulkner, Electrochemical Methods, Wiley, 1980, p. 701.
13. J. Mortensen and J. Heinze, Tet. Lett., 26, 415 (1985).
14. A. R. Garcia, L. B. Ebert, and B. G. Silbernagel, Extended Abstracts of the 18th Biennial Carbon Conference, July, 1987.
15. L. B. Ebert, G. E. Milliman, D. R. Mills, and J. C. Scanlon, in Advances in Chemistry Series No. 217 (Polynuclear Aromatic Hydrocarbons), Amer. Chem. Soc., 1987.
16. L. B. Ebert, D. R. Mills, and J. C. Scanlon, Preprints, Petroleum Division of the Amer. Chem. Soc., 32(2), 419 (1987).

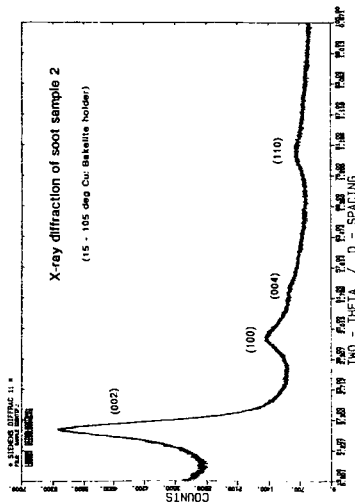


Figure 1. X-ray diffraction of sample 2.

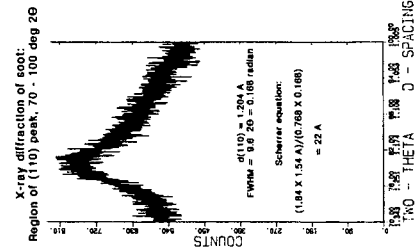
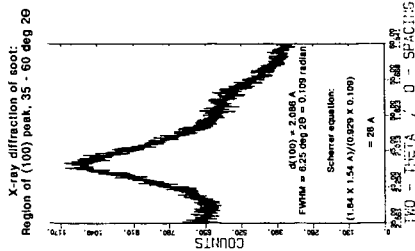


Figure 3. X-ray diffraction: (100) and (110) of sample 2

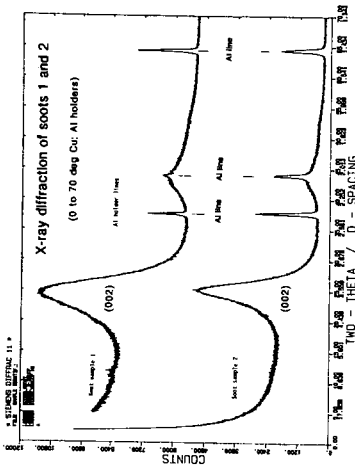


Figure 2. X-ray diffraction comparison: 1 vs. 2.

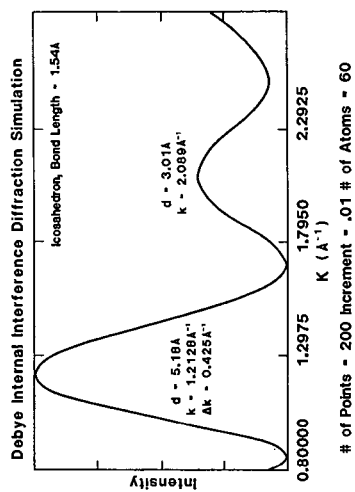


Figure 4. X-ray diffraction simulation: truncated icosahedron

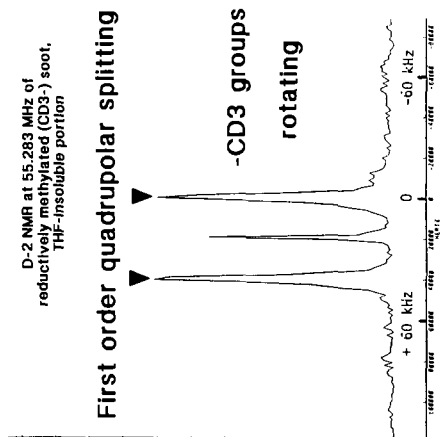
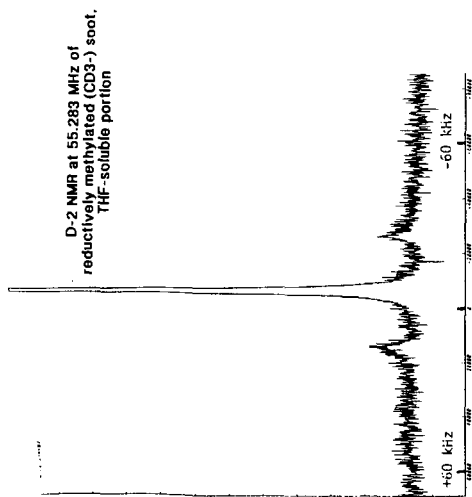


Figure 5. D-2 NMR of Me-soot THF-solubles

Figure 6. D-2 NMR of Me-soot THF-insolubles

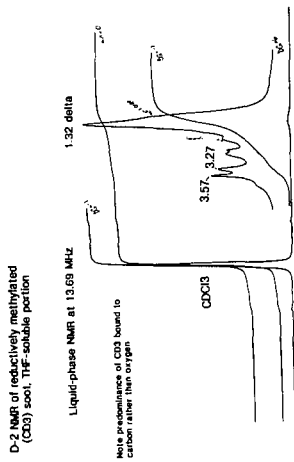


Figure 7. High resolution D-2 NMR of THF-sol

SINGLE PULSE SHOCK TUBE STUDIES ON
THE STABILITY OF 1-PHENYLBUTENE-2

J. P. Cui*, Y. Z. He* and W. Tsang

Chemical Kinetics Division
National Bureau of Standards
Gaithersburg, Maryland 20899

ABSTRACT

1-Phenylbutene-2(1-PHB-2) has been decomposed in single pulse shock tube experiments. Acetylene formation is used as a measure of the rate of cleavage of the benzyl-vinyl C-C bond. The rate expression for this reaction has been found to be

$$k(1\text{-PHB-2} \rightarrow \text{benzyl} + \text{propenyl}) = 2.4 \times 10^{16} \text{ Exp}(-43780/T) \text{ /s.}$$

The A-factor for this process is unexpectedly large. It may be indicative of a larger than usual combination rate constant for vinyl radicals. Possible sources of experimental errors are considered. Our results are consistent with a bond dissociation energy for the primary vinyl C-H bond in propylene of 475 ± 10 kJ/mol.

INTRODUCTION

This paper is concerned with the strength of the primary vinyl C-H bond in propylene. The present results should provide additional information on the energy of the vinyl C-H bond in ethylene. Within the past year there have been values ranging from 435 to 495 kJ/mol^{1,2}. Any effect from methyl substitution will be far smaller than the spread of such numbers. The importance of the this quantity is due to the evidence³ that vinyl radicals are key reactive intermediates for soot formation. Unfortunately, there is at present almost no rate data on vinyl radical reactions and the uncertainty with regard to its heat of formation prevents even the most rudimentary efforts at estimation.

The experiments are carried out in a heated single pulse shock tube⁴. Our target molecule is 1-phenyl butene-2 (1-PHB-2). The choice of this molecule is dictated by the weakening of the vinyl C-C bond by benzyl resonance and the decreased stability of the propenyl radical compared to that of the vinyl radical itself (had we chosen to work with allylbenzene). The former lowers the rate constant to a range which is more convenient for our purposes. Nevertheless, the rate constants are still very much smaller than those for alkane and alkene decomposition that we have hitherto studied. This creates certain problems. The existence of a unique reaction product, acetylene, from the decomposition of the propenyl radical, should reduce complications.

The key factors in obtaining high accuracy results from single pulse shock tube work are the great simplifications in the reaction mechanism and the use of an internal standard reaction to calibrate for the conditions in the experiments. The general methodology has been successfully used to give a complete picture of the decomposition of many organic compounds⁵.

*Guest Scientists: Permanent Address, Institute of Mechanics, Academia Sinica, Beijing, China

There have been no previous studies on 1-PHB-2 decomposition. In Figure I(1), we outline a number of possible competitive unimolecular decomposition processes. From published bond energies one expects that they will be close to that for the vinyl-benzyl bond⁶. Unfortunately, these decomposition channels do not lead to unique products and it will not be possible to obtain accurate information on the rate constants for these reactions. This also makes it important to work at extents of conversion.

EXPERIMENTAL

The experiments are carried out in a heated single pulse shock tube maintained at 110 °C. All of the gas sampling systems are maintained at temperatures close to or above this value. It is thus possible to work with very low volatility substances. Analysis of the products was by gas chromatography using a 30 meter polydimethylsiloxane capillary column for all substances with carbon numbers 5 or higher. For the light hydrocarbons we use a dinonylphthalate coated silica column. This column eluted acetylene between propylene and isobutene. Unfortunately, the retention time of allene also fell in this position. From separate experiments we determined that our yields of allene was uniformly of the order of 4% of the acetylene yield. The 1-PHB-2 from K & K⁷. Gas chromatographic analysis indicated that it is mostly the trans compound with about 3% cis. There are also a number of other impurities. These included n-butylbenzene and s-butyl benzene. In these molecules, the normal C-C bonds are weakened by benzyl resonance. Since these are much more labile than vinyl C-C bonds, we observe under all conditions large quantities of their dissociation products. However under our conditions it is not possible to form acetylene from these starting materials.

In Figure I we enumerate the most likely decomposition modes of 1-PHB-2. Note that for methyl or larger alkyl radicals addition will be reversed, while the abstraction products will be the same as that for hydrogen atoms. The key conclusion from an examination of these possibilities is that under conditions of small extent of decomposition of the parent compound there is no channel that can lead to acetylene formation except through the sequence of reaction initiated by the cleavage of the propenyl-benzyl bond, followed by beta elimination of the methyl group.

Our concern with these factors arises from the high stability of the 1-phenylbutene-2 which prevents us from carrying out our experiments under conditions of enormous excesses of scavenger (100 to 1000 to 1). Indeed, a scavenger such as toluene will have rates of decomposition less than an order of magnitude slower. With a 100 to 1 ratio the scavenger will be producing more radicals than our test compound and will then have the capability of inducing decomposition. With this in mind, our highest scavenger 1,2,4-trimethylbenzene (1,2,4-TMB) to 1-PHB-2 ratio was 8 to 1. This appeared to be sufficient since our results with a 2 to 1 ratio are within experimental error the same as that at 8 to 1. The composition of the mixtures used and the range of conditions are summarized in Figure II.

The internal standard used in these studies is the reverse Diels Alder decomposition of 1-methylcyclohexene (1-MCH). We have previously established⁸ its rate expression for decomposition into 2-methyl-butadiene-1,3(isoprene) and ethylene as

$$k(1\text{-MCH} \rightarrow \text{isoprene} + \text{C}_2\text{H}_4) = 10^{15} \text{ Exp}(-33500/T)/s$$

This standard is used because isoprene is not a reaction product in 1-PHB-2 decomposition and it elutes from our capillary column in a region where there are no interfering peaks.

RESULTS

The distribution of products from the shock induced decomposition of 1-phenylbutene-2 in the presence and absence of the scavenger 1,2,4-TMB can be found in Table I. The important points to be noted are the changes in relative concentrations. We assume that acetylene is essentially a primary product and its concentration will not be effected by the absence and presence of the scavenger. Our results are in accord with the expectation that some of the reactive radicals will be removed by the 1,2,4-TMB. However, although there is a decrease in the yields of the lighter products (for example, propylene, butadiene) relative to that of acetylene as the amount of the inhibitor, 1,2,4-TMB is increased, we cannot be certain that we have been able to stop completely the radical induced decomposition. This is not unreasonable, since as noted earlier the thermal stability characteristics of 1-PHB-2 is not that much different than the inhibitor. Thus there approaches a point where our inhibitor will in fact be contributing to the pool of active radicals. It is interesting to note that the material balance with regard to 1-MCH decomposition improves with scavenger addition. Paralleling this is the decrease in the quantity of 1-PHB-2 destroyed when the scavenger is added. Clearly in the absence of the scavenger there are radical catalyzed decomposition channels.

For our purposes we concentrate on the acetylene from 1-PHB-2 decomposition and isoprene from 1-MCH decomposition. Figure II contains the comparative rate plots for the formation of acetylene from 1-PHB-2 decomposition and isoprene from 1-MCH decomposition. The rate constants are derived from the relation

$$\begin{aligned} \text{Log}(k(\text{acetylene})) &= \text{Log}((\text{acetylene})_f / (1\text{-PHB-2})_i) / t \\ \text{Log}(k(\text{isoprene})) &= \text{Log}(1 - (X * (\text{isoprene})_f / (1\text{-MCH})_i)) / X t \end{aligned}$$

where $X = 1 + ((\text{MCH})_i - (\text{MCH})_f - (\text{isoprene})_f) / ((\text{isoprene})_f)$ and takes into account the possibility that some of the 1-MCH $((\text{MCH})_i - (\text{MCH})_f - (\text{isoprene})_f)$ will be decomposed through radical attack. We have no means of determining how much isoprene is destroyed. Thus it is essential in the 1-MCH decomposition to obtain the best possible mass balance. This is attained when the scavenger is added. As will be seen below, in the absence of scavenger comparative rate results are different than in its presence. The relation for acetylene appearance assumes negligible 1-PHB-2 disappearance. From the data in Table I it can be seen that this is attained in the studies with the scavenger. We assume that the conversion of the trans to the cis form will not effect our results. An interesting aspect of the data in Table I is that we can extract rate constants for the trans \rightarrow cis isomerization of 1-PHB-2 as well and the decomposition of nbutyl- and sbutyl-benzene. In all three cases they fall in the expected range.

The comparative rate expressions relating the rate constant for acetylene and isoprene formation in 1-PHB-2 and 1-MCH decomposition are as follows;

$$\text{Log}(k(\text{acetylene})) = 1.308 + .014 \text{Log}(k(\text{isoprene})) - 3.030 + .034$$

(1% 1-PHB-2 and 200 ppm 1-MCH)

$$\text{Log}(k(\text{acetylene})) = 1.312 + .015 \text{Log}(k(\text{isoprene})) - 3.256 + .036$$

(1% 1,2,4 TMB; .5% 1-PHB-2 and 100ppm 1-MCH)

$$\text{Log}(k(\text{acetylene})) = 1.304 + .034 \text{Log}(k(\text{isoprene})) - 3.198 + .087$$

(2% 1,2,4 TMB; .25% 1-PHB-2 and 50 ppm 1-MCH)

Substituting into these relations the rate expression for the reverse Diels-Alder decomposition of 1-MCH given above, we obtain the following rate expression for acetylene formation in 1-PHB-2 decomposition $k(\text{acetylene}) = 3.8 \times 10^{16} \text{Exp}(-43800/T) / \text{s}$, $k(\text{acetylene}) = 2.6 \times 10^{16} \text{Exp}(-43900/T) / \text{s}$ and $k(\text{acetylene}) = 2.3 \times 10^{16} \text{Exp}(-43670/T) / \text{s}$ respectively.

It will be noted that the last two expressions are virtually identical, while the first rate expression is about 30 % larger. This is due to the contribution from the radical induced decomposition of 1-MCH and isoprene and is of the magnitude expected on the basis of our mass balance considerations. The agreement in the other two cases suggest that enough inhibitor has now been added so that the radical induced decomposition no longer poses a serious problem. The similarity in the activation is also interesting. It suggests that the contribution from the induced decomposition has very similar temperature dependence as the direct unimolecular decomposition. Our best rate expression for the breaking of the vinyl-benzyl bond is thus the average of our results in studies carried out in the presence of 1,2,4 TMB or

$$k(1\text{-PHB-2} \rightarrow \text{benzyl} + \text{propenyl}) = 2.4 \times 10^{16} \text{Exp}(-43780/T) / \text{s}$$

DISCUSSION

We will now use our rate expression for the breaking of the benzyl-vinyl bond to derive the bond energy of the primary C-H bond in propylene. From the usual assumption regarding the absence of temperature dependence for the reverse combination reaction, the relations are

$$\Delta H (\text{reaction}) = \Delta E (\text{activation Energy}) + RT$$

or $\Delta H = 409.6 \text{ kJ/mol}$ at 1150K. Since

$$\Delta H (\text{reaction}) = H_f(\text{benzyl}) + H_f(\text{propenyl}) - H_f(1\text{-PHB-2}) \text{ at } 1150\text{K}.$$

substituting the heat of formation of benzyl and 1-PHB-2 lead to $H_f(\text{propenyl}) = 269.5 \text{ kJ/mol}$. at 1150K. We have calculated the thermodynamic quantities of benzyl using the prescription of Benson and O'Neal⁹ and a value of 205 kJ/mol for the heat of formation at 300K. This is 6 kJ/mol higher than the number recommended by McMillen and Golden⁶, but is a value that we obtained some years ago on the basis of isobutyl benzene decomposition¹⁰. This leads to a heat of formation of 180.7 kJ/mol at 1150K. The heat of formation of 1-PHB-2 at 1150K is taken to be 80.3 kJ/mol and is based on the heat of formation of butylbenzene and an average value of 133 kJ/mol for the heat of dehydrogenation¹¹. Assuming that the heat capacity of propenyl is an average of that of propene and propyne leads to

$$\text{BDE}(\text{propene} \rightarrow \text{propenyl} + \text{H}) = 484 \pm 8 \text{ kJ/mol}$$

There have been no previous measurement of this bond dissociation energy. However, it should not be too far off from the value for ethylene. Our number is extraordinarily high and had it not been for the recent value of Shiromaru and coworkers would be the highest ever reported for such a bond. Most kinetic results appear to favor very low values.

The A-factor for acetylene formation, 2.4×10^{16} /s, is large in comparison to that for processes that involve the breaking of a benzyl-alkyl bond. In these cases A-factors are more in the range of one-half to one order of magnitude smaller. Our high number is reflected in the rate constant of the reverse recombination reaction. It is of interest to calculate the combination rate constant for benzyl attack on propenyl using our A-factor. From the estimated entropies we find that $\Delta S = 148 \text{ J/mol-K}$. Substitution into the relation,

$$A_f/A_b = \exp(-\Delta S/R)/eRT$$

leads to $A_b = k_b = 11 \times 10^{10} \text{ l/mol-s}$, with an uncertainty of a factor of 3. This is a large rate constant. It is much larger than the values for comparable processes involving alkyl radicals. Thus an interesting consequence of this study is that higher vinyl C-H bond energies not only lead to longer lifetimes for the decomposition of vinyl type radicals but predicts higher combination rates with other radicals.

In view of the unexpectedly larger recombination rates, it is important to consider possible sources of uncertainties in our measurements. The chief source of error is probably in the definition of the reaction mechanism. We have assumed that all the acetylene must be formed from the cleavage of the benzyl-vinyl C-C bond and that this will be followed by beta C-C bond cleavage. While we believe that these embody the main reactions, the fact that we are making a slope measurement means that small errors may lead to substantial errors. Probably the most serious is the assumption of beta C-C bond cleavage in propenyl decomposition and ignoring the possibility of a 1-3 bond shift leading to an allyl radical which will be fairly stable under our conditions. This assumption is based on the behavior of alkyl radicals. In the present case there may be some enhancement due to the much larger reaction exothermicity for the 1-3 shift (in excess of 60 kJ/mol). However, since we are dealing with a doubly bonded structure there will be an extra degree of strain in the transition state. Furthermore, in the decomposition of o-iodotoluene where we make the o-methylphenyl radical, which is structurally very similar to propenyl, there does not appear to be any evidence for such a shift. It should be noted that if such an effect is to make a contribution it will bias the results towards higher activation energies. The A-factor for 1-3 H-shift is smaller than that for beta C-C bond fission and this must be compensated for by a lower activation energy if this process is to make any contribution. Similarly, since the lowest energy path for acetylene formation in our system is the breaking of the benzyl-vinyl bond, then any other contribution will also lead to an increase in measured activation energy. On this basis we believe that to some extent our activation energy is an upper limit. A lower limit is set by the A-factor for the decomposition of a compound such as ethylbenzene or 4×10^{15} /s. This leads to a more "normal" A-factor $1.8 \times 10^{10} \text{ l/mol-s}$. Scaling our activation energy to obtain the same rate constant will lead to a value of 346 kJ/mol or a bond dissociation energy

of 465 kJ/mol. Taking the average of these two values we arrive at 475±10 kJ/mol as the most likely value. This is still a very large number. It is a reflection of the fact that our measured rate constants are much too small to be consistent with a low vinyl-H bond energy.

In a similar fashion it is interesting to consider the consequences of a bond dissociation energy in the 435 kJ/mol range. Assuming our rate constant to be correct, this will imply an A-factor of 3×10^{14} /s and a rate constant for combination of close to 10^9 l/mol-s. This strikes us as an extremely low and unlikely value. Even more unlikely is the highest reported value for the C-H bond energy in ethylene since this will lead to an A-factor of 2.5×10^{17} /s and a recombination rate of 11×10^{11} l/mol-s. or larger than collisional. On the other hand, a somewhat higher rate constant for vinyl radical combination is in line with increasing evidence for a very small disproportionation to combination rate constant ratio for vinyl radicals reacting with itself.

REFERENCES

1. Shiromaru, H., Achiba, Y., Kimura, K., and Lee, Y. T. J. Phys. Chem., 1987 91,17
2. Kiefer, J. H., Wei, H. C., Kern, R. D., and Wu, C. H., Int'l J. Chem. Kin.,1985, 17, 225
3. Frenklach, M; Gardiner W. C., Clary, D. and Stein, S. E., 21st Symposium on Combustion, in press
4. Robaugh, D. and Tsang, W., J. Phys. Chem., 1986, 90, 5363
5. Tsang, W, "Comparative-Rate Single Pulse Shock Tube Studies on the Thermal Stability of Polyatomic Molecules," in Shock Waves in Chemistry (A.Lifshitz, ed) Marcel Dekker, New York, 1981, pg 59
6. McMillen, D.F. and Golden, D. M. Annu. Rev. Phys. Chem., 1982, 33, 493
7. Certain commercial materials and equipment are identified in this paper in order to specify adequately the experimental procedure. In no case does such identification imply recommendation of endorsement by the national Bureau of Standards, nor does it imply that the material or equipment is necessarily the best available for the purpose
8. Tsang, W., Int'l. J. Chem. Kin.,1978, 10, 599
9. O'Neal, H. E. and Benson, S. W., "Thermochemistry of Free Radicals" in "Free Radicals, Vol II" (J. Kochi, ed) John Wiley and Sons, 1973, pg 275
10. Tsang, W., Int'l. J. Chem. Kin., 1969, 1, 245
11. Stull, D. R., Westrum, E. F.; and Sinke, G. C.; "The Chemical Thermodynamics of Organic Compounds", John Wiley and Sons, 1969

Figure I: Important Steps in 1-Phenylbutene-2 Decomposition

1. Unimolecular Decomposition
 - a. C-H bond split $C_6H_5CH_2CH=CHCH_3 \rightarrow C_6H_5C\dot{C}H=CHCH_3 + H$
 $\rightarrow C_6H_5CH_2\dot{C}H=CHCH_2 + H$
 - b. C-C bond splits $C_6H_5CH_2CH=CHCH_3 \rightarrow C_6H_5 + \dot{C}H_2CH=CHCH_3$
 $\rightarrow C_6H_5CH_2 + \dot{C}H=CHCH_3$
2. Radical Attack (abstraction and addition)
 - a. $C_6H_5CH_2CH=CHCH_3 + R \rightarrow C_6H_5CHCH=CHCH_3 + RH$
 $\rightarrow C_6H_5CH_2CH=CH\dot{C}H_2 + RH$
 - b. $C_6H_5CH_2CH=CHCH_3 + H \rightarrow C_6H_6CH_2CH=CHCH_3$
 $\rightarrow C_6H_5CH_2CH_2\dot{C}HCH_3$
 $\rightarrow C_6H_5CH_2CHCH_2\dot{C}H_3$
3. Decomposition of Radicals

$CH_2\dot{C}H=CHCH_3 \rightarrow CH_2=CH\dot{C}H=CH_2$
 $C_6H_5CHCH=CHCH_3 \rightarrow C_6H_5\dot{C}H=CHCH=CH_2 + H$
 $C_6H_5CH_2CH=CHCH_2$
 (stabilized)
 $C_6H_6CH_2\dot{C}H=CHCH_3 \rightarrow C_6H_6 + CH_2\dot{C}H=CHCH_2$
 $C_6H_5CH_2CH_2\dot{C}HCH_3 \rightarrow C_6H_5CH_2 + C_3H_6$
 $C_6H_5CH_2CHCH_2\dot{C}H_3 \rightarrow C_6H_5CHCH=CH_3 + CH_3$
 $\dot{C}H=CHCH_3 \rightarrow \dot{C}H=CH + CH_3$
4. Decomposition Products from Impurities (nbutylbenzene, sbutylbenzene) leading to ethylene, styrene, methyl, methane, ethane, etc.

Figure II: Comparative Rate Studies on the Formation of Benzyl and Propenyl from 1-PHB-2 and 1-MCH Decomposition; 1% 1-PHB-2 and 200 ppm 1-MCH in Argon (□); 1% 1,2,4-TMB, .5% 1-PHB-2 and 100ppm 1-MCH in Argon (*); and 2% 1,2,4 TMB, .25% 1-PHB-2 and 50 ppm 1-MCH in Argon(●). Temperature, 1092-1221 K; Residence time 500 microseconds.; Pressure, 2.5-3.5 atms.

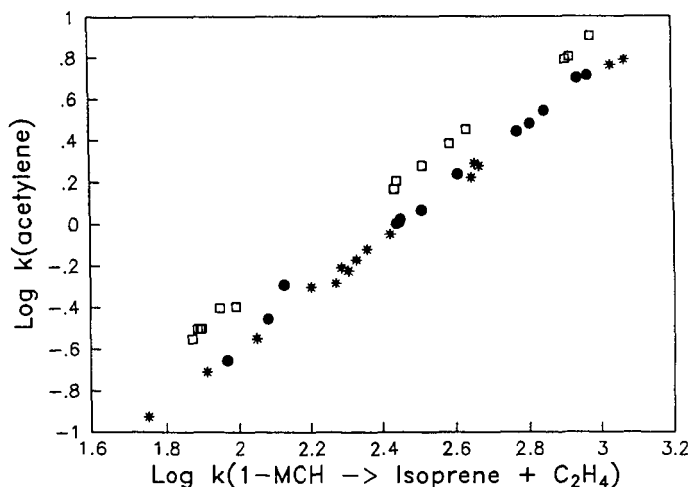


Table I: Typical Gas Analysis Results from the Decomposition of 1-Phenylbutene-2
(in units of 10³ x mole fraction)

A) Normalized against initial mixture (composition; 964, trans 1-PHb-2; 21, cis 1-PHB-2; 12, s-Butylbenzene; 2.6 n-Butylbenzene)

Mixtures	1% (1-PHB-2) in Argon	1% (1-PH-2) 200ppm (1-MCH) in Argon	1% (1,2,4TMB) .5% (1-PHB-2) 100ppm (1-MCH) in Argon	2% (1,2,4-TMB) .25% (1-PHB-2) 50 ppm (1-MCH) in Argon
Methane	8.3	6.6	5.8	11.4
Ethane, Ethene	6.9	2.0	4.2	8.2
Propylene	9.6	7.7	1.7	3.5
Acetylene	1.3	.81	.3	.74
Butenes	1.5	1.3	.45	.8
1,3 Butadiene	3.5	2.5	.76	1.7
Benzene	2.5	1.7	.57	1.2
Toluene	2.8	1.8	.82	1.8
Ethylbenzene	3.4	2.5	.5	1
m,p-Xylene			1.4	2.9
Styrene	6.5	5.0	2.0	3.6
o-Xylene			.5	1.0
Allylbenzene	5.8	4.6	1.1	2.1
s-Butylbenzene	7.4	8.5	11.2	10.4
n-Butylbenzene	2.2	2.2	2.3	2.5
1-PHB-2 trans	860	860	916	945
cis	62	57	30	50
				76
				85
				35

b) Normalized against 1-MCH

Isoprene	133	34	91	178	234	53
1-MCH	807	944	904	780	744	934
Temperature(K) (based on Isoprene yields)	1160	1105	1143	1172	1185	1121

Reaction Time: 500 microseconds; Pressure: 2.8-3.2 atm.

The Correlation of Benzene Production with Soot Yield Determined from Fuel Pyrolyses

R.D. Kern, C.H. Wu, J.N. Yong, K.M. Pamidimukkala and H.J. Singh

Department of Chemistry
University of New Orleans
New Orleans, Louisiana 70148

Introduction

The rate of production of soot in pyrolytic reaction systems has been studied in shock tubes using a variety of non-intrusive analytical techniques; laser extinction (LEX)¹⁻⁶, static analysis of the product distribution from single pulse shock tubes (SPST)⁷⁻⁹, and dynamic analysis of the reflected shock zone by time-of-flight mass spectrometry (TOF)¹⁰. The data reduction process often involves measurement of a changing bulk quantity; e.g., attenuation of a He-Ne laser beam due to absorption by high molecular weight gas phase species and discrete soot particles via LEX or deficiencies in the carbon atom mass balance via SPST or TOF. The concentrations of the various polycyclic hydrocarbons formed in the pre-particle soot chemistry phase are extremely low⁹ and are below the detectability limit of the TOF technique¹⁰ which is about 10^{-10} mol cm^{-3} . The non-detected hydrocarbons constitute the "missing" mass.

The ultimate goal of the work in this area is to write a complete chemical mechanism for soot formation. This formidable task has been attempted for acetylene¹¹. Some 180 species and 600 reactions were considered in an effort to model the soot yield obtained by LEX. Both the calculated and experimental yields were very low (< 1%). Comparison of the calculated results with the measured bulk quantity was obtained by assuming that all species in the model having $MW > 300$ absorbed 632.8 nm radiation. The summation of these high molecular weight concentrations converted to carbon atoms cm^{-3} and divided by the input carbon atom concentration yielded the computed soot yield.

The effort herein is to develop a correlation between a readily observable molecular species whose presence is diagnostic of subsequent soot formation and the bulk observables of laser extinction and mass balance deficiency.

Experimental Techniques Employed

LEX has been utilized behind incident and reflected shock waves during various observation times ranging from 0.5-2.5 ms¹⁻⁶. In order to compare the relative sooting tendencies of fuels, a total carbon atom concentration of 2×10^{17} atoms cm^{-3} was chosen for such fuels as ethylbenzene, toluene, benzene, pyridine, allene, 1,3 butadiene, vinylacetylene, and acetylene. The soot yield vs the no-reaction shock zone temperature curves are bell-shaped. Aromatic compounds produced the greatest amount of beam attenuation or soot yield while

acetylene exhibited the least. The early LEX work¹⁻³ reported values for the absolute soot yield on the order of 80 - 90% conversion of aromatic fuels to soot. It was subsequently realized that these values were too high due in part to uncertainty of the literature value for the refractive index of soot and to light absorption by pre-particle species.⁴ It was also known that a significant amount of soot formation occurred in the accompanying cooling wave.^{7,8} For these and other reasons, the ordinate for soot yield plots was taken to be $E(m) \times$ soot yield with the value of $E(m)$ left unspecified pending resolution of the uncertainties.^{4,5} This adjustment cast the LEX results as a measurement of relative rather than absolute soot yields.

The thrust of the mass balance deficiency procedure was to add up all of the carbon containing products detected and subtract from the total carbon atoms in the original fuel. Aromatic compounds showed the greatest deficiencies (with the notable exception of pyridine⁶) and acetylene the least. There was good agreement with regard to the relative sooting tendencies of fuels investigated with LEX and the mass deficiencies obtained by SPST and TOF.

The TOF method offers the advantage of recording the product distribution at selected times during the reaction. Concentration profiles of various observed species are constructed within the m/e range of 12 - 300 during typical observation times of ~ 0.75 ms. The data are fit with computed lines from proposed or known mechanisms. Benzene has been recorded during the pyrolyses of allene¹², 1,2 butadiene¹³, and 1,3 butadiene¹⁴. The profiles have been modeled using the CHEMKIN program^{15,16} with reasonable success.

Results and Discussion

In order to mimic the soot bells determined by LEX, benzene concentrations were modeled for the thermal decompositions of C_3H_4 ¹², 1,2 C_4H_6 ¹³, 1,3 C_4H_6 ¹⁴, C_4H_4 ¹⁷, C_5H_5N ¹⁸, and C_2H_2 ¹⁹. In each of these pyrolyses investigated by the TOF method, the total carbon atom concentration was approximately 2×10^{17} atoms cm^{-3} . The benzene concentrations were calculated for each of these fuels at 1 ms as a function of no-reaction shock temperature in order to compare with the LEX work. The TOF and LEX results are shown in Figures 1 and 2. Before discussing each fuel individually, we note that the benzene concentration curves are bell shaped, that the relative amounts of benzene formed are in the same general order as the sooting tendencies, and that the benzene maximum for each fuel precedes the respective soot tendency maxima.

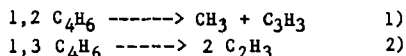
Allene

A 4.3% C_3H_4 -Ne mixture was investigated over the temperature and total pressure range of 1300-2000 K and 0.2-0.5 atm, respectively. TOF analysis revealed that the major products were C_2H_2 , C_4H_2 , CH_4 and C_6H_6 ; lesser amounts of C_2H_4 , C_2H_6 , C_4H_4 , and C_6H_2 were detected. The major product profiles were modeled with an 80 step reaction mechanism. The initial reactions involved the isomerization of allene to propyne²⁰; both isomers decompose to yield $C_3H_3 + H$ ^{21,22}. Benzene was produced via reaction of C_3H_3 with allene and by reaction of

two C_3H_3 radicals. The latter route was suggested by Hurd^{23,24} in which C_3H_3 initially forms $:CH-CH=CH$ via 1,2 H shift followed by cyclization to benzene. Benzene concentrations were calculated at 1 ms for various no-reaction temperatures. The resulting bell shaped curve is displayed in Figure 1 along with its respective LEX soot tendency bell⁵.

1,2 Butadiene

A 3% 1,2 C_4H_6 -Ne mixture was shocked over the ranges 1200-2000 K and 0.17-0.56 atm. The major stable species observed were C_2H_2 , CH_4 , C_2H_4 and C_4H_2 . At intermediate temperatures (around 1500 K), benzene and toluene were recorded. C_2H_2 and C_4H_2 were the only major products at high temperatures. Isomerization of 1,2 to 1,3 C_4H_6 precedes extensive decomposition. The two isomers decompose according to two pathways.



The decomposition of 1,3 C_4H_6 has been studied by laser schlieren densitometry (LS) and TOF¹⁴. The reaction mechanism used to model the various product profiles from 1,3 C_4H_6 was employed as a subset to the mechanism for 1,2 C_4H_6 . Reactions describing the isomerization and other key channels complete the model. Benzene concentrations were calculated at 1 ms and are plotted as a function of temperature in Figure 1. There are no LEX data available for comparison.

1,3 Butadiene

A 3% 1,3 C_4H_6 -Ne mixture was studied over the range comparable to 1,2 C_4H_6 . LS profiles obtained by Professor Kiefer provided conclusive evidence that the main pathway for decomposition was C-C bond rupture to produce two vinyl radicals. A 31 step mechanism modeled the LS profiles and the TOF profiles for 1,3 C_4H_6 , C_2H_2 , C_2H_4 , C_4H_2 and C_6H_6 ¹⁴. The amount of benzene produced was less than that recorded for 1,2 C_4H_6 and for an equivalent amount of C_3H_4 . The latter result is in agreement with the LEX work⁵ which is shown in Figure 1.

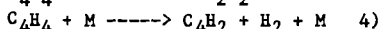
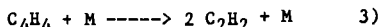
Acetylene

C_2H_2 is the major product in the high temperature thermal decompositions of many hydrocarbons; C_8H_{10} ²⁵, C_7H_8 ²⁶, C_6H_6 ²⁷⁻²⁹, C_5H_5N ¹⁸, C_3H_4 ¹², 1,2¹² and 1,3 C_4H_6 ¹⁴, and C_4H_4 ³⁰. A radical mechanism derived largely from those previously employed by Gardiner³¹ and Kiefer³² was used to model TOF data obtained on a series of C_2H_2 -Ne mixtures, 1-6.2%, over the range 1900-2500 K and 0.3-0.55 atm. The major species modeled were C_2H_2 , C_4H_2 , and C_6H_2 . Minor amounts of C_8H_2 and C_4H_3 were recorded; benzene was not detected. Reactions from the benzene mechanism²⁹ were added to the model and used to calculate the relatively minor amounts of benzene detected in the SPST work by Colket⁹. The results are shown in Figure 3. Although the fit is not completely satisfying, the computed profile is satisfactory for our purpose here; namely, the benzene yield is very low compared to the major species present. Benzene concentrations for an acetylene

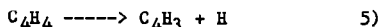
mixture containing 2×10^{17} C atoms cm^{-3} are plotted in Figure 2 along with the corresponding LEX soot bell⁵.

Vinylacetylene

Pyrolysis of C_4H_4 has been studied recently by LS and TOF over the range 1500–2500 K and 0.14–0.56 atm³⁰. Analysis of the LS profiles revealed that the decomposition was characterized by a heat release of ~ 40 kcal mol^{-1} . The LS profiles were all concave upward which ruled out any appreciable chain acceleration reactions. TOF measurements of the major products, C_2H_2 and C_4H_2 disclosed a near constant ratio of $\text{C}_2\text{H}_2/\text{C}_4\text{H}_2 \sim 5$ which was independent of the observation time and temperature. Trace amounts of C_6H_2 were recorded at higher temperatures; C_8H_2 and benzene were not detected. These facts support the proposal that the mechanism is molecular and occurs via the reactions



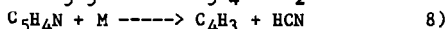
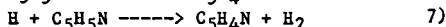
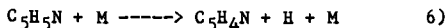
The LS profiles and the TOF profiles were fit with rate constants derived for this two channel dissociation. These conclusions are in conflict with two other shock tube reports that propose a radical mechanism for the pyrolysis in which the first step is C-H bond rupture^{33,34}.



The initiation is followed by a sequence of radical reactions. The benzene concentrations shown in Figure 2 were calculated using rxns 3) and 4) along with the C_2H_2 ¹⁹ and C_6H_6 ²⁹ mechanisms previously mentioned to fit the SPST data in Figure 3.

Pyridine

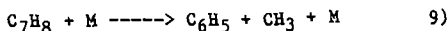
LS and TOF profiles have been recently obtained¹⁸ for the thermal decomposition of $\text{C}_5\text{H}_5\text{N}$ over the range 1700–2200 K and 0.13–0.5 atm. The LS profiles displayed local maxima which is a signature for chain acceleration of the net endothermic rate. The main products were identified by TOF to be HCN, C_2H_2 , and C_4H_2 . A 24 step mechanism was constructed which included the following steps:



Benzene concentrations were calculated in the manner employed for C_4H_4 and are extremely low which is in accord with the LEX result⁶. The near absence of this key building block inhibits polycyclic growth and subsequent soot formation. Intact pyridine rings are not suitable substitutes since polycyclic growth is retarded by the presence of the ring nitrogen.

Temperature Changes

Thermal decompositions are endothermic processes and the system temperature decreases as the reaction progresses. This point is illustrated in Figure 4 in which the soot bell for toluene at 1 ms observation time⁴ is shifted markedly when the system temperature at 1 ms is used to plot the sooting tendency instead of the usual practice which employs the no reaction temperature. The temperatures at 1 ms were calculated using a mechanism from recent LS and TOF work on C₇H₈²⁶ which identifies the major pathway for dissociation as



Temperature decreases for the pyrolyses represented in Figures 1 and 2 at 1 ms are listed in Table 1.

Conclusions

There appears to be sufficient evidence to support the correlation of benzene production and soot tendencies. It does not necessarily follow that the key to soot control is limiting solely those reactions and/or species which promote benzene formation. The pyrolyses considered herein were those of "pure" fuels. Synergistic effects have been reported for fuel mixtures; e.g., a 0.75% C₇H₈ - 0.75% C₅H₅N - Ar mixture produced almost as much soot as an equivalent amount of "pure" toluene, 1.5% C₇H₈ - Ar⁶. Nevertheless, the results herein are consistent with the proposal of relatively low concentrations of soot nuclei which subsequently increase in mass due to surface growth by C₂H₂³⁵.

Acknowledgments

We appreciate the collaboration of Professor Kiefer and his research group and thank the Department of Energy for support under contract DE-FG0585ER/13400.

References

1. Graham, S.C., Homer, J.B. and Rosenfeld, J.L.J., Proc. Roy. Soc. A344(1975) 259.
2. Graham, S.C., Homer, J.B. and Rosenfeld, J.L.J., Proc., 10th Int. Symp. on Shock Tubes and Waves, 1975, p.621.
3. Wang, T.S., Matula, R.A. and Farmer, R.C., 18th Symp. (Int.) on Combustion (1981), 1149.
4. Frenklach, M., Taki, S. and Matula, R.A., Combust. Flame, 49, (1983), 275.
5. Frenklach, M., Taki, S. Durgaprasad, M.B. and Matula, R.A., Combust. Flame, 54, (1983) 81.
6. Rawlins, W.T., Tanzawa, T., Schertzer, S.P., and Kreck, R.H., Final Report submitted to DOE, Contract DEAC2280PC30292, January 1983.
7. Vaughn, S.N., Ph. D. Thesis, Kansas State University, 1980.
8. Vaughn, S.N., Lester, T.W. and Merklin, J.F., Proc., 13th Int. Symp. on Shock Tubes and Waves, 1982, p. 860.
9. Colket, M.B., Proc., 15th Int. Symp. on Shock Tubes and Waves, 1986, p. 311.

10. Kern, R.D., Singh, H.J., Esslinger, M.A. and Winkeler, P.W., 19th Symp. (Int.) on Combustion, 1982, 1351.
11. Frenklach, M., Clary, D.W., Gardiner, W.C., and Stein, S.E., 20th Symp. (Int.) on Combustion, (1984), 887.
12. Wu, C.H. and Kern, R.D., manuscript submitted to J. Phys. Chem.
13. Singh, H.J. and Kern, R.D., work in progress.
14. Kiefer, J.H., Wei, H.C., Kern, R.D. and Wu, C.H., Int. J. Chem. Kinet., 17, (1985) 225.
15. Kee, R.J., Miller, J.A. and Jefferson, T.H., CHEMKIN: A General Purpose, Problem Independent Transportable, Fortran Chemical Kinetics Code Package, Sandia National Laboratories, SAND 80-8003, 1980.
16. Hindmarsh, A.C., LSODE Livermore Solver for Ordinary Differential Equations, Lawrence Livermore Laboratory, 1980.
17. Kiefer, J.H., Mitchell, K.I., Kern, R.D., and Yong, J.N., manuscript submitted to J. Phys. Chem.
18. Kern, R.D., Yong, J.N., Kiefer, J.H., and Shah, J.N., paper to be presented at the 16th Int. Symp. on Shock Tubes and Waves, 1987.
19. Wu, C.H. and Kern, R.D., manuscript submitted to Int. J. Chem Kinet.
20. Kakumoto, T., Ushirogouchi, T., Saito, K., Isamura, A., J. Phys. Chem., 91, (1987), 183.
21. Lifshitz, A., Frenklach, M., Burcat, A., J. Phys. Chem., 79, (1975), 1148.
22. Lifshitz, A., Frenklach, M., Burcat, A., J. Phys. Chem., 80, (1976), 2437.
23. Hurd, C.D., Macon, A.R., Simon, J.I., Levetan, R.V., J. Am. Chem. Soc., 84, (1962), 4509.
24. Hurd, C.D., Macon, A.R., J. Am. Chem. Soc., 84, (1962), 4524.
25. Pamidimukkala, K.M. and Kern, R.D., Int. J. Chem. Kinet., 18, (1986), 1341.
26. Pamidimukkala, K.M., Kern, R.D., Patel, M.R., Wei, H.C. and Kiefer, J.H., J. Phys. Chem., 91, (1987), 2148.
27. Singh, H.J. and Kern, R.D., Combust. Flame, 54, (1983), 49.
28. Kern, R.D., Wu, C.H., Skinner, G.B., Rao, V.S., Kiefer, J.H., Towers, J.A., and Mizerka, L.J., 20th Symp. (Int.) on Combustion (1984), 789.
29. Kiefer, J.H., Mizerka, L.J., Patel, M.R., and Wei, H.C., J. Phys. Chem., 89, (1985), 2013.
30. Kiefer, J.H., Mitchell, K.I., Kern, R.D., and Yong, J.N., manuscript submitted to J. Phys. Chem.
31. Tanzawa, T. and Gardiner, W.C., J. Phys. Chem., 84, (1980), 236.
32. Kiefer, J.H., Kapsalis, S.A., Al-Alami, M.Z., and Budach, K.A., Combust. Flame, 51, (1983), 79.
33. Colket, M.B., presented at the 21st Symp. (Int.) on Combustion, 1986, in press.
34. Hidaka, Y., Tanaka, K., and Suga, M., Chem. Phys. Lett., 130, (1986), 195.
35. Harris, S.J., and Weiner, A.M., Ann. Rev. Phys. Chem., 36, (1985), 31.

Table 1.

Temperature Decrease During Pyrolyses of Various Fuels

$T_0(K)$	$-\Delta T$ (1.0 msec, 2×10^{17} C atoms cm^{-3})						
	C_3H_4	1,2 C_4H_6	1,3 C_4H_6	C_4H_4	C_2H_2	C_5H_5N	C_7H_8
1500	-	57	88	36	<0.5	25	-
1600	-	114	149	95	1	75	93
1700	41	164	211	150	3	155	162
1800	110	206	268	186	6	235	236
1900	168	239	316	205	10	310	311
2000	206	269	354	208	14	375	379
2100	233	300	378	209	18	415	433
2200	249	325	393	210	23	433	462
2300	258	340	400	212	29	433	471
2400	264	349	402	212	33	433	508

Figure 1

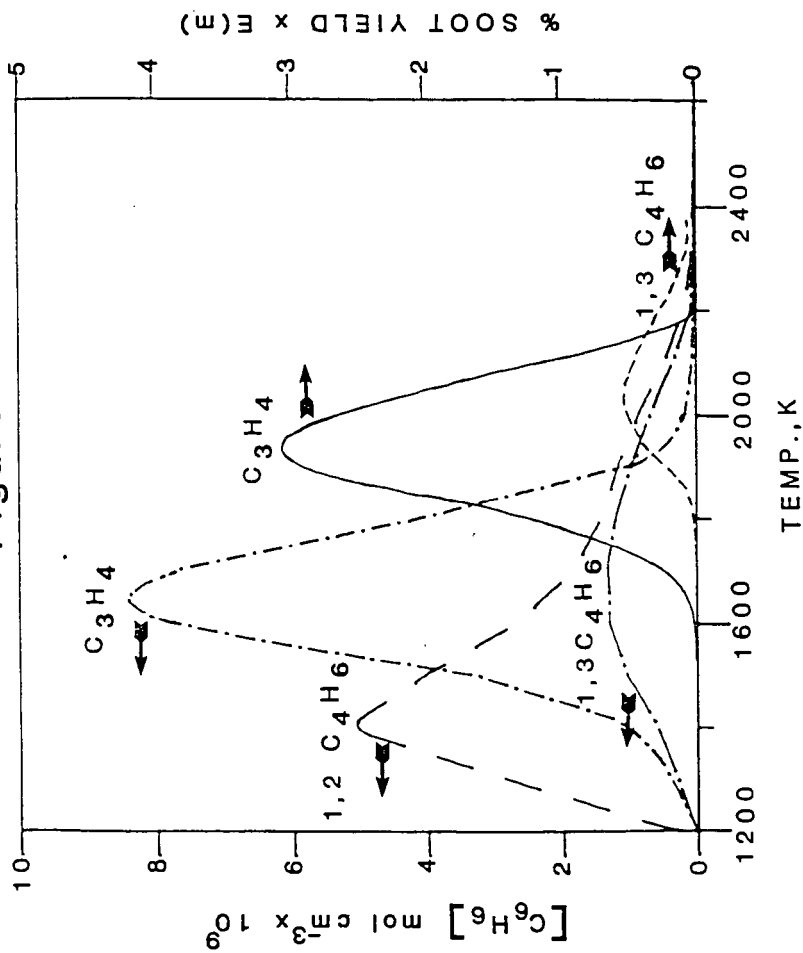


Figure 2

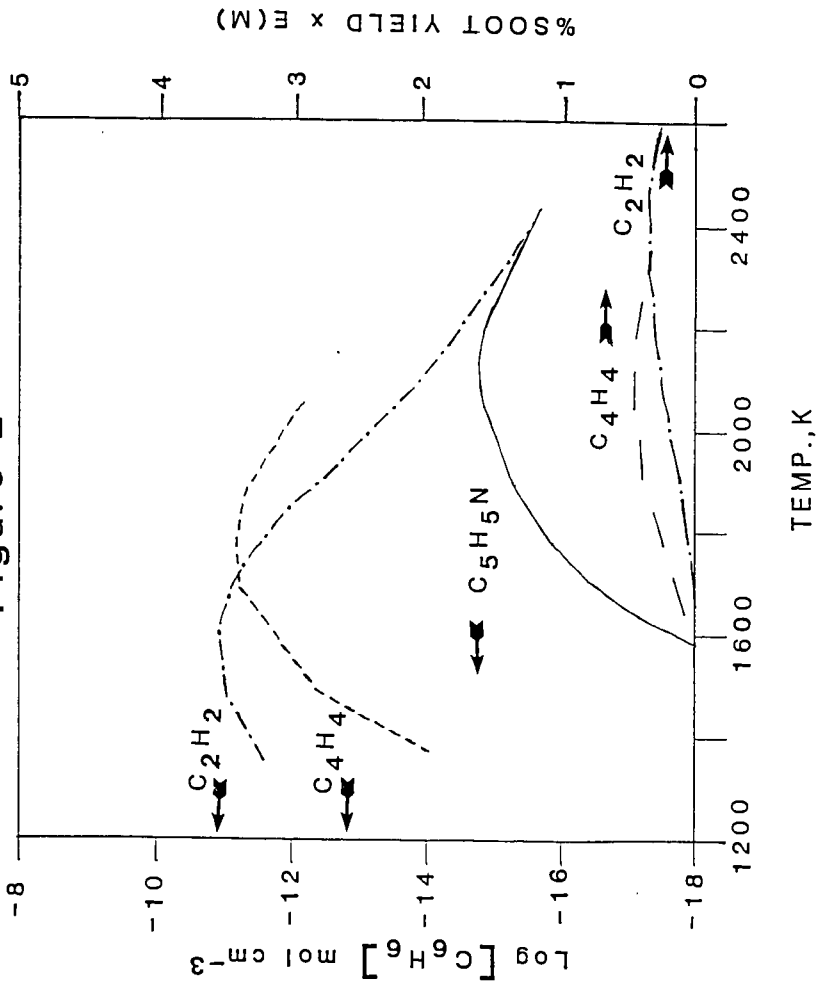


Figure 3
3.7% Acetylene

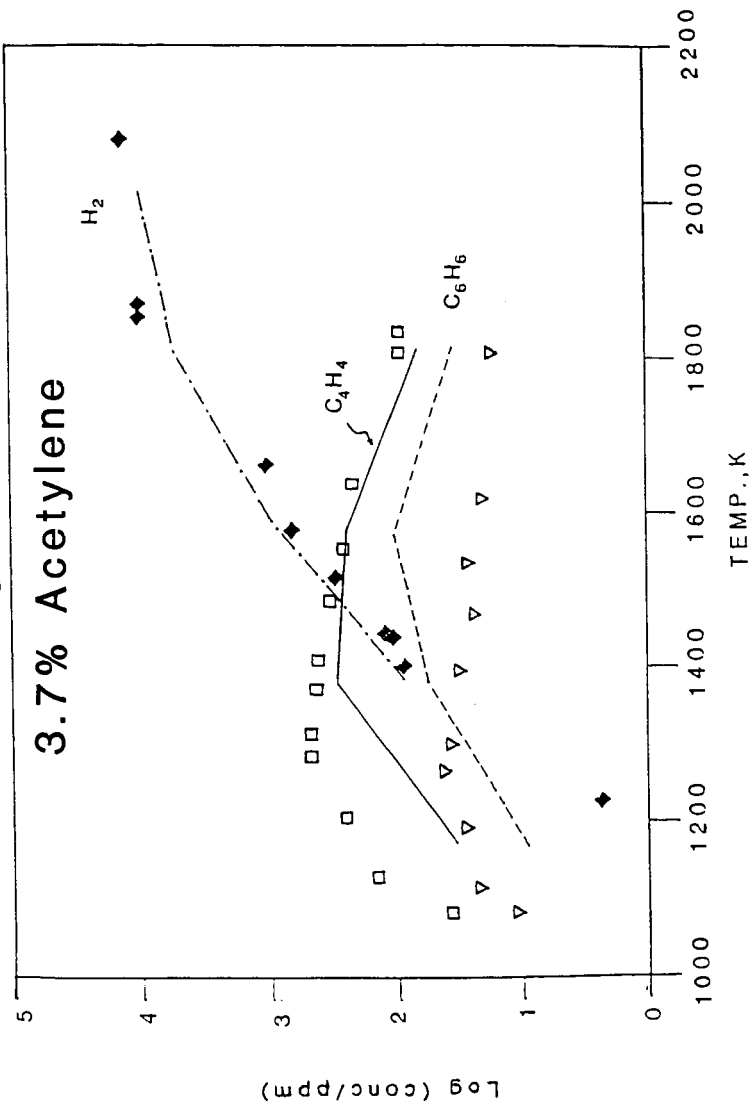
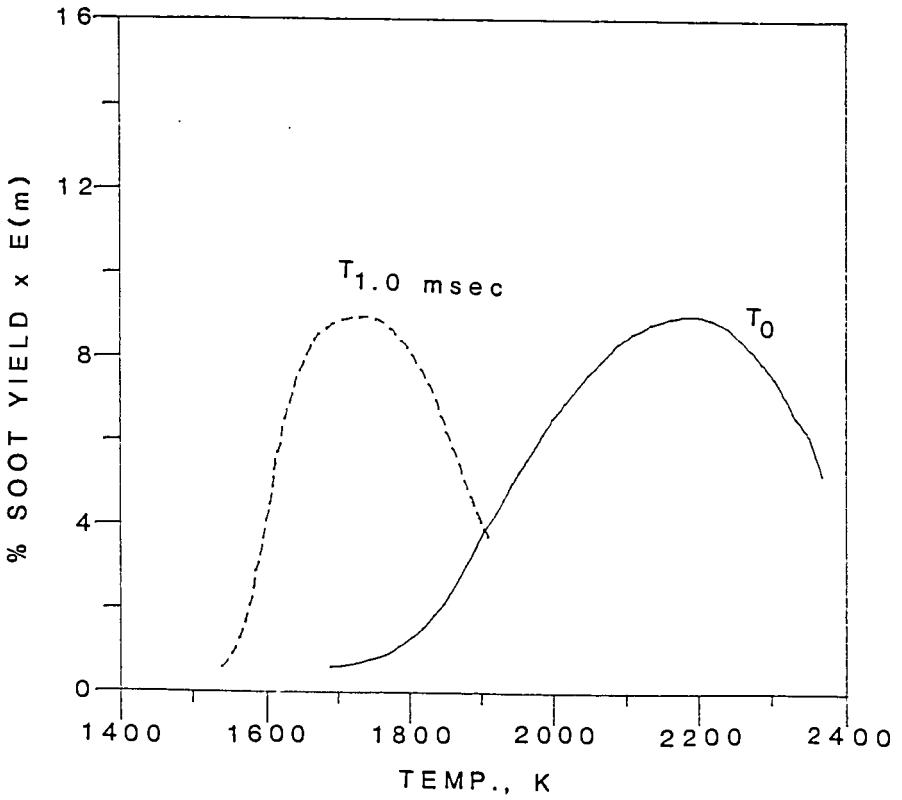


Figure 4



SHOCK-TUBE AND MODELING STUDY OF SOOT FORMATION IN MIXTURES OF HYDROCARBONS

M. Frenklach, T. Yuan and M.K. Ramachandra

Fuel Science Program
Department of Materials Science and Engineering
Pennsylvania State University
University Park, PA 16802

INTRODUCTION

Interest in soot formation in binary hydrocarbon mixtures has increased in recent years. Besides the very practical aspects of such knowledge, the subject is of interest from a fundamental point of view: to provide additional information for the elucidation of the soot formation mechanism. There is evidence, both experimental [1-8] and theoretical [9-11], that the key chemical reactions leading to soot formation in hydrocarbon systems are those between aliphatic and aromatic species. The importance of such reactions was suggested as early as 1960 by Stehling *et al.* [12].

This paper presents the results of a shock-tube pyrolysis study on soot formation from a series of binary hydrocarbon mixtures: benzene-additive, where the additives were acetylene, allene, vinylacetylene and 1,3-butadiene; and allene-acetylene, butadiene-acetylene and acetylene-hydrogen.

EXPERIMENTAL

The experiments were conducted behind reflected shock waves in a 7.62 cm i.d. shock tube [4-6]. Ten different mixtures were tested during the course of this study. The experimental conditions which were chosen such as to allow comparison with the previous results [5,6]. The experiments were carried out at temperatures from 1500 K to 2490 K, pressures from 1.3 to 3.1 bar, and carbon atom concentrations from 2.0 to 6.8×10^{17} atoms/cm³. The appearance of soot was monitored by the attenuation of a He-Ne laser beam (632.8 nm) at approximately 10 mm from the end plate of the shock tube. The term soot has been used in our work as a lumped property meaning "species absorbing at a 632.8 nm". For its practical measure, the amount of carbon atoms accumulated in soot is used in this work. The latter property is calculated following the usual Rayleigh approximation [13] using the complex refractive index of Dalzell and Sarofim [14].

The experimental results are presented for a reaction time of 1 ms; this time is chosen arbitrary — qualitatively similar results were obtained at all observation times.

RESULTS AND DISCUSSION

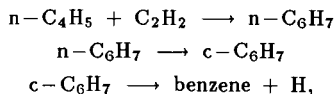
Acetylene-Hydrogen

Figure 1 depicts the comparison of soot carbon obtained in a acetylene-hydrogen mixture with those obtained at similar conditions from acetylene alone. As can be seen in this figure, hydrogen strongly suppresses soot formation from acetylene. Wang et al. [15] also observed the suppression effect of hydrogen in toluene-hydrogen mixtures. A chemical kinetic model [9,10] predicts this effect: addition of molecular hydrogen increases the reverse rate of the "reactivation", H-atom abstraction reactions.

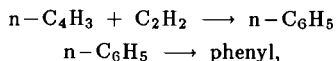
Allene-Acetylene and Butadiene-Acetylene

Figures 2 and 3 present the amount of soot formed in mixtures of acetylene with allene and 1,3-butadiene, respectively, and a comparison with the results for the individual fuels. A pronounced synergistic effect is observed for these cases.

A computer simulation for the conditions of a butadiene-acetylene mixture with a mechanism of butadiene pyrolysis [10] qualitatively predicts the experimentally observed synergistic effect (the lack of quantitative agreement, as discussed previously [10,16], is due to insufficient knowledge of thermochemical data). The results of the computer simulation are given in Fig. 4. The analysis of the computational results revealed that the main factor affecting soot formation is the increase in the rate of acetylene-addition reactions. This accelerates cyclization reactions and suppresses decomposition of $n-C_xH_y$ radicals to C_2H_2 and $n-C_{x-2}H_{y-2}$. The reaction pathway to soot is similar to that identified for pyrolysis of butadiene [10], except that cyclization via



becomes more prominent (yet still slower than the reaction sequence via $n-C_6H_5$ [9],



at the conditions of the soot yield maximum).

Based on the computational analysis of the butadiene-acetylene case, the experimental results obtained for allene-acetylene mixtures (Fig. 2) may indicate the importance of sequential addition of two acetylene molecules to $CH_2=C=CH\bullet$ radical followed by cyclization to a relatively stable benzyl radical. In other words, we propose that in an allene system the first-ring cyclization is not the formation of phenyl or benzene but rather that of benzyl.

Benzene-Additives

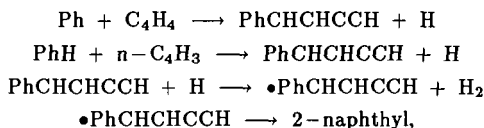
Figures 5 and 6 present the results obtained in mixtures of benzene with aliphatic hydrocarbons. Addition of acetylene (Fig. 5) enhances soot formation. However, the effect is pronounced only at relatively high (2.72 and 1.09 %) initial concentration of acetylene. With smaller amounts (0.54 %) of acetylene added, there is no significant increase in soot production; on the contrary, there is a slight suppression of soot formation at lower temperatures.

The main feature of the dominant reaction pathway to soot identified for benzene pyrolysis [10] is the formation of byphenyl by the addition of phenyl radical to benzene followed by sequential addition of two acetylene molecules to form pyrene. The initial presence of acetylene, as revealed by the results of a computer simulation using a benzene pyrolysis mechanism [10], increases the rate of the ring-growth process and suppresses the rate of phenyl fragmentation, both being promoting factors. However, reaction of acetylene with phenyl forming phenylacetylene removes phenyl radicals from a more efficient ring-forming pathway, addition to benzene molecules, which counteracts the promoting factors.

The experimental results reported in Fig. 6 show that vinylacetylene and 1,3-butadiene are more efficient soot promoters than acetylene. Soot-yield maxima in their mixtures with benzene are shifted to higher temperatures compared to that of benzene alone, which indicates that decomposition of the additives is important. The results of computer simulations, which reproduced (again, qualitatively) the experimental trends, support this conclusion. For instance, in the benzene-vinylacetylene case, decomposition of vinylacetylene via



initiates the pyrolysis. Reactions of C_4H_4 , C_4H_3 and C_2H_3 enhance the growth of aromatics compared to the pyrolysis of benzene alone. For example, reaction sequence



where $\bullet PhCHCHCCH$ is an *ortho*-substituted phenyl radical, is accelerated with the addition of vinylacetylene to benzene.

The results obtained in a benzene-allene mixture (Fig. 4) indicate a synergistic effect. Thus, not only does allene have a high sooting tendency itself [6], but it appears to be also an efficient soot promoter.

ACKNOWLEDGEMENT

The work was supported by Aerochemistry Branch of NASA-Lewis Research Center, Grants Nos. NAG 3-477 and NAG 3-668.

REFERENCES

1. Bittner, J.D. and Howard, J.B., *Eighteenth Symposium (International) on Combustion*, p. 1105, The Combustion Institute, 1981.
2. Bittner, J.D. and Howard, J.B., in *Soot in Combustion Systems and its Toxic Properties* (J. Lahaye and G. Prado, Eds.), p. 57, Plenum, 1983.
3. Bittner, J.D., Howard, J.B. and Palmer, H.B., *ibid.* p. 95.
4. Cole, J.A., Bittner, J.D., Longwell, J.P. and Howard, J.B., *Combust. Flame* **56**, 51 (1984).
5. Frenklach, M., Taki, S. and Matula, R.A., *Combust. Flame* **49**, 275 (1983).
6. Frenklach, M., Taki, S., Durgaprasad, M.B. and Matula, R.A., *Combust. Flame* **54**, 81 (1983).
7. Frenklach, M., Ramachandra, M.K. and Matula, R.A., *Twentieth Symposium (International) on Combustion*, p. 871, The Combustion Institute, 1985.
8. Bockhorn, H., Fetting, F. and Wenz, H.W., *Ber. Bunsenges. Phys. Chem.* **87**, 1067 (1983).
9. Frenklach, M., Clary, D.W., Gardiner, W.C., Jr. and Stein, S.E., *Twentieth Symposium (International) on Combustion*, p. 887, The Combustion Institute, 1985.
10. Frenklach, M., Clary, D.W., Gardiner, W.C., Jr. and Stein, S.E., *Twenty-First Symposium (International) on Combustion*, in press.
11. Frenklach, M. and Warnatz, J., *Combust. Sci. Technol.* **51**, 265 (1987).
12. Stehling, F.C., Frazee, J.D. and Anderson, R.C., *Eighth Symposium (International) on Combustion*, p. 744, Williams and Wilkins, 1962.
13. Frenklach, M., Taki, S., Li Kwok Cheong, C.K. and Matula, R.A., *Combust. Flame* **51**, 37 (1983).
14. Dalzell, W.H. and Sarofim, A.F., *Trans. ASME* **91**, 100 (1969).
15. Wang, T.S., Matula, R.A. and Farmer, R.C., *Eighteenth Symposium (International) on Combustion*, p. 1149, The Combustion Institute, 1981.
16. Frenklach, M., Clary, D.W., Gardiner, W.C., Jr. and Stein, S.E., *Proc. 15th Int. Symp. Shock Waves and Shock Tubes* (D. Bershader and R. Hanson, Eds.), p. 295, Stanford University, 1986.

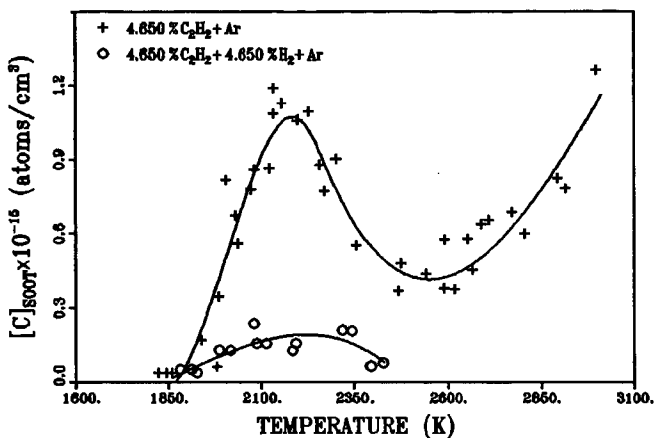


Figure 1. Comparison of soot carbon in pyrolysis of acetylene and acetylene-hydrogen mixture.

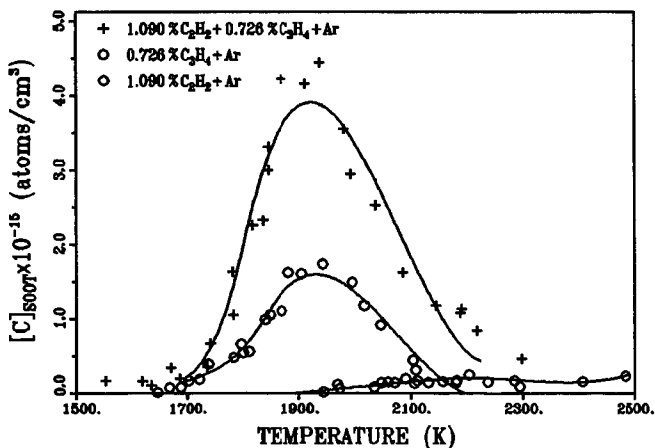


Figure 2. Comparison of soot carbon in pyrolysis of acetylene, allene, and acetylene-allene mixture.

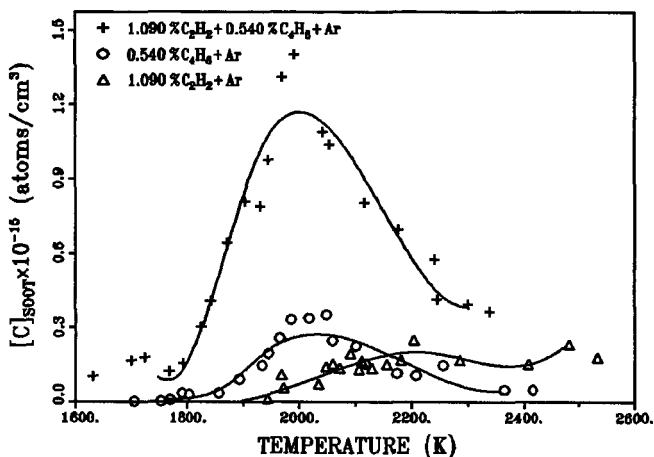


Figure 3. Comparison of soot carbon in pyrolysis of acetylene, 1,3-butadiene, and acetylene-butadiene mixture.

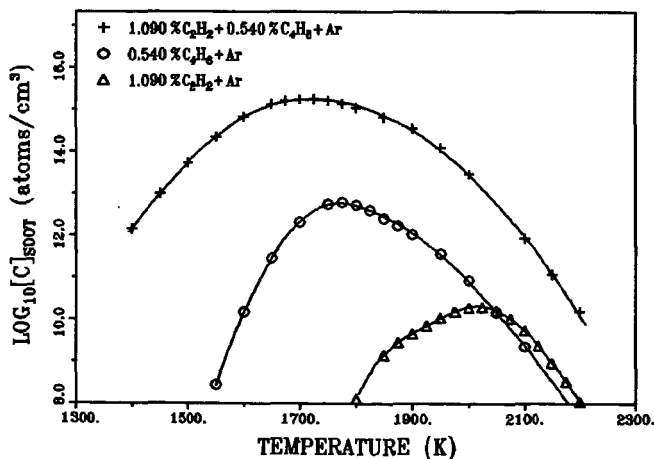


Figure 4. Comparison of computed soot carbon in pyrolysis of acetylene, 1,3-butadiene, and acetylene-butadiene mixture.

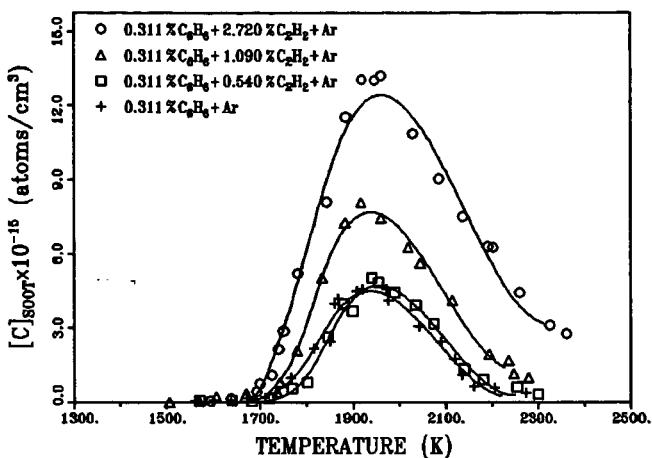


Figure 5. Comparison of soot carbon in pyrolysis of benzene, and benzene-acetylene mixture.

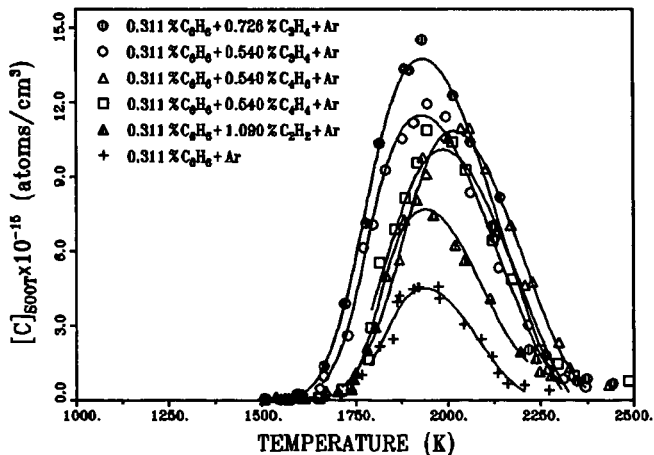


Figure 6. Comparison of soot carbon in pyrolysis of benzene, benzene-acetylene, benzene-allene, benzene-vinylacetylene, and benzene-butadiene mixtures.

THE MOLECULAR DISSOCIATION OF VINYLACETYLENE
AND ITS IMPLICATIONS FOR ACETYLENE PYROLYSIS

John H. Kiefer and Kevin I. Mitchell

Department of Chemical Engineering
University of Illinois at Chicago
Chicago, Illinois 60680

Perhaps the most extensively investigated of all fuel pyrolyses is that of acetylene. The reasons are compelling: acetylene is a major product of virtually all hydrocarbon pyrolysis and oxidation, and its reactions usually govern the later states of such processes, in particular the formation of soot. Acetylene is evidently essential to soot formation (1,2), and has also been selected as the prototype fuel in a recent detailed model of the soot formation process (3).

Although C_2H_2 pyrolysis has been observed over an enormous range of temperature (700-3500K) (4-17), and by many different and usually reliable methods, there is little agreement even on its initiation. The process looks much like a single second-order reaction over 700-2500K (5,7) and the early products are commonly dominated by multiples of the C_2H_2 unit. In particular, there is good evidence that vinylacetylene (C_4H_4 , 1-buten-3-yne) is the sole initial gaseous product below 1500K (4-8). This all suggests C_2H_2 pyrolysis is largely a molecular polymerization, but the reaction also shows induction periods (11,15), a sensitivity to NO (15), rapid isotopic scrambling in C_2H_2 - C_2D_2 mixtures (6), as well as minor products suggestive of radical intermediates (6,9,14). All this of course implies chain reaction, and most recent workers (7,9,10,12,17) have described this pyrolysis as an H-atom chain initiated by



There are also some interesting attempts to reconcile the evidence for chain and molecular reaction which postulate an intermediate triplet C_2H_2 (1,2-diradical) (5,7,18).

Given the effort expended on C_2H_2 pyrolysis the lack of consensus is striking. Much of this must simply reflect the complexity of the process. As noted by Palmer and Dormish (7), it is quite unlikely the same mechanism applies for all conditions. Certainly at very high temperatures, above 2500K, the reaction is a degenerate branched chain (10) which is probably initiated by simple dissociation. In the flow and static reactor studies below 1000K there is obviously a large heterogeneous component (5,7). At the lower temperatures impurities could readily compete as a source of chain initiation.

Some of the above complications may be avoided by observing the reverse process, which could well be the dissociation of vinylacetylene. Decomposition of C_4H_4 has recently been studied in the shock tube by Colket (9) and Hidaka et al. (19). They again suggest a radical chain mechanism initiated by



although they derive activation energies for this of 80-85 kcal/mol, which do seem low. The dominant products are C_4H_2 and C_2H_2 with a very consistent C_2H_2/C_4H_2 ratio of 5-10.

In a collaboration with R. D. Kern (20) we have reinvestigated the C_4H_4 decomposition at very high temperatures (1500-2500K) where the unimolecular dissociation should dominate, using laser-schlieren (LS) and

time-of-flight (TOF) mass spectroscopy techniques on shock waves. Here we present a brief reiteration of the C_4H_4 results together with their implications for the C_2H_2 pyrolysis, implications which have led to the proposal of a new mechanism for this reaction.

EXPERIMENTAL

Both the LS (2 and 4% C_4H_4 - Kr, 1650-2500K, 110-427 torr) and TOF (2% C_4H_4 - Ne, 1500-2200K, 150-300 torr) measurements used apparatus and procedures which have been fully described (21,22). Vinylacetylene was obtained from Wiley Organics, degassed and distilled for purification, finally showing no more than ~0.1% impurities. Thermodynamic properties of C_4H_4 were calculated from molecular properties (23), using an estimated $\Delta H_{f,298}^{\circ} = 69$ kcal/mol (24). A more detailed description of the experiments and calculations will be found in ref. (20).

RESULTS

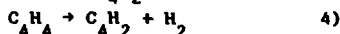
Example LS semilog density gradient profiles are presented in Figure 1. The important feature here is the upward concave shape. This concavity is consistent throughout the LS experiments and shows there can be no significant chain reaction in C_4H_4 pyrolysis. A chain will accelerate the endothermic decomposition producing a convex profile. For example, in benzene (25) and pyridine (26), which evidently dissociate by C-H scission, this acceleration is so severe it generates a local maximum. The likely consequences of such a chain in C_4H_4 are shown in Figure 2 where we have modeled one LS experiment with a "reasonable" chain mechanism, initiated by reaction 1) (see ref. (20) for details). As expected, the result is a strongly convex profile in complete disagreement with the measurements. In fact, even a small contribution from such a chain is excluded. In Figure 2 we also show the sensitivity to small amounts of chain reaction. Even 1% dissociation through reaction 1) produces noticeable deviation.

The TOF profiles also argue against a chain initiated by reaction 1). They show C_2H_2 and C_4H_2 as major products with $C_2H_2/C_4H_2 \sim 5$ independent of temperature (or even time) in essential agreement with the other recent shock tube studies (9,19). The problem is any chain initiated by 1) cannot maintain the required dominance of C_2H_2 at high temperatures where the products mainly arise from dissociation (and abstraction). Such a chain then produces the great excess of C_4H_2 shown in Figure 3.

The product distribution and the absence of discernable chain reaction suggest the main channel for C_4H_4 dissociation must be

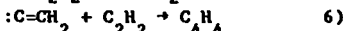
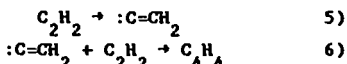


With almost no chain much of the C_4H_2 product must be formed through



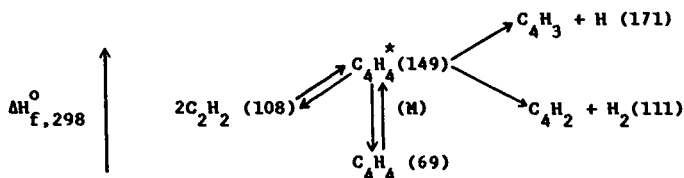
We have modeled the LS and TOF data using just these two reactions with the uniformly excellent results exemplified in Figures 1,2, and 4. Rate constants for the sum of reactions 3) and 4) (both have ΔH_{298}° very near 40 kcal/mol), derived from the zero-time density gradients, are shown in Figure 5. Here we also show a "routine" ERKM model fit to these data. This model

The detailed mechanism of the C_2H_2 dimerization would now be isomerization to vinylidene followed by insertion of this into the C-H bond of acetylene (33)



As long as 5) is equilibrated, the overall forward and reverse rates are still related by the equilibrium constant for 3). However, it is perfectly possible for 5) to be slow enough at low temperatures to generate a detectable induction period.

Although the calculated rates of dimerization to C_4H_4 in Figure 6 seem to account for the entire second-order rate above 1000K, this is rather misleading. Additional reaction paths are probably still necessary at both ends of the temperature range, i.e., outside 1000-1500K. For $T > 1500K$ the ERKM calculations show noticeable falloff even for the high pressures (3-10 atm) of the reflected shock experiments in Figure 6 (4,6,12). The use of k_∞ in the detailed balance calculation is then no longer valid, and the rates will begin to fall below the measured second-order data. However, consideration of the following reaction-enthalpy diagram



shows that when deactivation to C_4H_4 slows at high temperature (and/or low pressure) it opens the channels



These will now act to "pull" the dimerization forward, at least partially compensating for the falloff in C_4H_4 formation. The chain initiated by 8) can also convert both C_2H_2 and any residual C_4H_4 to C_4H_2 and higher polyacetylenes, particularly at very high temperatures. Note that here neither 7) nor 8) can proceed till there is falloff of the deactivation, i.e., above about 1500K. The onset of these two channels may provide a reasonable explanation for the crossover from C_4H_4 to C_4H_2 in C_2H_2 pyrolysis which occurs around 1500-1600K (6,7,9). However, a quantitative modeling on this basis may be quite difficult below 1600K, where production of H-atom through reaction 8) must be very slow and could be overwhelmed by impurity generation. We would also suggest the isotopic scrambling in C_2H_2/C_2D_2 mixtures (6), alluded to earlier, probably requires very little H-atom (34) which could be generated by a small contribution from 8) and/or various impurities.

Below 1000K the situation may be even more complex. The pyrolysis now involves polymer, tar, and char formation and has a significant heterogeneous component (5,7,11). Minor products which suggest chain reaction may be generated by polymer carbonization, heterogeneous reaction, or for that matter, impurity initiated chain reaction.

Finally, we offer a highly tentative explanation for the polymer formed at the lowest temperatures. Usually carbenes preferentially insert into multiple bonds (33), so the dominant insertion product should be methylenecyclopropene. This has now been synthesized (35,36) and is quite unstable. For one thing it evidently polymerizes (36); at high temperatures it probably reverts to C_2H_2 . This suggestion is closely analogous to the triplet diradical schemes (5, 7, 18) and can deal with the same phenomena. In addition to the right energetics, it also has the advantage of fading out at high temperatures where the methylenecyclopropene reverts to acetylene.

- 1.) H. B. Palmer and C. F. Cullis, "The Chemistry and Physics of Carbon", (P. L. Walker, Ed., Dekker, New York) 1, 265 (1985).
- 2.) S. J. Harris and A. M. Weiner, Comb. Sci. and Tech. 31, 155 (1983); 32, 267 (1983).
- 3.) M. Frenklach, D. W. Clary, W. C. Gardiner, Jr., and S. E. Stein, 20th (Int'l) Symposium on Combustion, The Combustion Institute, Pittsburgh, 1984, p 887.
- 4.) G. B. Skinner, and E. M. Sokoloski, J. Phys. Chem., 64, 1952 (1960).
- 5.) C. F. Cullis and N. H. Franklin, Proc. Roy. Soc. (London) A280, 139 (1964).
- 6.) H. Ogura, Bull. Chem. Soc. Jpn. 50, 1044 (1977).
- 7.) H. B. Palmer and F. L. Dormish, J. Phys. Chem. 68, 1553 (1964).
- 8.) C. F. Cullis and I. A. Read, Trans. Fara. Soc. 66, 920 (1970).
- 9.) M. B. Colket, presented at the 21st (Int'l) Symposium on Combustion, Munich, 1986.
- 10.) T. Tanzawa and W. C. Gardiner, Jr., 17th (Int'l) Symposium on Combustion, The Combustion Institute, Pittsburgh, 1978, p 563; J. Phys. Chem. 84, 236 (1980).
- 11.) C. G. Silcocks, Proc. Roy. Soc. (London) A242, 411 (1957).
- 12.) C. F. Aten and E. F. Greene, Combust. Flame 5, 55 (1961).
- 13.) G. D. Towell and J. J. Martin, AIChE J. 7, 693 (1961).
- 14.) M. S. B. Munson and R. C. Anderson, Carbon 1, 51 (1963).
- 15.) G. J. Minkoff, D. M. Newitt, and P. V. Rutledge, J. Appl. Chem. 7, 406 (1957).
- 16.) M. A. Nettleton, Ph.D. Thesis, University of London (1960).
- 17.) I. D. Gay, G. B. Kistiakowsky, J. V. Michael, and H. Niki, J. Chem. Phys. 43, 1729 (1965).
- 18.) G. J. Minkoff, Can. J. Chem. 36, 131 (1958).
- 19.) Y. Hidaka, K. Tanaka, and M. Suga, Chem. Phys. Lett. 130, 195 (1986).
- 20.) J. H. Kiefer, K. I. Mitchell, R. D. Kern, and J. N. Yong, Submitted to J. Phys. Chem.
- 21.) M. Z. Al-Alami and J. H. Kiefer, J. Phys. Chem. 87, 499 (1983).
- 22.) M. J. Singh and R. D. Kern, Combust. Flame, 54, 49 (1983).
- 23.) E. Tørnberg, C. J. Nielsen, P. Klæboe, H. Hopf, and H. Priebe, Spectrochimica Acta 36A, 975 (1980).
- 24.) S. W. Benson, "Thermochemical Kinetics", 2nd ed., Wiley, New York, 1976.
- 25.) J. H. Kiefer, L. J. Mizerka, M. R. Patel, and H. C. Wei, J. Phys. Chem. 89, 2013 (1985).
- 26.) R. D. Kern, J. N. Yong, J. H. Kiefer, and J. N. Shah, to be published.
- 27.) J. H. Kiefer, S. A. Kapsalis, M. Z. Al-Alami, and K. A. Budach, Combust. Flame 51, 79 (1983).
- 28.) Th. Just, P. Roth, and R. Damm, 16th (Int'l) Symposium on Combustion, The Combustion Institute, Pittsburgh, 1976, p 961, T. Tanzawa and W. C. Gardiner, Jr., Combust. Flame 39, 24 (1980).

- 29.) K. Raghavachari, M. J. Frisch, J. A. Pople, and P. von R. Schleyer, *Chem. Phys. Lett.* 85, 145 (1982).
- 30.) P. S. Skell, F. A. Fagone, and K. J. Klabunde, *J. Am. Chem. Soc.* 94, 7862 (1972); J. A. Pople, K. Raghavachari, J. H. Frisch, J. S. Brinkley, and P. von R. Schleyer, *J. Am. Chem. Soc.* 105, 6389 (1983); T. Carrington, Jr., L. M. Hubbard, H. F. Schaefer III, and W. H. Miller, *J. Chem. Phys.* 80, 4347 (1984).
- 31.) P. Davidson, H. M. Frey, and R. Walsh, *Chem. Phys. Lett.* 120, 227 (1985).
- 32.) J. S. Binkley, *J. Am. Chem. Soc.* 106, 603 (1984), and references therein.
- 33.) J. A. Berson, in "Rearrangements in Ground and Excited States", Academic Press, New York, 1980, p 311. See also P. J. Stang, *Chem. Rev.* 78, 383 (1978).
- 34.) A. Lifshitz, M. Bidani, and H. F. Carroll, *J. Chem. Phys.* 79, 2742 (1983).
- 35.) W. E. Billups, L-J. Lin, and E. W. Casserly, *J. Am. Chem. Soc.* 106, 3698 (1984)
- 36.) S. W. Staley and T. D. Norden, *J. Am. Chem. Soc.* 106, 3699 (1984).

PREDICTION OF KINETICS FOR C₄ SPECIES WHICH FORM BENZENE

Phillip R. Westmoreland

Chemical Engineering Department
University of Massachusetts - Amherst
Amherst, Massachusetts 01003

INTRODUCTION

C₄ species have long been proposed to be critical intermediates in forming aromatics from lighter aliphatics. Recent work (1) supports the hypotheses that 1-buten-3-ynyl (1-C₄H₃) and 1,3-butadienyl (1-C₄H₅) are the specific species involved in low-pressure flames of acetylene (C₂H₂) and 1,3-butadiene (1,3-C₄H₆).

1-C₄H₃ and 1-C₄H₅ have been suggested before as the key reactants (2-6), but the recent work shows that the earlier, thermal mechanisms are not justified; rather, only chemically activated pathways are feasible. Earlier studies generally assumed addition to C₂H₂, followed by thermal cyclization of the linear adduct to phenyl and cyclohexadienyl, respectively, and by thermal decomposition of the cyclohexadienyl to benzene and H. All reactions were implicitly assumed to be in the high-pressure limit. However, appropriate analysis of falloff indicates that this thermal sequence is too slow, even at 1 atm, while chemically activated intermediates from the same addition reactions lead directly to aromatics with fast enough rate constants.

Identifying the sources of 1-C₄H₃ and 1-C₄H₅ is plainly of interest. Literature analyses (2-6) assumed these sources were addition of C₂H and C₂H₃ to C₂H₂, again (implicitly) in the high-pressure limit. Also, the quantitative test in (1) was comparison of the measured, net rate of benzene formation to a rate calculated from predicted rate constants and the measured C₂H₂, C₄H₃, and C₄H₅ concentrations. An improved test would use concentrations of the specific isomers 1-C₄H₃ and 1-C₄H₅, which could not be resolved from other C₄H₃ and C₄H₅ isomers experimentally.

Rates are predicted and compared here for the reactions that form and destroy 1-C₄H₃, 1-C₄H₅, and other C₄H₃ and C₄H₅ isomers. Rate constants are estimated by analogy and thermochemical kinetics (7) for H-abstraction from 3-butenyne (C₄H₄ or vinylacetylene) and from 1,3-C₄H₆. Using Bimolecular Quantum-RRK (8-9), rate constants, branching and pressure dependence are predicted for the association reactions of radical addition (C₂H+C₂H₂ and C₂H₃+C₂H₂), H-addition (to C₄H₂ and C₄H₄), and H/radical and radical/radical recombination (H+C₄ radicals, C₂H+C₂H₃ and C₂H₃+C₂H₃).

EXPERIMENTAL AND THEORETICAL PROCEDURES

Experimental data. - Profiles of mole fractions were mapped for 38 stable species and free radicals in a lightly sooting flat flame of $C_2H_2/O_2/5\% Ar$ (10) using molecular-beam mass spectrometry. The fuel-equivalence ratio was 2.40, burner velocity (298 K) was 0.50 m/s, and pressure was 2.67 kPa (20 torr). Temperatures were measured using a 0.076-mm diameter Pt/Pt-13%Rh thermocouple, coated with a thin BeO/Y_2O_3 glass to eliminate catalytic heating and resistively heated to the flame temperature so as to eliminate convective heat transfer. Mole fractions were shifted 0.11 mm toward the burner (two orifice diameters), compensating for the shift caused by the probe.

Direct and indirect calibrations were used, and the smoothed data curves were used in the present calculations. Major stable species were calibrated directly within 3% except for H_2O (25%). Minor species were calibrated within a factor of two by the method of relative ionization cross-sections (11). Because of the correction for ^{13}C isotope effects and the low signals, the shapes of the radical profiles are less well defined than those of the minor stable species.

Complete profiles for all species of interest except C_2H and O were measured. For C_2H and O -atom in the present calculations, mole fractions were predicted (10) using a modified Warnatz (12-13) reaction mechanism.

Predicted rate constants. - Two types of reactions were considered: abstractions of H and association reactions, which include additions, combinations, and (by microscopic reversibility) unimolecular decompositions. Abstraction rate constants and high-pressure-limit association rate constants may be estimated by simple analogies or by more complex analogies such as thermochemical kinetics. However, as noted above, proper consideration of pressure effects is necessary for association reactions. Even at 1 atm and for relatively large molecules, these effects can be significant at combustion temperatures (14).

Bimolecular Quantum-RRK (8-9) was used here to predict falloff for addition and combination reactions. The method also predicts rate constants for the chemically activated decomposition paths, which numbered as many as three in the present study. These rate constants are also influenced by pressure but have an inverse falloff behavior (pressure-independent at low pressures (9)). Input data needed for the method are high-pressure-limit, Arrhenius pre-exponential factors and activation energies for each association and dissociation step; geometric mean frequency and number of frequencies in each adduct; and collisional properties of adduct and bath molecules.

Arrhenius parameters A and E_{act} were estimated for one direction of reaction, and the parameters for the reverse reaction then were calculated using the equilibrium constant (microscopic reversibility). For example, rate constants

for radical combinations were estimated by an extension (10) of a method of Benson (15) and were assumed independent of temperature.

ESTIMATION OF THERMODYNAMICS AND OF RATE CONSTANTS

Species involved in the reactions to be analyzed include H, H₂, O, OH, H₂O, C₂H, C₂H₂, C₂H₃, C₂H₄, C₄H₂, C₄H₄ (vinylacetylene), 1,2,3-C₄H₄ (butatriene), 1,3-C₄H₆, and the C₄H₃ and C₄H₅ radicals. Few data are available for the thermodynamics and kinetics of C₄ species. The necessary data may be estimated with useful accuracy, but data uncertainties and their effects must be examined.

Thermodynamics. - These properties (Table 1) were estimated using group additivity. The groups of Benson (7) were supplemented by the recent groups for unsaturates and rings by Stein and Fahr (16). Additional groups for vinyl (ethenyl) and ethynyl radical sites were derived from the heats of formation (298 K) of 70.4 kcal/mol for C₂H₃ (17) and 135 kcal/mol for C₂H (inferred from (18)). These values appear reliable, but other values as low as 63 and 127 have been suggested.

Structural assignments must be made in order to apply group additivity to the C₄H₃ and C₄H₅ radicals. For 1-C₄H₃ or 1-C₄H₅, the radical site is on a terminal alkene carbon, and properties are inferred by analogy of 1-C₄H₃/C₄H₄ or 1-C₄H₅/1,3-C₄H₆ with C₂H₃/C₂H₄. Similarly, properties of the CH₂CHCC· radical can be estimated from C₄H₄ and C₂H/C₂H₂, and for HCC-CH=CH·, from 1-butyne and C₂H₃/C₂H₄. Even for HCC-CH·-CH₃, the species is easily treated as an allylic radical of 1-butyne.

The remaining two radicals, HCC-C·=CH₂ (2-C₄H₃) and CH₂=CH-C·=CH₂ (2-C₄H₅), are more difficult. No groups are available for vinylic radical sites like these that are created inside conjugated pi-bond systems. Instead, thermodynamics are estimated for equivalent resonance structures for 2-C₄H₃ and 2-C₄H₅, respectively ·CH=C=C=CH₂ and ·CH₂-CH=C=CH₂. The first, allenic radical is assumed to be formed with the 110 kcal/mol bond dissociation energy of C₂H₄, while the second radical is treated as a simple allylic site.

The properties are summarized in Table 1. In addition, necessary geometric-mean frequencies were estimated from frequency assignments and are included in Table 1. Rougher estimates could have been used, as the quantized energy distribution is not affected greatly.

Table 1. Estimated thermodynamic properties and geometric-mean frequencies (enthalpy in kcal/mol; entropy in cal/mol K).

	$\Delta H_f, 298$ S298		C_p (cal/mol K) at T (K)=								$\langle \omega \rangle$, cm ⁻¹
			300K	400	500	600	800	1000	1500	2000	
C ₂ H	135.0	49.6	8.9	9.7	10.2	10.7	11.5	12.2	13.3	14.1	
C ₂ H ₃	70.4	54.5	10.9	12.4	13.8	15.1	17.2	18.8	21.3	23.2	
C ₄ H ₂ (HCC-CCH)	105.1	59.8	17.6	20.1	21.9	23.2	25.1	26.6	29.1	30.5	
1-C ₄ H ₃ (HCC-CH=CH)	126.1	66.5	17.2	20.1	22.4	24.4	27.2	29.2	32.7	34.4	1000
2-C ₄ H ₃ (HCC-C'=CH ₂)	138.7	68.3	17.5	20.2	22.5	24.4	27.4	29.6	33.2	34.7	1040
CH ₂ =CH-CC'	149.2	65.3	15.8	18.8	21.4	23.5	26.9	29.3	33.0	34.4	
C ₄ H ₄ (vinylacetylene)	68.2	65.1	17.5	21.2	24.2	26.6	30.3	33.1	37.6	39.7	1080
123-C ₄ H ₄ (butatriene)	80.9	63.1	18.0	21.5	24.4	26.9	30.7	33.5	37.7	39.5	
1-C ₄ H ₅ (CH ₂ =CH-CH=CH')	84.2	68.7	18.6	23.3	26.8	29.5	33.6	36.5	41.4	44.1	1140
2-C ₄ H ₅ (CH ₂ =CH-C'=CH ₂)	72.2	69.9	18.5	22.9	26.5	29.4	34.0	37.4	42.5	44.6	1160
HCC-CH ₂ -CH ₂ '	85.6	70.7	19.4	23.3	26.5	29.3	33.5	36.7	42.6	46.2	1450
HCC-CH'-CH ₃	96.6	73.1	18.8	22.4	25.5	28.3	32.7	36.1	41.5	43.9	1530
1,3-C ₄ H ₆ (butadiene)	26.3	66.6	19.0	24.3	28.5	31.8	36.9	40.5	46.3	49.9	1190
1-butyne	39.6	69.6	19.5	23.9	27.7	30.9	36.1	40.0	47.1	51.7	
2-butyne	35.0	68.2	18.7	22.7	26.4	29.7	35.2	39.3	45.5	49.2	

Radical additions. - Additions of C₂H and C₂H₃ to acetylene are the routes to 1-C₄H₃ and 1-C₄H₅ that have been assumed in previous analyses (2-6). One reason is that such addition leads only to an end radical on the C₄ adduct. Less recognized is that the adduct is initially rovibrationally excited (chemically activated) by the depth of the potential well where the ground-state adduct is located. Falloff can occur, and chemically activated decomposition of the hot adduct is possible to form H+C₄H₂ or H+C₄H₄. Thus, 1-C₄H₃ and H+C₄H₂ are not different types of C₂H+C₂H₂ reactions but different product channels from the same addition.

Calculation shows that the decomposition channels dominate over the simple additions for both these reactions over the range of 900 to 2000 K at 2.67 kPa CO. Even at 1 atm N₂, H+C₄H₂ is faster than the 1-C₄H₃ channel by a factor of 3 or more. For C₂H₃+C₂H₂ at 1 atm N₂, the addition/stabilization channel to 1-C₄H₅ is faster than addition/decomposition to H+C₄H₄ up to 1350 K, but the 1-C₄H₅ channel has fallen off to 1% of the high-pressure limit at 2000 K.

H-atom additions. - Addition of H to C₄H₂ or C₄H₄ also can form C₄H₃ and C₄H₅ radicals. In this case, the H can add (in principle) to any carbon, giving different isomers, and some chemically activated decompositions of the adducts may occur.

H-addition to the end carbons of C₄H₂ forms (2-C₄H₃)*, which can only be stabilized if 1,3-H shifts are disallowed. Addition to the internal carbons forms 1-C₄H₃ and C₂H+C₂H₂' in the reverse of the radical addition sequence described above. Calculation shows that falloff makes the 2-C₄H₃ product of H+C₄H₂

negligible, as the rate constants (2.67 kPa, 1500 K) are $2.6 \cdot 10^{11}$, $1.1 \cdot 10^{11}$, and $1.6 \cdot 10^9 \text{ cm}^3 \text{ mol}^{-1} \text{ s}^{-1}$ for 1-C₄H₃, C₂H+C₂H₂, and 2-C₄H₃. C₂H+C₂H₂ begins to dominate at 1600 K for 2.67 kPa, but 1-C₄H₃ remains dominant even at 2000 K at 1 atm.

The product spectrum from H+C₄H₄ is more complex because addition to each different carbon gives a different adduct. Of the additions forming (1-C₄H₅)* and (2-C₄H₅)*, C₂H₃+C₂H₂ dominates at 1500 K and 2.67 kPa ($2.2 \cdot 10^{12}$), followed by 1-C₄H₅ ($7 \cdot 10^{11}$), 2-C₄H₅ ($2.5 \cdot 10^{11}$), and H+butatriene ($6 \cdot 10^{10}$). Addition/stabilization to 1-C₄H₅ is dominant at 1 atm to 1900 K. Here, as for radical addition, C₄H₅ formation is less inhibited by falloff than is C₄H₃ formation.

Radical/radical and H/radical combinations. - Combination reactions have not generally been considered as paths to C₄ radicals. However, chemically activated decompositions to H+C₄H_x are possible from C₂H₃ combinations with C₂H, forming (C₄H₄)*, and with itself, forming (C₄H₆)*. Combinations of H with C₄H_x radicals are also of interest as sinks and as reactive-isomerization reactions for the radicals.

Formation of 1-C₄H₃ +H is dominant at 2.67 kPa for both C₂H+C₂H₃ and for 2-C₄H₃ +H reactions. Thermalized C₄H₄ is the only other significant product from 2-C₄H₃ +H, while C₂H+C₂H₃ forms minor amounts of C₄H₄ and 2-C₄H₃ +H. From the reaction of 1-C₄H₃ +H, formation of C₄H₄ is strongly favored at both pressures.

In contrast, C₂H₃+C₂H₃ leads predominantly to thermalized 1,3-C₄H₆. The 2-C₄H₅ +H and 1-C₄H₅ +H channels are within an order of magnitude of the C₄H₆ channel at 1500 K and 2.67 kPa, but C₄H₆ formation is even more strongly favored at 1 atm. Both C₄H₅+H channels are similarly dominated by C₄H₆ formation.

Thermal decompositions. - Thermal elimination of H by beta-scission can be an important loss mechanism for radicals. Thermal decompositions of molecules require more thermal activation and are usually not important in flames. In both cases, the kinetics may be calculated from unimolecular reaction theory, using the parameters developed for cases above, or from microscopic reversibility, using the rate constants developed above. In summary, elimination of H proved to be the dominant channel for the radicals, while formation of H + 1-C₄H₃ or 1-C₄H₅ was most important for decomposition of the molecules.

Application to flame data. - Only a few reactions prove to be important in determining the totals of formation and destruction rates. The above rate constants were combined with measured concentrations and temperature profiles to establish the dominant production and destruction channels of 1-

C_4H_3 , $2-C_4H_3$, $1-C_4H_5$, and $2-C_4H_5$. Rates were calculated as a function of position and also were integrated over distance.

$1-C_4H_3$, the apparent precursor of phenyl, is formed two orders of magnitude faster than $2-C_4H_3$. This difference would give super-equilibrium concentrations of $1-C_4H_3$ because equilibrium levels of $2-C_4H_3$ should exceed $1-C_4H_3$. Formation of $1-C_4H_3$ is primarily by H atom reactions with C_4H_2 (addition) and with C_4H_4 (abstraction), while destruction is dominated by loss of H to form C_4H_2 .

One puzzle is that the integrated amount of destruction should be less than or equal to the integrated rate of formation. However, the predicted destruction is greater by a factor of 20. One possible reason is error in the C_4H_3 calibration, as the destruction rate is proportional to C_4H_3 concentration, while formation is independent of it. An alternative is that some formation reaction is not considered. $C_2H_2 + C_2H_2$ was examined using a literature rate constant (19) but it was three orders of magnitude too slow to make any difference.

$1-C_4H_5$ was formed only at 45% of the rate of $2-C_4H_5$, in contrast to the C_4H_3 isomers. For both isomers, hydrogen abstraction by H was the principal source, with $H + C_4H_4$ (addition) and thermal decomposition of $1,3-C_4H_6$ making up 1/10 to 1/3 of the total rate. Simple addition to form $1-C_4H_5$ was important only very early in the flame. This mix is illustrated in Figure 1. Total destruction was higher than formation for C_4H_5 's by a factor of ten. Again, either calibration error or a missing source reaction are suggested as reasons for this difference.

CONCLUSIONS

Formation of $1-C_4H_3$ and $1-C_4H_5$ radicals is dominated by H-abstraction and H-addition. In contrast, previous workers had assumed that addition of C_2H and C_2H_3 to C_2H_2 were responsible. This conclusion is qualified by the excessive destruction that is predicted, but calibration error may be the cause. Detailed experimental data, combined with careful, comprehensive theoretical predictions of rate constants, account for this new understanding.

This study is continuing, further examining the rate constants and using them in predictive flame mechanisms.

ACKNOWLEDGEMENTS

Support of this C_4 study by the University of Massachusetts is gratefully acknowledged. The interest and insights of Professor Jack B. Howard, Professor John P. Longwell, and Dr. Anthony M. Dean are also appreciated.

REFERENCES

1. Westmoreland, P. R., A. M. Dean, J. B. Howard, and J. P. Longwell, submitted for publication.
2. Kinney, R. E., and D. J. Crowley, *Ind. Eng. Chem.*, **46**, 258 (1954).
3. Stehling, F. C., J. D. Frazee, and R. C. Anderson, *Sixth Symposium (International) on Combustion*, The Combustion Institute, Pittsburgh, 247, 1956.
4. Cole, J. A., J. D. Bittner, J. B. Howard, and J. P. Longwell, *Combustion and Flame*, **56**, 51 (1984).
5. Frenklach, M., D. W. Clary, W. C. Gardiner, Jr., and S. E. Stein, *Twentieth Symposium (International) on Combustion*, The Combustion Institute, Pittsburgh, 887, 1984.
6. Frenklach, M., D. W. Clary, T. Yuan, W. C. Gardiner, Jr., and S. E. Stein, *Combust. Sci. and Tech.*, **50**, 79 (1986).
7. Benson, S. W., *Thermochemical Kinetics*, 2nd Ed., Wiley, 1976.
8. Dean, A. M., *J. Phys. Chem.*, **89**, 4600 (1985).
9. Westmoreland, P. R., J. B. Howard, J. P. Longwell, and A. M. Dean, *AIChe J.*, **32**, 1971 (1986).
10. Westmoreland, P. R., *Experimental and Theoretical Analysis of Oxidation and Growth Chemistry in a Fuel-Rich Acetylene Flame*, Ph. D. thesis, Department of Chemical Engineering, Massachusetts Institute of Technology, 1986.
11. Lazzara, C. P., J. C. Biordi, and J. F. Papp, *Combustion and Flame*, **21**, 371 (1973).
12. Warnatz, J., *Combustion Science and Technology*, **34**, 177 (1983).
13. Westmoreland, P. R., J. B. Howard, and J. P. Longwell, *Twenty-First Symposium (International) on Combustion*, The Combustion Institute, Pittsburgh, in press.
14. Golden, D. M., and C. W. Larson, *Twentieth Symposium (International) on Combustion*, The Combustion Institute, Pittsburgh, 595, 1984.
15. Benson, S. W., *Can. J. Chem.*, **61**, 881 (1983).
16. Stein, S. E., and A. Fahr, *J. Phys. Chem.*, **89**, 3714 (1985).
17. McMillen, D. F., and D. M. Golden, *Ann. Rev. Phys. Chem.*, **33**, 493 (1982).
18. Wodtke, A. M., and Y. T. Lee, *J. Phys. Chem.*, **89**, 4722 (1985).
19. Tanzawa, T., and W. C. Gardiner, Jr., *J. Phys. Chem.*, **84**, 236 (1980).

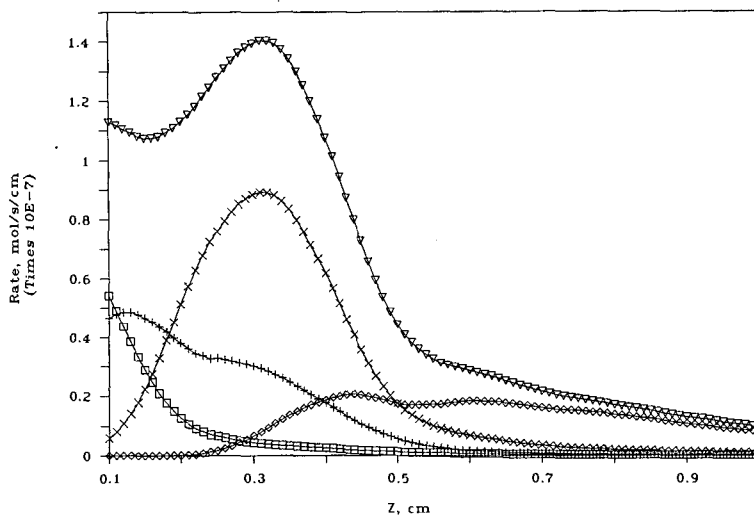


Figure 1. Predicted rates for reactions leading to 1-C₄H₅, using measured concentrations and predicted rate constants for C₂H₃+C₂H₂ (□), H+C₄H₄ (+), 1,3-C₄H₆ decomposition (◇), 1,3-C₄H₆ + H (×), and total (▽).

Formation of Small Aromatic Molecules in a Sooting Ethylene Flame

Stephen J. Harris

Anita M. Weiner

and

Richard J. Blint

Physical Chemistry Department, General Motors Research Laboratories, Warren, MI 48090-9055

Abstract

Small aromatic species are undoubtedly important precursor molecules in the formation of polycyclic aromatic hydrocarbons and soot, two important pollutants in diesel, direct-injection stratified charge (DISC), and other heterogeneous-combustion engines. Unfortunately, the chemical route to their formation is poorly understood, in part because rate constants for reactions of aromatic species at flame temperatures are largely unknown. In this work we used a quartz sampling probe to measure the concentration profiles of the single-ring aromatics benzene, phenylacetylene, and styrene in a heavily sooting premixed ethylene flame. A detailed chemical kinetics model was then constructed for the purpose of explaining the flame chemistry. The model, which uses estimated rate constants for many of the reactions involving aromatic species, gives good predictions for benzene and styrene and fair predictions for phenylacetylene. A sensitivity analysis has isolated a particular chemical reaction which controls their rate of formation, and it shows that even large errors in the other aromatic rate constants have relatively little effect on the predictions. Our approach will be applied in the future to trying to understand the formation of larger aromatic species and soot.

Introduction

Over the years there has been a considerable effort towards improving our understanding of the detailed chemistry in hydrocarbon combustion¹⁻³. Much of the work has concentrated on lean and stoichiometric flame environments, but understanding the processes that take place in rich systems is of great importance since many practical flames are diffusion flames. Unfortunately, rich combustion is a very difficult area for flame modeling because of the involvement of large hydrocarbon molecules and soot, species whose chemistry and thermodynamics are poorly known. In contrast, lean and near-stoichiometric flames involve a smaller number of species, nearly all of which are eventually converted to CO_2 and H_2O .

However, as knowledge of the kinetics and thermodynamics of hydrocarbons has increased, a growing number of studies have considered rich flame environments. These include, for example, the experiments of Homann and Wagner⁴, Howard and co-workers⁵, Bockhorn⁶, and Taylor⁷. In addition, detailed models have recently been constructed specifically to deal with rich flames⁸⁻¹⁰. In most of these cases, however, studies have been limited to non-sooting or lightly sooting flames because the presence of soot can make measurements difficult and because models have tended to avoid systems where pyrolysis chemistry and soot formation played major roles.

In recent work¹¹ we measured mole fraction profiles of a number of stable and radical species in a heavily sooting ethylene flame, and, building on previous work^{2,9,12}, we developed a model which predicted the profiles of many of the measured species with good accuracy. It would be very valuable to develop a reliable ethylene combustion model because many fuels such as octane are converted largely to ethylene on their way to being oxidized¹. Thus, an ethylene oxidation mechanism is an important component for models of more realistic fuels.

Unfortunately, our model severely underestimated the benzene mole fraction, and no other aromatic species was modeled. Since the goal of this research program is to understand the chemistry of soot formation, and since aromatic species undoubtedly play an important role in that process, our inability to model the chemistry of even the simplest aromatics was an important stumbling block. In this paper we describe modifications to our model which allow the successful prediction of the profiles of benzene, styrene, and, to a lesser extent, phenylacetylene. It is our hope that if the chemistry of large aromatics is similar to that of smaller aromatics, then semi-quantitative predictions of soot formation kinetics in well-studied systems such as premixed flat flames¹³ may be attainable in the foreseeable future.

Experiment and Model

The experimental conditions employed in this work have been described previously¹¹. Briefly, a flat premixed $C_2H_4/O_2/Ar$ flame with C/O ratio of 0.92 ($\phi = 2.76$) was stabilized on a water-cooled porous plug burner surrounded by a shroud of nitrogen. The $Ar : O_2$ mole ratio was 79 : 21. A quartz microprobe withdrew gases from the flame. No measurements could be taken beyond about 3.3 mm above the top of the burner because soot would clog the probe. Species mole fractions, X_i , were measured with a mass spectrometer and signal averaged on a computer. The complete species profiles were measured a number of

times. The resulting statistical uncertainties at the 90% confidence level (estimated from a Student's *t* distribution) were about $\pm 10\%$ for benzene. For styrene and phenylacetylene the uncertainty was about $\pm 25\%$ near their peaks and $\pm 50\%$ in the pre-flame zone where their concentrations were very low. There was also a potential systematic error of as much as 50% for styrene and phenylacetylene because of uncertainty in the mass spectrometer calibration. The pressure drop across the microprobe orifice was maintained at between 50:1 and 100:1 in order that the stable species chemistry would be adequately quenched. Tests and analysis on several species indicated that the quench was successful¹¹. We estimated that the profiles were shifted by approximately 2.5 probe orifice diameters (0.4 mm) from their true location¹¹. The figures in this paper have incorporated this shift. Temperatures were determined from measurements with both 3 mil and 5 mil diameter silica-coated, radiation-corrected Pt/Pt-Rh thermocouples. For measurements made in the sooting zone, thermocouple readings were difficult to take because the temperature dropped as soon as the thermocouple became coated with soot. Therefore, measurements were taken continuously with a computer as the flame was ignited. In this way the rise and fall in the thermocouple readings were recorded. We took the highest measured temperature as the true flame temperature, making sure that our results were unaffected by the rate at which the computer took the measurements. The two different thermocouples gave identical temperature profiles. The temperature peaked at 3.1 mm above the top of the burner at about 1640 K.

Concentration profiles were modeled using the Sandia burner code¹⁴ together with a mechanism that we developed for the flame. A number of reactions involving butane, butyl radical, 2-butene, propane, acetaldehyde, and acetaldehyde radical were considered, but they did not contribute to the profiles that we measured under our conditions. Therefore those species were eliminated. A partial mechanism is given in Table 1. (The complete mechanism is available from the authors.) For ease of comparison with previous work of Frenklach *et al.*^{10,15}, we have used the shorthand nomenclature that they suggested for aromatic species. In this system $A_n(R_m)$ refers to a species with *n* fused aromatic rings (fused to an *m*-membered non-aromatic ring). Radicals are indicated by a "*" or a "-". Table 2 shows structures for some of the species which appear in the mechanism. A complete table is given in Frenklach *et al.*¹⁵.

Most of the thermodynamics for small species comes from the Chemkin data base¹⁶, supplemented where necessary by other standard sources¹⁷. We assumed^{11,18a} a 70.5 kcal heat of formation for the vinyl radical (C_2H_3) and a 109 kcal heat of formation for C_4H_2 ^{18b}. For all the aromatic species we used the thermodynamics of Stein and Fahr¹⁹. (This set of data was called S6^{10,19b}.) In addition we used Stein and Fahr's thermodynamics for three aliphatic radicals which are closely related in our model to aromatic species, namely $n-C_4H_3$ ($\Delta H_f^{300} = 124$ kcal/mole), C_8H_5 ($\Delta H_f^{300} = 190$ kcal/mole), and C_6H_5 ($\Delta H_f^{300} = 138$ kcal/mole).

Information on the high temperature kinetics of most aromatic species, especially those larger than benzene, tends to be either too sparse or too tentative for us simply to use literature values for rate constants. In order to make progress we followed the approach of Frenklach, Clary, Gardiner, and Stein²⁰ (FCGS). These workers considered a very large number of elementary reactions for aromatic formation and growth. The reactions were grouped into classes, and all reactions of a given class were assigned the same rate constant.

For example, based on the measurement by Madronich and Felder²¹ for the rate of reaction between *OH* and benzene, all reactions involving *OH* abstraction of an aromatic hydrogen were assigned the rate constant $k_{T02} = 2.1 \times 10^{14} e^{-4600/RT}$. For other reaction classes rate constants were not available, and upper limit (nearly gas kinetic) values were assigned to their rate constants. In this way, they were able to identify the major reaction pathways as well as pathways which were not important.

However, use of upper limit values for rate constants entails certain disadvantages. First, because they are in general too large, this approach cannot be expected to yield results that are in quantitative agreement with experiment. Second, the usefulness of sensitivity coefficients cannot be expected to be great if the estimated rate constants are incorrect by very large factors. (However, FCGS²⁰ identified some pathways to aromatic formation whose relative importance is very small for almost any reasonable choice of rate constants.) Finally, if the rate constants are chosen to be sufficiently high the sensitivity coefficients may be smaller than they otherwise would be (As $k \rightarrow \infty$ its associated sensitivity coefficients will in general approach 0.), and the analysis may conclude that thermodynamics is relatively more important compared to kinetics than it actually is.

In our work we addressed these issues by using experimentally derived rate constants which have recently become available and by testing the effects of some very large changes in the rate constants (see Discussion section). The rate constants for aromatic species were derived as follows:

1. Mallard *et al.*²² measured the rate for reaction of the phenyl radical with acetylene (*U15*) and ethylene (*U18*). We used the same rate constants for *U16*, *U17*, *U19*, *U20*, and *G10*, which are similar.
2. Kiefer *et al.*²³ obtained the rate constant for abstraction of a benzene hydrogen by *H* (*T03*) from a model of his shock tube experiments. This rate constant extrapolates at 800 K to a value fairly close to that suggested by Nicovich and Ravishankara²⁴. We used the same value for *U02*, *G02*, and *G11*. We assumed that abstraction of an aromatic hydrogen by *C₂H* and *C₂H₃* is five times slower (*G04*, *G05*, *G08*, *G09*, *U04*, *U05*, *U09*, and *U10*).
3. Colket²⁵ used his shock tube results to obtain the rate constant for the displacement of a benzene hydrogen by *C₂H* (*U11*). We used the same value for displacement by vinyl (*U12*). The value for k_{T06} , the rate constant for ring formation, is taken from FW¹⁰, which at our temperatures is nearly identical to the value estimated by Colket²⁵. k_{U21} and k_{G12} were given the same value.
4. Hsu *et al.*²⁶ measured the rate constant for decomposition of benzene to phenyl and *H* (*T01*). We used this value for *U01*, *U06*, *G01*, and *G06*.
5. Cole *et al.*^{5b} estimated the rate of formation of benzene from *C₄H₅* and *C₂H₂* in their low pressure butadiene flame. We used their value for k_{T07} .
6. The rate constant for *U13* was given an upper limit value taken from Frenklach and Warnatz¹⁰; the same rate constant was used for *U14*.
7. k_{T08} and k_{U22} are evaluated below.

Reaction Path and Sensitivity Analysis

Principal reaction paths for species up to the *C₄*'s have been presented previously¹¹.

Graphs of the concentration profiles of many of those species were also presented¹¹. Here we discuss profiles and reaction paths for the single-ring aromatic species that we measured.

Benzene (A_1)

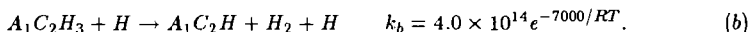
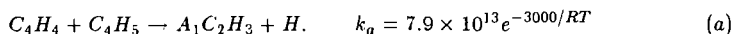
The calculated rate of benzene formation peaks between 1.6 and 2.2 mm (from 1450 - 1600 K), compared to peak formation rates of the C_3 and C_4 species between 1 and 1.6 mm. A single reaction path dominates at 1.8 mm, $T08$ followed by $T06$ and $-T01$ or $-T03$. The importance of $T08$ was emphasized originally by Bockhorn *et al.*⁶ and FCGS²⁰. In the pre-reaction zone $T07$ dominates, reflecting the higher concentration of C_4H_5 compared to $n-C_4H_3$ in the lower temperature environment found there (Figure 1). FW also found that ring formation was dominated by $T07$ in the pre-flame zone. We did not include any oxidation reactions which destroyed the aromatic ring since we have no evidence that such reactions are important in our flame and since the detailed kinetics of the species involved²⁷ would be entirely speculative.

A sensitivity analysis shows that the calculated benzene concentration in the region of its peak formation rate depends most strongly (sensitivity coefficient $\equiv \left| \frac{\partial \ln X_i}{\partial \ln k_j} \right| > 0.5$) on only three rate constants, k_{F01} , k_{A02} , and k_{T08} ; other rate constants to which the benzene concentration is sensitive include k_{H02} , k_{H03} , k_{A08} , k_{V04} , k_{V11} , and k_{F11} . k_{T01} and k_{T06} , with sensitivity coefficients between 0.05 and 0.06 are the only rate constants involving an aromatic ring with a sensitivity coefficient greater than 0.05. In the pre-flame region the above rate constants again have the highest sensitivities. Thus, among all the rate constants involving aromatic formation, many of whose values had to be guessed or extrapolated, only k_{T08} is critical. (This same conclusion was reached by FCGS²⁰ in their very extensive search for reaction paths leading to the formation of aromatic rings.) The calculated concentration is also sensitive to the thermodynamic values assumed for $n-C_4H_3$, a 5 kcal/mole increase in its heat of formation leading to a 3-fold reduction in the benzene concentration. A similar change in the assumed heat of formation of the aliphatic radical C_6H_5 has only a 10% effect. Assuming, then, that our pathway to form benzene is correct, that oxidation reactions which destroy the ring can be ignored, and that the thermodynamics is correct, we can estimate k_{T08} by comparing predicted and measured benzene concentrations. We chose $k_{T08} = k_{U22} = 1.5 \times 10^{12}$ cm³/molecule-sec, which is nearly identical to the value found¹⁰ to reproduce best the data of Bockhorn *et al.*⁶ (However, considering the differences between our mechanism and the one used in Ref. 10 as well as the differences in the pressure of the flames modeled, the significance of this agreement is not immediately clear.) With this choice, the rate of $T06$ at 1.8 mm is 50% faster than $-T06$, 2.5 times faster than $T08$, and about 10 times faster than $-T08$. Later in the flame, beyond 2.6 mm (1630-1640 K), the experiment shows that net benzene formation nearly comes to a halt. According to the model, in this region benzene is still being formed by $-T01$, but now it is being destroyed by $T03$ at about the same rate. Furthermore, $T06$ and $T08$ briefly run in the reverse (decomposition) directions, with the rate of $-T06$ being 0.6% faster than $T06$ and $-T08$ being 3.6% faster than $T08$. With such a fine balance, it is not surprising that the net directions in which $T06$, and $T08$ run are very sensitive to temperature. For example, our calculations show that if the peak temperature is assumed to be 1600 K, 40 K less than the measured value, these reactions always run in the direction of forming benzene.

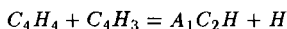
A comparison between the experiment and the model is shown in Figure 2. Adjustment of k_{T08} insures agreement at 3 mm, but we note that the model also reproduces fairly well the shape of the rise through the flame zone as well as the sharp leveling out in the profile beyond 2.5 mm.

Phenylacetylene (A_1C_2H) and Styrene ($A_1C_2H_3$)

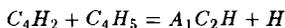
The predicted phenylacetylene profile (solid curve in Figure 3) differs by a factor of up to 6 from the experimentally measured profile. This discrepancy is more than a factor of two worse than for the C_3 and C_4 species from which phenylacetylene is ultimately formed, and it is much greater than the uncertainty in the measurements. Because all of the aromatic species showed similar first-order sensitivity coefficients to most of the same rate constants, no adjustment of a single rate constant to improve the agreement with phenylacetylene seemed possible without seriously degrading the agreement between the model and experiment for the other aromatic species. It is likely that the discrepancy is due to a combination of errors in more than one rate constant, requiring second- or higher-order sensitivity coefficients to identify them, or to errors in the precursor thermodynamics. However, we considered two alternate explanations for the discrepancy. First, we may not have identified the major pathway forming phenylacetylene. For example, Colket²⁵ has suggested an overall irreversible pathway to phenylacetylene.



Addition of these reactions increased the calculated phenylacetylene concentration by less than 10%, while reducing the styrene concentration by nearly an order of magnitude. Such a reduction would seriously degrade the agreement between measured and calculated styrene profiles (see below). (On the other hand, adding a detailed route from styrene to phenylacetylene analogous to the route from ethylene to acetylene—essentially a detailed version of Equation (b)—had hardly any effect on any of the aromatic profiles.) Inclusion of other possible routes to phenylacetylene,



or



with $k = 1.0 \times 10^{13}$ had little or no effect. Increasing k_{U22} by a factor of 5 had no effect on the phenylacetylene profile. We found no new reaction pathway which gave a substantial increase in the phenylacetylene concentration. A second possible explanation for the discrepancy between the model and the experiment could be uncertainty in the thermodynamics of phenylacetylene. To test for this possibility we lowered its assumed heat of formation at 300 K from 75 to 71 kcal/mole. The result, shown by the dashed line in Figure 3, is improved overall agreement, although the calculated and experimental profile shapes are still somewhat different. (The same effect could be obtained by changing the assumed entropy or the assumed heat capacity at high temperature.) Among other species, only the benzene and styrene concentrations were affected by this change, being reduced by about 10%.

The peak formation rate for phenylacetylene occurs in the same region as for benzene. Most of the phenylacetylene comes from the direct reaction between phenyl and acetylene (U_{15}); a smaller but still substantial amount comes from U_{22} followed by U_{21} and $-U_{09}$. The sensitivity coefficients for phenylacetylene are similar to those for benzene, although sensitivities to k_{F01} , k_{F08} , k_{F11} , k_{A02} , and k_{A08} are somewhat higher, reflecting among other factors a particular sensitivity to the acetylene concentration (which is modeled very well). There is also some sensitivity—about 0.1—to k_{U15} . (But increasing k_{U15} to 1.0×10^{13} increases the phenylacetylene concentration by only about 10%.)

The calculated net styrene formation rate peaks between 1.4–1.7 mm (1300–1500 K), somewhat earlier than the other aromatics. This is because the principal reaction forming styrene, U_{18} , involves C_2H_4 , whose concentration is falling rapidly with height. $-U_{12}$ is the major destruction reaction there. By 2.25 mm the rate of $-U_{12}$ exceeds U_{18} by a factor of 3, causing the styrene mole fraction to fall. Sensitivity coefficients for styrene are very similar to those for phenylacetylene, except for a much lower sensitivity to k_{U15} and some sensitivity to k_{U12} and k_{U18} .

A comparison between calculated and measured styrene mole fractions is shown in Figure 4. The agreement in shape and magnitude is good, although the calculated profile peaks earlier than the experimental one. It is interesting that the experiment showed benzene and phenylacetylene climbing rapidly through the reaction zone and then leveling off, while the styrene concentration peaks and falls. The model reproduces the proper qualitative behavior for all three species. The concentration of styrene falls in part because the mole fractions of ethylene and vinyl drop steeply through the post-flame region (*e.g.*, see Figure 1), increasing the net rate of $-U_{12}$ and decreasing the net rate of U_{18} . The most important reactions forming phenylacetylene (U_{15}) and benzene (T_{08}) run mainly in the forward direction throughout the flame, in part because the acetylene mole fraction does not change substantially in the post-flame region.

Naphthalene (A_2) and Acenaphthalene (A_2R_5)

Although we have no measurements for species larger than styrene, we continued the mechanism up to acenaphthalene in order that profiles of the species that we measured not become artificially high due to a lack of exit channels²⁸.

The path to larger aromatics funnels through phenylacetylene. Attack by H (U_{02}) (or OH (U_{03})) gives phenylacetylene radical, which almost irreversibly adds acetylene (G_{13}) and closes to form the naphthalene radical A_7^*X (G_{12}). This species can give naphthalene ($-G_{06}$ or $-G_{11}$) or react with acetylene (G_{10}) to give acenaphthalene.

Our analysis shows that the sensitivity spectra of naphthalene and acenaphthalene are very similar to that of phenylacetylene. In addition both are very sensitive to U_{02} and somewhat sensitive to G_{13} , while acenaphthalene is also quite sensitive to G_{10} .

Discussion

Comparison with Other Systems

Frenklach and Warnatz¹⁰ have very recently made the first detailed flame calculations to model the profiles of aromatic species in a flame. The flame modeled was a sooting ($\phi = 2.75$) 90 torr premixed acetylene flame studied by Bockhorn *et al.*⁶ Although they

obtained a certain qualitative agreement with Bockhorn's data, the calculated profiles of the aromatics declined precipitously in the post-flame gases, while the measured profiles dropped rather more slowly. The principal reason for this discrepancy¹⁰ comes from an apparent overestimate of the fragmentation rate of aromatic radicals *via* the reverse of reactions such as *T06*. It is possible that this overestimate is due to errors in the thermodynamic parameters, since those parameters determine the reverse reaction rates.

With the chosen value for k_{T08} , the measurements and calculations for benzene and styrene in our flame are in good agreement, both in the profile shapes and in their absolute values. The fact that the experimentally measured benzene and phenylacetylene concentrations do not decline in the post-flame region of our flame as they do in Bockhorn's flame can readily be explained by the fact that Bockhorn's flame is about 400 K hotter than ours. Graham *et al.*²⁹ interpreted the fall in the soot yield in their shock tube experiments for temperatures above 1800 K by postulating that at high temperatures the aromatic ring fragments more rapidly than it grows. Other data showing this "bell" have been explained in a similar way³⁰, and the aromatics in premixed flames may be subject to the same processes.

FCGS²⁰ have suggested that the driving force behind formation of larger aromatic species and soot is the superequilibrium of *H* atoms. They proposed R/K_{eq} as a measure of this superequilibrium, where $R = [H]^2/[H_2]$ and where $K_{eq} = [H_{eq}]^2/[H_2]$. They attributed the decline in the formation and growth rate of aromatics at long time to the decay of R/K_{eq} . We have plotted this ratio in Figure 2. The precipitous decline in R/K_{eq} to values below about 100 coincides very roughly with the slowdown in the formation of the benzene profile. However, our kinetic analysis and that of FW¹⁰ suggest that it is the increase in temperature through the reaction zone—leading to higher ring fragmentation rates—which is actually responsible for the cessation of net benzene and phenylacetylene formation. From this point of view, the fall in R/K_{eq} is simply a reflection of the fact that the temperature is rising in a region of constant or falling *H*-atom mole fraction. Furthermore, our model predicts that net benzene and phenylacetylene formation accelerates later in the flame where the temperature is lower, even though R/K_{eq} ultimately drops to about 2. (This secondary rise in net aromatic formation has previously been modeled¹⁰ and observed experimentally³¹.) The fact that net benzene and phenylacetylene formation is greater when $R/K_{eq} < 10$ than when $R/K_{eq} \sim 100$ suggests that the value of this ratio is not of fundamental significance in aromatic formation.

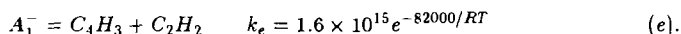
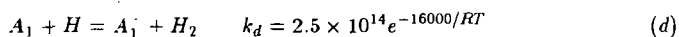
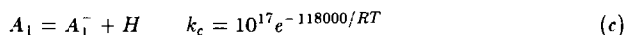
Robustness of the Model

The model that we have presented relies in many cases on analogies and estimates for rate constants of aromatic species because few of these rate constants are known. When they are measured the new values can replace those used here. Similarly, our knowledge of thermodynamic properties of large aromatic species can be expected to improve. The usefulness of this modeling effort, then, depends on the robustness of the calculations to potentially large changes in the values of the rate constants and to some changes in the thermodynamics. FW¹⁰ have shown the effects of changing certain thermodynamic assumptions, and we have reported above some effects on the calculated phenylacetylene profile. The effects are significant but not drastic for the species modeled here; additional efforts to measure or calculate thermodynamic properties, particularly for larger species,

would be very valuable in order to better understand hydrocarbon growth in flames.

The situation may be somewhat more promising with regard to uncertainty in the rate constants. The analyses done by FCGS²⁰, FW¹⁰, and ourselves show remarkably small values for most of the sensitivity coefficients. However, as we pointed out above, the model could still be quite sensitive to very large changes in the rate constants. In order to evaluate this possibility, we ran our flame code using the aromatic mechanism and rate constants of FW, only adding analogous reactions for styrene, which did not appear in their mechanism, and using our value for k_{T08} . This involved many significant changes. For example, FW's value for k_{T03} is about two orders of magnitude greater than that of Kiefer *et al.*²³ The profiles for the single-ring compounds changed by less than 50% compared to those obtained using the mechanism in the Table 1, supporting our conclusion that k_{T08} is the only critical unknown rate constant. (However, the predicted concentrations of 2-ring compounds changed substantially, reflecting their sensitivity to UO_2 .)

As a second test of the robustness of our mechanism we asked whether our model is consistent with benzene decomposition measurements made by Kiefer *et al.*²³ According to this proposed mechanism, benzene decomposition at 1 atmosphere follows the route:



Our mechanism already includes (d); we replaced $T01$ and $T06/T08$ with (c) and (e). The result is a reduction in the calculated aromatic concentration by 40-45%, with little effect on the qualitative shapes of the profiles. Since we have not used the same thermodynamic assumptions as Kiefer, use of his rate constants in our system is not really warranted. (The reactions are running in the reverse direction.) However, taken together with the fact that Kiefer's results were not highly sensitive to k_e , the modest effect of the change in rate constants suggests that the mechanism of Table 1 is in reasonable agreement with the shock tube results of Kiefer *et al.*

Conclusions

We believe that we have made progress in modeling the pyrolysis processes in our flame up to and including the formation of single-ring aromatic species, even though there is great uncertainty in many of the rate constants. Our sensitivity analysis shows that the basis for this success is that there is a single crucial unmeasured rate constant, k_{T08} , which largely controls the combined single-ring aromatic species concentrations. Our results are in accord with those of FCGS and FW, even though we used experimentally derived rate constants which were not available to them. The robustness of our model to future changes in most of the rate constants used in the aromatic part of our model appears to be high.

We hope in the future to continue our measurements and modeling work to species with more than one aromatic ring. If we are successful in modeling growth from one to two rings, we can have some hope for modeling much larger species if adequate thermodynamics are available.

The ability to model soot formation in a flame, however, requires overcoming several additional hurdles. First, the number of species becomes too large to handle with a code such as that used here. As an alternative we could model the growth to larger species by ignoring diffusion in the post-flame gases and using a much faster code which assumes a homogeneous environment. The burner code, then, would provide estimates for the concentrations of small radicals and hydrocarbons which could be crucial for the hydrocarbon growth. Second, in order to calculate soot particle inception, additional processes such as coagulation and surface growth would have to be included. Recent work³² suggests that these processes can be considered without significant additional demands on computer resources.

Acknowledgements

We are grateful to Professor Michael Frenklach of Pennsylvania State University for many helpful discussions and for providing us with an advance copy of his paper with Warnatz and with the thermodynamics of Stein and Fahr.

References

1. J. Warnatz, Twentieth Symposium (International) on Combustion, The Combustion Institute, p. 845 (1984).
2. Westbrook, C. K., Dryer, F. L., Schug, K. P., Nineteenth Symposium (International) on Combustion, The Combustion Institute, Pittsburgh, 1982, pg. 153.
3. Miller, J.A., Mitchell, R.E., Smooke, M.D., and Kee, R.J., Nineteenth Symposium (International) on Combustion, The Combustion Institute, p. 181 (1982).
4. Bonne, U., Homann, K.H., and Wagner, H.Gg., Tenth Symposium (International) on Combustion, The Combustion Institute, p. 503 (1965).
- 5a. Bittner, J.D. and Howard, J.B., Eighteenth Symposium (International) on Combustion, The Combustion Institute, p. 1105 (1982).
- b. Cole, J.A., Bittner, J.D., Longwell, J.P., and Howard, J.B. *Combustion and Flame* **56**, 51 (1984).
6. Bockhorn, H., Fetting, F., and Wenz, H.W., *Ber. Bunsenges. Phys. Chem.* **87** 1067 (1983).
7. Taylor, B.R., Thesis, Department of Chemical Engineering, MIT, 1984.
8. Warnatz, J., Bockhorn, H., Moser, A., and Wenz, H.W., Nineteenth Symposium (International) on Combustion, The Combustion Institute, Pittsburgh, p. 197 (1982).
9. Levy, J.M., Taylor, B.R., Longwell, J. P., and Sarofim, A. F., Nineteenth Symposium (International) on Combustion, The Combustion Institute, Pittsburgh, p. 167 (1982).
10. M. Frenklach and J. Warnatz, "Detailed Modeling of PAH Profiles in a Sooting Low-Pressure Acetylene Flame," *Combustion Science and Technology*, in press.
11. Harris, S.J., Weiner, A.M., Blint, R.J., and Goldsmith, J.E.M., Twenty-first Symposium (International) on Combustion, The Combustion Institute, in Press.
12. Cathonnet, M., Gaillard, F., Boettner, J. C., Cambray, P., Karmed, D., Bellet, J.C., "Twentieth Symposium (International) on Combustion", The Combustion Institute, Pittsburgh, 1984, pg. 819.
13. Harris, S.J., Weiner, A.M., Ashcraft, C.C., *Comb. and Flame* **64**, 65 (1986).
- 14a. Smooke, M.D., *J. Comp. Phys.*, **48**, 72 (1982).
- b. Kee, R.J., Grear, J.F., Smooke, M.D., and Miller, J.A., "A Fortran Program for Modeling Steady Laminar One-Dimensional Premixed Flames." Sandia Report SAND85-8240, 1985.
15. Frenklach, M., Clary, D.W., Yuan, T., Gardiner, W.C., and Stein, S.E., *Combustion Science and Technology* **50**, 79 (1986).
16. Kee, R.J., Rupley, F.M., and Miller, J.A., "The Chemkin Thermodynamic Data Base," Sandia Report SAND87-8215, April, 1987.
- 17a. Stull, D.R., Westrum, E.F., and Sinke, G.C., "The Chemical Thermodynamics of Organic Compounds," Wiley, New York, 1969.
- b. Burcat, A. in "Combustion Chemistry," W.C. Gardiner, ed., Springer-Verlag, New York, 1984, p. 455.
- 18a. McMillen, D.F. and Golden, D.M., *Ann. Rev. Phys. Chem.* **33**, 493 (1982).

- b. Bittner, J.D., Thesis, MIT, 1981.
- 19a. Stein, S.E. and Fahr, A. J. Phys. Chem. **94**, 3714 (1985).
- b. Frenklach, M., Clary, D.W., Gardiner, W.C., and Stein, S.E, 15th Symposium on Shock Waves and Shock Tubes, Stanford University Press, 1986, p. 295.
20. Frenklach, M., Clary, D.W., Gardiner, W.C., and Stein, S.E, Twentieth Symposium (International) on Combustion, The Combustion Institute, p. 887 (1985).
21. Madronich, S. and Felder, W., J. Phys. Chem. **89**, 3556 (1985).
22. a. Mallard, W.G., Fahr, A., and Stein, S.E., Chem. Phys. Proc. Combustion, Paper 92, 1984.
- b. Mallard, W.G., private communication.
23. Kiefer, J.H., Mizerka, L.J., Patel, M.R. and Wei, H.-C., J. Phys. Chem. **89**, 2013 (1985).
24. Nicovich, J.M. and Ravishankara, A.R., J. Phys. Chem. **88**, 2534 (1984).
25. Colket, M.B., "The Pyrolysis of Acetylene and Vinylacetylene in a Single-Pulse Shock Tube," Twenty-first Symposium (International) on Combustion, The Combustion Institute, in Press.
26. Hsu, D.S.Y., Lin, C.Y., and Lin, M.C., Twentieth Symposium (International) on Combustion, The Combustion Institute, p. 623 (1984).
27. Brezinsky, K., Prog. Energy Combust. Sci. **12**, 1 (1986).
28. Kiefer, J.H., Kapsalis, S.A., Al-Alami, M.S., Budach, K.A., Comb. and Flame **51**, 79 (1983).
29. Graham, S.C., Homer, J.B., and Rosenfeld, J.L., Proc. R. Soc. London **A344**, 259 (1975).
30. Frenklach, M., Ramachandra, M.K. and Matula, R.A., Twentieth Symposium (International) on Combustion, The Combustion Institute, p. 871 (1984).
31. Westmorland, P.R., "Experimental and Theoretical Analysis of Oxidation and Growth Chemistry in a Fuel-Rich Acetylene Flame," Ph. D. Thesis, Department of Mechanical Engineering, Massachusetts Institute of Technology, 1986.
32. Frenklach, M. and Harris, S.J., "Aerosol Dynamics Modeling Using the Method of Moments," J. Colloid and Interface Science, in Press.
33. Gardiner, W. C. and Troe, J., in "Combustion Chemistry," W.C. Gardiner, ed., Springer-Verlag, New York, 1984, p. 173.
34. Frank, P.I, Bhaskaran, K.A., and Just, T., Twenty-First Symposium (International) on Combustion, The Combustion Institute, in press.

Table 1

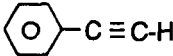
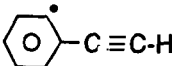
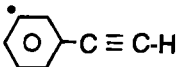
REACTIONS	A	n	E _a
A02) $C_2H_3 = C_2H_2 + H$	6.6E+19	-2.794	36130.0
A08) $C_2H_2 + OH = CH_2CO + H$	1.0E+14	0.0	11500.0
F01) $C_2H_3 + O_2 = HCO + CH_2O$	4.0E+12	0.0	-250.0
F11) $HCO + O_2 = CO + HO_2$	5.0E+11	0.5	835.0
H02) $H_2 + O = H + OH$	1.5E+07	2.0	7550.0
H03) $H + O_2 = O + OH$	1.2E+17	-907	16620.0
V04) $C_4H_4 + H = C_4H_3 + H_2$	7.9E+13	0.0	14500.0
V11) $C_2H_2 + C_2H_2 = C_4H_3 + H$	2.0E+12	0.0	45900.0
T01) $A_1 = A_1^- + H$	5.0E+15	0.0	108600.0
T02) $A_1 + OH = A_1^- + H_2O$	2.1E+13	0.0	4600.0
T03) $A_1 + H = A_1^- + H_2$	2.5E+14	0.0	16000.0
T04) $A_1 + C_2H = A_1^- + C_2H_2$	5.0E+13	0.0	16000.0
T05) $A_1 + C_2H_3 = A_1^- + C_2H_4$	5.0E+13	0.0	16000.0
T06) $C_6H_5 = A_1^-$	1.0E+10	0.0	0.0
T07) $C_4H_5 + C_2H_2 = A_1 + H$	3.2E+11	0.0	3700.0
T08) $C_4H_3 + C_2H_2 = C_6H_5$	1.5E+12	0.0	0.0
U01) $A_1C_2H = A_1C_2H^+ + H$	5.0E+15	0.0	108600.0
U02) $A_1C_2H + H = A_1C_2H^+ + H_2$	2.5E+14	0.0	16000.0
U03) $A_1C_2H + OH = A_1C_2H^+ + H_2O$	2.1E+13	0.0	4600.0
U04) $A_1C_2H + C_2H_3 = A_1C_2H^+ + C_2H_4$	5.0E+13	0.0	16000.0
U05) $A_1C_2H + C_2H = A_1C_2H^+ + C_2H_2$	5.0E+13	0.0	16000.0
U06) $A_1C_2H = A_1C_2H^- + H$	5.0E+15	0.0	108600.0
U07) $A_1C_2H + H = A_1C_2H^- + H_2$	2.5E+14	0.0	16000.0
U08) $A_1C_2H + OH = A_1C_2H^- + H_2O$	2.1E+13	0.0	4600.0
U09) $A_1C_2H + C_2H_3 = A_1C_2H^- + C_2H_4$	5.0E+13	0.0	16000.0
U10) $A_1C_2H + C_2H = A_1C_2H^- + C_2H_2$	5.0E+13	0.0	16000.0
U11) $A_1 + C_2H = A_1C_2H + H$	1.0E+12	0.0	0.0
U12) $A_1 + C_2H_3 = A_1C_2H_3 + H$	1.0E+12	0.0	0.0
U13) $A_1^- + C_2H = A_1C_2H$	1.0E+13	0.0	0.0
U14) $A_1^- + C_2H_3 = A_1C_2H_3$	1.0E+13	0.0	0.0
U15) $A_1^- + C_2H_2 = A_1C_2H + H$	3.2E+11	0.0	1350.0
U16) $A_1^- + C_4H_2 = A_1C_2H + C_2H$	3.2E+11	0.0	1350.0
U17) $A_1^- + C_4H_4 = A_1C_2H + C_2H_3$	3.2E+11	0.0	1350.0
U18) $A_1^- + C_2H_4 = A_1C_2H_3 + H$	3.2E+11	0.0	1900.0
U19) $A_1^- + C_4H_4 = A_1C_2H_3 + C_2H$	3.2E+11	0.0	1900.0
U20) $A_1^- + C_4H_6 = A_1C_2H_3 + C_2H_3$	3.2E+11	0.0	1900.0
U21) $C_8H_5 = A_1C_2H^-$	1.0E+10	0.0	0.0
U22) $C_4H_3 + C_4H_2 = C_8H_5$	1.5E+12	0.0	0.0
G01) $A_2R_5 = A_2R_5^- + H$	5.0E+15	0.0	108600.0
G02) $A_2R_5 + H = A_2R_5^- + H_2$	2.5E+14	0.0	16000.0
G03) $A_2R_5 + OH = A_2R_5^- + H_2O$	2.1E+13	0.0	4600.0

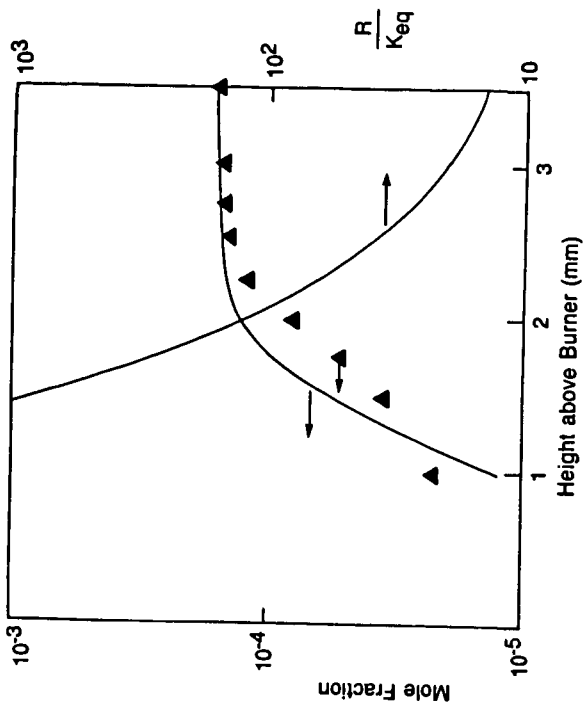
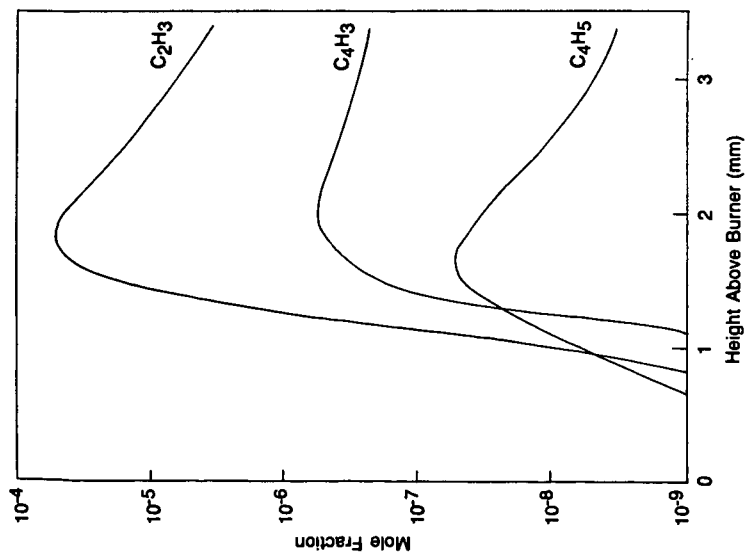
G04)	$A_2R_5 + C_2H = A_2R_5^- + C_2H_2$	5.0E+13	0.0	16000.0
G05)	$A_2R_5 + C_2H_3 = A_2R_5^- + C_2H_4$	5.0E+13	0.0	16000.
G06)	$A_2 = A_2^-X + H$	5.0E+15	0.0	108600.0
G07)	$A_2 + OH = A_2^-X + H_2O$	2.1E+13	0.0	4600.0
G08)	$A_2 + C_2H_3 = A_2^-X + C_2H_4$	5.0E+13	0.0	16000.0
G09)	$A_2 + C_2H = A_2^-X + C_2H_2$	5.0E+13	0.0	16000.0
G10)	$A_2^-X + C_2H_2 = A_2R_5 + H$	3.2E+11	0.0	1350.0
G11)	$A_2 + H = A_2^-X + H_2$	2.5E+14	0.0	16000.0
G12)	$A_1C_2HC_2H_2 = A_2^-X$	1.0E+10	0.0	0.0
G13)	$A_1C_2H^* + C_2H_2 = A_1C_2HC_2H_2$	1.0E+13	0.0	0.0

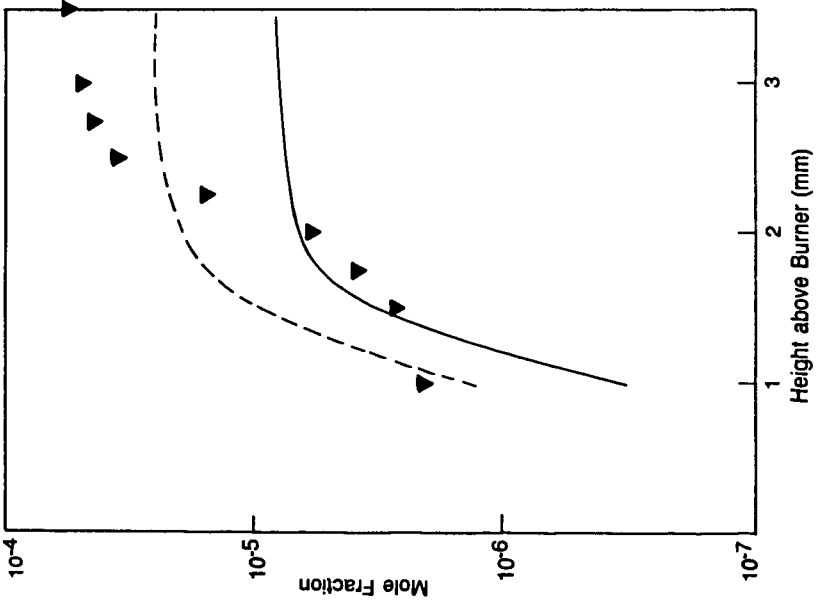
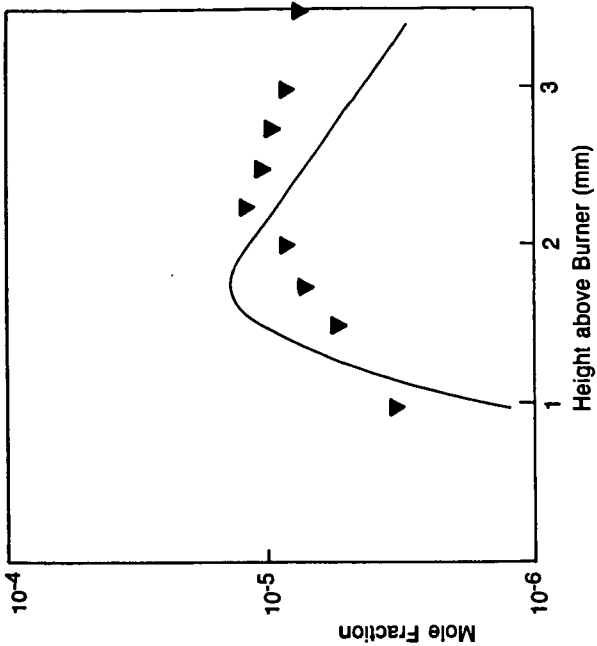
Units are cm³, moles, seconds, calories

Captions

1. Calculated mole fraction profiles for three radical species.
2. Left axis, benzene mole fraction. Symbols are experimental measurements, the curve is the model calculation. Right axis, calculated superequilibrium of H .
3. Phenylacetylene mole fraction. Symbols are experimental measurements, the solid curve is the model calculation, the dashed curve is the model calculation when the assumed heat of formation of phenylacetylene is lowered by 4 kcal/mole.
4. Styrene mole fraction. Symbols are experimental measurements, the solid curve is the model calculation.

<u>Structure</u>	<u>Name</u>
	A_1
	A_1^-
	A_1C_2H
	$A_1C_2H^*$
	$A_1C_2H^-$
	A_2R_5





SOOT FORMATION IN HYDROCARBON DIFFUSION FLAMES

J. Houston Miller, Anthony Hamins, and Trudy A. Kohout

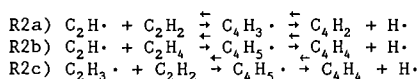
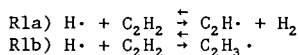
Department of Chemistry
The George Washington University
Washington, DC 20052

Kermit C. Smyth^a and W. Gary Mallard^b

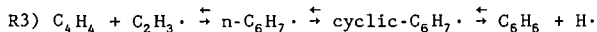
^aCenter for Fire Research and ^bCenter for Chemical Physics
The National Bureau of Standards
Gaithersburg, MD 20899

INTRODUCTION:

The chemistry of the combustion of simple hydrocarbons to form carbon dioxide and water has been extensively studied and is generally well established [1]. Our level of understanding of the chemistry which leads to the formation of polynuclear aromatic hydrocarbons (PAH) and soot particles is less fully developed. Numerous modelling efforts have been applied to the analysis of concentration data collected in shock tubes and premixed flames [2-6]. Although there are many proposed routes involving specific hydrocarbon free radicals, these models do share some common features. Fuel molecules are converted to relatively high concentrations of acetylene. Two-carbon atom free radicals formed during this pyrolysis process, or by hydrogen atom reactions with acetylene, can react with acetylene to form four carbon atom species.



Four-carbon atom species can react with either acetylene or two-carbon atom radicals to form six-carbon atom radicals, which may cyclize into aromatic structures. Finally, the cyclic radicals can lose or add hydrogen to form stable aromatic hydrocarbons such as benzene. For example:



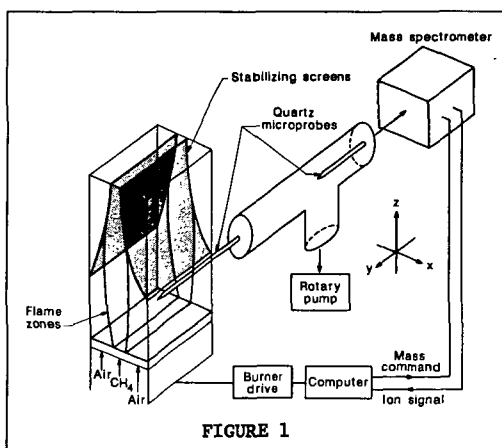
Analogous growth processes lead to the formation of larger ring structures and finally soot particles. The aromatic structures are believed to act as "islands of stability" along the reaction pathway [6], in effect providing a measure of irreversibility to the process. Because the thermodynamic stability of the aromatic structures increases with size, these subsequent ring formation steps occur more rapidly than the earlier ones. Our emphasis, therefore, has been on the chemical formation route for the first aromatic ring with the goal of verifying specific mechanisms for this process. A model

must not only account for observed concentrations of intermediate hydrocarbons but also for their net rate of production as a function of flame position.

In our laboratory, specific attention has been given to identifying the important chemistry leading to the formation of the key precursor molecules to soot particle formation in diffusion flames. To achieve this goal measurements of the important intermediate gas phase species, temperature, and velocity fields have been required. The results of these studies provide a comprehensive data base with which to examine the phenomenon of soot particle inception in flames. In this paper, a review of some of the results of these studies will be given along with a discussion of areas of future interest.

Experimental Approach

A study of the structure of laminar diffusion flames has been undertaken in which spatially detailed measurements of the gas phase species, velocity, and temperature fields have been obtained. The majority of the work has been carried out for flames burning methane in air, although some preliminary work has been done for ethylene/air diffusion flames. Only the methane flame results will be described in this paper. The design of the burner has been described elsewhere in detail and will only briefly be summarized here [7]. The fuel flowed through a central slot located between two air slots. The resulting flame sheets are symmetric about the plane through the center of the burner (see Figure 1). The burner assembly was mounted on a two-dimensional computer-controlled, micrometer stage so that movement laterally, through the flame sheets, and vertically was possible. Lateral profiles of temperature, velocity, and species concentrations were collected at relatively high spatial resolution (0.2 mm) at a series of heights (consecutive profiles were taken every 2 mm).



Species concentrations were determined by a direct sampling quartz microprobe system with mass spectrometric analysis. A probe following the

design of Fristrom and Westenberg [8] was inserted into the flame parallel to the fuel/air flow separators. Mass spectrometer signals were calibrated against room temperature mixtures, and the resulting calibration factors were corrected for the temperature dependence of the molecular flow through the sampling probe orifice. In a related series of experiments, molecular iodine from a side arm on the probe was mixed with the flame gas sample just inside the orifice [9]. Iodine reacts quantitatively with methyl radicals to form methyl iodide, which could survive the remainder of the sampling train and be detected mass spectrometrically.

Results

Figure 2 illustrates the temperature and velocity fields for the methane/air flame supported on the Wolfhard/Parker slot burner. Shown in solid lines are isothermal contours determined from thermocouple profiles⁷. Also shown are streamlines of convective velocity calculated from the two measured velocity components. The streamlines exhibit trajectories which begin in the lean region of the flame, cross the high temperature reaction zones, and continue into the fuel-rich regions.

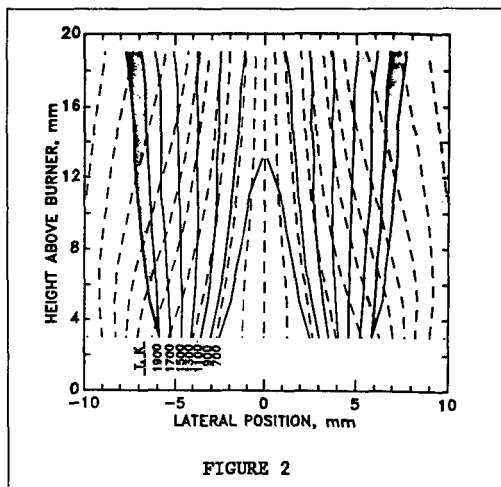


Figure 3 shows mass-spectrometric profiles of the concentrations of a variety of stable flame species at a height of 9 mm above the burner. A number of points are noteworthy in comparing Figures 2 and 3. First, the concentrations of oxygen and methane approach zero near the high temperature reaction zone at ± 6 mm from the burner centerline, where the concentration of water is a maximum. Second, the high concentration of nitrogen near the burner centerline reveals that significant entrainment of air (as shown by the velocity measurements in Fig. 1) and diffusion of nitrogen toward the burner centerline occur.

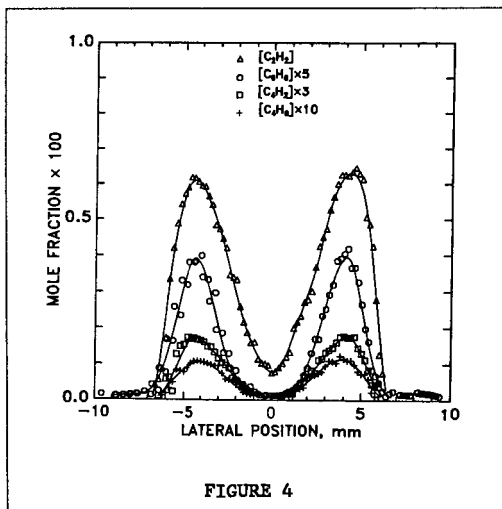
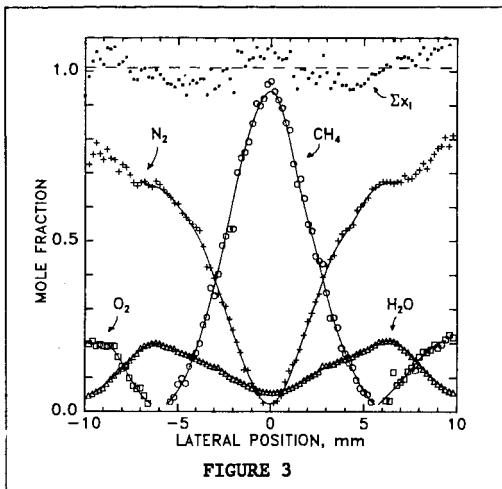
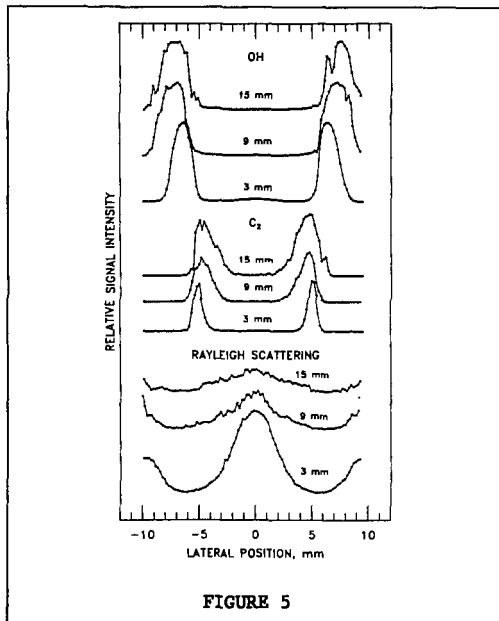


Figure 4 illustrates profiles collected at 9 mm above the burner surface for several intermediate hydrocarbons: acetylene, benzene, diacetylene, and butadiene. Peak concentrations at this height for these species are 6200, 800, 570, and 110 parts per million, respectively. Profiles for a large

number of additional intermediate hydrocarbons were obtained, and all have concentration maxima in the same region of the flame.

In addition to the probe studies described above, we have also applied optical diagnostic techniques to the study of the methane/air flame. Figure 5 compares the relative OH concentration profiles at various heights above the burner surface with profiles of C_2 fluorescence. Also shown is the Rayleigh light scattering signal for three flame heights. The absence of distinct peaks in the scattering signal profiles indicates that large soot particles are not detectable below 15 mm in the methane/air flame. The C_2 fluorescence is attributed to laser photolysis of large hydrocarbon molecules. Figure 5 shows that the OH concentration maximum occurs further away from the burner centerline (in more lean regions of the flame) than the area where hydrocarbons such as benzene and soot particles are observed.



Data Analysis and Discussion

A laminar flame is a steady-state system: the value of any macroscopic variable (such as a species concentration) does not change with time at a particular spatial location [10]. Because there is a flow of material into and out of a given volume element due to mass transport, there must be a corresponding change in species' concentrations due to chemical reactions:

$$R_i = \nabla[N_i (v + V_i)]. \quad (1)$$

Here, R_i is the net chemical rate, N_i is the species concentration, v is the mass average (convective) velocity, and V_i is the diffusion velocity of the species into the local mixture. All of the quantities on the right-hand side of Eq. 1 have been experimentally determined (N_i and v) or can be calculated directly from the experimental data (V_i).

Figure 6 illustrates the calculation of the chemical production rate, R_i , for acetylene at heights of 5 and 13 mm above the burner surface. Low in the flame, the rate profile exhibits a maximum destruction value near the high temperature, primary reaction zone, and a formation feature slightly toward the fuel side. This peak in the production rate is located on the lean, higher temperature side of the observed concentration peak (see Figure 4). Higher in the flame, the production rate is diminished by a new destruction feature (see arrow). This new destruction feature spatially overlaps an observed profile maximum for small soot particles, and this feature is believed to be due to acetylene participation in soot surface growth processes [10].

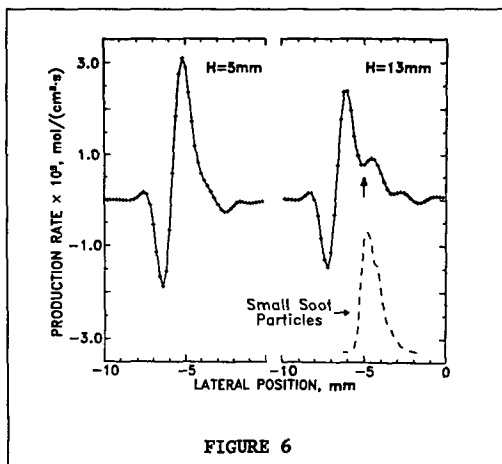
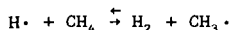


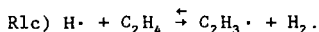
FIGURE 6

The concentration and production rate data have been used to critically evaluate proposed mechanisms for hydrocarbon condensation chemistry in the methane flame. For example, our data allows us to select between competitive reactions during specific growth steps in the formation of benzene. In the Introduction, alternative processes involving two, four, and six carbon-atom free radicals were suggested for the sequence leading from acetylene to benzene. For a given reaction to be important, its maximum forward rate must be faster than the observed production rate of the product benzene. For example, both ethynyl radicals and vinyl radicals can be formed by hydrogen atom reaction with acetylene. For these calculations, the concentration of

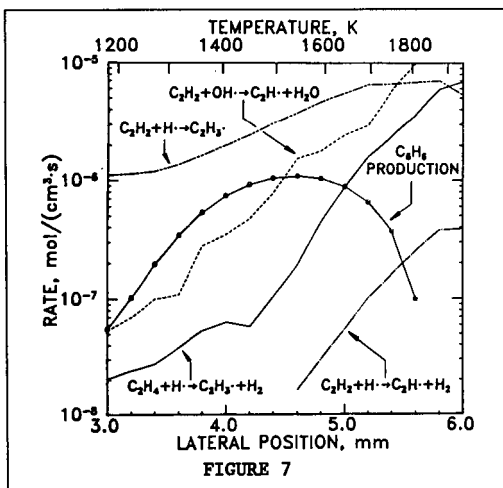
hydrogen atoms was determined by assuming equilibrium with methane in the reaction [10]:



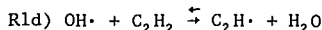
In Figure 7, the formation rates of these radicals via reactions 1a and 1b are compared with the observed net benzene formation rate. As this figure indicates, the ethynyl radical, $\text{C}_2\text{H} \cdot$, is produced too slowly to account for the observed rate of the formation of benzene in the methane flame. In contrast, the vinyl radical, $\text{C}_2\text{H}_3 \cdot$, formed through hydrogen atom addition to acetylene, is formed fast enough to account for our benzene rate data. Another route to vinyl formation is hydrogen abstraction from ethylene:



We have recently developed a method for distinguishing the individual contributions to the mass 28 signal from CO , N_2 , and C_2H_4 . Thus, the importance of reaction 1c) in the formation of benzene can be determined. The forward rate of R1c is plotted in Figure 7. Near the flame reaction zone, the magnitude of vinyl formation through R1c exceeds the observed net forward formation rate of benzene. Thus, in the methane flame, vinyl formation through both acetylene and ethylene can contribute to aromatic ring formation.



In a previous paper on the production rate calculations¹⁰, we concluded that the vinyl radical was the key two-carbon radical in the formation sequence leading to benzene. This result was predicated on the assumption that oxygen containing radicals such as OH were not involved directly in this process. However, OH abstraction of hydrogen from acetylene to form ethynyl is a fast reaction [11] and should be considered in our analysis. We have therefore added reaction 1d)



to the two-carbon radical formation processes plotted in Figure 7. Because laser induced fluorescence provides a determination of only the relative hydroxyl radical concentration, it is necessary to scale the profile results to a reasonable estimate of the actual OH concentration. To this end, the peak OH concentration was taken to be that predicted by the NASA combustion equilibrium code for methane/air mixtures at the local equivalence ratio, ≈ 0.7 , and the temperature, 2030 K, where the fluorescence maximum is observed [12]. This estimate should prove to be conservative: Mitchell et al. have found super-equilibrium concentrations for OH in fuel-rich regions of methane/air diffusion flames [13]. As Figure 7 demonstrates, formation of ethynyl from OH reactions with acetylene is fast enough to account for the observed benzene formation rate.

Further tests of benzene formation mechanisms will focus on competitive routes to four-carbon molecule formation (R2a-R2c). A critical concern will be the relative concentrations of vinyl and ethynyl radicals. If the vinyl radical concentrations far exceed the ethynyl radical concentrations, as has been observed in pre-mixed acetylene flame results [14], then processes such as reaction 2c will be far more important than the ethynyl radical reactions such as 2a or 2b. Reliable estimation or measurement schemes for these radicals remains as one of the great challenges in unravelling diffusion flame chemistry.

References

1. I. Glassman and P. Yaccarino, Eighteenth Symposium (International) on Combustion, The Combustion Institute, 1175 (1981).
2. J. Warnatz, Eighteenth Symposium (International) on Combustion, The Combustion Institute, 69, (1981).
3. T. Tanzawa and W.C. Gardiner, Jr., J. Phys. Chem. **84**, 236 (1980).
4. M.B. Colket, III, Chemical and Physical Processes in Combustion, Eastern States Section of the Combustion Institute, Paper 53, November 1985.
5. J.A. Cole, J.D. Bittner, J.P. Longwell, and J.B. Howard, Combustion and Flame **56**, 51 (1984).
6. M. Frenklach, J.W. Clary, W.C. Gardiner, and S.E. Stein, Twentieth Symposium (International) on Combustion, The Combustion Institute, 887 (1984).
7. K.C. Smyth, J.H. Miller, R.C. Dorfman, W.G. Mallard, and R.J. Santoro, Combustion and Flame **62**, 157 (1985).
8. R.M. Fristrom and A.F. Westenberg, Flame Structure, McGraw-Hill, New York, 1965.
9. J.H. Miller and P.H. Taylor, Combustion Science and Technology, in press.
10. J.H. Miller, W.G. Mallard, and K.C. Smyth, Twenty-first Symposium (International) on Combustion, The Combustion Institute, in press.
11. W. Tsang and R.F. Hampson, Journal of Physical and Chemical Reference Data **15**, 1087 (1986).
12. S. Gordon and B.J. McBride, NASA SP-273, 1971.
13. R. Mitchell, A.F. Sarofim, L.A. Clomburg, Combustion and Flame **37**, 201 (1980).
14. P.R. Westmoreland, D. Sc. Dissertation, Massachusetts Institute of Technology, 1986.

Soot Particle Formation in Diffusion Flames

Robert J. Santoro

Department of Mechanical Engineering
The Pennsylvania State University
University Park, PA 16802

I. Introduction

Over the past twenty five years a large number of investigations of soot formation, growth and oxidation have been reported. The extensive interest in this problem is a result of the important ramifications that the presence of soot particles have on practical combustion systems. Because of the diversity of these effects, a wide variety of experimental situations have been investigated. These range from small laboratory scale burners to full scale combustion devices. However, insights into the fundamental processes which control the formation and growth of soot particles have largely resulted from studies of simple premixed and diffusion flames. The results of such studies have been periodically reviewed and where applicable related to practical situations [1-4].

Recently a significant amount of attention has been given to the study of laminar and turbulent diffusion flames [5-15]. Many of these studies have utilized optical diagnostics to obtain quantitative information on soot particle size, concentration and spatial distribution in the flame. These techniques which were first applied to premixed flames [16] have allowed for a significant advance in our quantitative understanding of soot formation processes. In fact, the results of the premixed flames studies established the common sequence of events which is now viewed to govern the formation of soot particles in most combustion situations. These include (1) a chemically kinetically controlled reaction sequence which results in the formation of precursor species needed to form the first particles, (2) a particle inception stage which results in the formation of large numbers of small primary particles, (3) a particle growth period in which surface growth and particle coagulation processes contribute to the increase in particle size and (4) a stage in which material is no longer added to the soot particles and size is controlled by agglomeration or may even be reduced by oxidative attack. Recent work in premixed flames has concentrated on more firmly establishing quantitative measurements of the individual processes which constitute this description. Significant progress has been made in understanding the surface growth and particle coagulation processes which occur in premixed flames [17,18]. Results from these and other studies have emphasized the importance of acetylene (C_2H_2) and available surface area in the particle growth process and have established that soot particle coagulation accounts for the particle number concentration behavior observed in such flames. Presently efforts are focused on the particle inception stage in an effort to link the formation of large intermediate hydrocarbon species which are viewed as precursors to soot

particles and the initial particles observed by light scattering techniques in the flame [19,20]. Such measurements present serious challenges for current diagnostic approaches and progress has been possible only through a combination of experimental measurements and extensive computer modelling of the soot aerosol as it develops in time. In these studies, the effects of particle inception, surface growth and coagulation must be taken into account simultaneously.

Recent studies in laminar diffusion flames have essentially confirmed that the formation and growth of soot particles can be described by a similar series of processes. Using laser-based techniques to measure particle size [6,7], velocity [9,10] and temperature [21], workers have provided a much more detailed understanding of soot particle processes in these flames. Because particle formation is not spatially homogeneous throughout the flame, the high spatial resolution of these techniques have allowed investigation of the structure of the soot particle field and, at least to some degree of accuracy, to follow the time history of the particles as they proceed through the flame [10,11,22]. In particular, attention has been given to the study of effects of temperature [23,24] and pressure [22] on the production of soot particles. Of related interest are studies examining radiative transfer from these flames which indicate that radiation from soot particles represents a significant energy transfer mechanism [15]. This has led several workers to speculate that radiative transfer is important in controlling the emission of soot particles from the flame [7,11,15].

In addition to these studies, which have emphasized the detailed processes involved in soot particle and growth, a large body of work exists concerning the relative sooting tendency of fuels [12,25,26]. These works largely focus on the concept of a "smoke point" or "sooting height" which characterizes an individual fuel. The sooting height is an experimental measurement of the height of a laminar diffusion flame when soot particles are observed to issue from the tip of the flame. Fuels which have a higher tendency to soot are found to have a shorter flame height at this characteristic point. Although a qualitative measure of soot production tendencies, workers investigating soot formation from this approach have made several critical contributions to the phenomenological understanding of soot particle formation [27]. Recently work has appeared to relate the more detailed measurement results in laminar and turbulent flames to these sooting height results with some success [28,29]. This work is particularly significant in that it allows a quantitative relationship to be obtained from the previous relational information on a wide variety of fuels. The fact that information for turbulent flames could be derived from laminar flame measurements is encouraging since it points to the general utility of the laminar diffusion flame results.

It should be mentioned that a good deal of the understanding of the evolution of the soot particle field in diffusion flames draws substantially from the earlier work of Roper [30,31]. In these papers, and recently in an update to that work [32], a simple model of laminar diffusion flames is developed which clearly describes the effects of fuel flowrate, temperature and radiation on the structure of the flame. These works have widely influenced other researchers in this field.

In the above work on diffusion flames, the emphasis has been on the particle aspects of these flames. Studies of the important chemistry have been undertaken for the most part in low pressure and atmospheric laminar premixed flames, although shock tube work has also contributed in some respects [33,34]. These studies have established plausible reaction mechanisms leading to the formation of aromatic compounds with a few rings. There continues to be a debate concerning the role that ions may have in providing the rapid chemical reaction rates needed to form the particles in the reaction times available (~ 1 ms) [35]. However, in the area of diffusion flames a relatively smaller amount of work is available examining the preparticle chemistry [36]. Recently a significant effort has been made to study both the chemistry leading to soot precursors and the subsequent soot particle growth in diffusion flame environments [9]. These results have not yet progressed sufficiently to allow a complete quantitative picture to be drawn, but progress is continuing [37].

The experiments to be described here are an extension of our previous laminar diffusion flame studies of soot particle formation [7,10]. Specifically a detailed examination of the effect of fuel chemical structure has been undertaken. In our previous work, the emphasis has been on examining the effects of fuel flowrate and temperature on the production of soot in diffusion flames [7,10,24]. In addition, specific attention was given to the processes controlling the emission of soot particles from the flame. These results along with the findings of other researchers has established the complex, coupled nature of the processes determining the soot particle evolution in the flame. The individual effects of temperature, flow field (e.g. velocity), pressure and fuel constituents all must be investigated if a comprehensive understanding of the soot formation process is to be achieved.

II. Experimental Apparatus

For these studies, a coannular laminar diffusion flame has been used in which fuel is burned in air under atmospheric pressure conditions [7]. The burner consists of an 11.1 mm id fuel passage surrounded by 101.6 mm outer air passage. The flame is enclosed in a 405 mm long brass cylinder to shield the flame from laboratory air currents. Slots machined in the chimney provide for optical access while screens and a flow restrictor were placed at the exhaust of the chimney to achieve a stable flame. The burner is mounted on translating stages to provide three-dimensional positioning capability. Radial traversing of the burner is accomplished using a motorized translation stage.

The soot particle measurements were obtained using a laser scattering/extinction technique [16]. Laser extinction and scattering measurements were carried out using a 4 W argon ion laser which was operated at the 514.5 nm laser line. The incident laser power was 0.5 W and was modulated using a mechanical chopper. The transmitted power was measured using a photodiode and the scattered light was detected at 90° with respect to the incident beam using a photomultiplier tube. Signals from each detector were input to a lock-in amplifier and subsequently digitized signals were stored on a computer. The ratio of the measured scattering cross section to the extinction coefficient was used to determine particle size. For these calculations, the particle size

analysis was carried out using a data reduction approach based on Mie theory.

Previously obtained velocity measurements on a similar flame, obtained using a laser velocimeter technique, were used to calculate the particle paths and the residence time in the flame.

III. Results

As has been previously described, the amount of soot formed in a flame is a function of several variables. Temperature, pressure and fuel structure have been shown to be particularly important in determining the amount of soot formed. Thus, it is highly desirable to study soot particle formation under conditions where these variables can be systematically varied. This presents several problems, particularly in the case of fuel structure studies, because the sooting propensity of fuels varies widely [25-27]. This results in important variations in the velocity field and heat losses to the burner for different flames.

To overcome some of these difficulties, a fuel mixture approach has recently been tried for the study of soot particle processes in these flames. In this approach, an ethene/air diffusion flame which has been extensively characterized in terms of the particle, velocity and temperature fields has served as the baseline flame [7]. For the fuel composition studies, different fuel species were added to the baseline fuel (ethene), such that the additional carbon flow rate was the same in each case. Under these conditions, the total carbon flow rate is held constant. In addition, the flame size and shape remains similar for all the flames studied, thus minimizing changes in burner heat loss or particle transport in the flame. An ethene fuel flow rate of 3.85 cc/s (a carbon flow rate of 3.78×10^{-3} gm/s) was selected for the baseline flame since this diffusion flame has been extensively studied [7,10,22]. A second fuel was added to the ethene flow to produce a total carbon flow rate of 4.81×10^{-3} gm/s, an increase of 1.03×10^{-3} gm/s from the baseline case. Results have been obtained for methane, ethane, ethene, acetylene, propene, butene, and toluene. In the case of toluene, the fuel was vaporized using a technique similar to that described by Gomez et al. [12]. The flow conditions for these studies are given in Table 1 along with the calculated adiabatic flame temperatures for the fuel mixtures. Table 1 also includes the measured values for the percent carbon conversion to soot for the fuel increment introduced into the baseline flame. This value is obtained by taking the difference between the maximum soot mass flow rate observed in the flame for the fuel mixture case and the baseline flame divided by the carbon mass flow rate increase (1.03×10^{-3} gm/s). The percent conversion is observed to vary strongly as a function of fuel species with the aromatic fuel having the largest conversion percentage.

Using the previously obtained detailed information on the particle paths for the ethene flame, comparisons between the different fuels can be made for different regions of the flame. Two regions of the flame have been selected for illustration using the soot volume fraction (f_v) measurements. Figure 1 shows the time evolution of f_v along the particle path which traverses the annular region of the flame where the maximum f_v

Table 1

Baseline Fuel	Fuel Added	T _{ad}	Carbon Conversion
(cc/s)	(cc/s)	(K)	(%)
C ₂ H ₄ (3.85)	+ CH ₄ (2.10)	2333	13
"	+ C ₂ H ₆ (1.05)	2344	22
"	+ C ₂ H ₄ (1.05)	2369	18
"	+ C ₂ H ₂ (1.05)	2403	32
"	+ C ₃ H ₆ (0.70)	2368	36
"	+ C ₄ H ₈ (0.525)	2359	52
"	+ C ₇ H ₈ (0.30)	2361	98

is observed; Figure 2 shows a similar plot for the center line of the flame. The fuel mixtures shown include three alkenes (ethene, propene and butene) and an aromatic (toluene). As Table 1 indicates, the adiabatic flame temperatures for these fuel mixtures do not vary significantly. Thus, the temperature fields characterizing these flames should be similar, allowing a direct comparison between the flames.

Figures 1 and 2 clearly indicate that differences between the fuels are more pronounced in the annular region of the flame than near the center line. This implies that the higher temperatures and larger radical concentrations present in the annular region of the flame, which lies closer to the flame reaction zone, not only increase the soot formation rates, but also enhance the differences between fuel species. In the annular region (see Fig. 1), all the fuels are observed to reach a maximum in f_v at a similar residence time (≈ 60 ms). For the alkene fuels, the observed residence time for the first observation of soot particles and the value of f_v at this time are also very similar. However, the different alkene fuels are observed to have measurably different rates of growth in terms of the change in the soot volume fraction with time. For the toluene mixture, although soot particles are first observed at a similar residence time (≈ 21 ms), the initial concentration is much higher. This implies that soot particle inception occurred at an earlier time or that the inception process is much more vigorous. The particle size and number density measurements, along with the results from nearby particle paths, favor an interpretation indicating an earlier inception time. Thus, these results indicate that the specific nature of the fuel species is observed to affect the initial particle formation process as well as the subsequent growth rates. Comparisons with the data along the center line of the flame (see Figure 2) further support the argument that the aromatic fuel accelerates the inception process. However, the final soot volume fraction values observed in this region show smaller differences as compared to the annular region of the flame for the fuels studied. Thus, the particle growth processes may differ in this fuel rich region which also exhibits lower temperatures than observed in the annular region.

The approach of determining the influence of fuel structure based on fixed increments in the carbon flow rate provides an appropriate framework in which to consider the soot formation process in general. As an example, Fig. 3 shows a plot of the maximum soot mass flow rate as a function of fuel flow rate for a series of ethene/air flames [7,10]. A linear relationship is observed over the flow range studied, indicating that the conversion of fuel carbon to soot is constant beyond some minimum required flow rate to first produce soot particles in the flame. The observed value for the percent conversion for these ethene flames is 18%. Similar experiments for other fuels are presently underway.

IV. Discussion

The results described above, although preliminary nature, have identified several features which are deserving of further investigation. Attention should be focused on differentiating the particle inception and surface growth contributions for the various fuel types. The differences between the alkene and aromatic fuels is, obviously, of most interest in light of the large differences in their sooting tendencies. In addition, the occurrence of a constant conversion percentage based on fuel structure needs further investigation. Specifically, this relationship for fuel mixtures needs to be developed over a wider variation of fuel structures and as a function of temperature. Recently, Kent [28] has reported soot conversion percentages for a wide variety of fuels which were directly related to soot volume fraction measurements obtained at the sooting height [28,38]. In this case, the conversion percentages are based on the total amount of conversion of fuel to soot rather than on the incremental change as described above. However, the trends observed in terms of the contrast between the alkene and aromatic fuel species are similar to those observed here. Kent's results indicate the conversion percentage for ethene to be 12% while that for toluene is 38%. The values for acetylene and propene were 23% and 16% respectively which differs in the ordering observed in the present study. However, the present results agree with previous studies of sooting height measurements in terms of the sooting tendency of the studied fuels [12]. These results along with the previous studies mentioned represent the beginning steps to obtaining a quantitative understanding of the effect of fuel molecular structure on soot formation in diffusion flames. Significant progress is likely to continue as experimenters concentrate on specific aspects of the problems such particle inception and surface growth.

Acknowledgement

The support of the Air Force Office of Scientific Research under grant AFOSR-87-0145 is gratefully acknowledged. The author also wishes to acknowledge with great appreciation the contributions of coworkers at the National Bureau of Standards J.J. Horvath, H.G. Semerjian and T.T. Yeh. The U.S. government is authorized to reproduce and distribute reprints for governmental purposes notwithstanding any copyright notation thereon.

References

1. Palmer, H. B. and Cullis, C. F., in The Chemistry and Physics of Carbon, Walker, P. J., Jr. and Thrower, P. A., Marcel Dekker, 1965, Vol. 1, p. 265.
2. Haynes, B. S. and Wagner, H. Gg., Prog. Energy Combust. Sci., 7,22 (1981).
3. Wagner, H. Gg., in Particulate Carbon Formation During Combustion, Siegl, D. C. and Smith G. W., Eds., Plenum, New York, 1981, p. 1.
4. Howard, J. B. and Kausch, W. J. Jr., Prog. Energy Combust. Sci., 6, 263, (1980).
5. Haynes, B. S., and Wagner, H., Gg., Ber. Bunsenges Phys. Chem. 84, 498, (1980).
6. Kent, J. H., Jander, H., and Wagner, H., Gg., Eighteenth Symposium (International) on Combustion, The Combustion Institute, Pittsburgh, 1981, 1117.
7. Santoro, R. J., Semerjian, H. G. and Dobbins, R. A., Combustion and Flame, 51, 203, (1983).
8. Prado, G., Garo, A., Ko, A. and Sarofim, A., Twentieth Symposium (International) on Combustion, The Combustion Institute, Pittsburgh, 1984, p. 989.
9. Smyth, K. C., Miller, J. H., Dorfman, R. C., Mallard, W. G. and Santoro, R. J., Combustion and Flame, 62, 157, (1985).
10. Santoro, R. J., Yeh, T. T., Horvath J. J. and Semerjian, H. G., Combustion Science and Technology, in press (1987).
11. Kent, J. H. and Wagner, H. Gg., Combustion Science and Technology, 41, 245 (1984).
12. Gomez, A., Sidebotham, G. and Glassman, I., Combustion and Flame, 58, 45 (1984).
13. Kent, J. H. and Bastin, S. J., Combustion and Flame, 56, 29 (1984).
14. Kent, J. H., Combustion and Flame, 67, 223 (1987).
15. Markstein, G. H., Twentieth Symposium (International) on Combustion, The Combustion Institute, Pittsburgh, 1985, p. 1055.
16. D'Allessio, A., Di Lorenzo, A., Sarofim, A. F., Berretta, F., Masi, S. and Venitozzi, C., The Fifteenth Symposium (International) on Combustion, The Combustion Institute, Pittsburgh, 1975, p. 1427.

17. Harris, S. J. and Weiner, A. M., Combustion Science and Technology, 32, 155 (1983).
18. Bockhorn, H., Fetting, F., Heddrich, A. and Wannemacher, Twentieth Symposium (International) on Combustion, The Combustion Institute, Pittsburgh, 1985, p. 979.
19. Harris, S. J. and Weiner, A. M., Combustion and Flame, 64, 65 (1986).
20. Kennedy, I. A., Combustion and Flame, 68, 1 (1987).
21. Boedeker, L. and Dobbs, G. M., Combustion Science and Technology, 46, 31 (1986).
22. Flower, W. L. and Bowman, C. T., The Twentieth Symposium (International) on Combustion, The Combustion Institute, Pittsburgh, 1984, p. 1035.
23. Kent, J. H. and Wagner, H. Gg., Twentieth Symposium (International) on Combustion, The Combustion Institute, Pittsburgh, 1984, p. 1007.
24. Santoro, R. J. and Semerjian, H. G., Twentieth Symposium (International) on Combustion, The Combustion Institute, Pittsburgh, 1984, p. 997.
25. Schug, K. P., Manheimer-Timnat, Y., Yaccaino, P. and Glassman, I., Combustion Science and Technology, 22, 235 (1980).
26. Calcote, H. F. and Manos, D. M., Combustion and Flame, 49, 289 (1983).
27. Glassman, I. and Yaccarino, P., Eighteenth Symposium (International) on Combustion, The Combustion Institute, Pittsburgh, 1981, p. 1175.
28. Kent, J. H., Combustion and Flame, 63, 349 (1986).
29. Kent, J. H., Combustion and Flame, 67, 223 (1987).
30. Roper, F. G., Combustion and Flame, 29, 219 (1977)
31. Roper, F. G., Smith, C. and Cunningham, A. C., Combustion and Flame, 29, 227 (1977)
32. Roper, F. G., Combustion Science and Technology, 40, 323 (1984).
33. Bittner, J. D. and Howard, J. B. Eighteenth Symposium (International) on Combustion, The Combustion Institute, Pittsburgh, 1981, p. 1105.
34. Frenklach, M., Clary J., Gardiner, W. C. and Stein, S. E., Twentieth Symposium (International) on Combustion, The Combustion Institute, Pittsburgh, 1984, p. 887.

35. Calcote, H. F., Combustion and Flame, 42, 215 (1981).
36. Flossdorf, J., Jost, W. and Wagner, H. Gg., Ber. Bunsenges. Phys. Chem., 78, 378 (1974).
37. Santoro, R. J. and Miller, H. J., Langmuir, 3, 244 (1987).
38. Olson, D. B., Pickens, J. C. and Gill, R. J., Combustion and Flame [to appear].

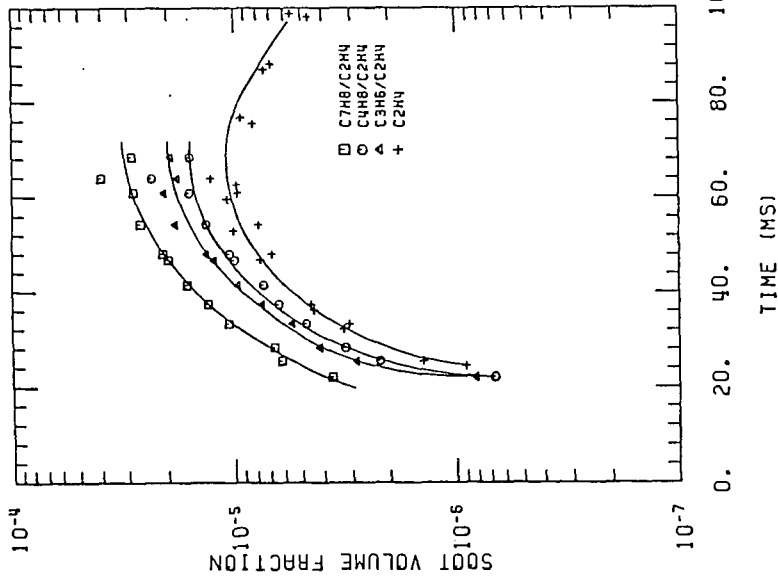


Figure 1. Comparison of the soot volume fraction, along the streak line exhibiting the maximum soot volume fraction for fuel mixtures containing ethene, propene, butene or toluene.

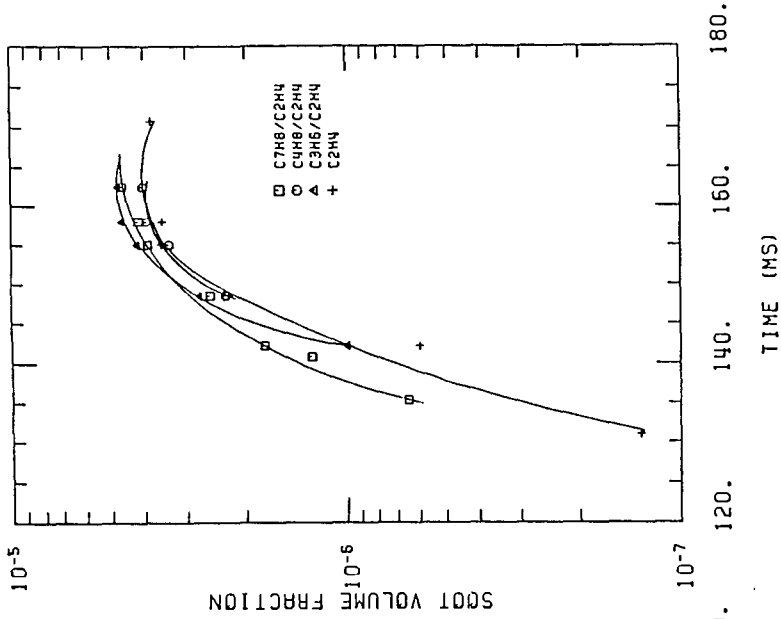


Figure 2. Comparison of the soot volume fraction along the center line of the flame for fuel mixtures containing ethene, propene, butene or toluene.

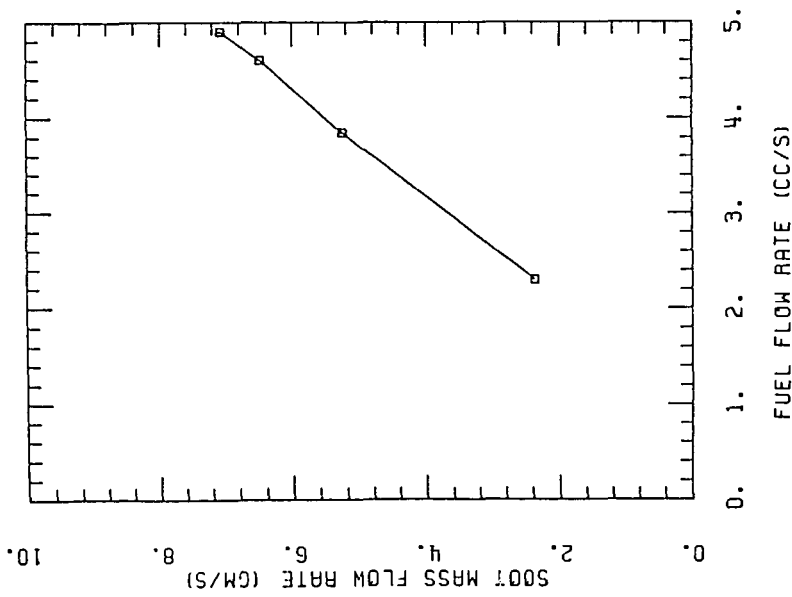


Figure 3. The maximum soot mass flow rate as a function of fuel flow rate for an ethene air diffusion flame.

ARE IONS IMPORTANT IN SOOT FORMATION?

H. F. Calcote, D. B. Olson, and D. G. Keil

AeroChem Research Laboratories, Inc.
P.O. Box 12, Princeton, NJ 08542

I. INTRODUCTION

Many chemical mechanisms have been proposed for the formation of incipient soot in flames. The ionic mechanism has not been widely embraced; it is considered a competitor to free radical mechanisms which have received more attention. It seems timely to review the evidence for the ionic mechanism, which we do here.

The precursor of soot formation is assumed to be the propargyl ion, $C_3H_3^+$ (1-3). The source of this ion is not clear but it is the dominate ion in fuel rich hydrocarbon flames and is generally considered to be a primary chemi-ion, i.e., derived from the reaction of neutral species. There are two isomers of $C_3H_3^+$, a linear structure and a more stable cyclic structure. Measurements of reaction rates for these two isomers at near room temperature demonstrate that reactions of the linear isomer are fast, generally equal to the Langevin rate, while reactions of the cyclic isomer are slower (4-6). Eyler and associates (7) have recently determined that the rate of linear $C_3H_3^+$ reacting with acetylene is small compared to Langevin theory (8,9). The validity of extrapolating these measurements to high temperatures is not clear. The Langevin theory, for ions reacting with non-dipolar molecules, does not predict a temperature dependence. Which isomer of $C_3H_3^+$ is formed initially in flames is also not known, nor is the rate of isomerization.

In the ionic soot formation mechanism, the precursor ion reacts with neutral species, e.g., acetylenes, to produce larger ions. These larger ions continue to react further to produce ever increasingly larger ions.

A major feature of this mechanism is the large rate coefficients for ion-molecule reactions and the ease with which ions isomerize (8). The formation of a cyclic structure does not represent a significant energy barrier as it does for a free radical mechanism. Some of the electrons produced in the chemi-ionization reaction produce negative ions by electron attachment to large molecules; these reactions are favored by low temperature and increasing molecular weight of the neutral reactant. As the ions grow larger their recombination rate coefficient for reaction with electrons or negative ions increases, so positive ions are removed, forming large neutral molecules, the equivalent of small neutral soot particles. The small neutral particles continue to grow and as they become larger their work function approaches that of bulk graphite. At sufficiently high temperature, these particles become thermally ionized; these thermally ionized particles are not of interest for soot nucleation.

In this paper we review the evidence for the sequence of reactions starting with $C_3H_3^+$ and proceeding through large soot ions; this sequence of reactions has been labeled "the ionic mechanism."

II. EVIDENCE

A. Concentration

Concentrations of ions have been measured by AeroChem (2,3,10), Delfau and associates (11,12), and Homann and associates (13,14) in what has been referred to as the "standard flame." This is a premixed, sooting acetylene/oxygen flame on a

flat flame burner at 2.7 kPa, an equivalence ratio of 3.0, and an unburned gas velocity of 50 cm/s. Ion concentrations are shown in Fig. 1 along with neutral soot concentrations, charged soot concentrations, and the flame temperature. The ion concentration in this flame is sufficient to account for the formation of the observed soot.

B. Reaction Rates

Ion-molecule rate coefficients are generally several orders of magnitude greater than for neutral species reactions (8), which, of course, means that the concentration of ions does not have to be as great to react at the same rate.

Figure 1 also contains evidence that the rates of ion-molecule reactions are sufficiently rapid in flames to account for soot formation. As the ion concentration decays by ion recombination, the soot concentration increases. The slopes are comparable within the accuracy of the data. We note, however, that soot particles are identified as those which can be detected using an electron microscope, i.e., their diameter exceeds 1.5 nm.

Several available sets of data on neutral soot particle diameters and positively charged soot particle diameters are presented in Fig. 2 for the standard C_2H_2/O_2 flame. These data have presented a dilemma (15); it appears that neutral particles grow faster than charged particles, but in the early part of the flame the charged particles have a larger diameter. This question seems to relate more to particle growth and thermal ionization than to soot nucleation; nevertheless the location of the phenomena in the flame is at just the distance where the initial ion concentration is falling and the concentrations of neutral particles and charged particles are increasing. In previous calculations (1,16) of thermal ionization of soot particles about 2 cm downstream from the burner, the assumption was made that equilibrium was approached from the side of excess neutral particles. This is difficult to rationalize if the concentration of charged particles exceeds the concentration of neutral particles at small distances where the particle diameters are the smallest.

The fraction of thermally ionized particles and the rate of thermal ionization are both very sensitive to particle diameter. For the small neutral particles the calculated ionization rate is slow compared to the experimental rate. Thus at 2.25 cm above the burner, with the Richardson equation modified for small particles (17), we calculate a rate of ionization of 2×10^{11} charged particles/(cm^3 s) and we measure a rate of 6×10^{11} charged particles/(cm^3 s) from the slope of the "charged soot" curve in Fig. 1. Between 2.5 and 3.0 cm the calculated rate exceeds the observed rate; here and at greater distances equilibrium controls the concentrations. Thus at the first appearance of soot the rate of thermal ionization of neutral particles is too small to account for the observed rate of charged particle appearance; close to the burner equilibrium is approached from the direction of excess charged particles. This is further evidence that charged species are involved in the formation of soot.

The difference in slopes of the neutral and charged particle concentrations in Fig. 2 is probably due to a faster rate of ion-electron recombination for large ions than for small ions. For example, increasing the particle diameter from 5 to 10 nm increases the rate coefficient of recombination from about 1.3×10^{-6} to about 3.8×10^{-6} cm^3/s . Thus the larger charged particles disappear more rapidly than the smaller ones. In the region of the flame where this occurs, the observed charged particles are derived from the chemi-ions produced early in the flame and are not derived from the neutral particles. This is not only further evidence for the ionic mechanism of soot formation, but it makes very awkward any explanation of the source of ions being the thermally ionized particles as some have suggested.

C. Confirmation of Ions

All of the individual ions involved in the postulated mechanism, up to mass 557, have been observed in sooting flames (2,3,11,12). The confirmation that ions larger than these are present in the flame, prior to the appearance of soot, has also been documented (13,14).

D. Location of Ions in Flame

The order of appearance of ions and soot, Fig. 1, in a flame is not in itself evidence that ions are produced before soot in the reaction sequence; the order of appearance would be reversed if the rate of production of soot from ions were fast compared to the rate of production of ions. However, when the species peak at considerable distance apart in the flame it seems safe to assume that the first peak precedes the second in the reaction sequence as well as in order of appearance. This assumption is further warranted when there is no clear means of proceeding from soot to ions (18). With these caveats, the appearance of ions in the flame with respect to the appearance of soot is evidence for ions being the precursors of soot.

Further evidence of a similar nature comes from observations in diffusion flames at one atmosphere. We have made ion concentration measurements (19) in the same methane/air flame on which Smyth et al. (20) made a number of measurements. Our temperature profiles agreed with theirs. The data for this diffusion flame are summarized in Fig. 3 and the rationale for the estimates of concentrations are summarized in the caption. The soot concentration profile was not measured by Smyth et al., but the position of the soot maximum in the flame was determined by laser induced ionization. The relative concentrations of polycyclic aromatic hydrocarbons, PCAH, were estimated from laser induced fluorescence. We confirmed the radial location of the soot maximum by laser extinction measurements at a wavelength of 633 nm somewhat higher in the flame. We estimate from our measurements that the volume fraction of soot is about 5×10^{-8} , which for 20 nm diameter particles would correspond to about 10^{10} particles/cm³.

The location of soot, Fig. 3, with respect to the possible reactants is evidence for the ionic mechanism as opposed to a mechanism involving only acetylene and a PCAH. For a reaction of acetylene and PCAH to be to be reasonable, it is necessary to assume something else is involved, such as hydrogen atoms (21,22), or that the rate limiting reaction has a very high activation energy. The soot is located between the peak concentrations of acetylenes and ions, just where it would be anticipated if these were the two reactants producing it.

An important question with respect to soot formation is "why does inception stop?" (23). Harris has recently suggested that the falloff in oxygen concentration may be responsible due to its promotion of the formation of high energy species which are important for soot formation and which disappear along with the oxygen. He suggested that the production of excess H-atoms is possibly responsible for the effect. An even more obvious explanation for the termination of soot inception would be the termination of ion formation and the rapid decrease in ion concentration, see e.g., Fig. 1. It is a long established fact that ions show a sharp peak in the flame front of hydrocarbon flames (24,25).

E. Changes With Equivalence Ratio

In premixed flames dramatic changes in ion concentrations occur at the threshold fuel concentration for soot formation as shown in Fig. 4. Small flame ions are replaced by large ions as the equivalence ratio is increased through the threshold soot point. This simple observation would be consistent with an ionic

mechanism of soot formation; there are, however, complications. Why does the total concentration of ions increase at higher equivalence ratios beyond the soot threshold? This observation has, in fact, been used to argue against the ionic mechanism; namely that the occurrence of the increase in ion concentration with equivalence ratio was due to ionization of charged particles (11,15). We have subsequently demonstrated that thermal ionization of soot particles cannot be the explanation for this increase (10) but the phenomenon remains unexplained. Both the maximum flame temperature (26) and the total ion recombination coefficient (10) change at the soot threshold concentration. The temperature drop is probably due to increased radiative losses.

F. Fuel Effects

The occurrence of ions and the appearance of soot in flames of various fuels are consistent with the ionic mechanism of soot formation, i.e., fuels which do not produce ions do not produce soot (1).

Another indication of a correlation between fuel effects on soot formation and ionization can be gleaned from the correlation made by Takahashi and Glassman (27) between the equivalence ratio for soot formation and the number of carbon bonds; the tendency to soot increases with the number of carbon bonds. This is similar to the tendency of compounds to produce ions under various conditions. In flame ionization detectors for gas chromatography the magnitude of the signal produced correlates with the number of carbon atoms in the molecule (28). In premixed fuel/oxygen flames, Bulewicz and Padley (29) found that the electron current increased with the number of carbon atoms in the molecule. Interestingly acetylene differed from their correlation as it does in the Takahashi and Glassman correlation.

G. Chemical Additive Effects

Some of the first evidence quoted for an ionic mechanism of soot formation was from observations of the effect on soot formation of chemical additives with low ionization potentials. Strong correlations are observed between the effectiveness of additives on soot formation and their ionization potentials (30). Alkaline earths are a special case because the level of ionization is greater than anticipated by thermal equilibrium; ions are produced by chemi-ionization (31).

The same additives have been observed to both promote or inhibit (30) the formation of soot, and the results have been interpreted as affecting either the nucleation or the coagulation step. Much of the confusion arises because of the number of possible roles an additive can play and the fact that these roles can vary with the experimental conditions, e.g., the concentration of the additive (32).

The effects of additives on soot nucleation are based on two processes as suggested by Addecutt and Nutt (33): (1) the transfer of charge from a chemi-ion to a metallic atom, A, (34) e.g.:



where M^+ is any hydrocarbon ion, such as $C_3H_3^+$, or (2) by increasing the concentration of electrons due to thermal ionization of easily ionized metals. This would increase the rate of dissociative recombination of chemi-ions:



Either one of these mechanisms would remove the precursor chem-ion from the system and thus reduce the number of soot nuclei produced. Reaction 1 will be important under conditions such that the equilibrium concentration of M^+ is lower than that of A^+ . In fact, the rate coefficient for Reaction 1 is so much greater than for Reaction 2 that equilibrium concentrations of A^+ may be approached via Reaction 1 rather than Reaction 2. The metal ion, A^+ , may also be produced in greater than equilibrium concentrations by Reaction 1 (35). Thus the specific mechanism by which the addition is effective will be determined by the relative equilibrium concentration of A^+ to M^+ and the time available to approach equilibrium.

Miller (36), in a study of additive effects on flame quenching, observed that the addition of carbon tetrachloride to a spherical low pressure diffusion flame transformed a nonsooting flame to a sooting flame and simultaneously completely altered the ionic composition of the flame. The chlorine from the additive forms compounds which attach electrons producing large concentrations of negative ions. These reduce the rate of recombination of positive ions because recombination coefficients with negative ions are about 100 times smaller than with electrons. Thus the positive ion concentration is increased, and this increase, via the ionic mechanism of soot formation, produces observable soot.

Bulewicz et al. (32) have studied the effect of metal additives on soot formation in flames and have given a detailed interpretation of their results which is in complete accord with our current concepts of the mechanism of soot formation via an ionic mechanism. A number of chemical additives were added to the fuel side of an acetylene/oxygen diffusion flame. The soot was collected on a glass fiber filter and weighed. The soot particle size was determined by electron microscopy of samples taken at 2 cm, about 1 ms, above the burner rim, and the total positive ion concentration was determined by Langmuir probe. Flame temperatures were in the range of 1400 to 1800 K.

The same additive acted as a pro-soot or an anti-soot additive, depending upon the total ion concentration due to the additive. With increasing ion concentration, the total quantity of soot increases and then decreases so that at one specific additive concentration, the amount of soot is the same as without the additive. At this additive concentration the particle number density reaches a maximum. Beyond this concentration the number density, total mass of soot, and the soot particle size all decrease so that the dominant effect of the additive is on the nucleation rather than the coagulation step. In other flames the dominant effect of additives is on coagulation, see e.g., Haynes et al. (37).

Bulewicz et al. (32) explain both the pro-soot and the anti-soot effects by means of an ionic mechanism. The reader is referred to their paper for the detailed arguments. Briefly, the anti-soot effect is due to charge transfer from the precursor hydrocarbon ion, M^+ , to the metal atom as in Reaction 1. They point out that in their flame, thermal ionization of the metal atom would be too slow to produce electrons above the natural flame level so that Reaction 3 cannot be effective in reducing the concentration of hydrocarbon flame ions. The pro-soot effect is explained by demonstrating that small concentrations of additive may, in fact, maintain the level of M^+ at a higher value throughout the flame than when no additive is present. The potassium level in the range of concentration near the cross-over point from pro-sooting to anti-sooting varies from about 10^{10} to 10^{14} atom/cm³. At about 1600 K, the equilibrium concentration of K^+ varies from about 10^8 to 10^{10} ion/cm³ (function of solution molarity). The natural flame ionization concentration is about 10^{10} ion/cm³, several orders of magnitude above equilibrium levels. When the concentration of K is 10^{14} and the concentration of M^+ is 10^{10} it is clear that Reaction 1 can proceed at a significant rate, thus reducing the concentration of M^+ . At this high level of additive concentration the equilibrium

concentration of K^+ cannot be exceeded. On the other hand when the K concentration is only 10^{10} atom/cm³, the M^+ concentration can be only negligibly reduced in the time available. However, the equilibrium level of K^+ , which is only about 10^8 ion/cm³, may be significantly exceeded because the recombination rate is slow compared to the rate of charge transfer from chemi-ions, Reaction 1 (see e.g., Ref. 35). Farther downstream the slow decay of K^+ maintains a higher level of total ionizations and at this point Bulewicz et al. (32) suggest that the reverse of Reaction 1 maintains the concentrations of M^+ . In the absence of this reaction, M^+ would have decayed because dissociative recombination of molecular ions is about two orders of magnitude greater than for atomic ions which must decay by a three body process. Thus new ionic nuclei are available at later stages in the combustion process to grow to incipient soot particles.

The pro-soot action of higher ionization elements, e.g., Pb 7.42 eV; Mg 7.64 eV; Cr 6.76 eV; Co 7.86 eV; Mn 7.43 eV; and even Li 5.39 eV, are explained by the above argument. Their equilibrium ionization levels are very low and their ionization potentials are somewhat less than those for hydrocarbon ions, so a concentration above the equilibrium concentration is expected. Clearly this analysis merits more detailed modeling in which all of the simultaneous reactions can be accounted for more quantitatively. It does, however, at this stage of development, support the ionic mechanism of soot formation.

III. SUMMARY

The answer to the question raised in the title seems to be "yes."

ACKNOWLEDGEMENTS

This paper is based on work funded by the Air Force Office of Scientific Research under contract F49620-83-C-0150 and National Science Foundation grant CBT-8502122. The United States Government is authorized to reproduce and distribute reprints for government purposes not withstanding any copyright notation hereon.

REFERENCES

1. Calcote, H.F., *Combust. Flame* **42**, 215 (1981).
2. Olson, D.B. and Calcote, H.F., *Eighteenth Symposium (International) on Combustion* (The Combustion Institute, Pittsburgh, 1981) p. 453.
3. Calcote, H.F., and Keil, D.G., submitted to *Combust. Flame*.
4. Smyth, K.C., Lias, S.G., and Ausloos, P., *Combust. Sci. Tech.* **28**, 147 (1982).
5. Eyler, J.R., in *The Chemistry of Combustion Processes*, T.M. Sloane, Ed., ACS Symposium Series 249 (American Chemical Society, Washington, DC, 1984) p. 49.
6. Baykut, G., Brill, F.W., and Eyler, J.R., *Combust. Sci. Tech.* **45**, 233 (1986).
7. Eyler, J.R., Ozlark, F., Baykut, and Moini, M., to be submitted to *J. Phys. Chem.*

8. Bowers, M.T., Ed., Gas Phase Ion Chemistry, Vol. 1 and 2, (Academic Press, 1979).
9. Patrick, R. and Golden, D.M., J. Chem. Phys. **82**, 75 (1985).
10. Keil, D.G., Gill, R.J., Olson, D.B., and Calcote, H.F., Twentieth Symposium (International) on Combustion (The Combustion Institute, Pittsburgh, 1985) p. 1129.
11. Delfau, J.L., Michaud, P., and Barassin, A., Combust. Sci. Tech. **20**, 165 (1979).
12. Michaud, P., Delfau, J.L., and Barassin, A., Eighteenth Symposium (International) on Combustion (The Combustion Institute, Pittsburgh, 1981) p. 443.
13. Homann, K.H., Ber. Bunsenges. Phys. Chem. **93**, 738 (1979).
14. Homann, K.H. and Stroofer, E., Soot in Combustion Systems and Its Toxic Properties, J. Lahaye and G. Prado, Eds. (Plenum, New York, 1983) p. 217.
15. Haynes, B.S. and Wagner, H. Gg., Progr. Energy Combust. Sci. **7**, 229 (1981).
16. Howard, J.B. and Prado, G.P., Combust. Sci. Tech. **22**, 189 (1980).
17. Sodha, M.S. and Guha, S., Adv. Plasma Phys. **4**, 219 (1971).
18. Calcote, H.F., in Soot in Combustion Systems and Its Toxic Properties, J. Lahaye and G. Prado, Eds. (Plenum Press, New York, 1983) p. 197.
19. Keil, D.G. and Calcote, H.F., paper in preparation.
20. Smyth, K.C., Miller, J.H., Dorfman, R.C., Mallard, W.G., and Santoro, R.J., Combust. Flame **62**, 157 (1985).
21. Frenklach, M., Clary, D.W., Gardiner, W.C., Jr., and Stein, S.E., Twentieth Symposium (International) on Combustion (The Combustion Institute, Pittsburgh, 1985) p. 887.
22. Frenklach, M. and Warnatz, J., accepted for publication in Combust. Sci. Tech.
23. Harris, S.J., Combust. Flame **66**, 211 (1986).
24. Calcote, H.F., Combust. Flame **1**, 385 (1957).
25. Wilson, H.A., Rev. Mod. Phys. **3**, 156 (1931).
26. Calcote, H.F., Olson, D.B., and Keil, D.G., paper in preparation.
27. Takahashi, F. and Glassman, I., Combust. Sci. Tech. **37**, 1 (1984).
28. Bulewicz, E.M., Nature **211**, 961 (1966).
29. Bulewicz, E.M. and Padley, P.J., Ninth Symposium (International) on Combustion (Academic Press, New York, 1963) p. 638.
30. Howard, J.B. and Kausch, W.J., Jr., Prog. Energy Combust. Sci. **6**, 263 (1980).

31. Schofield, K. and Sugden, T.M., Tenth Symposium (International) on Combustion (The Combustion Institute, Pittsburgh, 1965) p. 589.
32. Bulewicz, E.M., Evans, D. G., and Padley, P. J., Fifth Symposium (International) on Combustion (Reinhold Publishing Corp., New York, 1955) p. 1461.
33. Addecutt, K.S.B. and Nutt, C.W., Symposium on Deposit, Wear, and Emission Control, ACS Meeting, September 1969, p. A69.
34. Prado, G.P. and Howard, J.B., in Evaporation - Combustion of Fuels, Advances in Chemistry Series No. 166, J.T. Zung, Ed. (American Chemical Society, Washington, DC, 1978) p. 153.
35. Calcote, H.F., in Ion-Molecule Reactions, Vol. 2, J.L. Franklin, Ed. (Plenum Press, New York, 1972) p. 673.
36. W. J. Miller, Comment following Place and Weinberg paper, Eleventh Symposium (International) on Combustion (The Combustion Institute, Pittsburgh, 1967) p. 252, and unpublished work (AeroChem TP-151, 1967).
37. Haynes, B.S., Jander, H., and Wagner, H.Gg., Seventeenth Symposium (International) on Combustion, (The Combustion Institute, Pittsburgh, 1979), p. 1365.
38. Howard, J.B., Mersborg, B.L., and Williams, G.C., Faraday Soc. Symp. 7, 109 (1973).
39. Bonne, U., Homann, K.H., and Wagner, H. Gg., Tenth Symposium (International) on Combustion (The Combustion Institute, Pittsburgh, 1965), p. 503.

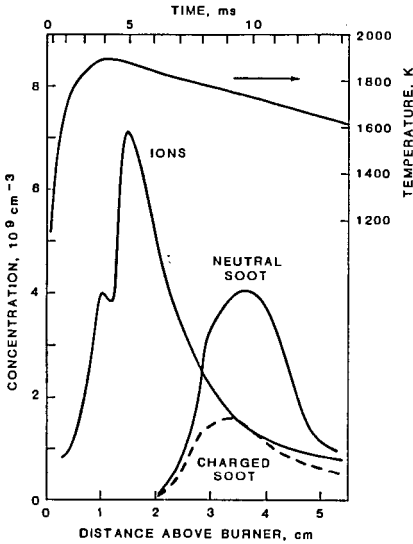


FIGURE 1 COMPARISON OF TOTAL ION CONCENTRATION AND SOOT CONCENTRATION PROFILES IN LOW PRESSURE (2.67 kPa), $\phi = 3.0$ ACETYLENE/OXYGEN FLAME (50 cm/s UNBURNED GAS VELOCITY)

The temperature, ion profiles, and time axis are from AeroChem (10). The soot profiles are from Howard et al. (38) and have been reduced by 50% so the charged soot and ion concentrations agree at 3.5 cm (10).

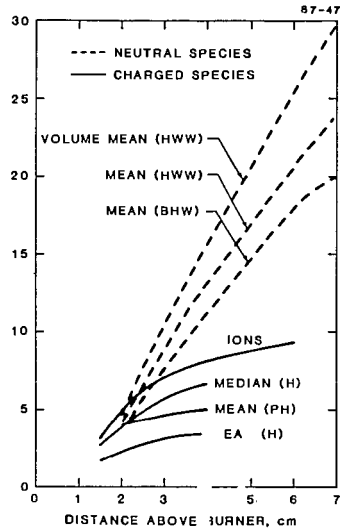


FIGURE 2 NEUTRAL SOOT PARTICLE AND CHARGED SOOT PARTICLE DIAMETERS IN SAME ACETYLENE/OXYGEN FLAME AS FIG. 1
HWW = Ref. 38. BHW = Ref. 39.
(Median) IONS = Refs. 13 and 14.
PH = Ref. 34.

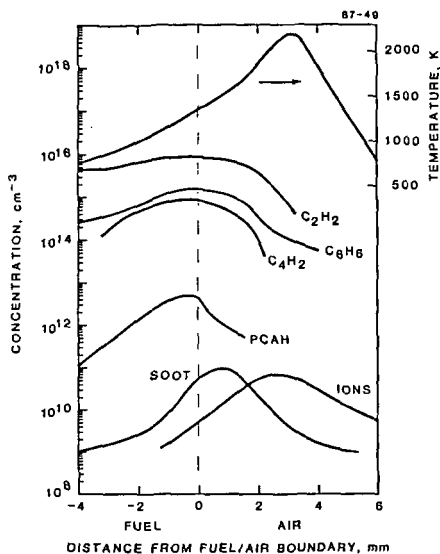


FIGURE 3 PROFILES 15 mm ABOVE A WOLFTHARD PARKER SLOT BURNER SUPPORTING AN ATMOSPHERIC PRESSURE METHANE/AIR DIFFUSION FLAME

Fuel velocity = 9.7 cm/s. Air velocity = 19.4 cm/s. TEMPERATURE and positive IONS (concentration measured with Langmuir probe, 1000 amu ion mass assumed) profiles measured at AeroChem (19). Other profiles from Smyth et al. (20). Profile for C_4H_2 represents experimental profiles at 9 mm scaled to 15 mm by the acetylene ratio at the two heights. PCAH is visible laser induced fluorescence profile approximately scaled with a constant factor based on the ratio of $C_{14}H_9$ to C_6H_6 concentrations in the low pressure flame of Figs. 1 and 2. SOOT is in arbitrary units and was scaled to maximize at the same concentration as IONS.

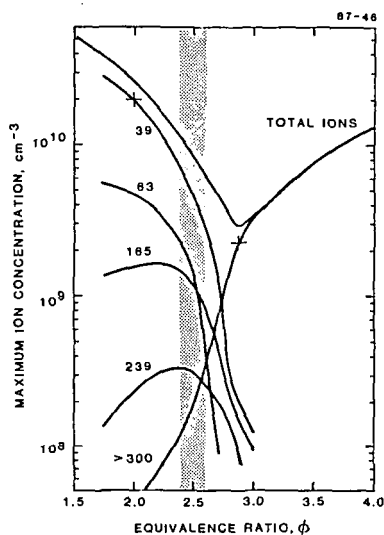


FIGURE 4 VARIATION OF MAXIMUM ION CONCENTRATION WITH EQUIVALENCE RATIO IN LOW PRESSURE ACETYLENE/OXYGEN FLAME TOTAL IONS are Langmuir probe measurements. Profiles of individual ions indicated by mass in amu were measured with flame ion sampling mass spectrometry. The ratio of TOTAL IONS to the sum of the individual currents at $\phi = 3$, where mass 39 dominates (+) provided a calibration of the mass spectrometer for lighter masses. Similarly, > 300 , representing all heavy masses between 300 amu and the high mass cut-off of the mass spectrometer, was put on an absolute scale at $\phi = 2.9$ (+). Shading indicates the threshold for soot formation.

Cluster Size Distribution for Free Molecular Agglomeration

G. W. Mulholland¹, R. J. Samson², R. D. Mountain¹, and M. H. Ernst³

1. INTRODUCTION

Dobbins and Megaridis (1) have observed soot agglomerates in a diffusion flame via thermophoretic sampling. The agglomerates are made up of spherules with a typical diameter of about 30 nm. A characteristic of the agglomerate is the relatively low density of the structure with much open space as indicated in Fig. 1. This study is concerned with modeling the agglomeration growth process.

Within the flame, the mean free path of the gas is on the order of 300 nm. Under these conditions, the particle continues in a straight path for a distance long compared to the particle size. Such behavior is termed free molecular. Mountain *et al.* (2) and Sullivan *et al.* (3) developed a computational technique for simulating particle agglomeration under these conditions, though in these studies the investigators were limited to a total of 500 primary particles in their simulations. The results were very limited in regard to the size distribution function. In this study, we have extended the simulations to 8000 primary particles in order to determine the size distribution function for agglomerates in the free molecular limit.

In addition to the computer simulation results, an expression for the coagulation kernel is developed based on the apparent fractal structure of the agglomerate and the free molecular particle dynamics condition. The size distribution function appropriate to the coagulation kernel is derived in the limit of long time based on the dynamic scaling analysis of van Dongen and Ernst (4). We also directly compute the size distribution function based on a numerical solution of the coagulation equation.

Previous studies of free molecular particle coagulation have been based on spherical particles. Lai *et al.* (5) have shown that free molecular coagulation with coalescence leads to a so called self-preserving size distribution. Dobbins and Mulholland (6) considered simultaneous particle formation and free molecular growth, but again with the assumption of spherical particle shape. They find that for conditions similar to those existing in a flame, the simultaneous particle formation can lead to a much broader size distribution than the self-preserving distribution obtained by Lai *et al.* As indicated above, the soot in the flame exists as an agglomerate. It is of obvious interest to determine the size distribution, structure, and growth kinetics for agglomerates.

Meakin *et al.* (7) have studied the effect of the cluster diffusivity on the resulting cluster-size distribution. In their study, the diffusion coefficient of a cluster of size k is assumed to be proportional to k^γ . Meakin *et al.* find a critical value of γ , $\gamma_c \approx 1/2$, at which the shape of the cluster-size distribution crosses over from a monotonically decreasing function to a bell-shaped curve. A Monte Carlo simulation is used with the diffusional motion of the clusters represented by random walks on a three-dimensional cubic lattice. In all cases considered, the primary particle size corresponds to one lattice site and the diffusion step is one lattice site. This differs from the free molecular condition that the particle move several particle

¹National Bureau of Standards, Gaithersburg, Maryland 20899

²Vista Chemical Co., 3441 Fairfield Rd., Baltimore, Maryland 21226

³Institute for Theoretical Physics, State University, P.O. Box 80.006, 3508 TA Utrecht, The Netherlands.

diameters before changing its trajectory. It is this latter case of free molecular motion that is the focus of this paper.

2. Description of Computer Simulation

The initial condition consists of 8000 spheres of mass m_0 and unit diameter σ randomly located in a cube of size L . The initial velocities are obtained using a random number generator which produces normally distributed numbers with unit variance so that the particles are in thermal equilibrium with the background gas through which they diffuse.

The dynamics of a particle are governed by the Langevin equation

$$d(mv_x)/dt = -m\beta v_x + f_x \quad [1]$$

where v_x is the x th cartesian component of the velocity of the center of mass of the agglomerate of mass m and f_x is a stochastic force satisfying $\langle f_x^2 \rangle = 2\beta mk_B T$. As can be seen from Eq. [1], β^{-1} represents the relaxation time of the agglomerate. The numerical solution of Eq. [1] to obtain the velocity and coordinates for each particle after a time interval h is described in Mountain et al. (2).

After each time interval h , the system is examined to see if any agglomeration events have occurred. It is assumed that whenever two particles "touch", they stick and the resulting agglomerate diffuses as a rigid assembly. Also, the agglomerates are thermally accommodated after each collision, since thermal accommodation with the host gas may not occur before a second collision at the high particle concentration.

The product $m\beta$ in Eq. [1] is termed the friction coefficient, K . We approximate the friction coefficient of k spheres as k times the friction coefficient of a single sphere. In making this approximation we neglect the shielding effect of the other spheres, but for a tenuous, low density agglomerate this is a reasonable first approximation. Both the mass m and the friction coefficient K are proportional to the number of particles in the agglomerate k ; therefore, β is independent of the size of the agglomerate in this independent particle approximation. Dividing both sides of Eq. [1] by m , it is seen that the quantity β is the controlling parameter for the particle dynamics.

The free molecular condition corresponds to the particle relaxation time, β^{-1} , being long compared to the time, $\tau = (m_0 \sigma^2 / k_B T)^{1/2}$, to free stream a particle diameter; that is,

$$\beta \tau \ll 1. \quad [2]$$

The following result is derived for $\beta \tau$ in the free molecular limit in Mountain et al. (2):

$$\beta \tau = 4P(2m_0 m_g)^{1/2} / (\rho_g k_B T), \quad [3]$$

where m_0 is the mass of an individual sphere, ρ_g refers to the density, and m_g is the mass of the gas molecules. The surface accommodation is assumed to have a value of unity. The simulations are carried out for $\beta \tau = 0.2$, which corresponds to a 16 nm particle diameter for a 1500 K flame temperature, and for $\beta \tau = 0.05$, which corresponds to a 6 nm diameter. The density of the individual particle is taken to be 2.0 g/cm³ and ambient pressure is assumed.

Another important parameter concerning the simulation is the number density, ρ , defined as the number of particle per volume, where volume is in units of σ^3 . Simulations were performed for the following values of ρ : 0.05, 0.0167, and 0.005. Even the lowest of these densities is several orders of magnitude larger than the value of about 10^{-6} observed in flames. The density dependence of the results

provides insight regarding the applicability of the simulations to an actual flame. A value of ρ of 0.005 is the lowest density for which the simulation can be carried out for 8000 particles with 5 runs to obtain adequate statistics using a Cyber 205 computer⁴.

3. RESULTS

While the primary focus of this study is the results regarding the size distribution function, it is also of interest to analyze the structure of the agglomerates and the cluster growth rate. The structural information will be used in the next section for deriving an effective collision kernel for the agglomerates. Given the collision kernel, the size distribution can be determined as shown in the next section. The cluster growth rate is of interest in its own right but is also needed for obtaining the scaled size distribution function.

3.1 Structure

The structure of the agglomerates is quite open as indicated in Fig. 1 for a planar projection of the structure. It is also seen that there is a similarity between the actual structure of soot produced by an acetylene diffusion flame and the results of the computer simulation. As has been demonstrated in a number of studies of agglomerate growth including Meakin (8,9) and Mountain *et al.* (2), the degree of openness can be conveniently characterized in terms of a fractal dimensionality, D_f , which in the case of an agglomerate is conveniently defined by the equation

$$k \propto R_g^{D_f} \quad [4]$$

where R_g is the radius of gyration of the cluster. In Fig. 2, $\log R_g$ is plotted versus $\log k$ for the case $\beta\tau=0.05$ and $\rho=0.005$. A linear least square fit of the data over the range 10-500 in k with a uniform weighting on a log scale leads to $D_f=1.91\pm 0.06$. The choice of the lower bound is determined by onset of power law behavior and the upperbound by condition that agglomerate not extend from one edge of the cell to the other. As indicated in Table I, the mean values of D_f are in the range 1.89 - 2.07. This is to be compared with a value of $D_f=1.87\pm 0.04$ obtained by Meakin (10) for cluster in the size range 10-500 with $\rho=0.005$. The model used by Meakin consists of random linear trajectories by both particles and clusters. The model was originally introduced by Sutherland and Goodarz-Nia (11). This model would correspond to the limiting case $\beta\tau=0$ for the free molecular simulation.

3.2 Cluster Growth

The average cluster size, \bar{k} , is defined by

$$\bar{k} = N_0 / N(t) \quad [5]$$

where N_0 is the number of primary particles and $N(t)$ is the total number of clusters at time t . In Fig. 3, \bar{k} is plotted versus number of time steps, t_N , on a log-log plot for all of the simulations. The mean cluster size increases asymptotically as

$$\bar{k} \propto t^z \quad (t \rightarrow \infty) \quad [6]$$

The exponent z is obtained from a linear least square fit of the log-log plot for the

⁴Certain commercial equipment is identified in this paper to specify adequately the calculation method. In no case does such identification imply recommendation or endorsement by the National Bureau of Standards, nor does it imply that the equipment identified is necessarily the best available for the purpose.

range in t over which $20 < \bar{k} < 100$. As indicated in Table I, there seems to be a decrease in z with decrease in density.

An alternative method for determining the exponent z is suggested by the analysis of van Dongen and Ernst (4). They obtain the following relationship between \bar{k} and t_N :

$$\bar{k} \propto (t_N + t_N^0)^z \quad [7]$$

The value of t_N^0 is obtained as the value for which $\log(\bar{k})$ versus $\log(t_N + t_N^0)$ has no curvature. The value of the exponent z obtained in this way is also given in Table I.

In Fig. 4, all of the data is reduced to a single curve by plotting \bar{k} vs. τ_1 , where

$$\tau_1 = (t/\tau)\rho \quad [8]$$

3.3 Cluster Size Distribution

The cluster-size distribution, N_k , is plotted in Fig. 5 at several times. As a test for the existence of a self-preserving cluster distribution, we also plot the size distribution in terms of the similarity variables, ψ and η , introduced by Friedlander (12),

$$N_k = \bar{k}^2 N_0 \psi(\eta) \quad [9]$$

$$\eta = k/\bar{k} \quad [10]$$

It is seen from Fig. 6 that the similarity variables do reduce all of the cluster-size distributions to a single curve. The possibility of deriving this universal size distribution is treated in the next section.

Perhaps the size distribution function affording the best comparison with experiment is the number distribution in terms of the radius of gyration, R_g .

$$dN/dR_g = AD_r R_g^{-1} N_k \quad [11]$$

Such a size distribution is plotted in Fig. 7. While it may not be practical to evaluate R_g for every cluster by electron microscopy, one might rapidly determine an effective size of the agglomerate based on its length and width.

4. Coagulation Equation

The most widely used tool for studying irreversible clustering phenomena in many fields of science is Smoluchowski's coagulation equation:

$$\dot{n}_k = k \sum K(i, j) n_i n_j - n_k \sum K(k, j) n_j \quad [12]$$

where n_k is the number concentration of clusters of size k and $K(i, j)$, the coagulation kernel, represents the rate coefficient for a specific clustering mechanism between clusters of sizes i and j . Below an estimate is made for the coagulation kernel for the case of free molecular growth and then Eq. [12] is solved analytically in the asymptotic limit as well as numerically. Finally the results are compared with the results of the computer simulation.

4.1 Coagulation Kernel

For the case of small droplets that coalesce upon contact, the free molecular coagulation kernel is given by

$$K(i, j) = a(i^{1/3} + j^{1/3})^2 (1/i + 1/j)^{1/2} \quad [13]$$

$$a = (3v_0/4\pi)^{1/6} (6k_B T/\rho_g)^{1/3} . \quad [14]$$

The first factor in Eq.[13] corresponds to the size dependence of the collision cross section and the second term to the dependence of the average relative velocity on the reduced cluster mass. The quantity $K(i,j)$ given above is essentially identical to the kinetic theory prediction of the volume swept out per second by colliding molecules.

The collision cross section of two low density agglomerates (fractal objects with Hausdorff dimension $D_f=1.9$) in free flow (ballistic trajectories) is much larger than for compact spheres, mainly because of their large radii of gyration,

$$R_g \propto k^{1/D_f} .$$

However, there is a subtlety in the argument. Since $D_f < 2$, the planar projection of a cluster or cross-sectional area (see Fig. 1) is still a fractal object with Hausdorff dimension $D_f=1.9$. Therefore, the effective scattering area for two free moving fractal clusters with $D_f < 2$ and sizes i and j respectively is:

$$\begin{aligned} \text{cross-section} &\propto (R_g(i) + R_g(j))^{D_f} \\ \text{" " " " } &\propto (i^{1/D_f} + j^{1/D_f})^{D_f} \end{aligned} \quad [15]$$

If however the fractal dimension of the clusters would be $2 \leq D_f \leq 3$, then their projections would be compact objects and their collision cross-section would be:

$$\begin{aligned} \text{cross-section} &\propto (R_g(i) + R_g(j))^2 \\ \text{" " " " } &\propto (i^{1/D_f} + j^{1/D_f})^2 \end{aligned} \quad [16]$$

Note that the cross-section in both cases [15] and [16] is bounded by $\text{const.} \cdot xj$ for $j \gg i$. This is a physically obvious requirement. Equation [16] for $D_f < 2$ would violate this condition (See Mountain *et al.* (2)).

The agglomerate speed is not affected by the particle structure based on the equipartition of energy so that the coagulation kernel for the agglomerate in the free molecular limit is given by

$$K(i,j) = a_1 (i^{1/D_f} + j^{1/D_f})^{D_f} (1/i + 1/j)^{1/2} . \quad [17]$$

Van Dongen and Ernst (4) have obtained asymptotic solutions to the coagulation equation, Eq.[14], for coagulation kernels classified on the basis of three exponents defined below:

$$K(ai, aj) = a^\lambda K(i, j) = a^\lambda K(j, i) , \quad [18]$$

$$K(i, j) \approx i^\mu j^\nu \quad (j \gg i; \lambda = \mu + \nu) . \quad [19]$$

For $K(i,j)$ given by Eq.[17], $\lambda = 1/2$, $\mu = -1/2$, and $\nu = 1$. For $\lambda \leq 1$, van Dongen and Ernst (4) show that the exponent z is given by

$$z = 1/(1 - \lambda) . \quad [20]$$

So for $\lambda = 1/2$, $z = 2$. The general form of the reduced size distribution for large η is given by van Dongen and Ernst (13).

$$\psi(\eta) = A\eta^{-z} \exp(-\alpha\eta) , \quad \eta \rightarrow \infty . \quad [21]$$

For coagulation kernels with $\nu < 1$, the θ exponent is simply given by $\theta = \lambda$. However, for kernels with $\nu = 1$, such as given in Eq.[17], the θ exponent is more complicated. It has been calculated by van Dongen and Ernst (13), and we conclude from their Eqs.[12] through [15] that the exponent θ is determined from the following transcendental equation:

$$J(\theta) = 0, \quad [22]$$

where $J(\theta)$ is defined by

$$J(\theta) = \int_0^1 dx (K(x, 1-x) [x(1-x)]^{-\theta} - x^{\mu-\theta}) - \int_0^{\infty} dx x^{\mu-\theta}. \quad [23]$$

Since the first integrand diverges at $x=0$, an asymptotic expansion is made for the integrand to obtain the small x contribution to the integral. For the remainder of the range in x , the integration is obtained numerically. For the case $D_c = 1.90$, we obtain $\theta = 0.72$.

For large values of D_c the asymptotic solution of Eq.[23] is (14)

$$\theta = 1/2 + 2^{1-D_c} / \pi \quad (D_c \gg 1)$$

This relation gives at $D_c = 1.9$ the fair estimate $\theta = 0.67$ and at $D_c = 1$ is even close to the exact value $\theta = 1$.

The size distribution plots given in Fig. 6 suggest a power law region followed by an exponential region. However, one finds a wide range in the value of θ , 0.4 to 0.8, depending on the range in η over which the line is drawn. A better method is to first obtain k from the large η asymptotic slope of $\ln \psi$ vs η and, then obtain θ from the slope of $k\eta + \ln \psi$ vs $\ln \eta$. This approach applied to the case $\beta_T = 0.05$ and $\rho = 0.005$ yields $\alpha = 0.67$ and $\theta = 0.53$ compared to the predicted value of θ of 0.72. There is still some ambiguity in the value of θ , because of the interplay between the value of α and θ . That is, a lower value of α and a larger value of θ will also lead to a good fit to the simulation results.

In the limit of small cluster size and long time, van Dongen and Ernst (4) predict that

$$\psi(\eta) \propto \eta^{-2} \exp(-1/\eta^k) \quad \text{for } \eta \rightarrow 0. \quad [24]$$

Unlike this predicted exponential behavior, it appears that $\psi(\eta)$ decreases only slightly for small η . Presumably this discrepancy results from the simulations not being carried out to long enough time.

Another approach to comparing the results of the simulations with coagulation theory is to numerically solve for N_k vs k from Eq.[13] based on the kernel given by Eq.[17]. One thousand twenty four coupled rate equations given by Eq.[13] were solved by the Runge Kutta method with fourth order predictor corrector. This is analogous to the technique used by Hidy et al. (15,16) for solving the coagulation equation. Starting from a monodisperse size distribution as in the simulations, it was found that the loss of mass due to particles reaching $k=1024$ represented a 4% effect when the total number concentration had dropped by a factor of 100. It is seen from Fig. 6 that the reduced size distribution obtained from the numerical solution of the coagulation equation is both self-preserving and agrees very well with the results of the computer simulation. The value of the exponent z characterizing the cluster growth rate is found to be in good agreement with the computer simulation results (1.84 for the coagulation equation vs 1.72 for the simulation).

5. Discussion

The computer simulations of free molecular agglomeration lead to much more rapid growth than is predicted for coalescing droplets in the free molecular limit, which has been the basis for predicting coagulation rates in flames in previous studies (5,6). The agglomeration leads to an exponent z of about 2.0 compared to a value of about 1.2 based on coalescence.

The results of the computer simulations in terms of the fractal structure and the size distribution function seem to vary only slightly with the choice of β (0.2 and 0.05) and ρ (0.05, 0.0167, 0.005). There appears to be a more pronounced affect of the density on the value of the exponent z with the higher density leading to a higher value of z . The value reported by Mountain et al. (2) for a system with 500 primary particles was larger yet with a value of about 2.6 for z . We expect the simulation with the lowest density ($\rho=0.005$) and lowest value of β (0.05) to give the most appropriate value for physical systems. For the limited range in k , Eq.[7] is the most accurate method for determining the exponent z , and this leads to $z=2.05$ for the simulation.

We do not observe as large a density effect in the free molecular limit as has been observed by Mountain et al. (2) in the continuum limit and by Ziff et al. (17) for agglomerates with diffusion coefficient proportional to the cluster size raised to a power.

We find that a coagulation kernel derived based on the fractal structure of the agglomerate leads to an average growth rate and self-preserving size distribution in good agreement with the computer simulations. The computer simulations have not been run for long enough time to afford a comparison with the predicted small η behavior..

Ziff et al. (17) demonstrated that for a size dependent diffusion coefficient the kinetic rate kernel predicted by taking into account the fractal geometry of the agglomerate is in agreement with the computer simulation results. We have shown that in the free molecular limit that using a kinetic rate kernel based on fractal geometry leads to a size distribution in agreement with the computer simulation. One is encouraged to conjecture that the coagulation equation can be applied to agglomerates provided the agglomerate structure information is included in the kinetic rate.

1. Dobbins, R.A., and Megaridis, C.M., Langmuir accepted for publication.
2. Mountain, R.D., Mulholland, G.W., and Baum H., J. Colloid Interface Sci., **114**, 67 (1986).
3. Sullivan, F., Mountain, R.D., and O'Connell, J., J. Comput. Phys., in press.
4. van Dongen, P.G.J., and Ernst, M.H., Phys. Rev. Lett., **54**, 1396 (1985).
5. Lai, F.S., Friedlander, S.K., Pich, J., and Hidy, G.M., J. Colloid Interface Sci. **39**, 395 (1972).
6. Dobbins, R.A., and Mulholland, G.W., Comb. Sci. and Tech., **40**, 175 (1984)
7. Meakin, P., Vicsek, T., and Family, F., Phys. Rev. B, **31**, 564 (1985).
8. Meakin, P., J. Colloid Interface Sci., **102**, 491 (1984).
9. Meakin, P., Phys. Review A, **29**, 997 (1984).
10. Meakin, P., J. Colloid Interface Sci., **102**, 505 (1984).
11. Sutherland, D.N., and Goodarz-Nia, I., I. Chemical Engineering Sci., **26**, 2071 (1971).
12. Friedlander, S.K., "Smoke, Dust, and Haze", Wiley, New York, 1977.
13. van Dongen, P.G.J., and Ernst, M.H., "Fractals in Physics", L. Pietronero and E. Tosatti, ed., Elsevier, 1986.
14. van Dongen, P.G.J., private communication.
15. Hidy, G., and Lilly, D., J. Colloid Sci. **20**, 867 (1965)
16. Hidy, G., J. Colloid Sci. **20**, 123 (1965).
17. Ziff, R.M., McGrady, E.D., and Meakin, P., J. Chem. Phys. **82**, 5269 (1985).

TABLE I. Exponents D_z and z for Free Molecular Simulations

βr	ρ	D_z	z^a	z^b	t_N^0
0.20	0.05	2.05 ± 0.03	1.98 ± 0.05		
0.05	0.05	2.07 ± 0.08	2.40 ± 0.16	4.06 ± 0.19	500
0.05	0.0167	1.89 ± 0.08	1.92 ± 0.07	2.53 ± 0.05	900
0.05	0.005	1.91 ± 0.06	1.72 ± 0.05	2.05 ± 0.03	2000

^a The exponent z is defined by $\bar{k} \propto (t_N)^z$.

^b Here the exponent z is defined by $\bar{k} \propto (t_N + t_N^0)^z$.

Soot (acetylene fuel)

Agglomeration Model



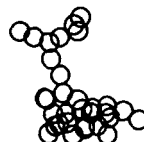
10 Spheres



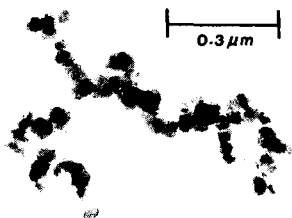
12 Spheres



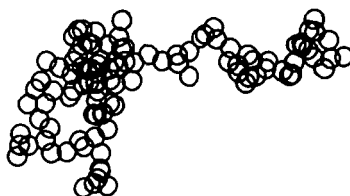
33 Spheres



33 Spheres



107 Spheres



108 Spheres

Fig. 1. Qualitative comparison of soot clusters and clusters obtained by computer simulation of free molecular growth.

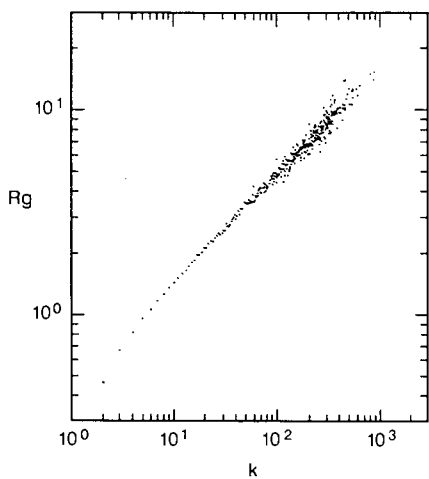


Fig. 2. R_g versus k for $\beta\tau=0.05$ and $\rho=0.005$.

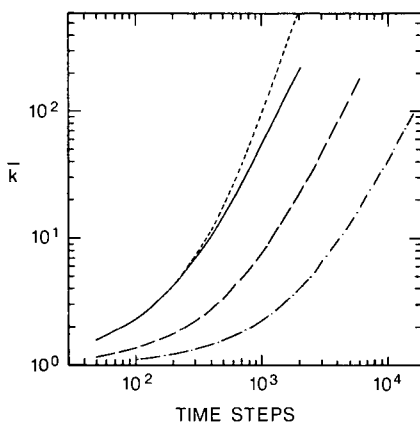


Fig. 3. \bar{k} versus time steps for $\beta\tau=0.2$, $\rho=0.05$ (—); $\beta\tau=0.05$, $\rho=0.05$ (---), $\rho=0.0167$ (- · -), $\rho=0.005$ (- - -).

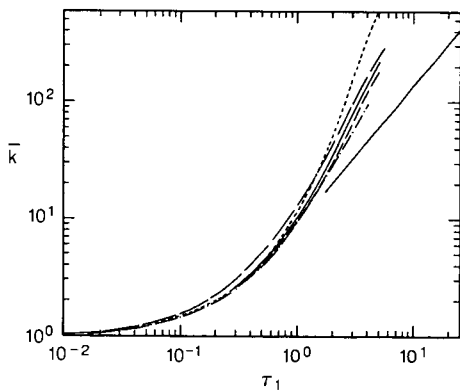


Fig. 4. \bar{k} versus τ_1 , for $\beta\tau=0.2$, $\rho=0.05$ (—); $\beta\tau=0.05$, $\rho=0.05$ (---), $\rho=0.0167$ (- · -), $\rho=0.005$ (- - -), fractal coagulation (—), coalescence (—) slope=1.2.

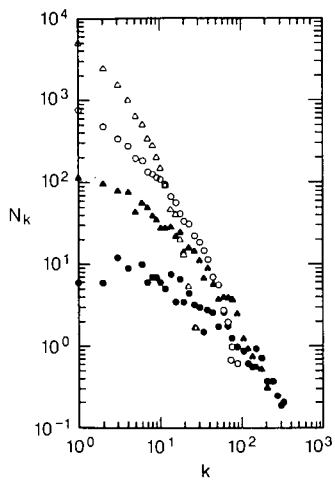


Fig. 5. Size distribution for $\beta r=0.05$, $\rho=0.005$, $t_N=1500(\Delta)$, $t_N=4200(\circ)$, $t_N=8000(\Delta)$, $t_N=16,000(\bullet)$.

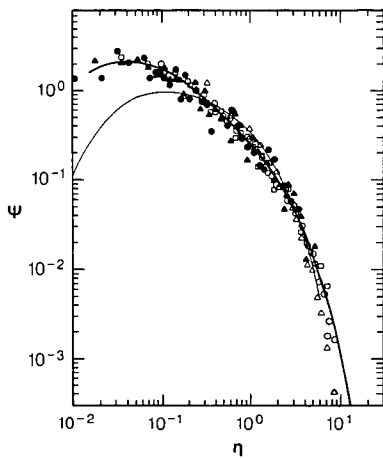


Fig. 6. Self-preserving sized distribution for simulation, fractal coagulation(Δ), coalescence(\square).

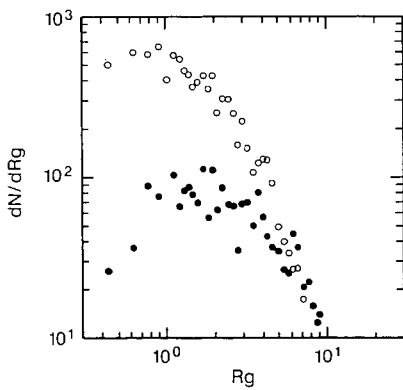


Fig. 7. dN/dR_g versus R_g for $t_N=8000(\circ)$ and $t_N=16,000(\bullet)$.

A SIMPLE METHOD FOR PREDICTING SOOTING TENDENCIES OF HYDROCARBON FUELS IN PREMIXED FLAMES

Stamoulis Stournas and Euripides Lois

Chemical Engineering Department, National Technical University
42 Patission Street, 106 82 Athens, Greece

ABSTRACT

One of the accepted measures of sooting tendencies of hydrocarbon fuels in premixed flames is the threshold fuel/oxidizer ratio, φ_c , which assumes combustion to CO_2 and H_2O . In this analysis it has been found that this sooting can be accurately predicted by using the group additivity approach based on the nature of the individual carbon atoms that exist in the fuel molecule. The only parameters needed for this prediction are the numbers of sp^3 , sp^2 , sp , aromatic and benzylic carbons along with the total number of hydrogen atoms in the molecule.

This approach has been used for the calculation of the sooting tendencies of 73 fuels whose measured φ_c has been reported in the literature. Even though the structure of these fuels varied widely and included alkanes, olefins, alkynes and aromatics, the calculated values were always very close to the measured ones. In fact, in 88% of the cases the predicted values lie within 5% of the measured ones, whereas the deviation in the rest never exceeds 10%.

INTRODUCTION

The sooting tendencies of hydrocarbon fuels, either in premixed or diffusion flames, has been studied in the past by a number of investigators (1-12).

A number of parameters have been recognized as important aspects for the sooting tendency of a fuel, such as its molecular structure, fuel/oxygen ratio, flame temperature, etc.

Most of the recent work refers to efforts made to quantify these parameters into a unified approach that will predict the soot threshold of each fuel. More recently, Olson and Pickens (1) investigated a number of probable expressions defining soot thresholds for premixed flames for a large number of hydrocarbons, including alkanes, alkenes, alkynes and aromatics. A few years earlier, Haynes and Wagner (5) discussed soot thresholds for premixed flames, in a comprehensive review of soot formation in terms of critical C/O ratios, $(\text{C/O})_c$.

Olson and Pickens assumed two modified equivalence ratios, one giving combustion products CO_2 and H_2O (φ_c), and the other CO and H_2O ($\varphi_{c'}$); the former was linked eventually with the Threshold Soot Index (TSI) as defined by Calcote and Manos (6).

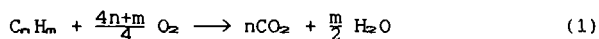
In the present analysis, we have found that, by using the group additivity principle (13) the sooting tendency of hydrocarbon fuels can be predicted with good accuracy. Group additivity has been successfully used in the past to predict properties such as heat of formation, heat capacity, refractive index, etc. (14); more recently, it has been found useful in the prediction of ignition quality (cetane number) of diesel fuels. (15) Our approach was to divide the carbon atoms that comprise the fuel molecules into groups according

to their chemical nature (sp^3 , sp^2 , aromatic, etc.) and to assign a different weighting factor to each group. The only other information that is needed for the prediction is the total number of hydrogen atoms in the molecule.

ANALYTICAL APPROACH

Soot threshold is defined by the appearance of the first visible yellow emission as the fuel to air ratio was increased (1,16). This critical fuel to air ratio (F_c), when compared to the stoichiometric fuel to air ratio (F) that is required by the combustion process, gives a measure of the sooting tendency of each particular fuel.

If complete combustion to CO_2 and H_2O is taken as the basis of comparison, then the required stoichiometry for any hydrocarbon fuel C_nH_m is:



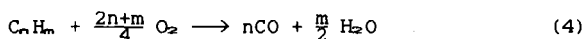
In this case the stoichiometric fuel/air ratio is given by

$$F = \frac{4}{4n+m} \quad (\text{moles fuel/moles oxygen}) \quad (2)$$

and the sooting tendency depends on ϕ_c , defined as

$$\phi_c = \frac{F}{F_c} = \frac{4}{(4n+m)F_c} \quad (3)$$

On the other hand, by assuming combustion to CO and H_2O , the stoichiometry is:



with

$$F = \frac{4}{2n+m} \quad (\text{moles fuel/moles oxygen}) \quad (5)$$

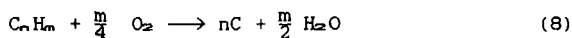
The sooting tendency criterion is now ψ_c , defined as:

$$\psi_c = \frac{F}{F_c} = \frac{4}{(2n+m)F_c} \quad (6)$$

It is clear that ϕ_c and ψ_c are related by the expression

$$\psi_c = \frac{(4n+m)\phi_c}{2n+m} \quad (7)$$

A third criterion, s_c , may be employed as a measure of sooting tendency, if we assume incomplete combustion to elemental carbon and water:



In this case,

$$F = \frac{4}{m} \quad (\text{moles fuel/moles oxygen}) \quad (9)$$

and the sooting tendency criterion, s_c , is defined as:

$$s_c = \frac{F}{F_c} = \frac{4}{mF_c} \quad (10)$$

Also

$$s_c = \frac{(4n+m)\varphi_c}{m} \quad (11)$$

This last expression permits the computation of the actual s_c for all fuels whose φ_c has been measured experimentally and whose gross structure (i.e. number of carbon and hydrogen atoms in the molecule) is known.

It is recognized that combustion to carbon and water is a rather unrealistic process; as will be shown later, however, s_c is a useful criterion for a unified approach to the prediction of sooting tendencies of hydrocarbon fuels and, by employing relations (7) and (11), it can lead to the better known quantities φ_c and ψ_c .

The relative amounts of carbon and hydrogen in a fuel molecule (in the form of hydrogen content) has been used as a rather intuitive guide to the sooting tendency of hydrocarbon fuels in both premixed and laminar flames, albeit with rather limited success. If, however, the effect of each carbon atom in the fuel molecule is accorded a weighting factor according to its chemical nature, an almost quantitative prediction of sooting tendency can result. We have found that it is sufficient to divide the various types of carbon atoms into five categories:

1. Saturated (sp^3) carbon atoms (C_1)
2. Olefinic (sp^2) carbon atoms (C_2)
3. Acetylenic (sp) carbon atoms (C_3)
4. Aromatic carbon atoms (C_A)
5. Benzylic carbon atoms, i.e. those directly coupled to an aromatic ring (C_B).

For the purpose of this definition, olefinic carbon atoms that belong to conjugated double bonds are counted as aromatic.

Based on the above definitions, the sooting tendency of any hydrocarbon fuel can be accurately predicted in the form of s_c by the relation:

$$s_c = \frac{3.5C_1 + 2.9C_2 + 1.9C_3 + 3.1C_A + 5C_B}{m} \quad (12)$$

where C_1 , C_2 , etc. are the numbers of each type of carbon atoms as defined above, and m is the total number of hydrogen atoms in the molecule.

Alternatively, φ_c and ψ_c can be calculated for any fuel by changing the denominator in (12) with $(4n+m)$ and $(2n+m)$ respectively, where n is the total number of carbon atoms in the molecule.

RESULTS AND DISCUSSION

Relation (12) was applied to 73 hydrocarbon fuels whose sooting tendencies have been measured experimentally. (1,2,4,12) The calculated value of φ_c was within $\pm 5\%$ of the experimental value in 64 of the cases, and even in the worst case (1,5-cyclooctadiene) the difference was less than 10%. The linear correlation coefficient (r) between calculated φ_c and experimental φ_c for all the fuels was 0.95; this value can be considered as quite acceptable, given the wide variation in the molecular structure of the fuels (26 paraffins, 20 olefins, 7 alkynes, and 20 aromatics) and the inherent experimental uncertainties in measuring the critical fuel to air ratio. In several cases the values reported by different

investigators for the same fuel differ by more than 10%; the experimental values employed in this work were the averages of the reported values. The results of the calculations are depicted graphically in Figure 1, whereas Table I contains some examples that illustrate the calculation procedure.

Similar results were obtained in the calculation of ψ_c for the same fuels, except that the linear correlation coefficient was somewhat better ($r=0.97$).

TABLE I
EXAMPLES OF CALCULATED SOOTING TENDENCIES

FUEL	FORMULA	C ₁	C ₂	C ₃	C ₄	C ₅	EXPERIMENTAL		CALCULATED	
							ψ_c	s_c	ψ_c	s_c
Propane	C ₃ H ₈	3	0	0	0	0	0.524	1.309	0.525	1.313
iso-Octane	C ₈ H ₁₈	8	0	0	0	0	0.556	1.543	0.560	1.556
Decalin	C ₁₀ H ₁₈	10	0	0	0	0	0.613	1.977	0.603	1.944
n-Tetradecane	C ₁₄ H ₃₀	14	0	0	0	0	0.575	1.648	0.570	1.633
1-Heptene	C ₇ H ₁₄	5	2	0	0	0	0.552	1.657	0.555	1.664
1-Pentyne	C ₅ H ₈	3	0	2	0	0	0.529	1.852	0.518	1.813
Toluene	C ₇ H ₈	0	0	0	6	1	0.658	2.961	0.656	2.950
Indene	C ₉ H ₈	0	0	0	8	1	0.676	3.716	0.677	3.725
Propylbenzene	C ₉ H ₁₂	2	0	0	6	1	0.633	2.532	0.638	2.550
Tetralin	C ₁₀ H ₁₂	2	0	0	6	2	0.676	2.928	0.685	2.967

The best correlation with experimental measurements was obtained in the calculation of s_c for the 73 fuels; in this case the linear correlation coefficient has an excellent value, being equal to 0.994. The results, as depicted in Figure 2, show ancillary advantages of the employment of s_c as a sooting tendency criterion:

a. The values of s_c (approx. 0.9 to 3.8) cover a wider range than those of ψ_c (approx. 0.4 to 0.7), thus making it easier to discern the differences between various fuels.

b. What is more important, s_c tends to divide the sooting tendencies of the fuels into more rational and intuitively acceptable classes. Thus paraffins have s_c values averaging around 1.5, olefins and alkynes average around 1.8, whereas the average for aromatics is close to 3. Such distinctions are difficult to make with ψ_c as the sooting tendency criterion.

The above observations, which show a dependence of sooting tendency on molecular structure similar to that observed for diffusion flames, (3) has led us to attempt a correlation of sooting tendencies in diffusion flames with those in premixed flames. Figure 3 shows a plot of s_c vs. the diffusion flame threshold soot index, TSI(3), for 65 fuels. The linear correlation coefficient has an acceptable value of 0.925, which rises to 0.96 if the four points that are circled in Figure 3 are omitted and the correlation employs 61 fuels. When diffusion flame TSI is compared to ψ_c , the correlation coefficient has a much less acceptable value of 0.76, whereas the correlation with ψ_c gives results that are only slightly better ($r=0.86$).

CONCLUSIONS

1. By employing appropriate weighting factors on the carbon atoms that comprise a fuel molecule, its premixed flame sooting tendency in the form of ϕ_s can be predicted with acceptable accuracy. The prediction is even better if the sooting tendency criterion is s_{sc} , which assumes incomplete combustion to elemental carbon and water.

2. A linear correlation exists between sooting tendency in premixed flames as expressed by s_{sc} , and sooting tendency in diffusion flames as expressed by TSI.

REFERENCES

1. Olson, D.B. and Pickens, J.C., *Combust. and Flame* **57** 199 (1984)
2. Wright, F.J., 12th Symposium (International) on Combustion, The Combustion Institute, 1969, p. 867
3. Olson, D.B., Pickens, J.C. and Gill, R.J. *Combust. and Flame* **62** 43 (1985)
4. Blazowski, W.S., *Combust. Sci. Technol.* **21**, 87 (1980)
5. Haynes, B.S. and Wagner, H.G. *Prog. Energy and Combust. Sci.* **7** 229 (1981)
6. Calcote, H.F. and Manos, D.M. *Combust. Flame* **49** 289 (1983)
7. Glassman, I. and Lara, P.V., Fall Technical Meeting, Eastern Section, The Combustion Institute, 1981
8. Calcote, H.F. and Olson, D.B. *Combust. Sci. Technol.* **28** 315 (1982)
9. Dyer, T.M. and Flower, W.L., in "Particulate Carbon: Formation during Combustion" (D.C. Singh and G.W. Smith, eds.), New York (Plenum), 1981 p. 363
10. Glassman, I. and Yaccarino, P., 18th Symposium (International) on Combustion, The Combustion Institute, 1981, p.1175
11. Siddall, R.G. and McGrath, I.A., 9th Symposium (international) on Combustion, Academic Press, New York, 1963, p.102
12. Street, J.C. and Thomas, A., *Fuel* **34**, 4 (1955)
13. Benson, S.W. and Buss, J.H. *J. Chem. Phys.* **29**, 546 (1958)
14. Benson, S.W. "Thermochemical Kinetics" New York (Wiley) 1976
15. DeFries, T.H., Indritz, D. and Kastrup, R.V. *Ind. Eng. Chem. Res.* **26**, 188 (1987)
16. Burke, S.P. and Schumann, T.E.W., *Ind. Eng. Chem.* **20**, 998 (1928)

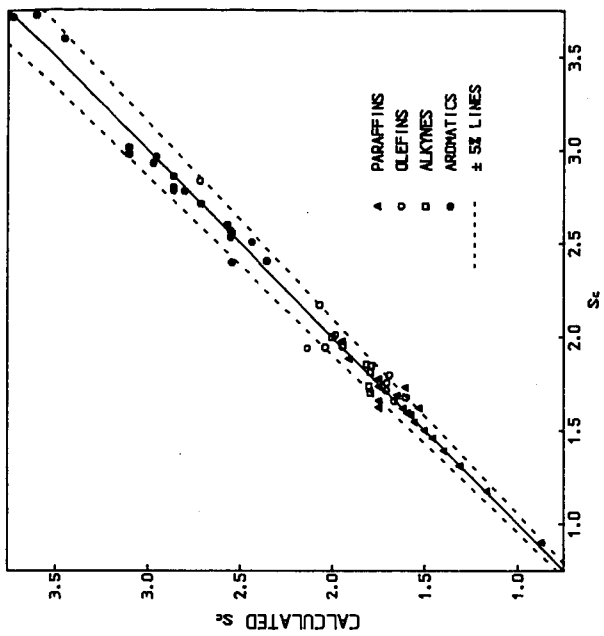


FIGURE 2. CALCULATION RESULTS FOR S_c

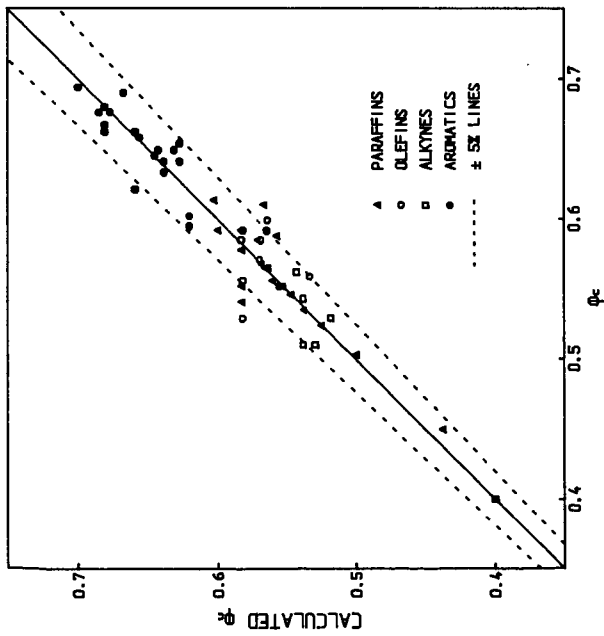


FIGURE 1. CALCULATION RESULTS FOR ϕ_c

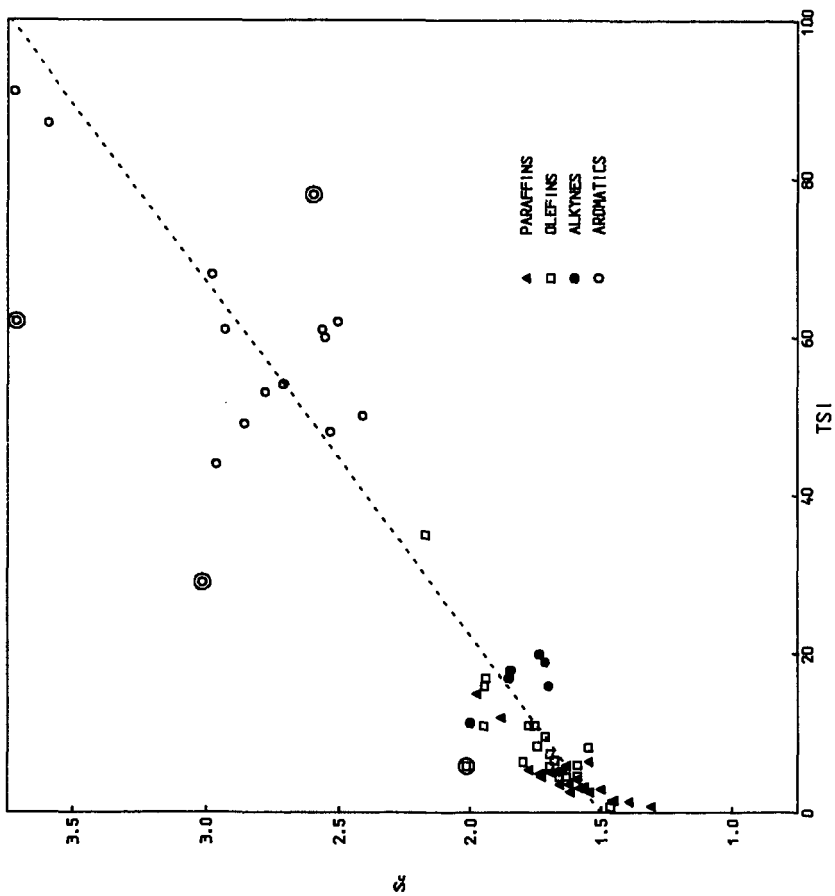


FIGURE 3. CORRELATION OF DIFFUSION FLAME TSI WITH S_c

Oxidation Kinetics of Carbon Blacks over 1300-1700 K*

W. Felder, S. Madronich,† and D. B. Olson

AeroChem Research Laboratories, Inc.
P.O. Box 12, Princeton NJ 08542

I. INTRODUCTION

The oxidation of carbonaceous particulate matter is of wide practical concern in power generation and pollution reduction. Typically, in fuel-rich portions of combustion flames, OH radicals can be the major oxidizing species (1-3). However, in regions of combustors and in the exhaust where soot is present and OH concentrations are essentially negligible (regions in which particles spend the major portion of their lifetimes within a device), oxidation by excess oxygen is important. The work described here utilized an entrained flow reactor (a modified High Temperature Fast Flow Reactor, HTFFR) to determine the reactivity of two carbon blacks with O₂ in the 1300-1700 K range. A wide range of oxygen concentration was investigated while maintaining independent control of total pressure and flow velocity (particle residence time). A method and apparatus were developed for feeding particles to the HTFFR and assuring that particle sizes lie below specified limits.

II. METHODS AND APPARATUS

The primary measurement is the number of moles of carbon converted to CO_x (= CO + CO₂) in a residence time, t . Collected gas samples were analyzed gas chromatographically to determine the amount of CO_x evolved after the particle and oxidizer mixture had traversed the flow tube reactor at a temperature, T , in a time, t . For surface oxidation of monodisperse spherical particles, evolving CO_x at the expense of particle size (4):

$$u(t) = 1 - (1 - (R_e S_0 t / 3)) ^3 \quad (1)$$

where: $u(t) = (m_0 - m_t) / m_0$, is the burnoff at time t ; m_0 and m_t are the mass of carbon input (g/s) and the mass of carbon remaining unoxidized at time t , respectively

R_e = the external surface oxidation reactivity coefficient, g cm² s⁻¹, a function of [O₂]

S_0 = specific surface area of unoxidized carbon particles, cm²/g

Equation 1 assumes that the oxidation is chemically controlled (i.e., diffusion is rapid compared to reaction), and that the surface reactivity is a function only of available area. In this work, it was shown that the assumptions of surface reaction and chemical control are valid. The possible change in surface reactivity with oxidation was not addressed; thus the R_e values are referred to the original surface area.

To determine $u(t)$, it is necessary to measure [CO_x] for the experimental condition and [CO_x(max)], the amount of CO_x produced by complete particle oxidation. The [CO_x(max)] gives m_0 in the expression for $u(t)$ and is obtained by replacing the N₂ diluent flow to the HTFFR with an equivalent O₂ flow, thus com-

* This work supported by the U.S. Army Research Office, Contract No. OAG29-83-C-0023.

† Present address: National Center for Atmospheric Research, Boulder, CO.

pletely converting input carbon to CO_x . Measurement of $[\text{CO}_x]$ at other than complete oxidation conditions (replacing part of the N_2 flow with O_2) gives $(m_0 - m_x)$. Frequent $[\text{CO}_x(\text{max})]$ determinations were interspersed with the $[\text{CO}_x]$ measurements.

The HTFFR described by Fontijn and Felder (5) was modified for this work. Optical observation ports in the reaction tube were eliminated, allowing the isothermal zone of the reactor to include between 50 and 70 cm of the overall 90 cm length of the tube, depending on the flow conditions used in the experiments. The reaction tubes (two different diameter tubes were used in the present work, a 4.5 cm i.d. mullite tube, and a 2.5 cm i.d. 998 alumina tube) were resistively heated in three separately controlled zones of ≈ 30 cm each with 0.127 cm diam Pt/40% Rh resistance wire. At the reaction tube exit a HeNe laser beam crossed the particle-laden flow; scattered laser light was detected perpendicular to the beam. A 10 cm diam filter support and filter were mounted in a downstream bypass line so that the entire flow could be routed through it to collect partially oxidized particles for subsequent surface area measurements.

Particle feed was from a 10 cm i.d., 40 cm long tumbling bed supported $\approx 30^\circ$ from horizontal on two bearings. The particle bed charge consists of 90% (wt.) silica sand and 10% carbon black. A small N_2 flow through the bed formed a carbon black aerosol, some of which entered a particle takeoff tube and flowed to a "settling chamber." Feed rates at the bed outlet of 1-100 mg/min (10^{-5} to 10^{-4} moles C/s) were achieved. In the 15 cm i.d., 75 cm long settling chamber the flow was smoothed with a conically shaped flow straightener and slowed to ≈ 0.5 cm/s so that particle aggregates with aerodynamic diameters $\geq 4 \mu\text{m}$ settled out of the flow. In some experiments, settling chamber flow speeds up to 2 cm/s were used; under these conditions, particle aggregates up to $\approx 10 \mu\text{m}$ could have passed through the settling chamber. This range of particle sizes is below the size at which bulk diffusion affects the oxidation rate measurements.

The flow from the settling chamber entered the HTFFR reaction tube, where the major portion of the N_2 diluent and O_2 were added radially to the flow. The mass flow of carbon to the reactor indicated by $[\text{CO}_x(\text{max})]$ measurements was 0.05-5.0 mg/min (10^{-7} to 10^{-5} mol C/s), or about 5% of the output of the particle feeder. The remaining carbon black particles were collected in the settling chamber. The flow of O_2 in the experiments ranged from 5×10^{-5} to 5×10^{-3} mol/s and always exceeded the molar "carbon" flow by a factor of at least 20; for measurements of $[\text{CO}_x(\text{max})]$, the oxygen flow was 10^3 to 10^4 times in excess of the "carbon flow."

Laser scattering was also used to obtain kinetic data by measuring the concentration of O_2 required to consume all of the input carbon in exactly the residence time. The O_2 flow to the reactor was progressively incremented while recording the scattered light intensity; a plot was made of relative (to $[\text{O}_2] = 0$) scattered light intensity against $\log [\text{O}_2]$. The intensity decreased linearly on such plots as the particles were consumed; the curve went to zero at the value of $[\text{O}_2]$ at which the input carbon was consumed in the burnup time, t_b . The burnup time is simply related to R_p . The R_p values obtained using the scattered light method were identical with those obtained using the gc method.

Partially oxidized particles were collected on the inline filter for surface area measurements which yield information on the physical mechanism of the oxidation process. An adsorption analyzer (Quantachrome MS-8) was used for N_2 adsorption at 77 K, and the results were analyzed using the one point BET method (7). Specific surface area ratios were measured as a function of fractional burn-off, u , from $u = 0$ (particles that have traversed the reactor with $[\text{O}_2] = 0$) to $u = 0.7$.

The carbon blacks, Raven 16 (R16), a lampblack, and Conductex SC (CSC), a conducting black, were chosen to have a wide difference in initial specific surface area and iron impurity concentration. Both have "high" sulfur concentrations. The materials were donated by Columbian Chemical Corporation, Tulsa, OK, and their properties are summarized in Table I.

III. RESULTS AND DISCUSSION

1. Specific Surface Area Measurements

The interaction between O_2 and the carbon black particles can occur between two extreme modes (4,7,8): (1) reaction on an external non-porous surface; (2) reaction within a completely porous mass. In the first extreme, a particle of constant density, ρ , is oxidized and its radius decreases with burnoff. In the second extreme, a porous particle of constant radius is oxidized internally and its density decreases with burnoff. The ratio of specific surface areas of the unoxidized and partially oxidized particles, $S_0/S(t)$, are given by (9):

$$\begin{aligned} S_0/S(t) &= (1-u)^{0.33} && \text{(constant density)} \\ S_0/S(t) &= (1-u) && \text{(constant radius)} \end{aligned}$$

Representative data for the two carbon blacks are compared with these functions in Fig. 1; the results indicate that the external surface area available for reaction increases in a manner consistent with a constant density (case 1 above) burning. The present measurements can thus be interpreted as the oxidation of non-porous spherical particles (assumed monodisperse) which react at constant density and with no change in particle number density.

2. Oxidation Rates

Oxidation rates were measured over 1300-1700 K for R16 and 1400-1700 K for CSC, more than three decades of oxygen partial pressure (0.02-60 kPa) and total pressures ($O_2 + N_2$) from 20 to 60 kPa. Particle residence times were varied from 50-800 ms. The majority of the data were obtained using the gc method; additional data were obtained using the laser scattering method. Representative burnoff data from the gc measurements, plotted against $[O_2]$ are shown in Fig. 2. Figure 3 shows data obtained using the laser scattering diagnostic as discussed above from one experiment on CSC at 1580 K and a total pressure of 27 kPa.

There were no discernible total pressure effect on the measured $[CO_x]$ yields over the approximately factor of two-to-three variation in total pressure covered at each temperature investigated, and no gas velocity effects over a factor of six at any temperature, nor did changing the reaction tube diameter from 2.5 to 4.5 cm have any effect. The measured burnoff depended only on reactor temperature, $[O_2]$ and residence time.

The gc data were analyzed to extract R_e by rearranging Eq. 1:

$$R_e = (3/S_0 t) \cdot (1 - (1 - u)^{0.33})$$

Representative results are plotted in in Figs. 4 and 5. For the laser scattering measurements, $u = 1$ when the scattered intensity is zero and

$$R_e = 3/S_0 t_0$$

where t_0 is the residence time for complete burnoff at the $[O_2]$ determined from plots such as Fig. 3. Values of R_e so determined are included in Figs. 4 and 5.

These observed surface reactivities are chemically controlled as can be seen by comparing the calculated diffusion limited and observed reactivities. For diffusion controlled reaction on a spherical particle of radius, r (4):

$$R_{e,o} = (\psi D/r) \cdot (C_0 - C_x) \quad (2)$$

where $R_{e,o}$ = diffusion controlled reactivity based on external surface area, $g \text{ cm}^{-2} \text{ s}^{-1}$

$\psi = (M_c/M_o \nu)$ where ν is the molar stoichiometric coefficient for the gas and M_c/M_o is the molecular weight ratio of carbon to the reactant gas. For the present studies, $C + 1/2 O_2 \rightarrow CO$, and $\nu = 1/2$, with $\psi = (12/32) \cdot 2 = 3/4$

D = Binary diffusion coefficient of the oxidant gas, $\text{cm}^2 \text{ s}^{-1}$.

C = mass density of the gas at the particle surface, C_x , and in the free stream, C_0 , $g \text{ cm}^{-3}$.

Thus, diffusion control (small values of $R_{e,o}$) is favored by high pressure (low diffusion rates), large particle size, and high temperature (high surface reaction rates). For pure diffusion control, i.e., when the surface reaction rate is infinitely rapid, $C_x \rightarrow 0$. Figure 6 shows the range of $R_{e,o}$ calculated from Eq. 2) with $C_x = 0$ at the temperature and pressure extremes used in the present work (60 kPa and 1700 K) compared to the experimentally measured values. For the nominal particle diameters of the carbon blacks, ≈ 10 -100 nm, diffusion controlled rates are large and the reaction rate is controlled by surface chemistry processes. Figure 6 shows that even if aggregates as large as 100 μm were present in the reactor (and the settling chamber ensures that they were not), bulk diffusion rates would still be ≈ 10 times larger than the observed reaction rates under the present experimental conditions. On this basis, mass transfer to the carbon black particles does not significantly affect the observed measurements.

In the absence of diffusion effects, the slopes of plots like Figs. 4 and 5 give the apparent reaction order in $[O_2]$. The reaction orders, n , lie between 0.6 and 0.8. Table II contains a summary listing of the values of R_e for the present experiments in the form $\log R_e = \log R_0 + n \log [O_2]$. R_0 is a fitting constant with units of $g \text{ cm}^{-2} \text{ s}^{-1} [O_2]^{-n}$.

3. Discussion

Figures 2, 4, and 5 show comparisons of the observed u and R_e with the predictions of the Nagle and Strickland-Constable, NSC, formulation (10) which has been successful in describing the reactivity of several carbonaceous materials with O_2 , especially at higher temperatures than those used here (10,11). From the plots it is clear that the present results are not well described by two site NSC kinetics (cf. Blyholder, et al. (12)). In particular, the present results show no indication of the change in reaction order in $[O_2]$ suggested by the two site theory (12).

In Fig.7, the R_e values are compared with previous studies of soot and carbon black oxidation at $[O_2] = 3.5 \times 10^{17} \text{ cm}^{-3}$. The data are those of NSC (10), Park and Appelton (11), PA, on carbon black oxidation in a shock tube (the PA and NSC results are identical), and of Lee, Thring, and Beér (13), LTB, on soot oxidation in an O_2 -rich flame. At this $[O_2]$ and higher, R16 and CSC oxidation are significantly slower than that of previously studied carbon blacks and soot. An "activation energy" of $\approx 170 \text{ kJ}$ is consistent with all of the measurements. At lower $[O_2]$ ($\approx 2 \times 10^{14}$), the present results are compared with those of Rosner and

Allendorf (14), (RA), and NSC in Fig. 8. At this low $[O_2]$, RA's measurements on isotropic and pyrolytic graphite bracket those predicted by NSC and those measured in the present work. The "turnover" in the reactivity coefficient values predicted by NSC and observed by RA may be present for R16, but it is not suggested by the CSC data.

Figures 9 and 10 display the probability of reaction, $\bar{\tau}$, per O_2 -surface collision calculated using kinetic theory to determine the number of collisions/s per unit surface area and the measured R_p values. The data of RA on pyrolytic graphite over a range of low $[O_2]$ at ≈ 1500 K are shown for comparison in Fig. 9. In Fig. 10, $\bar{\tau}$ for R16 and CSC is shown for most of the wide range of $[O_2]$ covered in this work at the extremes of the temperature ranges investigated. The low reactivity of these carbon blacks translates into collision efficiencies as low as $\approx 1 \times 10^{-6}$ at $[O_2] = 1 \times 10^{18} \text{ cm}^{-3}$ and as high as $\approx 4 \times 10^{-3}$ at $[O_2] = 1 \times 10^{15} \text{ cm}^{-3}$. These values are comparable to those for graphitic carbons.

Thus, the present results indicate low reactivity for R16 and CSC for $[O_2]$ values of practical interest. The complex $[O_2]$ -dependence of R_p required by NSC kinetics is not observed over the temperature range studied, despite extremely wide variations in $[O_2]$. The data show no significant differences which can be attributed to metallic content. We speculate that the high sulfur content in these carbon blacks may be the cause of their low reactivity and the failure of the two site model to describe their oxidation kinetics. The sulfur content (mole fraction ≈ 40 ppm) may be sufficient to poison potential metallic catalytic sites (on a molar basis, sulfur is ≈ 20 times more abundant than metals in R16 and 10 times more in CSC) as well as to interfere with active sites in both carbon blacks. If correct, this speculation suggests that it is important to avoid sulfur contamination where carbonaceous burnout at "low" temperature is desired.

REFERENCES

1. Neoh, K.G., Howard, J.B., and Sarofim, A.F., in Particulate Carbon: Formation During Combustion, D.C. Siegl and G.W. Smith, Eds., Plenum Press, New York, (1981), p. 261.
2. Page, F.M. and Ates, F., in Evaporation and Combustion of Fuels, J.T. Zung, Ed., Advances in Chemistry 166, American Chemical Society, Washington, D.C. (1978), p. 190.
3. Fenimore, C.P. and Jones, G.W., *J. Phys. Chem.* 71, 593 (1967).
4. Laurendeau, N.M., *Prog. Energy Combust. Sci.* 4, 221 (1978).
5. Fontijn, A. and Felder, W., in Reactive Intermediates in the Gas Phase: Generation and Monitoring, D.W. Setser, Ed., Academic Press, New York, (1979) Chap. 2.
6. Lowell, S. Introduction to Powder Surface Area, Wiley-Interscience, New York (1979).
7. Mulcahy, M.F.R. and Smith, I.W., *Pure and Appl. Chem.* 19, 81 (1969)
8. Essenhigh, R.H., in Chemistry of Coal Utilization, 2nd Supplementary Volume, M.A. Elliott, Ed., Wiley, New York, (1981) Chap. 19.
9. Smith, I.W., *Combust. Flame* 17, 303 (1971)

10. Nagle, J. and Strickland-Constable, R.F., Proceedings of the Fifth Conference on Carbon, Volume 1, Macmillan, New York (1962), p. 154.
11. Park, C. and Appelton, J.P., Combust. Flame **20**, 369 (1973).
12. Blyholder, G., Binford, J.S., Jr., and Eyring, H., J. Phys. Chem. **62**, 263 (1958).
13. Lee, K.B., Thring, M.W., and Beer, J.M., Combust. Flame **6**, 137 (1962).
14. Rosner, D.E. and Allendorf, H.D., AIAA J. **6**, 650 (1968).

TABLE I. PHYSICAL AND CHEMICAL PROPERTIES OF CARBON BLACKS^a

Trade Name	Mean Particle Diam. (nm)	BET (N ₂) Surface Area (m ² g ⁻¹)	Volatiles (wt %)	Metal Content (wt %) ^c	Ash (wt %)	Sulfur (wt %)
Raven 16	61	25 (29 ^b)	0.9	0.1 ^c	0.098	1.67
Conductex SC	20	220 (190 ^b)	1.5	0.08 ^c	0.075	0.85

^a Data supplied by manufacturer.

^b Measured in this work.

^c Metallic impurities, wt. %:

	R16	CSC
I Mn, Mg, Al, Ti	0.007	0.008
Fe	0.045	0.005
Na	0.021	0.047
Ca	0.025	0.016

TABLE II. EXTERNAL SURFACE REACTIVITY FOR CARBON BLACK OXIDATION BY O₂

$$\log_{10} R_e = \log_{10} R_0 + n \log_{10} [O_2]$$

Carbon Black	T (K)	$\log_{10} R_0$ (g cm ⁻² s ⁻¹ [O ₂] ⁻ⁿ)	n	[O ₂] range (10 ¹⁶ cm ⁻³)
Raven 16	1300	-16.3 ± 0.5 ^a	0.62 ± 0.04 ^a	0.02 - 158
	1400	-16.5 ± 2.0	0.64 ± 0.12	2.0 - 104
	1470	-16.1 ± 1.3	0.66 ± 0.10	0.02 - 98
	1580	-14.9 ± 1.7	0.59 ± 0.10	0.12 - 177
	1680	-15.1 ± 1.0	0.61 ± 0.07	0.03 - 154
Conductex SC	1410	-18.6 ± 0.5	0.76 ± 0.13	0.03 - 200
	1580	-18.8 ± 1.1	0.82 ± 0.17	0.02 - 130
	1650	-14.2 ± 1.4	0.57 ± 0.09	0.02 - 75

^a One standard deviation

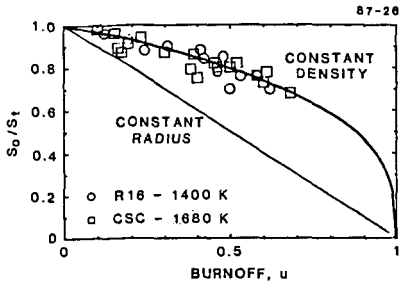


FIGURE 1 VARIATION OF CARBON BLACK SURFACE AREA WITH BURNOFF

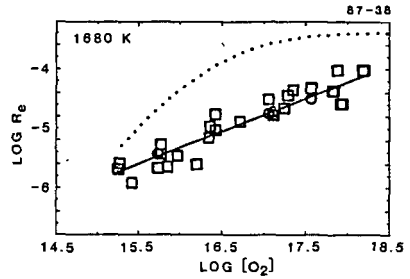


FIGURE 4 R16 OXIDATION BY O_2
 □ - gc data; ○ - scattering data;
 ... -NSC (10) prediction

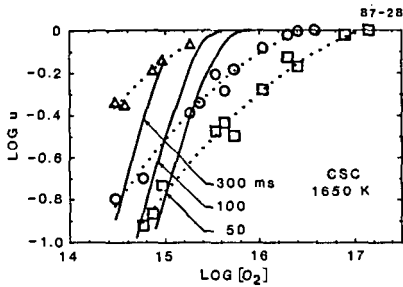


FIGURE 2 BURNOFF OF CSC AT 1650 K
 Residence times: □ - 50 ms; ○ - 100 ms;
 Δ - 300 ms. Solid lines are NSC (10)
 predictions.

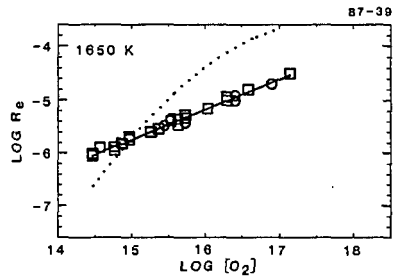


FIGURE 5 CSC OXIDATION BY O_2
 □ - gc data; ○ - scattering data;
 ... -NSC (10) prediction

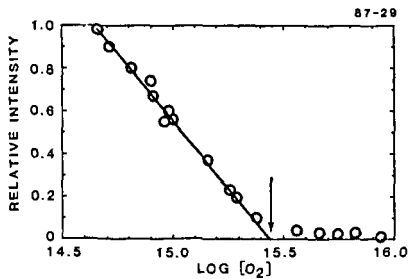


FIGURE 3 LASER SCATTERING MEASUREMENT
 OF CSC OXIDATION AT 1650 K
 $[O_2] = 2.8 \times 10^{15}$ (arrow), $t_0 = 380$ ms

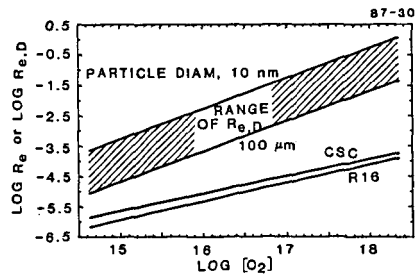
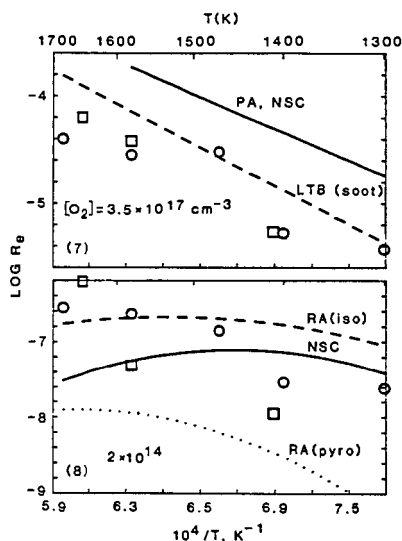
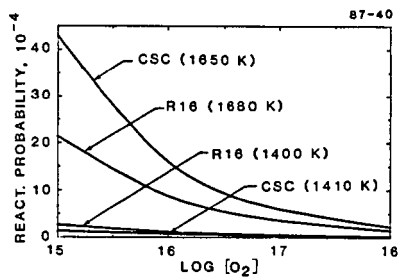
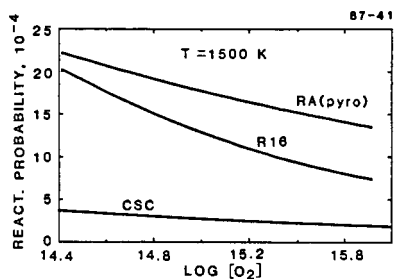


FIGURE 6 COMPARISON OF DIFFUSION-LIMITED
 REACTIVITY WITH OBSERVED VALUES AT 1700K

87-44



FIGURES 7 and 8 TEMPERATURE DEPENDENCE OF CARBON BLACK OXIDATION
 o - R16; \square -CSC; NSC - Nagle and Strickland-Constable (10); PA - Park and Appelton (11); LTB -Lee, Thring and Beer (13); RA - Rosner and Allendorf (14) for isotropic (iso) and pyrolytic (pyro) graphite



FIGURES 9 and 10 DEPENDENCE OF REACTION PROBABILITY ON $[\text{O}_2]$
 RA(pyro) - results of Rosner and Allendorf (14) on pyrolytic graphite.